

Aims and Scope: Cell Journal (Yakhteh) is a quarterly English publication of Royan Institute of Iran. The aim of the journal is to disseminate information through publishing the most recent scientific research studies on exclusively Cellular, Molecular and other related topics. Cell J, has been certified by Ministry of Culture and Islamic Guidance since 1999 and also accredited as a scientific and research journal by HBI (Health and Biomedical Information) Journal Accreditation Commission since 2000. **This journal holds the membership of the Committee on Publication Ethics (COPE).**

1. Types of articles

The articles in the field of Fertility and Sterility can be considered for publications in Cell J. These articles are as below:

A. Original articles are scientific reports of the original research studies. The article consists of English Abstract (structured), Introduction, Materials and Methods, Results, Discussion, Conclusion, Acknowledgements, Author's Contributions, and References (**Up to 40**).

B. Review articles are the articles written by well experienced authors and those who have excellence in the related fields. The corresponding author of the review article must be one of the authors of at least three published articles appearing in the references. The review article consists of English Abstract (unstructured), Introduction, Conclusion, Author's Contributions, and References (**Up to 70**).

C. Systematic Reviews

Systematic reviews are a type of literature review that collect and critically analyzes multiple research studies or papers. The Systematic reviews consist of English Abstract (unstructured), Introduction, Materials and Methods, Results, Discussion, Conclusion, Acknowledgements, Author's Contributions, and References (**Up to 70**).

D. Short communications are the articles containing new findings. Submissions should be brief reports of ongoing researches. The short communication consists of English Abstract (unstructured), the body of the manuscript (should not hold heading or subheading), Acknowledgements, Author's Contributions, and References (**Up to 30**).

E. Case reports are short discussions of a case or case series with unique features not previously described which make an important teaching point or scientific observation. They may describe novel techniques or use equipment, or new information on diseases of importance. It consists of English Abstracts (Unstructured), Introduction, Case Report, Discussion, Acknowledgements, Author's Contributions, and References (**Up to 30**).

F. Editorial should be written by either the editor in chief or the editorial board.

G. Imaging in biology should focus on a single case with an interesting illustration such as a photograph, histological specimen or investigation. Color images are welcomed. The text should be brief and informative.

H. Letter to the editors are welcome in response to previously published Cell J articles, and may also include interesting cases that do not meet the requirement of being truly exceptional, as well as other brief technical or clinical notes of general interest.

I. Debate.

2. Submission Process

It is recommended to see the guidelines for reporting different kinds of manuscripts here. This guide explains how to prepare the manuscript for submission. Before submitting, we suggest authors familiarize themselves with Cell J format and content by reading the journal via website (www.celljournal.org). The corresponding author ensures that all authors are included in the author list and agree with its order, and they must be aware of the manuscript submission.

A. Author contributions statements

It is essential for authors to include a statement of responsibility in the manuscript that specifies the contribution of every one of them. This participation must include conception and design of the manuscript, data acquisition or data analysis and interpretation, drafting of the manuscript and/or revising it for critically important intellectual content, revision and final approval of the manuscript and statistical analysis, obtaining funding, administrative, technical, or material support, or supervision. Authors who do not meet the above criteria should be acknowledged in the **Acknowledgments Section**.

B. Cover letter

Each article should be accompanied by a cover letter, signed by all authors specifying the following statement: "The manuscript has been seen and approved by all authors and is not under active consideration for publication. It has neither been accepted for publication nor published in another journal fully or partially (except in abstract form). I hereby assign the copyright of the enclosed manuscript to Cell J. Corresponding author must confirm the proof of the manuscript before online publishing. Also, is it needed to suggest three peer reviewers in the field of their manuscript.

C. Manuscript preparation

Authors whose first language is not English encouraged to consult a native English speaker in order to confirm his manuscripts to US or British (not a mixture) English usage and grammar. The manuscript should be prepared in accordance with the "International Committee of Medical Journal Editors (ICMJE)". Please send your manuscript in two formats (word and Pdf). The abstract and text pages should have consecutive line numbers in the left margin beginning with title page and continuing through the last page of the written text. Each abbreviation must be defined in the abstract and text when they are mentioned for the first time. Avoid using abbreviation in title. Please use the

international and standard abbreviations and symbols.

It should be added that an essential step toward the integration and linking of scientific information reported in published literature is using standardized nomenclature in all fields of science and medicine. Species names must be italicized (e.g., *Homo sapiens*) and also the full genus and species written out in full, both in the title of the manuscript and at the first mention of an organism in a paper.

It is necessary to mention that genes, mutations, genotypes, and alleles must be indicated in italics. Please use the recommended name by consulting the appropriate genetic nomenclature database, e.g., HUGO for human genes. In another words; if it is a human gene, you must write all the letters in capital and italic (e.g., *OCT4*, *c-MYC*). If not, only write the first letter in capital and italic (e.g., *Oct4*, *c-Myc*). **In addition, protein designations are the same as the gene symbol but are not italicized.**

Of note, Cell J will only consider publishing genetic association study papers that are novel and statistically robust. Authors are advised to adhere to the recommendations outlined in the STREGA statement (<http://www.strega-statement.org>). The following criteria must be met for all submissions:

1. Hardy-Weinberg Equilibrium (HWE) calculations must be carried out and reported along with the P-values if applicable [see Namipashaki et al. 2015 (Cell J, Vol 17, N 2, Pages: 187-192) for a discussion].
2. Linkage disequilibrium (LD) structure between SNPs (if multiple SNPs are reported) must be presented.
3. Appropriate multiple testing correction (if multiple independent SNPs are reported) must be included.

Submissions that fail to meet the above criteria will be rejected before being sent out for review.

Each of the following manuscript components should begin in the following sequence:

Authors' names and order of them must be carefully considered (full name(s), highest awarded academic degree(s), email(s), and institutional affiliation(s) of all the authors in English. Also, you must send mobile number and full postal address of the corresponding author).

Changes to Authorship such as addition, deletion or rearrangement of author names must be made only before the manuscript has been accepted in the case of approving by the journal editor. In this case, the corresponding author must explain the reason of changing and confirm them (which has been signed by all authors of the manuscript). If the manuscript has already been published in an online issue, an erratum is needed.

Title is providing the full title of the research (do not use abbreviations in title).

Running title is providing a maximum of 7 words (no more than 50 characters).

Abstract must include Background, Materials and Methods, Results, and Conclusion (no more than **300** words).

Keywords, three to five, must be supplied by the authors at the foot of the abstract chosen from the Medical Subject Heading (MeSH). Therefore; they must be specific and relevant to the paper.

The following components should be identified after the abstract:

Introduction: The Introduction should provide a brief background to the subject of the paper, explain the importance of the study, and state a precise study question or purpose.

Materials and Methods: It includes the exact methods or observations of experiments. If an apparatus is used, its manufacturer's name and address should be stipulated in parenthesis. If the method is established, give reference but if the method is new, give enough information so that another author can perform it. If a drug is used, its generic name, dose, and route of administration must be given. Standard units of measurements and chemical symbols of elements do not need to be defined.

Statistical analysis: Type of study and statistical methods should be mentioned and specified by any general computer program used.

Ethical considerations: Please state that informed consent was obtained from all human adult participants and from the parents or legal guardians of minors and include the name of the appropriate institutional review board that approved the project. It is necessary to indicate in the text that the maintenance and care of experimental animals complies with National Institutes of Health guidelines for the humane use of laboratory animals, or those of your Institute or agency.

Clinical trial registration: All of the Clinical Trials performing in Iran must be registered in Iranian Registry of Clinical Trials (www.ircct.ir). The clinical trials performed abroad, could be considered for publication if they register in a registration site approved by WHO or www.clinicaltrials.gov. If you are reporting phase II or phase III randomized controlled trials, you must refer to the CONSORT Statement for recommendations to facilitate the complete and transparent reporting of trial findings. Reports that do not conform to the CONSORT guidelines may need to be revised before peer reviewing.

Results: They must be presented in the form of text, tables, and figures. Take care that the text does not repeat data that are presented in tables and/or figures. Only emphasize and summarize the essential features of the main results. Tables and figures must be numbered consecutively as appeared in the text and should be organized in separate pages at the end of article while their location should be mentioned in the main text.

Tables and figures: Tables should have a short descriptive heading above them and also any footnotes. Figure's legend should contain a brief title for the whole figure and continue with a short explanation of each part and also the symbols used (no more than 100 words). All figures must be prepared based on cell journal's guideline in color (no more than **6** Figures and Tables) and also in GIF or JPEG format with 300 dpi resolutions.

Supplementary materials would be published on the online version of the journal. This material is important to the understanding

and interpretation of the report and should not repeat material within the print article. The amount of supplementary material should be limited. Supplementary material should be original and not previously published and will undergo editorial and peer review with the main manuscript. Also, they must be cited in the manuscript text in parentheses, in a similar way as when citing a figure or a table. Provide a legend for each supplementary material submitted.

Discussion: It should emphasize the present findings and the variations or similarities with other researches done by other researchers. The detailed results should not be repeated in the discussion again. It must emphasize the new and important aspects of the study.

Conclusion: It emphasizes the new and important aspects of the study. All conclusions are justified by the results of the study.

Acknowledgements: This part includes a statement thanking those who contributed substantially with work relevant to the study but does not have authorship criteria. It includes those who provided technical help, writing assistance and name of departments that provided only general support. You must mention financial support in the study. Otherwise; write this sentence "There is no financial support in this study".

Conflict of Interest: Any conflict of interest (financial or otherwise) and sources of financial support must be listed in the Acknowledgements. It includes providers of supplies and services from a commercial organization. Any commercial affiliation must be disclosed, regardless of providing the funding or not.

References: The references must be written based on the Vancouver style. Thus the references are cited numerically in the text and listed in the bibliography by the order of their appearance. The titles of journals must be abbreviated according to the style used in the list of Journals Indexed in PubMed. Write surname and initials of all authors when there are six or less. In the case of seven or more authors, the names of first six authors followed by "et al." must be listed. The reference of information must be based on the following order:

Article:

Surname(s) and first letter of name & middle name(s) of author(s). Manuscript title. Journal title (abbr).publication date (year); Volume (Issue): Page number.

Example: Manicardi GC, Bianchi PG, Pantano S, Azzoni P, Bizzaro D, Bianchi U, et al. Presence of endogenous nicks in DNA of ejaculated human spermatozoa and its relationship to chromomycin A3 accessibility. *Biol Reprod.* 1995; 52(4): 864-867.

Book:

Surname(s) and first letter of name & middle name(s) of author(s). Book title. Edition. Publication place: publisher name; publication date (year); Page number.

Example: Edelman CL, Mandle CL. Health promotion throughout the life span. 2nd ed. ST Louis: Mosby; 1998; 145-163.

Chapter of book:

Surname(s) and first letter of name & middle name(s) of author(s). Chapter title. In: Surname(s) and first letter of name & middle name(s) of editor(s), editors. Book title. Edition. Publication place: publisher name; publication date (year); Page number.

Example: Phillips SJ, Whisnant JP. Hypertension and stroke. In: Laragh JH, Brenner BM, editors. Hypertension: pathophysiology, diagnosis, and management. 2nd ed. New York: Raven Press; 1995; 465-478.

Abstract book:

Example: Nabavi SM. Stem cell therapy for multiple sclerosis. *Cell J.* 2013; 5 Suppl 1: Os-13.

Thesis:

Name of author. Thesis title. Degree. City name. University. Publication date (year).

Example: Eftekhari Yazdi P. Comparison of fragment removal and co-culture with Vero cell monolayer's on development of human fragmented embryos. Presented for the Ph.D., Tehran. Tarbiyat Modarres University. 2004.

Conferences:

Name(s) of editor(s). Conference title; Holding date; Holding place. Publication place; Publisher name; Publication date (year).

Example: Harnden P, Joffe JK, Jones WG, editors. Germ cell tumors V. Proceedings of the 5th Germ Cell Tumors Conference; 2001 Sep 13-15; Leeds, UK. New York: Springer; 2002.

Internet References

Article:

Surname(s) and first letter of name & middle name(s) of author(s). Manuscript title. Journal title (abbr). Publication date (year); Volume (Issue): Page number. Available from: URL link. (Observation date).

Example: Jahanshahi A, Mirnajafi-Zadeh J, Javan M, Mohammad-Zadeh M, Rohani M. Effect of low-frequency stimulation on adenosine A1 and A2A receptors gene expression in dentate gyrus of perforant path kindled rats. *Cell J.* 2008; 10 (2): 87-92. Available from: <http://www.celljournal.org>. (20 Oct 2008).

Book:

Example: Anderson SC, Poulsen KB. Anderson's electronic atlas of hematology.[CD-ROM]. Philadelphia: Lippincott Williams & Wilkins; 2002.

Law:

Example: Embryo donation law. Iran Judicature, Official Gazette of the Islamic Republic of Iran. Available from: <http://www.dastour.ir/Brows/?lid=245069>.(20 Jul 2013).

D. Proofs are sent by email as PDF files and should be checked and returned within 72 hours of receipt. It is the authors' responsibility to check that all the text and data as contained in the page proofs are correct and suitable for publication. **We are requested to pay particular attention to author's names and affiliations as it is essential that these details be accurate when the article is published.**

E. Pay for publication: Authors do not have to pay any Manuscript Processing Charge or Open Access Publication Fee. **Before publishing author's article, it would be the author's responsibility to pay for the expenses, if the editor feels the level of English used in the manuscript requires editing.**

F. Ethics of scientific publication: Manuscripts that have been published elsewhere with the same intellectual material will refer to duplicate publication. If authors have used their own previously published work or work that is currently under review, as the basis for a submitted manuscript, they are required to cite the previous work and indicate how their submitted manuscript offers novel contributions beyond those of the previous work. Research and publication misconduct is considered a serious breach of ethics. The Journal systematically employs iThenticate, a plagiarism detection and prevention software designed to ensure the originality of written work before publication.

Plagiarism of text from a previously published manuscript by the same or another author is a serious publication offence. Some parts of text may be used, only where the source of the quoted material is clearly acknowledged.

3. General information

A. You can send your article via online submission system which is available at our website: <http://www.celljournal.org>. If the article is not prepared according to the format of **Cell J**, it will be returned to authors.

B. The order of article appearance in the Journal is not demonstrating the scientific characters of the authors.

C. **Cell J** has authority to accept or reject the articles.

D. The received articles will be evaluated by one epidemiologist. Then associate editor will determine its reviewers. If three reviewers pass their judgments on the article, it will be presented to the editorial board of **Cell J**. If the editorial board has a positive judgment about the article, reviewers' comments will be presented to the corresponding author (the identification of the reviewers will not be revealed). The executive member of journal will contact the corresponding author directly within 7-8 weeks by email. If authors do not receive any reply from journal office after the specified time, they can contact journal office. Executive manager will respond promptly to authors' message.

The Final Checklist

The authors must ensure that before submitting the manuscript for publication, they have to consider the following parts:

1. Title page should contain title, name of the author/coauthors, their academic qualifications, designation & institutions they are affiliated with, mailing address for future correspondence, email address, phone, and fax number.
2. Text of manuscript and References prepared as stated in the "guide for authors" section.
3. Tables should be in a separate page. Figures must be sent in color and also in GIF or JPEG format with 300 dpi resolutions.
4. Covering Letter.

The Editor-in-Chief: Ahmad Hosseini, Ph.D.

Cell Journal (Yakhteh),

P.O. Box: 16635-148, Iran

Tel/Fax: + 98-21-22510895

Emails: Celljournal@royaninstitute.org

info@celljournal.org



IN THE NAME OF GOD

Gone But not Forgotten

In the memory of the late Director of Royan Institute,
Founder of Stem Cells Research in Iran and Chairman of
Cell Journal (Yakhteh). May he rest in peace.

Dr. Saeed Kazemi Ashtiani

OWNED:

Royan Institute, Iranian Academic Center for Education Culture and Research (ACECR)

CHAIRMAN:

Hamid Gourabi, Ph.D., (Professor, Royan Institute, Tehran, Iran)

EDITOR IN CHIEF:

Ahmad Hosseini, Ph.D., (Professor, Shahid Beheshti Medical University, Tehran, Iran)

EDITOR ASSOCIATE:

Saeid Abroun, Ph.D., (Associate Professor, Tarbiat Modares University, Tehran, Iran)

EDITORIAL BOARD:

Saeid Abroun, Ph.D., (Associate Professor, Tarbiat Modares University, Tehran, Iran)
Kamran Alimoghadam, M.D., (Associate Professor, Tehran Medical University, Tehran, Iran)
Alireza Asgari, Ph.D., (Professor, Baghyatallah University, Tehran, Iran)
Mohammad Kazem Aghaee Mazaheri, D.D.S., (Assistant Professor, ACECR, Tehran, Iran)
Gila Behzadi, Ph.D., (Professor, Shahid Beheshti Medical University, Tehran, Iran)
Hossein Baharvand, Ph.D., (Professor, Royan Institute, Tehran, Iran)
Mary Familiar, Ph.D., (Senior Lecturer, University of Melbourne, Melbourne, Australia)
Hamid Gourabi, Ph.D., (Professor, Royan Institute, Tehran, Iran)
Jurgen Hescheler, M.D., (Professor, Institute of Neurophysiology of University Zu Koln, Germany)
Ghasem Hosseini Salekdeh, Ph.D., (Assistant Professor, Agricultural Biotechnology Research Institute, Karaj, Iran)
Esmail Jabbari, Ph.D., (Associate Professor, University of South Carolina, Columbia, USA)
Suresh Jesuthasan, Ph.D., (Associate Professor, National University of Singapore, Singapore)
Bahram Kazemi, Ph.D., (Professor, Shahid Beheshti Medical University, Tehran, Iran)
Saadi Khochbin, Ph.D., (Professor, Inserm/Grenoble University, France)
Ali Khademhosseini, Ph.D., (Associate Professor, Harvard Medical School, USA)
Kun Ping Lu, M.D., Ph.D., (Professor, Harvard Medical School, Boston, USA)
Navid Manuchehrabadi, Ph.D., (Angio Dynamics, Marlborough, USA)
Hosseinali Mehrani, Ph.D., (Professor, Baghyatallah University, Tehran, Iran)
Marcos Meseguer, Ph.D., (Clinical Embryology Laboratory IVI Valencia, Valencia, Spain)
Seyed Javad Mowla, Ph.D., (Professor, Tarbiat Modares University, Tehran, Iran)
Mohammad Hossein Nasr Esfahani, Ph.D., (Professor, Royan Institute, Tehran, Iran)
Toru Nakano, M.D., Ph.D., (Professor, Osaka University, Osaka, Japan)
Donald Newgreen, Ph.D., (Professor, Murdoch Children Research Institute, Melbourne, Australia)
Mojtaba Rezazadeh Valojerdi, Ph.D., (Professor, Tarbiat Modares University, Tehran, Iran)
Mohammad Hossein Sanati, Ph.D., (Associate Professor, National Institute for Genetic Engineering and Biotechnology, Tehran, Iran)
Eimei Sato, Ph.D., (Professor, Tohoku University, Sendai, Japan)
Andreas Serra, M.D., (Professor, University of Zurich, Zurich, Switzerland)
Abdolhossein Shahverdi, Ph.D., (Professor, Royan Institute, Tehran, Iran)
Michele Catherine Studer, Ph.D., (Institute of Biology Valrose, IBV University of Nice Sophia-Antipolis, France)
Daniela Toniolo, Ph.D., (Head, Unit of Common Disorders, San Raffaele Research Institute, Milano, Italy)
Gianpaolo Zerbini, M.D., Ph.D., (San Raffaele Scientific Institute, Italy)
Shubing Zhang, Ph.D., (Associate Professor, Central South University, China)
Daniele Zink, Ph.D., (Institute of Bioengineering and Nanotechnology, Agency for Science Technology & Science, Singapore)

EXECUTIVE MANAGER:

Farideh Malekzadeh, M.Sc., (Royan Institute, Tehran, Iran)

EXECUTIVE BOARD:

Parvaneh Afsharian, Ph.D., (Royan Institute, Tehran, Iran)
Ahmad Vosough Taqi Dizaj, M.D., (Royan Institute, Tehran, Iran)
Reza Omani-Samani, M.D., (Royan Institute, Tehran, Iran)
Elham Amirchaghmaghi, M.D., Ph.D., (Royan Institute, Tehran, Iran)
Leila Daliri, M.Sc., (Royan Institute, Tehran, Iran)
Mahdi Lotfipanaah, M.Sc., (Royan Institute, Tehran, Iran)

ENGLISH EDITOR:

Naser Ansari-Pour, Ph.D., (University of Tehran, Tehran, Iran)
Saman Eghtesad, Ph.D., (Royan Institute, Tehran, Iran)
Vahid Ezzatizadeh, Ph.D., (Royan Institute, Tehran, Iran)
Jane Ferrie, Ph.D., (University College of London, London, UK)
Mojtaba Nemat, M.Sc., (Royan Institute, Tehran, Iran)
Ramin Rezaee, Pharm.D., Ph.D., (Mashhad University of Medical Sciences, Mashhad, Iran)
Kim Vagharfard, M.Sc., (Royan Institute, Tehran, Iran)
Hamid Zahednasab, M.Sc., (Royan Institute, Tehran, Iran)

GRAPHICS:

Laleh Mirza Ali Shirvani, B.Sc., (Royan Institute, Tehran, Iran)

PUBLISHED & SPONSORED BY:

Publication of Royan Institute (ACECR)

Indexed in:

1. Thomson Reuters (ISI); *Impact Factor: 2.363*
2. PubMed
3. PubMed Central (PMC)
4. National Library Medicine (NLM)
5. Biosis Preview
6. Index Medicus for the Eastern Mediterranean Region (IMEMR)
7. Index Copernicus International
8. Cambridge Scientific Abstract (CSA)
9. EMBASE
10. Scopus
11. Cinahl Database
12. Google Scholar
13. Chemical Abstract Service (CAS)
14. Proquest
15. Directory of Open Access Journals (DOAJ)
16. Open Academic Journals Index (OAJI)
17. Directory of Research Journals Indexing (DRJI)
18. Scientific Information Database (SID)
19. Iranmedex
20. Regional Information Center for Sciences and Technology (RICeST)
21. Islamic World Science Citation Center (ISC)
22. Magiran
23. Science Library Index

ACECR

Copyright and license information:

The *Cell Journal* (Yakhteh) is an open access journal which means the articles are freely available online for any individual author to download and use the providing address. The journal is licensed under a Creative Commons Attribution-Non Commercial 3.0 Unported License which allows the author(s) to hold the copyright without restrictions that is permitting unrestricted use, distribution, and reproduction in any medium provided the original work is properly cited.

Editorial Office Address (Dr. Ahmad Hosseini):

Royan Institute, P.O.Box: 16635-148,
Tehran, Iran

Tel & Fax: (+9821)22510895

Website: www.celljournal.org

Emails: info@celljournal.org

celljournal@royaninstitute.org

Printing Company:

Jurband Ghaemprint Co.
NO. 5, Jalil khoob alley, Niroo Havaei Street,
Tehran, Iran



CONTENTS

Review Articles

- **FACT or PACT: A Comparison between Free-Acrylamide and Acrylamide-Based Passive Sodium Dodecyl Sulfate Tissue Clearing for whole Tissue Imaging**
Huimei Wang, Arezoo Khoradmehr, Amin Tamadon 103
- **The Expression of Microvesicles in Leukemia: Prognostic Approaches**
Ali Ehsanpour, Najmaldin Saki, Marziye Bagheri, Masumeh Maleki Behzad, Saeid Abroun 115

Original Articles

- **Histone Modification Marks Strongly Regulate *CDH1* Promoter in Prostospheres as A Model of Prostate Cancer Stem Like Cells**
Fateme Shokraii, Maryam Moharrami, Nasrin Motamed, Maryam Shahhoseini, Mehdi Totonchi, Vahid Ezzatizadeh, Javad Firouzi, Pardis Khosravani, Marzieh Ebrahimi 124
- **Preparation and Evaluation of A Novel Liposomal Nano-Formulation in Metastatic Cancer Treatment Studies**
Fateme Barzegari Firouzabadi, Shahrbanoo Oryan, Mohammad Hasan Sheikhha, Seyed Mehdi Kalantar, Ameneh Javed 135
- **Effectiveness of Plasmocure™ in Elimination of *Mycoplasma* Species from Contaminated Cell Cultures: A Comparative Study versus Other Antibiotics**
Vahid Molla Kazemiha, Shahram Azari, Mahdi Habibi-Anbouhi, Amir Amanzadeh, Shahin Bonakdar, Mohammad Ali Shokrgozar, Reza Mahdian 143
- ***In Vitro* and *In Vivo* Comparison of Different Types of Rabbit Mesenchymal Stem Cells for Cartilage Repair**
Mohammad Ali Khalilifar, Mohamadreza Baghaban Eslaminejad, Mohammad Ghasemzadeh, Samaneh Hosseini, Hossein Baharvand 150
- **Generation and Characterization of Induced Pluripotent Stem Cells from Mononuclear Cells in Schizophrenic Patients**
Qing Liu, Jiang Du, Jinyu Fan, Wenqiang Li, Weiyun Guo, Huigen Feng, Juntang Lin 161
- ***MafA* Overexpression: A New Efficient Protocol for *In Vitro* Differentiation of Adipose-Derived Mesenchymal Stem Cells into Functional Insulin-Producing Cells**
Dian Dayer, Mohammad Reza Tabandeh, Eskandar Moghimipour, Mahmood Hashemi Tabar, Ata.A Ghadiri, Elham Allah Bakhshi, Mahmoud Orazizadeh, Mohammad Ali Ghafari 169
- **Endometriotic Mesenchymal Stem Cells Epigenetic Pathogenesis: Deregulation of *miR-200b*, *miR-145*, and *let7b* in A Functional Imbalanced Epigenetic Disease**
Parisa Mashayekhi, Mehrdad Noruzinia, Sirous Zeinali, Sepideh Khodaverdi 179
- **Differential Proliferation Effects after Short-Term Cultivation of Mouse Spermatogonial Stem Cells on Different Feeder Layers**
Hossein Azizi, Hatef Ghasemi Hamidabadi, Thomas Skutella 186
- **Dynamics of The Expression of Pluripotency and Lineage Specific Genes in The Pre and Peri-Implantation Goat Embryo**
Pouria HosseinNia, Mehdi Hajian, Farnoosh Jafarpour, Seyed Morteza Hosseini, Mojtaba Tahmoorespur, Mohammad Hossein Nasr-Esfahani 194
- **Synergetic Effect of Silver Nanoparticles and UVC Irradiation on *H2AX* Gene Expression in TK6 Cells**
Tahereh Zare, Reza Fardid, Samaneh Naderi 204
- ***Panax ginseng* Extract Improves Follicular Development after Mouse Preantral Follicle 3D Culture**
Abbas Majdi Seghinsara, Hamed Shoorei, Mohammad Mehdi Hassanzadeh Taheri, Arash Khaki, Majid Shokoohi, Moloud Tahmasebi, Amir Afshin Khaki, Hossein Eyni, Sadegh Ghorbani, Khadijeh Riahi Rad, Hossein Kalarestaghi, Leila Roshangar 210
- **Neuroprotective Effects of Combined Treatment with Minocycline and Olfactory Ensheathing Cells Transplantation against Inflammation and Oxidative Stress after Spinal Cord Injury**
Soheila Pourkhodadad, Shahrbanoo Oryan, Gholamreza Kaka, Seyed Homayoon Sadraie 220
- **Front page of Cell Journal (Yakhteh): Figure 1, Page: 188**

FACT or PACT: A Comparison between Free-Acrylamide and Acrylamide-Based Passive Sodium Dodecyl Sulfate Tissue Clearing for whole Tissue Imaging

Huimei Wang, M.Sc.^{1#}, Arezoo Khoradmehr, M.Sc.^{2#}, Amin Tamadon, D.V.M., Ph.D.^{3*}

1. Department of Integrative Medicine and Neurobiology, School of Basic Medical Sciences, Institute of Acupuncture and Moxibustion, Fudan Institutes of Integrative Medicine, Fudan University, Shanghai, China
2. Research and Clinical Center for Infertility, Shahid Sadoughi University of Medical Sciences, Yazd, Iran
3. The Persian Gulf Marine Biotechnology Research Center, The Persian Gulf Biomedical Sciences Research Institute, Bushehr University of Medical Sciences, Bushehr, Iran

#The first two authors equally contributed to this work.

*Corresponding Address: P.O.Box: 7514763448, The Persian Gulf Marine Biotechnology Research Center, The Persian Gulf Biomedical Sciences Research Institute, Bushehr University of Medical Sciences, Bushehr, Iran
Email: amintamaddon@yahoo.com

Received: 21/April/2018, Accepted: 26/August/2018

Abstract

Major biological processes rely on the spatial organization of cells in complex, highly orchestrated three-dimensional (3D) tissues. Until the recent decade, most of information on spatial neural representation primarily came from microscopic imaging of "2D" (5-50 μm) tissue using traditional immunohistochemical techniques. However, serially sectioned and imaged tissue sections for tissue visualization can lead to unique non-linear deformations, which dramatically hinders scientists' insight into the structural organization of intact organs. An emerging technique known as CLARITY renders large-scale biological tissues transparent for 3D phenotype mapping and thereby, greatly facilitates structure-function relationships analyses. Since then, numerous modifications and improvements have been reported to push the boundaries of knowledge on tissue clearing techniques in research on assembled biological systems. This review aims to outline our current knowledge on next-generation protocols of fast free-of-acrylamide clearing tissue (FACT) and passive CLARITY (PACT). The most important question is what method we should select for tissue clearing, FACT or PACT. This review also highlights how FACT differs from PACT on spanning multiple dimensions of the workflow. We systematically compared a number of factors including hydrogel formation, clearing solution, and clearing temperatures between free-acrylamide and acrylamide-based passive sodium dodecyl sulfate (SDS) tissue clearing and discussed negative effects of polyacrylamide on clearing, staining, and imaging in detail. Such information may help to gain a perspective for interrogating neural circuits spatial interactions between molecules and cells and provide guidance for developing novel tissue clearing strategies to probe deeply into intact organ.

Keywords: Acrylamide, Imaging, Staining and Labeling, Three-Dimensional, Tissues

Cell Journal(yakhteh), Vol 21, No 2, July-September (Summer) 2019, Pages: 103-114

Citation: Wang H, Khoradmehr A, Tamadon A. FACT or PACT: a comparison between free-acrylamide and acrylamide-based passive sodium dodecyl sulfate tissue clearing for whole tissue imaging. Cell J. 2019; 21(2): 103-114. doi: 10.22074/cellj.2019.5989.

Introduction

Biological systems are capable of forming complex neuronal network of feedforward, feedback and horizontal circuits (1), the most prominent biological systems being the neural basis of spatial codes. Decades of research on the neurobiology of tissue imaging mainly focused on neuroanatomical structures by mechanical slicing procedures, which laid the foundations for understanding neural maps of 2D spatial representations. However, tissue opacity and light scattering greatly limit the tissue depth which can be sectioned optically. Furthermore, high-resolution reconstruction techniques for 3D image require sophisticated image computation, which are markedly labor-intensive and time-consuming. Moreover, although several novel brain imaging techniques including magnetic resonance imaging (MRI) (2), computed tomography (CT) (3, 4), positron emission tomography (PET) (5), confocal microscopy (6) and two-photon microscopy (7) have garnered considerable success owing to their higher attainable resolution and deeper penetration depths, high cytoarchitectural resolution and large-volume organ details still remain to be achieved.

An emerging theme is that many optical clearing techniques have been developed recently and refined continually. Of these approaches, benzyl alcohol and benzyl benzoate (BABB) are among the first to make fixed tissues as large as 2 cm^2 transparent for deep microscopic imaging (8), compared with 5-20 μm sections for conventional immunohistochemical techniques. The potential to analyze complex neural networks make tissue-clearing methods extremely intriguing for subcellular and cellular analyses of complex structures. Enormous advances have since been made for high-resolution and large-scale imaging of tissue clearing, including scale (9), dibenzyl ether (DBE) (10), 3D imaging of solvent-cleared organs (3DISCO) (11, 12), see deep brain (seeDB) (13), ClearT (14), clear unobstructed brain imaging cocktails (CUBIC) (15, 16), system-wide control of interaction time and kinetics of chemical (SWITCH) (17), and ultimate DISCO (uDISCO) (18). However, these protocols were still limited by fluorescence quenching of samples, incomplete clearing of specimens and not permitted antibody labelling, effectively. Attempts to

address these issues and refine conditions of tissue processing have provided initial stimulation for optical clearing techniques.

A cutting-edge technique (termed CLARITY) developed by Chung and Deisseroth (19), provided a new tissue-processing platform for elucidating the 3D cellular connectome and arrangement in toto. This rapidly organ-clearing method, which has been the most common classical method for studying intact-tissue imaging and can be applied for probing molecular and structural underpinnings of intact tissue, largely broke through the limitations of using tissue-specific or application-specific reagents as described in prior clearing protocols. Since then, extensive research is accumulating on redesigning or optimization of clearing steps and reagents based on clarity method, including passive CLARITY (20), passive CLARITY technique (PACT) (21), active clearing technique-pressure related efficient and stable transfer of macromolecules into organs (ACT-PRESTO) (22), free-of-acrylamide and sodium dodecyl sulfate (SDS)-based tissue clearing (FASTClear) (23), and fast free-of-acrylamide clearing tissue (FACT) (24).

Three clear contributions have been made via these techniques: stabilizing tissue structures using hydrogel embedding (19), use of fluorochrome signal-compatible clearing reagents (15) and large-scale and challenging tissue imaging improvement (25). Remarkably, of these approaches, application of the PACT and the FACT methods have been identified "effective" for their high-resolution and high-speed of clearing, simplicity, cost-effectiveness, until now (20, 24). Regarding the differences between the FACT and the PACT, the outstanding questions are: How does gel formation by acrylamide affect the preservation of protein of cell structure? What are the advantages and disadvantages of utilization of different concentrations of clearing solutions and different temperatures for solving acrylamide, for making tissues optically transparent? Another hallmark improvement in the FACT is removing polyacrylamide in its protocol; do the acrylamide and VA-044 initiator play redundant or parallel roles in the PACT, compared with paraformaldehyde used in the FACT? What are the negative effects of polyacrylamide? There are indeed some initial clues to address these questions regarding the characteristics of reconstructed 3D images of biological tissues in the FACT and the PACT protocols.

In this review, we summarize some important findings related to the FACT and the PACT for whole tissue imaging, with systematically comparing differences on recent published protocols between free-acrylamide method and PACT method for whole tissue imaging, including gel formation, clearing solution concentrations, clearing temperature, and negative effect of polyacrylamide. Before, it should be noted that this article discusses most of published

research and review articles comparing or introducing acrylamide-based methods together or with other methods of clearing. It means the newly developed method, the FACT, has not been compared with acrylamide-based clearing methods. Based on comprehensive comparisons between the two tissue clearing techniques, FACT and PACT, we propose that FACT method performs better in the whole clearing processing, which may give novel insights into mapping the architecture of neural circuits and developing new approaches for tissue visualization.

Overview of two tissue clearing processes used for three-dimensional imaging

CLARITY technique has gained considerable success owing to its potential for mapping detailed structural and molecular information of intact biological systems and is supported by extensive research data, the applications of hydrogel embedding and electrophoretic tissue clearing (ETC) are at the very heart of the CLARITY clearing procedures associated with tissue preservation and clearing efficiency, both of these two techniques have had broad impact on the rate of tissue clearing, and had been incorporated into the design, or redesign, continually.

Although active transport organ-electrophoresis approach which capitalizes on the highly charged nature of ionic micelles, can accelerate the lipid extraction by orders of magnitude, the payoffs of ETC are inevitable tissue degradation during sample heating and complexity to implement. Extending their prior work, Chung et al. (26) developed a novel approach (defined as passive CLARITY) (20) for intact tissues imaging without electrophoretic instrumentation, optimizing objectives and compatibility with light-sheet optics. Enormous studies have since done to understand the native biological molecules and fine structure underlying the passive CLARITY (Table 1).

Nevertheless, the main limitation of the slow rate of clearing makes the protocol impractical for scaling up, not to mention intact biological body mapping. On the basis of the passive CLARITY method, the concept of the PACT was first scientifically described by Yang et al. (21), when they presented a "passive tissue clearing and immunostaining" protocol for whole organisms with passive lipid extraction and proposed that such a method increased the speed of clearing, reduced tissue damage and promoted scalability. Furthermore, their work optimized reagents for the hydrogel embedding, clearing, and imaging, which provides important insights into how this technique is compatible with immunohistochemistry, endogenous-fluorescence. According to this modified passive CLARITY method, the PACT, corresponding successful applications have also been brought under the spotlight (Table 2). However, application of hydrogel caused tissue deformation in the clearing process, which results in adversely impacting the evaluation of fine cellular structures and long-term imaging.

Table 1: Successful applications of the passive CLARITY protocol for tissue clearing and three-dimensional imaging

Tissue/organ	Species	Hydrogel perfusion/ embedding	Clearing solution	Clearing time	RI* homogenization	References
Skeletal muscle (whole)	Mouse	+/+	4% SDS in boric acid (pH=8.5)	42 days (adult)	80% glycerol	(27)
Brain (whole)	Mouse	+/+	4% SDS in boric acid (pH=8.5)	21 days (adult)	FocusClear/85-87% glycerol	(20)
Brain (section)	Mouse	+/+	4% SDS in boric acid (pH=8.5)	7 days (adult)	PBST	(28)
Brain (whole)/lung (whole)/testis (whole)/kidney (whole)/intestine (whole)/spleen (whole)	Mouse	+/+	4% SDS in boric acid (pH=8.5)	30 days (adult)	FocusClear/80% glycerol	(29)
Brain (whole)/spinal cord (whole)	Mouse	+/+	4% SDS in boric acid (pH=8.5)	28-42 days (adult brain)/14-28 days (adult spinal cord)	TDE	(30)
Brain (whole)/spinal cord (whole)	Mouse	+/+	4% SDS in boric acid (pH=7.5)	36 days (adult brain)/21 days (adult spinal cord)	FocusClear	(31)
Brain (section)/spinal cord (section)	Mouse/rat	+/+	8% SDS in boric acid (pH=7.5)	4 days (adult mouse)/6 days (adult rat)	80% Glycerol/65% TDE	(32)
Brain (whole)	Rat	+/+	4% SDS in boric acid (pH=8.5)	28-56 days (adult)	RapiClear	(33)
Brain (section)	Rat	+/+	4% SDS in boric acid (pH=8.5)	6 days (age P0) to 20 days (age P24)	TDE	(34)
Brain (section)	Human	-/+	4% SDS in boric acid (pH=8.5)	14 days (adult)	ScaleA2 solution	(35)
Brain (whole)	Mouse/rat /human (section)	+/+	4% SDS in boric acid (pH=8.5)	21 days (adult mouse)/60 days (adult rat)/5-10 days (adult human)	87% glycerol/ScaleA2 solution	(36)
Cerebellum (whole)	Mouse/human (section)	-/+	4% SDS in boric acid (pH=8.5)	7 days (adult mouse)/>28 days (human adult)	RIMS+PBS+Tween-20	(37)
Spinal cord (whole)	Mouse	+/+	4% SDS in boric acid (pH=7.5)	14 days (adult)	CUBIC clearing solution	(38)
Whole body	Zebrafish	-/+	8% SDS in boric acid (pH=8.5)	5-7 days (adult)	RIMS	(39)
Fetus (whole)/brain (whole)/lung (whole)/heart (whole)/kidney (whole)/muscle [†] (whole)	Mouse	+/+	4% SDS in boric acid (pH=8.5)	3-10 days (fetus)/10 days (other tissues)	RIMS	(40)
Liver (section)	Mouse	+/+	4% SDS in boric acid (pH=8.5)	30 days (adult)	RIMS	(41)

Table 1: Continued

Tissue/organ	Species	Hydrogel perfusion/ embedding	Clearing solution	Clearing time	RI* homogenization	References
Retina	Rat	-/+	4% SDS	5 days	RIMS	(42)
Lung (whole)	Mouse	-/+	8% SDS in boric acid (pH=8.5)	ND	RIMS	(39)
Intestine (section)	Mouse/ human	+/+	4% SDS in boric acid (pH=8.5)	12-14 days (adult)	80% glycerol	(43)
Ovary (whole)	Mouse	+/+	4% SDS in boric acid (pH=8.5)	35 days (adult)	FocusClear	(44, 45)
Testis (whole)	Zebrafish	-/+	8% SDS in boric acid (pH=8.5)	13 days (adult)	RIMS	(46)
Stem-cell-derived cortical cultures	Mouse	ND	ND	ND	ND	(47)

RI; Refractive index, SDS; Sodium dodecyl sulfate, TDE; 2,20-thiodiethanol, RIMS; Refractive index matching solution, PBS; Phosphate-buffered saline, ND; No data, PBST; Phosphate-buffered saline+Triton X-100, and †; The passive CLARITY was performed on muscle until the clearing stage and without immunolabelling and imaging.

Table 2: Application of successful PACT for different tissue clearing and three-dimensional imaging

Tissue/organ	Species	Hydrogel perfusion/ embedding	Clearing solution	Clearing time	RI* homogenization	References
Brain (whole/section)/kidney (section)/heart (section)/lung (section)/intestine (section)/basal cell carcinoma (section)	Mouse/human	+/+	8% SDS in PBS (pH=7.5)	3-14 days (adult mouse brain)/ND (other tissues)	80% glycerol/ RIMS/ sRIMS	(21)
Fetus (whole)/brain (whole)/lung (whole)/heart (whole)/kidney (whole)/muscle† (whole)	Mouse	+/+	8% SDS in PBS (pH=7.5)	3-10 days (fetus)/25-30 days (other adult tissues)	RIMS	(40)
Brain (whole)/spinal cord (whole)/ lung (whole)/heart (whole)/liver (whole)/stomach (whole)/salivary gland (whole)/pancreas (whole)/ fetus (whole)/spleen (whole)/ parotid gland (whole)/genital organ (whole)/kidney (whole)/ bone (whole)	Mouse/Rat/ Guinea Pig	+/+	8% SDS in PBS (pH=7.5)	17-23 days (adult)	nRIMS	(48)
Brain (section)	Mouse	-/+	8% SDS in PBS (pH=7.6)	1-3 days (adult)	RIMS	(49)
Intestine (section)	Mouse/ human	+/+	8% SDS in PBS (pH=7.5)	12-14 days (adult)	80% glycerol	(43)
Mammary gland (whole)/ mammary tumor	Mouse	+/+	8% SDS in distilled water (pH=7.5)	4 days (adult)	sRIMS	(49)

RI; Refractive index, SDS; Sodium dodecyl sulfate, PBS; Phosphate buffer saline, PBST; Phosphate buffer saline+triton X100, RIMS; Refractive index matching solution, nRIMS; Nycodenz-based refractive index media solution, sRIMS; Sorbitol-based refractive index matching solution, TDE; 2,20-thiodiethanol, ND; No data, and †; The PACT is done on muscle until clearing stage and without immune-labeling and imaging.

Recently, an exciting new wave of improvements has emerged from free-of-acrylamide SDS-based tissue clearing (FASTClear), which greatly reduces the whole clearing time. Most notably, the replacement of acrylamide hydrogel by formaldehyde largely

avoids incomplete tissue hydrogel hybridization and fine cytostructure destruction in this protocol. However, the most prominent disadvantages of FASTClear is being limited by immunolabelling to the full thickness of tissue. Moreover, problems of tissue shrinkage and archival

formalin-fixed tissues clearing still exist. To challenge the above imperfections in 3D tissue imaging, simultaneously with FASTClear, the FACT (24) was introduced for tissue clearing and imaging pertaining to immunolabeled fluorescent or transgenic proteins by further merging and modifying the PACT (21) and the FASTClear (50) methods. In a compelling set of experiments, it has been demonstrated that the FACT further improves the speed of clearing, preservation of cytoarchitecture, depth of tissue penetration, long-term storage of fluorescent signal, the

signal to noise ratio by comprehensively comparing the FACT protocol with the FASTClear methods, the PACT, and the passive CLARITY, demonstrating the higher potential of the FACT for rapid and high-resolution imaging on 3D biological tissue applications. A variety of successful applications of free-acrylamide tissue clearing are listed in Table 3. To better understand the optical transparency process of FACT, FASTClear and PACT, passive CLARITY, a more systematical comparison of workflow with these protocols has been shown in Figure 1.

Table 3: Application of successful free-acrylamide tissue clearing for different tissue clearing and three-dimensional imaging

Tissue/organ	Species	Hydrogel perfusion/ embedding	Clearing solution	Clearing time	RI [†] homogenization	References
Brain (section)	Mouse	-/-	8% SDS in PBS (pH=7.5)	3 days	FocusClear	(24)
Brain (section)	Mouse/human	-/-	4% SDS in sodium borate buffer	40 days (human)/ND (other tissues)	Histodenz-RIMS (mouse) 47% 2,2'-Thidiethanol in 10 mM phosphate buffer (human)/ND (other tissues)	(52)
Brain (section)	Human	-/-	4% SDS in sodium borate buffer	Minimum of 5 days	FASTClear	(51)
Heart (section)	Dog/human	-/-	4% SDS buffer	4 day	FASTClear	(23)

RI; Refractive index, SDS; Sodium dodecyl sulfate, PBS; Phosphate buffer saline, RIMS; Refractive index matching solution, and ND; No data.

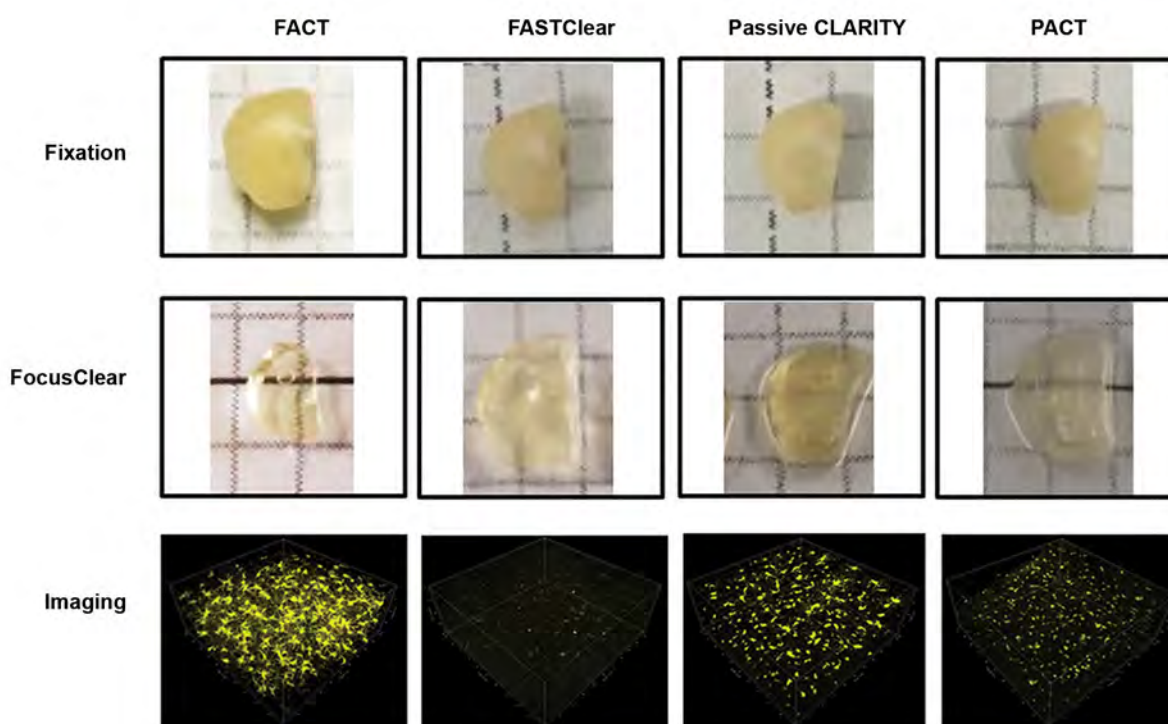


Fig.1: Whole-brain transparency comparison and representative fluorescence images of microglia obtained using different techniques. Images were adapted with permission (24).

Role of gel formation by acrylamide and protein of cell structure

Increase of our knowledge on gel formation that preserves proteins of cytoarchitecture but may conversely influence tissue expansion by clear solution, depth of antibody or light penetration in tissue, and speed of lipid removal is crucial. The hydrogel-embedding clearing protocols, including active CLARITY, passive CLARITY, PACT and so on, were developed based on polymerizing the fixed tissue into an acrylamide hydrogel prior to the process of lipid-removal. This hypothesis of hydrogel embedding provides a beautiful and simple account for how the use of hydrogel may provide physical framework for the cleared tissues and act as an impediment allowing for deep penetration of the antibodies into the tissue (30). It stems from one of the most influential reasoning that delipidation removes lipid bilayers which are essential for cellular integrity. Therefore, these formaldehyde-modified amines may crosslink proteins to acrylamide via nucleophilic addition reactions. Through this process, the acrylamide attached will be polymerized and form physical support to prevent excessive protein loss from samples in the steps of SDS delipidation, conversely, lipids and other biomolecules will be washed off due to the absence of the amine grouping (26). These features make hydrogel an extremely attractive crosslink substrate for maintaining cellular and molecular integrity of tissues thus they are vastly applied in researches on imaging of 3D tissues. Complications arisen in the past years, opened this hypothesis to debate (23, 24, 50, 51).

Interestingly, a more careful examination of different polyacrylamide concentrations in modified CLARITY protocol, found that the retention of RNA and penetration of antibodies improved with reducing acrylamide hydrogel composition from 4 to 1% (53). Furthermore, evidence began to mount that removing hydrogel from steps of perfusion and embedding can increase the amount, speed, and penetration depth of antibodies. Comparing the effects of samples morphologies between acrylamide-free and acrylamide-embedded tissues, which is consistent with the notion of reducing polyacrylamide concentration, revealed that using formaldehyde fixation singly could replace the acrylamide embedding of tissues for the steps of SDS-mediated delipidation and tissue clearing without affecting the tissue physical structure for high-resolution 3D histological analysis (52). Moreover, a series of problems using acrylamide hydrogel has also been brought under the spotlight. Tissues undergo expansion in the processing of polyacrylamide by SDS clearing and lose structural integrity as well (21, 36). Moreover, uncompleted hydrogel hybridization will block diffusion of hydrogel monomers when transcordial perfusion cannot be performed (17). On the basis of these observations, FASTClear protocol has been proposed for 3D visualization, and this technique has been successfully applied for human brain tissues (50) and myocardial tissue (23), so far. As reflected by a multitude of expounded theories, these modifications are SDS-based, avoid the

use of acrylamide during gel formation, which are vastly simplified and more user-friendly, and range from overall processing time to immunostaining and visualization, leading to optimal tissue transparency conditions.

Simultaneous with the FASTClear, the FACT was developed (24) for further optimizing tissue clearing protocols for moving deep into fine cytoarchitectural details of brain cells in both genetically and chemically labelled tissues. Xu et al. (24) provided a systematic comparison between hydrogel-based and free-acrylamide clearing methods, which, for the first time, revealed that PFA-based FACT techniques can clear tissue faster. As it is shown in Figure 2, principles of PFA-based FACT methods may brought new insights into how different PFA serve to make strong chemical bonds with the cytoskeleton between proteins, which may challenge the classical theories that polyacrylamide serves to build cross-links between formaldehyde and hydrogel for assisting fixation of nucleic acids and protein upon the process of delipidation (54).

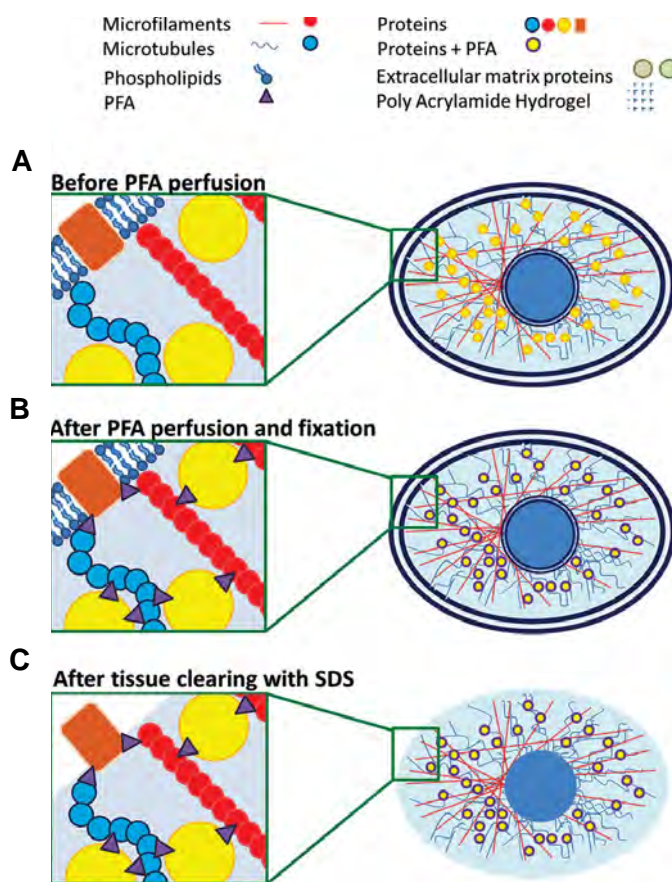


Fig.2: Mechanisms underlying the efficiency of the Fast Free-of-Acrylamide Clearing Tissue (FACT) protocol. **A, B.** During the paraformaldehyde (PFA)-mediated tissue fixation in the FACT protocol, membrane and intracellular cytoplasmic proteins (including the transgenic fluorescent proteins) make chemical bonds with the cytoskeleton, including microfilaments and microtubules, and/or with the extracellular matrix, including proteoglycans. These bonds help to construct a massive 3D matrix that provides structural support and essential tensile strength to the tissue during processing, and **C.** After removing the cell walls by 8% sodium dodecyl sulfate (SDS) in pH=7.5 (optimum pH for preserving normal protein structures), the tissue scaffold is chemically bonded by PFA. Images were adapted with permission (24).

One plausible explanation for PFA connection with peptides which is consistent with most of these data, is that aldehyde plays a crucial role in reaction with nitrogen or other atoms within proteins and peptides and therefore, creates a methylene bridge made of a $-CH_2-$ cross link (Fig.3). The majority of proteins are located in fixed places by these connections, which may form a large-scale 3D network. These kinds of bonds therefore provide essential tensile strength and structural rigidity of tissue upon harsh conditions. Most notably, although it has been reported that pores in polyacrylamide matrices motivate lipid exchange (21), no significant differences were observed in protein retention among these protocols. In a compelling set of experiments, a variety of related indicators, such as tissue weight, weight change ratio, the area change ratio were comprehensively measured in their experiments (24). There is considerable discrepancy between this discovery and prior works as significantly lower protein loss was observed in acrylamide-embedded tissues upon the SDS delipidation step compared to non-hybridized tissues (26, 54). Expanding on this, given that not all proteins can be trapped in the extracellular matrix or intracellular space, such as cytoplasmic membrane or extracellular proteins, protein loss to some degree, cannot be avoided in all protocols, so far. Further experiments are needed to explore the potential possibility of having better protein preservation. Furthermore, based on our knowledge, there is no experiment defining the type of proteins removed during the clearing process.

Different concentrations for different purposes (RNA and protein)

The optimal methods for 3D tissue mapping depend

on a set of processing factors that include selection of appropriate ingredients, optimization of pH, suitable incubation temperatures, thickness of sample, and perhaps also effort-based manipulation proficiency. For lipid removal, the clear solution composition at certain pH and solution concentration, could contribute to the speed of diffusion of detergent micelles and the rate of lipid solvation by detergent micelles in tissues (55). Each of several candidate detergents introduced during the past several years, either quenched native fluorescence (15, 55) or compromised tissue structure (9), opening these reagents to reexamination and debate (56). Useful operational comparisons were made by Yang et al. (21) in their PACT protocol. They tested various detergents at different concentrations for validity undergoing passively clearing brain tissue and revealed that SDS at all concentrations showed a superior effect for lipid solvation and delipidation as compared to other detergents. In traditional immunohistochemistry, SDS is proposed for protein denaturation for antigen retrieval. Delipidation properties of SDS have been also heavily implicated in tissue clearing in current years (20, 27, 34). Another intriguing discovery in their work is uniform clearing of the whole tissue only at 8% SDS concentration with less protein loss. Moreover, PACT studies also revealed that 8% SDS acts faster than 4% SDS in passive CLARITY technique. These features make SDS an extremely attractive reagent for tissue delipidation. Through this process, 8% SDS concentration is proposed for tissue clearing step in processing different samples for general applications.

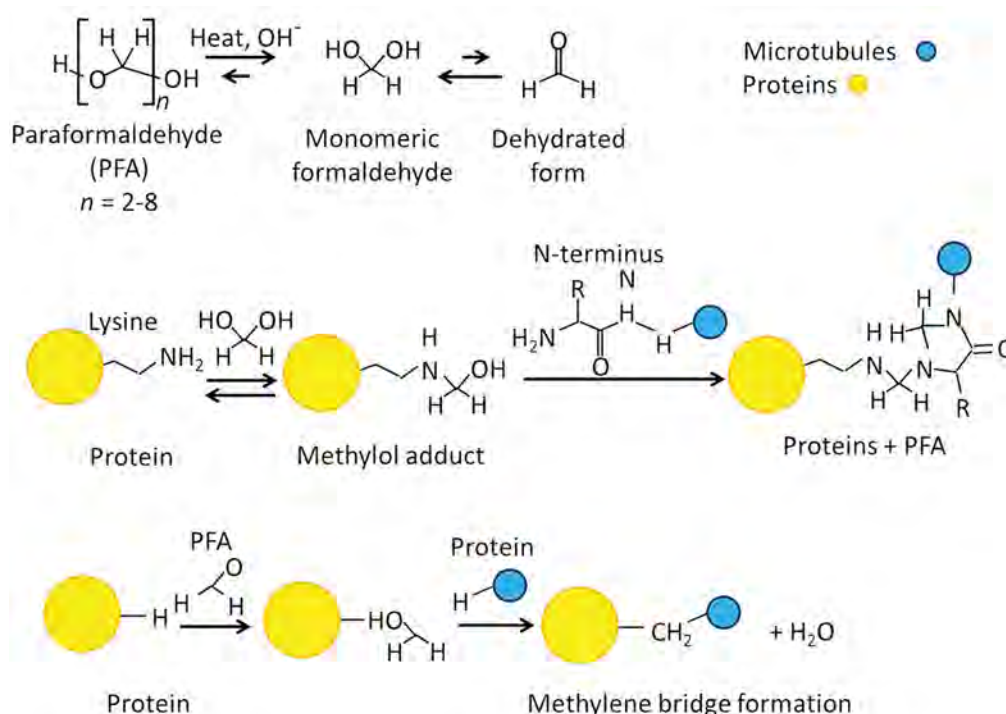


Fig.3: Chemical mechanisms through which paraformaldehyde crosslinks proteins. Images were adapted with permission (24).

Early recordings revealed that the presence of free radicals which is associated with pH value of solution used in the tissue clearing process, closely affect the clearing speed (20, 21, 57-59), presumably reflecting that considerable heterogeneity of pH produces various effects during tissue clearing process. Some of these studies adopted the modifications of the clear solution with the inclusion of boric acid and a basic pH=8.5 for increasing clearing speed, which also increases protein loss at the same time. It can provide one reasonable explanation consistent with frequent observation of fluorescent bleaching in both hydrogel-based and PFA-based protocols, which used clearing solution of pH=8.5 in clearing step. However, by adjusting the clearing solution pH to 7.5, quenching of fluorescent transgenic labels was decreased (24), suggesting that pH=7.5 can optimize the effects of tissue clearing. Consistent with these correlative studies, further optimized preservation of fluorescent signal for tissue clearing was provided by adjusting pH at 7.5 and SDS solution concentration at 8% (24) specially for transgene labelled tissue.

Different temperatures for removing polyacrylamide side effects

Recent studies have also revealed that temperature is also one of the most sensitive factors during clearing incubation process to preserve the fluorescent signal. Exposure to high temperatures can accelerate delipidation of tissue; however, 50°C adopted in FASTClear method (50) was shown to induce yellowness or even burn or melt of the tissues reported in some protocols (20), resulting in increased tissue expansion, increased protein loss, and decreased imaging depth of endogenous fluorescent signals. In the FACT protocol (24), it was proven that a temperature of 37°C is crucial in non-acrylamide based protocol. Keeping pH at 7.5, temperature at 37°C and SDS concentration at 8% can reduce bleaching of transgene fluorescent signals and also remove lipids in a logic time period. All these modifications increased the quality of 3D tissue imaging in comparison with other methods (24). Temperatures >37°C in non-acrylamide-based protocols, despite increasing fluorescent signals bleaching, can increase tissue size and also increase protein loss such as observed in FASTClear.

Negative effect of polyacrylamide on clearing (speed, protein loss, and tissue character)

The limitations of hydrogel crosslinking have substantial effects on the clearing process, including clearing speed, protein preservation, tissue character, which are thought to contribute to the index of clearing quality. The slow clearing speed using polyacrylamide has been brought under the spotlight. Theoretical basis of the FASTClear (50) postulates that the functions of polyacrylamide hydrogel in the intracellular and intercellular spaces, are not necessary to support sample spatial structure (19), but to impede clearing speed of removing of lipids by SDS.

Moreover, tissue transparency techniques are much more diverse than originally thought, ranging from not only tissue with transcordial perfusion but also tissues that cannot be perfused. However, a large block of tissue could be limited by diffusion of hydrogel monomers which results in incomplete tissue hydrogel hybridization when samples are not suitable for transcordial perfusion (17). On the contrary, omission of polyacrylamide hydrogel from the process of tissue fixation facilitated lipid removal both in SDS 4% at 37% and the FACT protocols (24). Thus, as long as the tissue is well fixed in formaldehyde, free-of-acrylamide protocol is recommended to increase the speed of the tissue-clearing procedure.

Preservation of structural integrity is the most prominent factor of 3D tissue imaging, which is thought to provide an intuitive and detailed picture of how neural circuits and other connectomics work. Polyacrylamide was once considered to chemically incorporate native biomolecules into the hydrogel mesh, however, investigation of the necessity of hydrogel involvement has just started. Although, analysis based on daily measurement of tissue weight (served as an indicator of tissue and water absorption) and tissue size (served as an indicator of tissue size change) area revealed increased daily protein loss by removal of hydrogel from brain fixation comparing with the PACT and passive Clarity approaches. Intriguingly, the total protein losses showed no significant differences among hydrogel-based and FACT groups (24). This discrepancy could potentially be explained as follows: increased tissue clearing speed in FACT protocols decreased the days of protein loss and therefore caused minor lesion to protein preservation, comparing with hydrogel-embedded protocols with the lowest speed of tissue clearing.

Furthermore, the field has begun to appreciate that acrylamide-embedded tissues during SDS clearing undergo expansion and become more fragile because of loss of structural integrity (17, 36). Consistent with this hypothesis, extreme expansion and irreversible contraction of hydrogel are even more evident when absorbed water is removed from swelled tissue by FocusClear in hydrogel-embedded methods, inducing changes of cellular microstructures, such as microglia branches (17). However, the free-of-acrylamide protocols (24, 50) revealed that the omission of hydrogel from clearing procedure but relying on the structural support of cytoskeleton (lower water absorbance), can prevent deformities from polyacrylamide hydrogel expansion.

Therefore, PFA-based tissue clearing protocols can achieve a rapid clearing without influencing total protein loss and tissue area under specific conditions, comparing with hydrogel-based protocols. However, given that some degree of protein loss is inevitable in all protocols, and given the potential of more or less deformation of samples during lipid removing process occur no matter it is in PACT or FACT approaches. More effort should be made to further preserve more tissue structure details upon tissue transparency.

Negative effects of polyacrylamide on staining (need specific antibody, non-specific staining, antibody penetration, and time consuming)

A variety of unfavorable factors of polyacrylamide, such as specific antibody, non-specific staining, low antibody penetration, and being time consuming on staining, made it heavily implicated. According to hydrogel-based hypothesis, pores of polyacrylamide matrices assist lipid exchange and therefore enhance antibody penetration by changing hydrogel composition (21). This hypothesis has a major impact on providing conditions of antibody labelling of tissue, and application of transgenic labels in animal models. However, compared with protocols which are hybridized with hydrogel and PFA, it appeared that the immunolabelled tissues showed higher quality than transgene labelled ones (54). This discovery prompted the hypothesis of hydrogel crosslinking to proteins or network trapping of cellular proteins and therefore provided the possibility of trapping antibodies in immunohistochemical steps. Consistent with this hypothesis, background staining appear to increase after tissue washing, because antibodies are deeply trapped within tissue or they non-specifically bind primary or secondary antibodies. A possible explanation is that the low porosity of hydrogel contributes to non-specific accumulation of antibodies in dense tissues, which elicits non-specific labelling, as reflected by staining of striosomes in passive CLARITY technique (24, 60). On the contrary, absence of hydrogel in the FACT approach reduces these lesions during staining process. These observations are consistent with the discovery of FACT that the process of free-of-polyacrylamide fixation and perfusion accelerate the immunostaining time of tissue and increase the depth of antibody penetration (24), which provide the possibility for better staining of full-thickness tissues.

Negative effects of polyacrylamide on imaging (depth and light scattering)

Polyacrylamide hydrogel application in imaging are also subjected to modifications such as alteration of depth of penetration and light scattering, to increase background during imaging. Tissues are opaque for conventional light microscopy, mainly owing to their lipids, induce light scattering (15, 19) which occurs to materials with different refractive indices (RIs). The development of the tissue transparency technique stems from the theoretical principle that minimizing the light scattered by an object to achieve transparency. Lipids are the major source of light scattering in fixed brain, therefore, removing lipids or/and adjustment of the discrepancy of the RI between the surrounding areas and lipids, are potential approaches to increase sample transparency. Importantly, both transparency and integrity play a crucial role in achieving a high quality 3D imaging.

As mentioned above, hydrogel polymerization can be considered for the expansion and fragility of tissue during the imaging procedure. Deformation of tissue disrupts the evaluation of fine structures such as neuronal

processes and microglia. In addition, lesions to tissue swelling is irreversible, a major adverse event for 3D tissue imaging quality, which RI cannot be corrected by using FocusClear. Abnormalities in tissue processing caused by polyacrylamide, heavily influence fluorescent signal intensity, antibody penetration depth as well as light scattering. In contrast, the absence of hydrogel in the FACT method circumvents these limitations and optimizes the preservation of antigenicity (24). Moreover, compared with other tissue clearing protocols (passive Clarity, PACT, and FASTClear), the FACT, which is based on optimizing all conditions in the whole procedure, is the most effective protocol in imaging procedure with the strongest signal detecting the depth of 300-700 μm .

Price, environmental concerns, and complications

Aided by merging and adjusting the FASTClear and PACT methods, Xu et al. (24) effectively simplified the tissue clearing protocol by removing acrylamide and VA-044 initiator used during tissue clearing process and avoiding the steps of degassing tubes with hydrogel solution, which has provided the most cost-effective and simplest protocol of 3D tissue imaging with maximal preservation of fluorophore signal, decreasing protein loss, and offering high speed clearing. Importantly, not using poisonous acrylamide for the polymerization of hydrogel largely provided the researchers with environment-friendly and less-toxic experiments. Furthermore, 3 to 5 times faster clearing of brain tissue by the FACT compared to PACT reduces SDS content in clearing solution. Moreover, all reagents and solvents provided in FACT protocols are easily accessible in most laboratories. In addition, by deleting excess gel removing step in the FACT protocol in comparison with the PACT after gel formation, the fragile tissues such as fat tissue can be cleared and imaged by the FACT method. Being more accurate and simple, but less toxic, less laborious, and less time-consuming, contributed to the optimization of FACT protocol with respect to price, environmental concerns and complications.

Concluding remarks and future perspectives

We have witnessed tremendous progress in refining clearing methods introduced for identifying complex cytoarchitecture and mapping neural circuitry, involved in simplified protocols, higher quality and speed of data generation, safety and economical materials and reagents application. Notably, the PACT and the FACT methods have recently attracted considerable attention as they could optimize the clearing time, temperature, and reagents and preserve the fluorochrome signal. Notably, the FACT technique which has been developed by merging and modifying the FASTClear and PACT methods, including avoiding hydrogel perfusion and embedding, decreasing the temperature to 37°C, adjusting the clear solution pH to 7.5, has been identified with reinforcing properties compared with PACT for mapping detailed structures such as neuronal processes and branches. As FACT facilitates the whole workflow of tissue clearing including clearing time saving, fluorescent signals preservation, cytoarchitectural retention, confocal microscopy optimization, data collection

acceleration, the distribution of such a 3D tissue map provides a more intuitive brain tissue picture of how connections of large populations of cells and their networks and how physiological and pathological conditions lead to changes in expression of corresponding proteins and molecules. The FACT protocol suggests optimized conditions of rapid high-resolution imaging for brain tissue, which has made a big step over the PACT protocol. In the following, we highlight several frontiers which should be addressed by further investigations to deepen our understanding of the FACT.

To test the validity and versatility of the FACT in 3D tissue imaging, a compelling set of experiments with tissue-type specificity and temporal precision recordings, remains warranted. Recently, a series of other tissue clearing methods has strongly established the visualization efficiency of various tissues including the spinal cord (61), whole embryo (62), bone (63), thymus, testis (22), pancreas, kidney, liver, intestine, lung (64), muscle (27), stomach, vasculature (65) and so on in different species including zebra fish (66, 39), mouse (10), rats (67), dogs (23), marmoset (15), and humans (21) in three dimensions. The FACT protocol has been tested on mouse, rat (68) and partridge (69) tissues for clearing various tissues of these species; nevertheless, reexamination of the proofs of necessity is still needed.

Although some articles have been recently done using FACT protocol (68, 69); but it remains to be reexamined whether the FACT can be applied to general use other than brain tissue and whether tissue specificity affects tissue process and image quality. Furthermore, to specifically dissect the adaptability of the FACT protocol in large volume tissue imaging, it is necessary to resolve whether thick hard tissues -even whole body tissues- would abolish the advantages of the FACT in imaging quality of 3D tissue compared with other tissue clearing protocols. The FACT have been successfully applied for whole imaging, while only 1-mm-thick brain cortex slices handled with FACT method were reported for testing this property so far (24). The lack of such studies is perhaps owing to the difficulties in achieving a complete image of intact biological tissue due to the limitation of confocal microscope in a spatially and temporally precise manner.

A potential problem of using scanning microscopes is that low scanning speeds make them impractical for imaging large fields of samples, resulting in light fall-off, lens distortions, potential micro movements of the tissues inside the chamber (70). The molecular-structural evaluation of intact tissues therefore may not be precisely mapped using this kind of objective with high power but low working distance. Application of appropriate imaging setup, such as light sheet microscopy, can partly overcome this problem by enhancing optical penetration depth and accelerating data collection. Light-sheet microscopy, which selectively confines the illumination to the interest layer to achieve optical sectioning, are powerful, efficient and empirical methods used for reducing sample bleaching, large fields of view, high acquisition speed, and

high dynamic range, compared with common classical method point-scanning microscopy (confocal or two-photon). For this, it will be helpful to image large volumes of tissue samples with the FACT approach.

Conclusion

It would be an effective and reliable tool to simultaneously map subcellular molecular architecture between neighboring or distant cells of various organs, such as the brain and stomach, using multiple fluorophore signal in the same biological samples to examine how feedback loops and neuronal circuits works among central and peripheral system. Moreover, based on molecular-level and projection-based neural circuit tracing, it would be especially useful to comprehensively explore pathological and physiological conditions by comparing the functionality of protein and cell population. The advantages of the FACT protocol, such as maximal preservation of fluorophore signal hold promise for classifying and sub-classifying cytoarchitectures, and for molecular localization and projection in other projects.

Authors' Contributions

A.T., H.W., A.K.; Contributed to conception and design, reviewed the literature for the manuscript. H.W., A.K.; Made substantial contribution to the discussions, wrote, and reviewed. A.T.; Edited and finalized the manuscript before submission, were responsible for overall supervision. All authors read and approved the final manuscript.

Acknowledgments

This study was financially supported by The Persian Gulf Marine Biotechnology Research Center, The Persian Gulf Biomedical Sciences Research Institute, Bushehr University of Medical Sciences, Bushehr, Iran. There is no conflict of interest in this study.

References

1. Angelucci A, Bijanzadeh M, Nurminen L, Federer F, Merlin S, Bressloff PC. Circuits and Mechanisms for Surround Modulation in Visual Cortex. *Annu Rev Neurosci*. 2017; 40: 425-451.
2. Taghizadeh Asl M, Nematı R, Chabi N, Salimipour H, Nabipour I, Assadi M. Brain perfusion imaging with voxel-based analysis in secondary progressive multiple sclerosis patients with a moderate to severe stage of disease: a boon for the workforce. *BMC Neurol*. 2016; 16: 79.
3. Taghizadeh Asl M, Nematı R, Yousefi F, Salimipour H, Nabipour I, Assadi M. A pictorial essay on brain perfusion SPECT in various neuro-psychiatric disorders and intoxication: though practical, it is not very commonly used. *Iran J Nucl Med*. 2017; 25 Suppl 1: 1-14.
4. Assadi M, Salimipour H, Seyedabadi M, Saberifard J, Javadi H, Nabipour I, et al. Brain single photon emission computed tomography with Tc-99m MIBI or Tc-99m ECD in comparison to MRI in multiple sclerosis. *Clin Nucl Med*. 2010; 35(9): 682-686.
5. Karnabi E. Positron emission tomography. In: Hendel RC, Kimmelsstiel C, editors. *Cardiology procedures: a clinical primer*. London: Springer-Verlag; 2017; 81-90.
6. Hasaballa Al, Sands G, Wilson A, Young A, Wang Y, LeGrice I, et al. Three-dimensional quantification of myocardial collagen morphology from confocal images. In Pop M, Wright G, editors. *Functional Imaging and Modelling of the Heart: 9th International Conference, FIMH 2017*. Toronto: Springer; 2017; 3-12.

7. Bijeesh MM, Shakhi PK, Arunkarthick S, Varier GK, Nandakumar P. Confocal imaging of single BaTiO₃ nanoparticles by two-photon photothermal microscopy. *Sci Rep.* 2017; 7(1): 1643.
8. Dodt HU, Leischner U, Schierloh A, Jährling N, Mauch CP, Deininger K, et al. Ultramicroscopy: three-dimensional visualization of neuronal networks in the whole mouse brain. *Nat Methods.* 2007; 4(4): 331-336.
9. Hama H, Kurokawa H, Kawano H, Ando R, Shimogori T, Noda H, et al. Scale: a chemical approach for fluorescence imaging and reconstruction of transparent mouse brain. *Nat Neurosci.* 2011; 14(11): 1481-1488.
10. Becker K, Jährling N, Saghafi S, Weiler R, Dodt HU. Chemical clearing and dehydration of GFP expressing mouse brains. *PLoS One.* 2012; 7(3): e33916.
11. Ertürk A, Becker K, Jährling N, Mauch CP, Hojer CD, Egen JG, et al. Three-dimensional imaging of solvent-cleared organs using 3DISCO. *Nat Protoc.* 2012; 7(11): 1983-1995.
12. Ertürk A, Bradke F. High-resolution imaging of entire organs by 3-dimensional imaging of solvent cleared organs (3DISCO). *Exp Neurol.* 2013; 242: 57-64.
13. Ke MT, Fujimoto S, Imai T. SeeDB: a simple and morphology-preserving optical clearing agent for neuronal circuit reconstruction. *Nat Neurosci.* 2013; 16(8): 1154-1161.
14. Kuwajima T, Sitko AA, Bhansali P, Jurgens C, Guido W, Mason C. ClearT: a detergent-and solvent-free clearing method for neuronal and non-neuronal tissue. *Development.* 2013; 140(6): 1364-1368.
15. Susaki EA, Tainaka K, Perrin D, Kishino F, Tawara T, Watanabe TM, et al. Whole-brain imaging with single-cell resolution using chemical cocktails and computational analysis. *Cell.* 2014; 157(3): 726-739.
16. Tainaka K, Kubota SI, Suyama TQ, Susaki EA, Perrin D, Ukai-Tadenuma M, et al. Whole-body imaging with single-cell resolution by tissue decolorization. *Cell.* 2014; 159(4): 911-924.
17. Murray E, Cho JH, Goodwin D, Ku T, Swaney J, Kim SY, et al. Simple, scalable proteomic imaging for high-dimensional profiling of intact systems. *Cell.* 2015; 163(6): 1500-1514.
18. Pan C, Cai R, Quacquarelli FP, Ghasemigharagoz A, Loubopoulos A, Matryba P, et al. Shrinkage-mediated imaging of entire organs and organisms using uDISCO. *Nat Methods.* 2016; 13(10): 859-867.
19. Chung K, Deisseroth K. CLARITY for mapping the nervous system. *Nat Methods.* 2013; 10(6): 508-513.
20. Tomer R, Ye L, Hsueh B, Deisseroth K. Advanced CLARITY for rapid and high-resolution imaging of intact tissues. *Nat Protoc.* 2014; 9(7): 1682-1697.
21. Yang B, Treweek JB, Kulkarni RP, Deverman BE, Chen CK, Lubeck E, et al. Single-cell phenotyping within transparent intact tissue through whole-body clearing. *Cell.* 2014; 158(4): 945-958.
22. Lee E, Choi J, Jo Y, Kim JY, Jang YJ, Lee HM, et al. ACT-PRESTO: Rapid and consistent tissue clearing and labeling method for 3-dimensional (3D) imaging. *Sci Rep.* 2016; 6: 18631.
23. Perbellini F, Liu AKL, Watson SA, Bardi I, Rothery SM, Terracciano CM. Free-of-Acrylamide SDS-based Tissue Clearing (FASTClear) for three dimensional visualization of myocardial tissue. *Sci Rep.* 2017; 7(1): 5188.
24. Xu N, Tamadon A, Liu Y, Ma T, Leak RK, Chen J, et al. Fast free-of-acrylamide clearing tissue (FACT)-an optimized new protocol for rapid, high-resolution imaging of three-dimensional brain tissue. *Sci Rep.* 2017; 7(1): 9895.
25. Becker K, Jährling N, Saghafi S, Dodt HU. Ultramicroscopy: light-sheet-based microscopy for imaging centimeter-sized objects with micrometer resolution. *Cold Spring Harb Protoc.* 2013; 2013(8): 704-713.
26. Chung K, Wallace J, Kim SY, Kalyanasundaram S, Andalman AS, Davidson TJ, et al. Structural and molecular interrogation of intact biological systems. *Nature.* 2013; 497(7449): 332-337.
27. Zhang WL, Liu SH, Zhang WC, Hu W, Jiang M, Tamadon A, et al. Skeletal muscle CLARITY: A preliminary study of imaging the three-dimensional architecture of blood vessels and neurons. *Cell J.* 2018; 20(2): 132-137.
28. Poguzhelskaya E, Artamonov D, Bolshakova A, Vlasova O, Bezprozvanny I. Simplified method to perform CLARITY imaging. *Mol Neurodegener.* 2014; 9: 19.
29. Epp JR, Niibori Y, Liz Hsiang HL, Mercado V, Deisseroth K, Josselyn SA, et al. Optimization of CLARITY for clearing whole-brain and other intact organs. *eNeuro.* 2015; 2(3). pii: ENEURO.0022-15.2015.
30. Roberts DG, Johnsonbaugh HB, Spence RD, MacKenzie-Graham A. Optical clearing of the mouse central nervous system using passive CLARITY. *J Vis Exp.* 2016; (112).
31. Spence RD, Kurth F, Itoh N, Mongerson CR, Wailes SH, Peng MS, et al. Bringing CLARITY to gray matter atrophy. *Neuroimage.* 2014; 101: 625-632.
32. Jensen KH, Berg RW. CLARITY-compatible lipophilic dyes for electrode marking and neuronal tracing. *Sci Rep.* 2016; 6: 32674.
33. Stefaniuk M, Gualda EJ, Pawlowska M, Legutko D, Matryba P, Koza P, et al. Light-sheet microscopy imaging of a whole cleared rat brain with Thy1-GFP transgene. *Sci Rep.* 2016; 6: 28209.
34. Zheng H, Rinaman L. Simplified CLARITY for visualizing immunofluorescence labeling in the developing rat brain. *Brain Struct Funct.* 2016; 221(4): 2375-2383.
35. Ando K, Laborde Q, Lazar A, Godefroy D, Youssef I, Amar M, et al. Inside Alzheimer brain with CLARITY: senile plaques, neurofibrillary tangles and axons in 3-D. *Acta Neuropathol.* 2014; 128(3): 457-459.
36. Liu AK, Hurry ME, Ng OT, DeFelice J, Lai HM, Pearce RK, et al. Bringing CLARITY to the human brain: visualization of Lewy pathology in three dimensions. *Neuropathol Appl Neurobiol.* 2016; 42(6): 573-587.
37. Phillips J, Laude A, Lightowers R, Morris CM, Turnbull DM, Lax NZ. Development of passive CLARITY and immunofluorescent labelling of multiple proteins in human cerebellum: understanding mechanisms of neurodegeneration in mitochondrial disease. *Sci Rep.* 2016; 6: 26013.
38. Liang H, Schofield E, Paxinos G. Imaging serotonergic fibers in the mouse spinal cord using the CLARITY/CUBIC technique. *J Vis Exp.* 2016; (108): 53673.
39. Cronan MR, Rosenberg AF, Oehlers SH, Saelens JW, Sisk DM, Jurcic Smith KL, et al. CLARITY and PACT-based imaging of adult zebrafish and mouse for whole-animal analysis of infections. *Dis Model Mech.* 2015; 8(12): 1643-1650.
40. Orlich M, Kiefer F. A qualitative comparison of ten tissue clearing techniques. *Histol Histopathol.* 2018; 33(2): 181-199.
41. Sindhwani S, Syed AM, Wilhelm S, Chan WC. Exploring passive clearing for 3D optical imaging of nanoparticles in intact tissues. *Bioconjug Chem.* 2017; 28(1): 253-259.
42. Singh JN, Nowlin TM, Seedorf GJ, Abman SH, Shepherd DP. Quantifying three-dimensional rodent retina vascular development using optical tissue clearing and light-sheet microscopy. *J Biomed Opt.* 2017; 22(7): 76011.
43. Neckel PH, Mattheus U, Hirt B, Just L, Mack AF. Large-scale tissue clearing (PACT): technical evaluation and new perspectives in immunofluorescence, histology, and ultrastructure. *Sci Rep.* 2016; 6: 34331.
44. Hu W, Tamadon A, Hsueh AJW, Feng Y. Three-dimensional reconstruction of vascular architectures of passive CLARITY-cleared mouse ovary. *J Vis Exp.* 2017; (130).
45. Frétaud M, Rivière L, Job É, Gay S, Lareyre JJ, Joly JS, et al. High-resolution 3D imaging of whole organ after clearing: taking a new look at the zebrafish testis. *Sci Rep.* 2017; 7: 43012.
46. Moore S, Evans LD, Andersson T, Portelius E, Smith J, Dias TB, et al. APP metabolism regulates tau proteostasis in human cerebral cortex neurons. *Cell Rep.* 2015; 11(5): 689-696.
47. Woo J, Lee M, Seo JM, Park HS, Cho YE. Optimization of the optical transparency of rodent tissues by modified PACT-based passive clearing. *Exp Mol Med.* 2016; 48(12): e274.
48. Shah S, Lubeck E, Schwarzkopf M, He TF, Greenbaum A, Sohn CH, et al. Single-molecule RNA detection at depth by hybridization chain reaction and tissue hydrogel embedding and clearing. *Development.* 2016; 143(15): 2862-2867.
49. Lloyd-Lewis B, Davis FM, Harris OB, Hitchcock JR, Lourenco FC, Pasche M, et al. Imaging the mammary gland and mammary tumours in 3D: optical tissue clearing and immunofluorescence methods. *Breast Cancer Res.* 2016; 18(1): 127.
50. Richardson DS, Lichtman JW. SnapShot: tissue clearing. *Cell.* 2017; 171(2): 496. e1.
51. Liu AKL, Lai HM, Chang RC, Gentleman SM. Free of acrylamide sodium dodecyl sulphate (SDS)-based tissue clearing (FAST-Clear): a novel protocol of tissue clearing for three-dimensional visualization of human brain tissues. *Sci Rep.* 2017; 43(4): 346-351.
52. Lai HM, Liu AK, Ng WL, DeFelice J, Lee WS, Li H, et al. Rationalisation and validation of an acrylamide-free procedure in three-dimensional histological imaging. *PLoS One.* 2016; 11(6): e0158628.
53. Sylwestrak EL, Rajasethupathy P, Wright MA, Jaffe A, Deisseroth K. Multiplexed Intact-Tissue Transcriptional Analysis at Cellular Resolution. *Cell.* 2016; 164(4): 792-804.
54. Treweek JB, Chan KY, Flytzanis NC, Yang B, Deverman BE, Greenbaum A, et al. Whole-body tissue stabilization and selective extractions via tissue-hydrogel hybrids for high-resolution intact

- circuit mapping and phenotyping. *Nat Protoc.* 2015; 10(11): 1860-1896.
55. Hoffman AS. Hydrogels for biomedical applications. *Adv Drug Deliv Rev.* 2002; 54(1): 3-12.
 56. Magliaro C, Callara AL, Mattei G, Morcinelli M, Viaggi C, Vaglini F, et al. Clarifying CLARITY: quantitative optimization of the diffusion based delipidation protocol for genetically labeled tissue. *Front Neurosci.* 2016; 10: 179.
 57. Chiang AS. Aqueous tissue clearing solution. U.S. Patent No. 6,472,216. Washington, DC: U.S. Patent and Trademark Office 2002; 2002 Oct 29.
 58. Beeckman T, Engler G. An easy technique for the clearing of histochemically stained plant tissue. *Plant Molecular Biology Reporter.* 1994; 12 Suppl 1: 37-42.
 59. Matthews JB. Influence of clearing agent on immunohistochemical staining of paraffin-embedded tissue. *J Clin Pathol.* 1981; 34(1): 103-105.
 60. Kupferschmidt DA, Cody PA, Lovinger DM, Davis MI. Brain BLAQ: Post-hoc thick-section histochemistry for localizing optogenetic constructs in neurons and their distal terminals. *Front Neuroanat.* 2015; 9: 6.
 61. Ertürk A, Mauch CP, Hellal F, Förstner F, Keck T, Becker K, et al. Three-dimensional imaging of the unsectioned adult spinal cord to assess axon regeneration and glial responses after injury. *Nat Med.* 2011; 18(1): 166.
 62. Yokomizo T, Yamada-Inagawa T, Yzaguirre AD, Chen MJ, Speck NA, Dzierzak E. Whole-mount three-dimensional imaging of internally localized immunostained cells within mouse embryos. *Nat Protoc.* 2012; 7(3): 421-431.
 63. Greenbaum A, Chan KY, Dobрева T, Brown D, Balani DH, Boyce R, et al. Bone CLARITY: Clearing, imaging, and computational analysis of osteoprogenitors within intact bone marrow. *Sci Transl Med.* 2017; 9(387): pii: eaah6518.
 64. Lee H, Park JH, Seo I, Park SH, Kim S. Improved application of the electrophoretic tissue clearing technology, CLARITY, to intact solid organs including brain, pancreas, liver, kidney, lung, and intestine. *BMC Dev Biol.* 2014; 14: 48.
 65. Renier N, Wu Z, Simon DJ, Yang J, Ariel P, Tessier-Lavigne M. iDISCO: a simple, rapid method to immunolabel large tissue samples for volume imaging. *Cell.* 2014; 159(4): 896-910.
 66. Santi PA, Johnson SB, Hillenbrand M, GrandPre PZ, Glass TJ, Leger JR. Thin-sheet laser imaging microscopy for optical sectioning of thick tissues. *Biotechniques.* 2009; 46(4): 287-294.
 67. Ryan DP, Gould EA, Seedorf GJ, Masihzadeh O, Abman SH, Vijayaraghavan S, et al. Automatic and adaptive heterogeneous refractive index compensation for light-sheet microscopy. *Nat Commun.* 2017; 8(1): 612.
 68. Khoradmehr A, Mazaheri F, Anvari M, Tamadon A. A simple technique for three-dimensional imaging and segmentation of brain vasculature using Fast Free-of-Acrylamide Clearing Tissue (FACT) in murine. *Cell J.* 2019; 21(1): (A head of print).
 69. Mohammad Rezazadeh F, Saedi S, Rahmanifar F, Namavar MR, Dianatpour M, Tanideh N, et al. Fast free-of-acrylamide clearing tissue (FACT)-for clearing, immunolabeling and three-dimensional imaging of partridge tissues. *Microsc Res Tech.* 2018: (A head of print).
 70. Ahrens MB, Orger MB, Robson DN, Li JM, Keller PJ. Whole-brain functional imaging at cellular resolution using light-sheet microscopy. *Nat Methods.* 2013; 10(5): 413-420.

The Expression of Microvesicles in Leukemia: Prognostic Approaches

Ali Ehsanpour, M.D.¹, Najmaldin Saki, Ph.D.¹, Marziye Bagheri, M.Sc.¹, Masumeh Maleki Behzad, M.Sc.¹,
Saeid Abroun, Ph.D.^{2*}

1. Thalassemia and Hemoglobinopathy Research Center, Research Institute of Health, Ahvaz Jundishapur University of Medical Sciences, Ahvaz, Iran
2. Department of Hematology, Faculty of Medical Sciences, Tarbiat Modares University, Tehran, Iran

*Corresponding Address: P.O.Box: 14115-331, Department of Hematology, Faculty of Medical Sciences, Tarbiat Modares University, Tehran, Iran
Email: abroun@modares.ac.ir

Received: 29/February/2018, Accepted: 18/June/2018

Abstract

Microvesicles (MVs) are the smallest subclass of the extracellular vesicles (EVs) spontaneously secreted by the external budding from the cell membranes in physiologic and pathologic conditions. The MVs derived from leukemic cells (LCs) can be detected by the expression of specific cluster of differentiation (CD) markers indicating their cellular origin while they can transfer different agents such as microRNAs, cytokines, and chemokines. The secretion of these agents from MVs can affect the vital processes of LCs such as cell cycle, proliferation, differentiation, and apoptosis. According to the effects of MVs components on the vital processes of LCs, it has been postulated that a change in the expression of MVs might be involved in the progression and prognosis of leukemia. However, further studies are needed to confirm the association between the presence of MVs and their components with the prognosis of leukemia. It seems that the identification of the prognostic values and the application of them for the detection of MVs in leukemia can provide new therapeutic targets for monitoring the status of patients with leukemia.

Keywords: CD Markers, Leukemia, microRNAs, Microvesicles, Prognosis

Cell Journal (Yakhteh), Vol 21, No 2, July-September (Summer) 2019, Pages: 115-123

Citation: Ehsanpour A, Saki N, Bagheri M, Maleki Behzad M, Abroun S. The expression of microvesicles in leukemia: prognostic approaches. Cell J. 2019; 21(2): 115-123. doi: 10.22074/cellj.2019.5847.

Introduction

A cell can secrete the different types of vesicles, the extracellular vesicles (EVs), into the extracellular environment with a range from a few nanometers to several microns in size (1). According to either the size or source, EVs are divided into three subclasses: apoptotic bodies, microvesicles (MVs), and exosomes (2). MVs are the smallest subclass of vesicles, which differ in size from between 100 nm and 1000 nm, and they are secreted by the external budding from the membrane of the normal cells such as platelets, endothelial cells, and leukocytes (2-4). It has been shown that these secretory factors can also be released under pathological conditions such as cancers, inflammation, coronary heart disease, diabetes, pre-eclampsia, and hematological malignancies (3, 4). Despite their small size, MVs can contain several biological agents such as growth factors, enzymes, adhesion molecules, and nucleic acids including microRNAs (miRNAs) (5, 6). The production rate of MVs and the cellular lineage markers for their membranes are different depending on the cell origin (7).

MVs can affect the cell fate via direct binding to receptors of the target cell there by secreting their components into the extracellular medium, as well as

endocytosis (3, 8, 9). However, MVs do not transfer their components into target cells in a random manner, but their secretion is regulated by several small GTPases such as ADP-ribosylation factors 1 and 6 (ARF1 and ARF6), rhodopsin A (Rho A), Rac family small GTPase 1 (Rac1), and Rab (6, 9). Indeed, these GTPases can indirectly regulate the MVs secretion pathways (6). miR-containing MVs can lead to genetic changes in the target cell due to their effect on the expression regulation of specific genes (10-12).

These genetic changes can indirectly affect the vital processes such as differentiation, proliferation, and apoptosis (12, 13). In addition, MVs can also participate in biological processes such as thrombosis because of the transportation of the other components such as tissue factor (TF), cytokines, and chemokines receptors (4). Therefore, the elevated levels of TF-containing MVs can be associated with reduced survival in patients.

Leukemias are a group of hematological malignancies namely lymphocytic and myelocytic leukemia which is further divided into the acute and chronic types depending on the origin of the cell types and clinical manifestations, respectively.

The hallmark of these malignancies is an increase in leukemic cells (LCs) in bone marrow (BM) and their release into the peripheral blood (PB) (14). It has been shown in these malignancies that LCs MVs can stimulate some processes such as the cell growth, angiogenesis induction, and the escape of blast cells from the detection by the immune system through the secretion of their components (4, 15). MVs secretion in leukemia is increased during the onset and progression of the disease and their ectopic secretion is associated with the increased invasion and progression towards the progressive stages (4). Moreover, these secretory components can result in multidrug resistance (MDR) in leukemias by transporting certain proteins (15). The significance of this issue is revealed when the plasma levels of some MVs are reduced following chemotherapy in leukemias, while an increase in their levels is observed sometime after the treatment (16).

It can be inferred that although these types of MVs are not resistant to treatments, their increase following the treatment may be considered a marker of the relapse phase during the disease. Hence, the assessment of these vesicles can provide a better understanding of chemotherapy-resistant leukemias. Given that the secretion of MVs components can have a significant impact on critical processes of LCs, it seems that their presence could play a key role in the progression and prognosis of leukemias (17, 18). In this review article, we attempt to examine the role of MVs expression in the progression of leukemia and their potential effects on the prognosis of these abnormalities.

Microvesicles in the progression of acute lymphocytic leukemia

Acute lymphocytic leukemia (ALL) is the most common childhood leukemia, which results from the clonal proliferation of lymphoid precursors in BM (15). Most studies have indicated the miRs are as the most prevalent components in ALL MVs components. MiR-150 is among these miRs, in which its expression is decreased in ALL Nalm-6 cell line MVs (16, 17). MiR-150 can inhibit the differentiation of lymphocytes by preventing the cell transition from pro-B to the pre-B stage. On the other hand, miR-150 can directly contribute to the reduced expression of the c-Myc transcription factor which is involved in controlling the development of lymphocytes (17, 18). Thus, it seems that the reduced expression of miR-150 can, directly and indirectly, increase the upregulation of the immature lymphoid cells in ALL.

Similar to miR-150, the expression levels of some other miRs such as miR-15b, miR-424, and miR-101 are decreased in B-ALL Nalm-6 cell line MVs. It has been shown that the reduced expression of these miRs can be associated with the increased expression of

a number of genes such as cyclin D1 (CCND1) and B-Cell CLL/Lymphoma 9 (BCL9) in this cell line (16). BCL9 is a component of the Wnt/ β -catenin signalling pathway that plays an important role in the regulation of self-renewal, proliferation, and differentiation in normal and malignant cells. On the other hand, BCL9 can increase β -catenin activity which has a key role in the increases self-renewal and maintenance of leukemic stem cells (LSCs) (19, 20). CCND1 is a cell cycle regulator with a recognized role in the control of the G1/S transition by regulating the function of cyclin-dependent kinases (CDKs) (21). Song et al. (21) have shown that CCND1 overexpression in T and B-cell lymphomas may function as an oncogene through the activation of the proliferation and differentiation processes. Similar to B-ALL Nalm-6 cell line, CCND1 and BCL9 overexpression as a post-translational phenomenon following the reduced expression of miR-15b, miR-424, and miR-101 in MVs may be useful as a potential therapeutic target in ALL patients.

Unlike the Nalm-6 cell line in which the reduced expression of some MVs miRs have been shown, the accumulation of miR17-92 cluster containing (e.g. miR-92a, miR-92b, miR-18a, miR-18b, and miR-96) in T-ALL Jurkat cell line MVs has been reported by a study of Li et al. (16). Many tumor suppressor proteins such as phosphatase and Tensin homolog (PTEN), and apoptotic proteins including BIM (BCL2) and E2F transcription factor1 (E2F1) can be targeted by this aberrantly expressed miRs in this cell line (16, 22). BIM induces apoptosis via activating a number of proapoptotic family members such as BCL-2 associated proapoptotic x protein (Bax) and BCL-2 antagonist killer-1 (Bak) (23). On the other hand, PTEN can phosphorylate and activate BCL2-associated agonist of cell death (BAD), which leads to the induction of apoptosis (24). E2F1 is a protein that plays an important role in the regulation of apoptosis mediators such as retinoblastoma protein (pRb) and murine-double-minute-2 (MDM-2). PRb is a negative cell cycle regulator that can be activated by binding E2F1 in a hypo-phosphorylated form. On the other hand, MDM-2 activates P53 and controls the cell cycle during the transition from G1 to S phase (25). Also, it has been shown that miR-1246-containing MVs can suppress the function of P53 and prevent the LCs apoptosis (Fig.1) (16).

Similar to T-ALL Jurkat cell line, the reduced expression of these proapoptotic proteins due to the secretion of the above-mentioned miRs from ALL MVs results in LCs survival. Since miR-containing MVs can play a critical role in the progression of ALL by inhibition of apoptosis, as well as increasing the survival and proliferation of LCs, the overexpression of this miRs can be a poor prognostic marker in ALL.

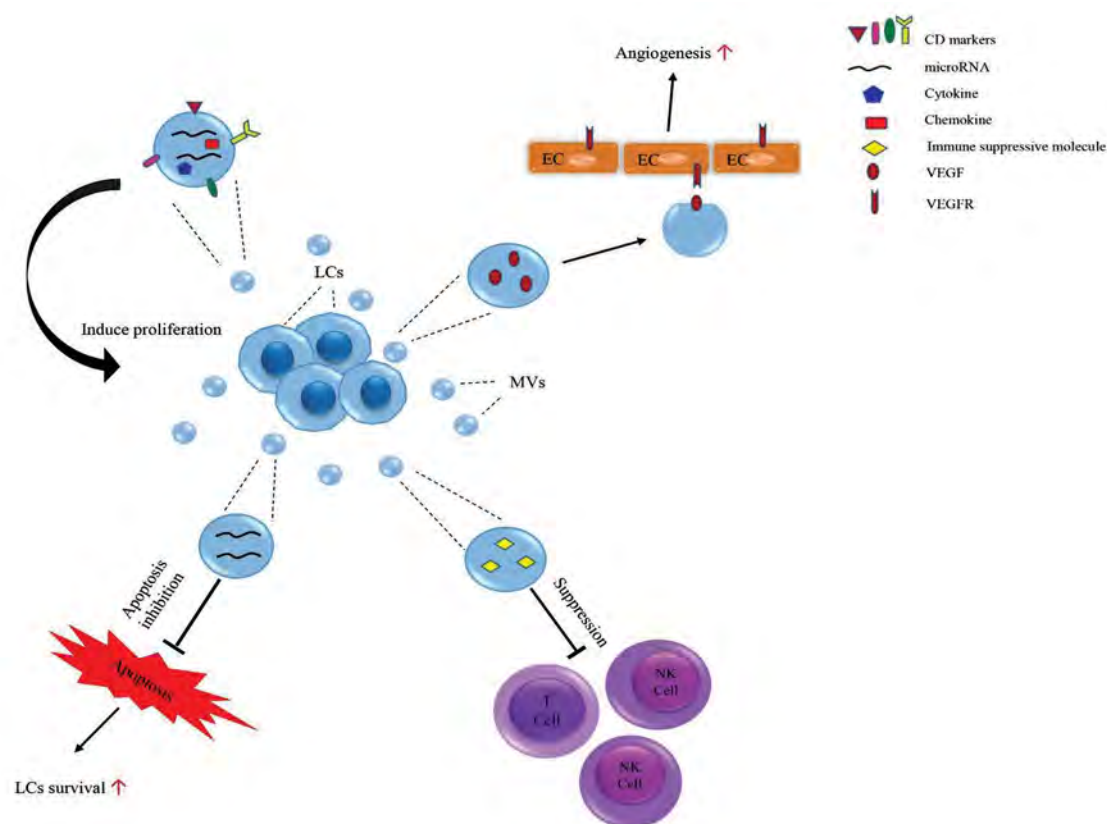


Fig.1: The mechanism of MVs in leukemia progression. LCs-derived MVs affect the cell fate via direct binding to receptors of the target cells. In fact, these vesicles can play a role in vital processes of target cells by transfer different agents such as microRNAs, cytokines, and chemokines. LCs-derived MVs as autocrine positive feedback could be a cause of LCs progression. Also, MVs can increase LCs survival by a decrease in anti-leukemia activity via the suppression of the immune cells, the reduction of proapoptotic proteins, and the induction of angiogenesis. Therefore, LCs-derived MVs play an important role in the progression of leukemia via disrupting the balance of these processes. MVs; Microvesicles, LCs; Leukemic cells, ECs; Endothelial cells, VEGF; Vascular endothelial growth factor, and VEGFR; VEGF receptor.

Chronic lymphocytic leukemia-derived microvesicles

Chronic lymphocytic leukemia (CLL) is a leukemia of apoptosis-resistant mature B-cells which is characterized by the expression of CD5⁺, CD19⁺, CD23⁺, CD10⁺, CD20⁺, CD22⁺, CD79 α , and CD79 β . These cells can clonally aggregate in PB, BM, lymph nodes, and spleen (26). Some MVs are derived from B-cell CLL possessing AXL receptor tyrosine kinase (27). AXL acts as an active regulator of kinases such as Lyn and phosphatidylinositol 3-kinase (PI3K)/AKT serine-threonine kinase (4). On the other hand, AXL-containing MVs can enhance the expression of vascular endothelial growth factor (VEGF) by activating the AKT/mammalian target of rapamycin (mTOR)/P70S6K/hypoxia-inducible factor-1 α (HIF-1 α) signalling pathway in BM stromal cells (BMSCs) (28). VEGF has a well-known role in inducing angiogenesis by binding to its cognate receptor on the endothelial cells (Fig. 1) (4, 28). On the other hand, these MVs can promote the expression of CCND1 and c-MYC by activating the AKT/ β -catenin signalling pathway in BMSCs (29). CCND1 and c-MYC play important roles in cell cycle regulation. Several studies have shown that the induction of the expression of CCND1 and c-MYC by AXL-containing MVs can dysregulate the cell cycle in BMSCs and lead to the increased proliferation of these cells (4, 27,

28, 30). Therefore, this is inferred that the release of AXL from B-cell CLL MVs may result in a higher BM density due to angiogenesis and BMSCs proliferation induction. In these conditions, high BM density can cause a problem in BM aspiration in CLL patients.

Another type of MVs in B-CLL patients has the certain CD markers on their surface that can indicate their origin. The overexpression of CD20, CD19, CD37, and CD52 is among the changes observed on MVs surface in CLL patients (Table 1) (7, 28, 31, 32). Interestingly, De Luca et al. (31) in their study on newly diagnosed B-CLL patients showed that an increase in the number of MVs bearing these CD19 and CD37 had a direct correlation with a high tumor burden and an inverse relationship with the overall survival. This finding suggests that the overexpression of MVs bearing these CD markers could be a poor prognostic biomarker for the patient survival. CD52 is a specific target of humanized monoclonal antibody Alemtuzumab (CAMPATH-1H) used for the treatment of relapsed or refractory CLL (33). A higher expression of CD52 in serum vesicles has been reported in a B-CLL patient with poor risk karyotype (17p- and 11q-) and more advanced disease (Rai stage III) (7). In addition, Albitar et al. (34) demonstrated a high level of soluble CD52 in the plasma of patients which is inversely associated with the plasma concentration of Alemtuzumab and also can cause

a nearly 4-fold increase in the risk of death in CLL patients. Therefore, the presence of MVs bearing CD52 could be a poor prognostic biomarker for the CLL progression toward the advanced stage. Also, the assessment of MVs bearing CD52 in CLL patients can provide useful information for the analysis of Alemtuzumab therapy and minimal residual disease (MRD).

MiRs are the components of CLL MVs that can affect various aspects of LCs function by binding their targets. Yeh et al. (35) have shown that MVs-containing miR-150 and miR-155 can boost B-cell receptor (BCR) expression in B-cells via the secretion of their components. Also, they showed the increased BCR activation through α -IgM stimulation which can lead to the increased secretion of MVs containing these miRs. BCR is the main functional receptor on B-cells, and several processes of these lymphocytes, including antibody production, are linked to its downstream signalling pathways (36). Therefore, a change in the expression of BCR can affect the activity of B lymphocytes. Since BCR signalling plays an essential role in the proliferation and maintenance of malignant B-cells, increasing the activity of the cell signalling via the secretion of miR-150 and miR-155 from MVs may be associated with the survival of LCs in CLL (35, 37). Considering the cross-talk between MVs containing biological molecules and CLL cells, the assessment of the impact of MVs on the processes of LCs such as maintenance, proliferation as well as the response therapy and MRD in this disease can reveal the prognostic value of MVs expression in the prediction of CLL progression.

Circulating microvesicles in acute myeloid leukemia

Acute myeloid leukemia (AML) is a hematological

malignancy associated with a rapid proliferation of myeloblasts in BM and their release into PB (38). Studies have shown that MVs secreted from LCs, especially in AML patients, can induce the proliferation, migration, and apoptosis inhibition in these patients (39). Additionally, these MVs can suppress the immune system through the release of immune suppressive molecules such as transforming growth factor beta1 (TGF β 1), Fas ligand, programmed cell death 1 ligand (PD-L1), CD39, CD73, MHC class I polypeptide-related sequence A (MICA), and MHC class I polypeptide-related sequence B (MICB) (11, 40). Therefore, these vesicles as the immune suppressors are able to decrease anti-leukemia activity and play a role in LCs escape from the immune defense processes. Natural killer cells (NK cells) play a vital role in the eradication of tumor cells in a wide range of cancers, including leukemia (41). The function of these cells is controlled by activating and inhibiting the receptors expressed on their surface. NKG2D is among the active receptors located on the surface of NK cells that its expression is a sign of the active function of NK cells (42). In a study conducted on the function of these types of cells in AML patients, Szczepanski et al. (43) found that the expression of NKG2D on NK cells is decreased following the secretion of TGF β 1 from blast-derived MVs. In fact, this type of MVs suppresses the function of NK cells by the secretion of their components (Fig.1). On one hand, interleukin-15 (IL-15) can protect NK cells from the adverse effects of these MVs. Considering the role of NK cells in the killing of LCs, the suppression of NKs function by TGF β 1-containing MVs seems to provide conditions for LCs survival and thereby AML progression. Therefore, an increase in this type of MVs can be a poor prognostic factor in AML.

Table 1: Prognostic value of CD markers' expression in leukemia MV

Leukemia	CD markers	Cho.	Expression	Prognosis	Ref.
CLL	CD19	16p11.2	High	Can be associated with CLL progression via increased BCR signalling in B-cells	(31, 32, 44)
	CD37	19q13.33	High	Associated with the progression of pre-B to mature B-cell lymphocyte and subsequently increased proliferation	(31, 45)
	CD20	11q12.2	High	Can be associated with CLL progression	(28, 32, 46)
	CD52	1p36.11	High	Maybe associated with poor prognosis via increased progression and invasion of B-cells	(7, 28, 33)
AML	CD13	15q26.1	High	Poor prognosis via increased migration of cells	(47, 48)
	CD33	19q13.41	High	Associated with increased myeloid blast cells	(40, 47, 49)
	CD117	4q12	High	Can be associated with poor prognosis via interaction with SCF and subsequently increased blast cells survival	(40, 47, 50)
	CD34	1q32.2	High	Maybe associated with increased blast cells	(40, 47, 51)
CML	CD34	1q32.2	High	Can be associated with increased blast cells	(12)
	CD123	Xp22.33	High	Can be associated with poor prognosis by increased proliferation	(12)

CD; Cluster of differentiation, MVs; Microvesicles, CLL; Chronic lymphocytic leukemia, AML: Acute myeloid leukemia; CML; Chronic myeloid leukemia, BCR; B-cell receptor, and SCF; Stem cell factor.

On the other hand, it may be inducing the expression of IL-15 by new immunotherapy agents which can protect NK cells from the adverse effects of these MVs. The relapse is a problem can complicate the process of the treatment for AML patients. Studies displayed that in addition of the genetic background of individuals, some AML MVs contain proteins that play a crucial role in drug resistance and relapse in this disease (52). AML MVs contain chemoattractants such as I-309, monocyte chemoattractant protein 1 (MCP-1), and MCP-4, which can lead to the resistance of AML blasts to chemotherapy by trafficking, proliferation, migration, and mobilization of these blasts (52, 53). Considering the impact of I-309, MCP-1, and MCP-4 MVs on AML blasts drug resistance, it may be targeting these MVs by chemotherapeutic agents reduce the MRD, as well as relapse in this disease. Another AML MVs also have procoagulants such as TF which is a component of AML MVs that could be associated with hypercoagulable state and increased the risk of thrombosis in this malignancy (52). Considering some AML MVs contain VEGF, the secretion of them can lead to elevated angiogenesis and hence increased the chance of thrombosis (4). It can be mentioned that the disturb balance between pro- and anti-coagulant factors by AML MVs may have a potential role in the incidence of thrombotic events in AML patients.

The increased expression of myeloid markers is an early indicator of the presence of blasts in BM and PB of AML patients. Some of these blasts can secrete MVs bearing myeloid-specific CD markers, which can be thus distinguished from MVs of normal cells. Several studies indicated that the expressions of CD13, CD34, CD117, and CD33 in blast-derived MVs in AML patients can be associated with the presence of activated blasts in this disease (Table 1) (11, 40, 47). Regarding CD13, CD34, CD117, and CD33 are the immature myeloid specific markers; it seems that a higher expression of these markers in AML MVs may be displayed the presence of active myeloid neoplastic clone in BM. However, few studies indicated the possible correlation between the AML MVs markers and clinical findings or response/resistance to the therapeutic agents of this disease. Therefore, more studies are required to reveal the prognostic value of AML MVs markers in clinical outcomes and disease aggressiveness.

MiRs are another type of secreted MVs in AML patients. Among these miRs, the expression of miR-155 has been shown to increase in AML MVs. Interestingly, the presence of this type of MVs is associated with the increased white blood cell (WBC) counts and a complex karyotype such as genotype FLT3-ITD in combination with NPMc⁺ (37, 54). Since miR-155-containing MVs are associated with high WBC counts and the FLT3-ITD combination, it seems that a higher level of this MVs has a poor prognostic value in AML patients. Unlike miR-155, the increase in some miRs (like miR34a) can be associated with a favorable prognosis. Wang et al. (38) in

their recent study demonstrated that the increased miR34a level in MVs of KG1a cell line can be associated with the suppression of proliferation and induce apoptosis in this cell line. In this situation, miR-34a could act as a tumor suppressor by affecting factors involved in apoptosis such as caspase-3 and T cell immunoglobulin mucin-3 (Tim-3). According to these findings, it may be inducing the expression of miR34a level in KG1a cell line MVs and transferring them to patients with AML as new therapeutic agents which can improve the management of these patients. Since AML MVs can be associated with AML progression, we believe that the MVs may be used as an independent prognostic biomarker in monitor AML progression. However, further studies are required to substantiate this notion.

Chronic myeloid leukemia microvesicles

Chronic myeloid leukemia (CML) is a clonal myeloproliferative disorder characterized by the presence of translocation (9, 22) and a range of immature myeloid cells (12, 13). Several recent study demonstrated that MVs which are derived from LAMA84 CML cell line through secretion of interleukin-8 (IL-8) can induce the intercellular adhesion molecule 1 (ICAM-1) and vascular cell adhesion molecule 1 (VCAM-1) expression in human umbilical vein endothelial cells (HUVECs), which is associated with an increase in the adhesion and migration of CML cells (4, 11, 55, 56). Considering the fact that ICAM-1 and VCAM-1 can mediate CML cells adhesion to endothelial cells, it may be similar to LAMA84 CML cell line, the release of IL-8 from MVs-derived CML can induce thrombotic process in this malignancy.

MiR-containing MVs are secreted by LSCs in CML, which can reflect the abnormal function of these stem cells. Chen et al. (13) in a recent study have shown that the overexpression of miR 23-27-24 cluster and onco-miR cluster, which includes several miRs such as miR-17, miR19a, miR-19b, miR-20a, and miR-92a that play an important role in development and proliferation of CML K562 cell line. The increase in miR 23-27-24 cluster can enhance angiogenesis by promoting angiogenic signalling including Ras/MAP kinase and vascular endothelial growth factor receptor 2 (VEGFR2) signalling in endothelial cells (56, 57). On the other hand, Tadokoro et al. (58) exhibited that the co-culture of the K562 cell line containing miR-210 in hypoxic conditions with HUVECs enables miR-210 to induce angiogenesis by reducing ephrin A3 (EFNA3) as a negative regulator of angiogenesis. Although a high level of immature myeloid progenitors is the main cause of the thrombotic event in CML, it may be similar to K562 cell line, the release of miRs-210 from CML MVs in hypoxic conditions induces the thrombotic activity in CML patients.

It has been demonstrated several miRs derived from K562 cell line MVs including miR-27b, miR-24, miR-23b, miR-126, has-let-7f, has-let-7a, miR-1249, miR-185, miR-7,

and miR-130b/let-7b may contribute to the development of this cell line. These miRs have been demonstrated to be involved in a number of biological processes, including development, differentiation, apoptosis, and proliferation of K562 cell line. For example, miR-7 may play a role in leukemogenesis by abnormally regulating their target genes such as retinoblastoma 1 (RB1), breakpoint cluster region (BCR), phosphatidylinositol-4,5-bisphosphate 3-kinase catalytic subunit delta (PIK3CD), phosphoinositide-3-kinase regulatory subunit 3 (PIK3R3), BCL2 like 1 (BCL2 L1), and v-raf-leukemia viral oncogene 1 (RAF1). Furthermore, miR-126 can activate the PI3K/AKT signalling pathway by affecting the v-crck avian sarcoma virus CT10 oncogene homolog (CRK) (13).

A large number of these target genes were involved in the activation of PI3K/AKT signalling pathway, cell cycle, and P53 signalling, which involved in various processes such as development, proliferation, and apoptosis of LCs (13, 59). Since most of these pathways are involved in the vital processes of LCs; therefore, miRs derived MVs may contribute to the uncontrolled development, as well as resistance to apoptosis in LCs. Furthermore, Zhang et al. (60) have shown that a high level of miR-146b-5p in K562 cell line MVs can promote hematopoietic cells to a leukemic state. Silencing NUMB gene in the recipient cells by

miR-146b-5p in K562-MVs is a possible mechanism for leukemic transformation of hematopoietic cells. NUMB can inhibit LCs proliferation by preventing degradation of p53 and Notch signalling pathway, which is involved in apoptosis and cell cycle respectively (Table 2) (61). So that, it is implied that MVs containing miR-146b-5p can have a role in the promotion of LCs proliferation by silencing NUMB gene indirectly.

Certain MVs are secreted in CML patients bearing CD markers which are indicating their derivation from blast cells. For example, the overexpression of CD34 and CD123 in MVs derived from CML CD34⁺ blasts can be associated with an increase in immature cells in PB (12). The CD123 or interleukin 3 receptor subunit alpha (IL-3RA) is one of the markers expressed on the majority of CD34⁺/CD38⁻ MVs derived from CML blasts (62, 63). IL-3 is a pleiotropic cytokine that functions as a multi-colony stimulating factor (multi-CSF), and its binding to its receptor (CD123) on hematopoietic cells can be associated with their development in BM (Table 1) (63). Given the low expression of CD123 in normal hematopoietic cells, the overexpression of this marker on MVs derived from CML cells indicated the stimulation of CML cells proliferation. Due to constitutive role of MVs in biological process and clinical finding in CML, MVs could be a powerful prognostic biomarker and target therapy in this malignancy.

Table 2: Prognostic value of miRs contents of MVs in leukemia

Leukemia	miRs	Cho.	Expression	Prognosis	Ref.
ALL	miR-150	19q13.33	Low	Good prognosis via transition of B-cell from pro-B to pre-B and subsequent increase in differentiation and development of B-cells	(16, 18)
	miR-101	1p31.3	Low	Associated with a poor prognosis via decreased apoptosis	(15, 16)
	miR-424	Xq26.3	Low	Associated with poor prognosis via induction of cell-cycle and subsequent increase of proliferation	(16, 64)
	miR-15b	3q25.33	Low	Can be associated with poor prognosis via decrease of caspase signalling cascade and decreased apoptosis	(16, 65)
	miR-1246	2q31.1	High	Poor prognosis via down-regulation of P53 and subsequently decreased apoptosis	(16)
CLL	miR-155	21q21.3	High	Can be associated with a poor prognosis via activating BCR signalling and increased proliferation	(35, 37, 64)
	miR-150	19q13.33	High	Maybe associated with a poor prognosis via inhibiting lymphocyte differentiation and decreased B-cell maturation	(18, 35)
AML	miR-34a	1p36.22	High	Good prognosis via the induction of apoptosis and decreased proliferation	(38, 66)
	miR-155	21q21.3	High	Associated with a poor prognosis via increased proliferation	(37, 39, 64)
CML	miR-210	11p15.5	High	Can be associated with poor prognosis through induced angiogenesis and cell-cycle	(11, 40)
	miR-146b-5p	10q24.32	High	Poor prognosis via inhibition of NUMB, Notch 2, BRCA1 and subsequently increased proliferation	(60)

MVs; Microvesicles, ALL; Acute lymphocytic leukemia, CLL; Chronic lymphocytic leukemia, AML; Acute myeloid leukemia, CML; Chronic myeloid leukemia, BCR; B-cell receptor, Cho; Chromosome, NUMB; Endocytic adaptor protein, and BRCA1; DNA repair associated.

MVs are the smallest subclass of vesicles secreted by the external budding from the membrane of cells in physiologic and pathologic states (1-4). These vesicles contain various biological agents and can release their components via interaction with target cells, leading to functional and phenotypic changes in these cells (3, 8, 9). MVs can be secreted from LCs in hematological malignancies and play an important role as bioactive vesicles. In addition, these particles can carry different biological mediators such as miRs, cytokines, and chemokines (4). The secretion of these agents, especially miRs, from MVs can cause genetic changes in target cell due to their effects on the regulation of the gene expression. For example, miRs-containing MVs can be associated with the ALL progression and prognosis by the impact on molecules and signalling pathways that involved in a vital process of LCs such as differentiation, proliferation, and apoptosis. On the other hand, LCs derived MVs can be recognizable via the expression of specific CD markers showing their origin. Elevated levels of some MVs CD markers expression such as CD52 can be associated with the CLL progression toward advanced stage (33). Similarly, a higher expression of myeloid progenitor CD markers in AML MVs may display the presence of the active myeloid neoplastic clone in BM (11, 40, 47). Hence, flow cytometry analysis of MVs related to CD markers in alongside the specific diagnostic CD markers in leukemias can reveal their prognostic value in disease progression. In addition to the biological process of LCs, the secretion of MVs components such as ICAM-1, VCAM-1, TF, and VEGF, which mediate the thrombotic event and angiogenesis process, can be associated with the incidence of unfavorable clinical outcomes in leukemia patients. Furthermore, MVs containing TGF- β can act as anti-leukemic agents by suppression of the immune cell activation in AML (43). It seems that these MVs function may have a role in drug resistance, as well as AML relapse by helping LCs to escape from the defective immune system. Accordingly, MVs can be used as prognostic biomarkers for the disease monitoring in hematological malignancies. It is conceivable that the inactivation of MVs function by new drug strategies can minimize the side effects of these particles on the clinical finding of leukemia patients and leads to improve the condition of those patients.

Conclusion

Leukemia-derived MVs can play an indispensable role in LCs maintenance by the impact on the vital process including survival, proliferation, and apoptosis of these cells. So that, MVs can have a crucial role in the leukemias progression. In spite of the important role of MVs in LCs survival, most studied of MVs function has been done on leukemic cell lines. Therefore, further clinical trials for a better understanding of MVs mechanisms in leukemias are required to confirm the relationship between these particles with the leukemias prognosis. It may reduce their undesirable effects by preventing the secretion of MVs

components from leukemic cells, removing them from the circulation, and blocking the binding of MVs to their corresponding receptors by a new therapeutic approach that leads to improving the patients' condition.

Acknowledgments

We wish to thank all our colleagues in Shafa Hospital and Allied Health Sciences School, Ahvaz Jundishapur University of Medical Sciences. The authors declare no conflict of interest.

Authors' Contributions

S.A., N.S.; Were responsible for overall supervision and provided critical revision of the manuscript. A.E., N.S., M.B., M.M.B., S.A.; Participated in study design, data collection, evaluation, and drafting. All authors read and approved the final manuscript.

References

- Borger V, Bremer M, Ferrer-Tur R, Gockeln L, Stambouli O, Betic A, et al. Mesenchymal stem/stromal cell-derived extracellular vesicles and their potential as novel immunomodulatory therapeutic agents. *Int J Mol Sci.* 2017; 18(7): pii: E1450.
- Ciregia F, Urbani A, Palmisano G. Extracellular vesicles in brain tumors and neurodegenerative diseases. *Front Mol Neurosci.* 2017; 10: 276.
- Razmkhah F, Soleimani M, Mehrabani D, Karimi MH, Amini Kafi-Abad S, Ramzi M, et al. Leukemia microvesicles affect healthy hematopoietic stem cells. *Tumour Biol.* 2017; 39(2): 1010428317692234.
- Aharon A, Rebibo-Sabbah A, Tzoran I, Levin C. Extracellular vesicles in hematological disorders. *Rambam Maimonides Med J.* 2014; 5(4): e0032.
- Butler JT, Abdelhamed S, Kurre P. Extracellular vesicles in the hematopoietic microenvironment. *Haematologica.* 2018; 103(3): 382-394.
- Raposo G, Stoorvogel W. Extracellular vesicles: exosomes, microvesicles, and friends. *J Cell Biol.* 2013; 200(4): 373-383.
- Boysen J, Nelson M, Magzoub G, Maiti GP, Sinha S, Goswami M, et al. Dynamics of microvesicle generation in B-cell chronic lymphocytic leukemia: implication in disease progression. *Leukemia.* 2016; 13(2): 350-360.
- Cocucci E, Racchetti G, Meldolesi J. Shedding microvesicles: artefacts no more. *Trends Cell Biol.* 2009; 19(2): 43-51.
- Tricarico C, Clancy J, D'souza-Schorey C. Biology and biogenesis of shed microvesicles. *Small GTPases.* 2016; 8(4): 220-232.
- Moldovan L, Batte K, Wang Y, Wisler J, Piper M. Analyzing the circulating microRNAs in exosomes/extracellular vesicles from serum or plasma by qRT-PCR. *Methods Mol Biol.* 2013; 1024: 129-145.
- Pando A, Reagan JL, Quesenberry P, Fast LD. Extracellular vesicles in leukemia. *Leuk Res.* 2017; 64: 52-60.
- Zhang J, Zhao A, Sun L, Chen W, Zhang H, Chen Z, et al. Selective surface marker and miRNA profiles of CD34+ blast-derived microvesicles in chronic myelogenous leukemia. *Oncol Lett.* 2017; 14(2): 1866-1874.
- Chen X, Xiong W, Li H. Comparison of microRNA expression profiles in K562-cells-derived microvesicles and parental cells, and analysis of their roles in leukemia. *Oncol Lett.* 2016; 12(6): 4937-4948.
- Kumar B, Garcia M, Weng L, Jung X, Murakami JL, Hu X, et al. Acute myeloid leukemia transforms the bone marrow niche into a leukemia-permissive microenvironment through exosome secretion. *Leukemia.* 2018; 32(3): 575-587.
- Qian L, Zhang W, Lei B, He A, Ye L, Li X, et al. MicroRNA-101 regulates T-cell acute lymphoblastic leukemia progression and chemotherapeutic sensitivity by targeting Notch1. *Oncol Rep.* 2016; 36(5): 2511-2516.
- Li WY, Chen XM, Xiong W, Guo DM, Lu L, Li HY. Detection of microvesicle miRNA expression in ALL subtypes and analysis of

- their functional roles. *J Huazhong Univ Sci Technolog Med Sci*. 2014; 34(5): 640-645.
17. Hajizamani S, Shahjahani M, Shahrabi S, Saki N. MicroRNAs as prognostic biomarker and relapse indicator in leukemia. *Clin Transl Oncol*. 2017; 19(8): 951-960.
 18. Vasilatou D, Papageorgiou S, Pappa V, Papageorgiou E, Dervenoulas J. The role of microRNAs in normal and malignant hematopoiesis. *Eur J Haematol*. 2010; 84(1): 1-16.
 19. Mani M, Carrasco DE, Zhang Y, Takada K, Gatt ME, Dutta-Simmons J, et al. BCL9 promotes tumor progression by conferring enhanced proliferative, metastatic, and angiogenic properties to cancer cells. *Cancer Res*. 2009; 69(19): 7577-7586.
 20. Ahmadzadeh A, Norozi F, Shahrabi S, Shahjahani M, Saki N. Wnt/ β -catenin signalling in bone marrow niche. *Cell Tissue Res*. 2016; 363(2): 321-35.
 21. Song JY, Song L, Herrera AF, Venkataraman G, Murata-Collins JL, Bedell VH, Chen YY, et al. Cyclin D1 expression in peripheral T-cell lymphomas. *Mod Pathol*. 2016; 29(11): 1306-1312.
 22. Nagel S, Venturini L, Przybylski GK, Grabarczyk P, Schmidt CA, Meyer C, et al. Activation of miR-17-92 by NK-like homeodomain proteins suppresses apoptosis via reduction of E2F1 in T-cell acute lymphoblastic leukemia. *Leuk Lymphoma*. 2009; 50(1): 101-108.
 23. Molitoris JK, McColl KS, Distelhorst CW. Glucocorticoid-mediated repression of the oncogenic microRNA cluster miR-17~92 contributes to the induction of Bim and initiation of apoptosis. *Mol Endocrinol*. 2011; 25(3): 409-420.
 24. Wang X, Gjørloff-Wingren A, Saxena M, Pathan N, Reed JC, Mustelin T. The tumor suppressor PTEN regulates T cell survival and antigen receptor signalling by acting as a phosphatidylinositol 3-phosphatase. *J Immunol*. 2000; 164(4): 1934-1939.
 25. Bi B, Littlewood NK, Crispe IN. Cleavage of E2F-1-regulating proteins and activation of E2F-1 during CD95-induced death of thymocytes. *Immunology*. 2001; 104(1): 37-42.
 26. Crompot E, Van Damme M, Pieters K, Vermeersch M, Perez-Morga D, Mineur P, et al. Extracellular vesicles of bone marrow stromal cells rescue chronic lymphocytic leukemia B-cells from apoptosis, enhance their migration and induce gene expression modifications. *Haematologica*. 2017; 102(9): 1594-1604.
 27. Ghosh AK, Secreto C, Boysen J, Sassoon T, Shanafelt TD, Mukhopadhyay D, et al. The novel receptor tyrosine kinase Axl is constitutively active in B-cell chronic lymphocytic leukemia and acts as a docking site of nonreceptor kinases: implications for therapy. *Blood*. 2011; 117(6): 1928-1937.
 28. Ghosh AK, Secreto CR, Knox TR, Ding W, Mukhopadhyay D, Kay NE. Circulating microvesicles in B-cell chronic lymphocytic leukemia can stimulate marrow stromal cells: implications for disease progression. *Blood*. 2010; 115(9): 1755-1764.
 29. Nomura S. Extracellular vesicles and blood diseases. *Int J Hematol*. 2017; 105(4): 392-405.
 30. Zhang ZK, Davies KP, Allen J, Zhu L, Pestell RG, Zagzag D, et al. Cell cycle arrest and repression of cyclin D1 transcription by INI1/hSNF5. *Mol Cell Biol*. 2002; 22(16): 5975-5988.
 31. De Luca L, D'Arcena G, Simeon V, Trino S, Laurenzana I, Caivano A, et al. Characterization and prognostic relevance of circulating microvesicles in chronic lymphocytic leukemia. *Leuk Lymphoma*. 2017; 58(6): 1424-1432.
 32. Domnikova NP, Dolgikh TY, Sholenberg EV, Vorontsova EV, Goreva OB, Mel'nikova EV, et al. Blood microvesicles during chronic lymphoproliferative diseases. *Bull Exp Biol Med*. 2013; 156(1): 94-97.
 33. Rodig SJ, Abramson JS, Pinkus GS, Treon SP, Dorfman DM, Dong HY, et al. Heterogeneous CD52 expression among hematologic neoplasms: implications for the use of alemtuzumab (CAMPATH-1H). *Clin Cancer Res*. 2006; 12(23): 7174-7179.
 34. Albitar M, Do KA, Johnson MM, Giles FJ, Jilani I, O'Brien S, et al. Free circulating soluble CD52 as a tumor marker in chronic lymphocytic leukemia and its implication in therapy with anti-CD52 antibodies. *Cancer*. 2004; 101(5): 999-1008.
 35. Yeh YY, Ozer HG, Lehman AM, Maddocks K, Yu L, Johnson AJ, et al. Characterization of CLL exosomes reveals a distinct microRNA signature and enhanced secretion by activation of BCR signaling. *Blood*. 2015; 125(21): 3297-3305.
 36. Ten Hacken E, Burger JA. Microenvironment interactions and B-cell receptor signaling in chronic lymphocytic leukemia: implications for disease pathogenesis and treatment. *Biochim Biophys Acta*. 2016; 1863(3): 401-413.
 37. Caivano A, La Rocca F, Simeon V, Girasole M, Dinarelli S, Laurenzana I, et al. MicroRNA-155 in serum-derived extracellular vesicles as a potential biomarker for hematologic malignancies—a short report. *Cell Oncol (Dordr)*. 2017; 40(1): 97-103.
 38. Wang Y, Cheng Q, Liu J, Dong M. Leukemia stem cell-released microvesicles promote the survival and migration of myeloid leukemia cells and these effects can be inhibited by microRNA34a overexpression. *Stem cells Int*. 2016; 2016: 9313425.
 39. Caivano A, Del Vecchio L, Musto P. Do we need to distinguish exosomes from microvesicles in hematological malignancies? *Leukemia*. 2017; 31(9): 2009-2010.
 40. Boyiadzis M, Whiteside TL. The emerging roles of tumor-derived exosomes in hematological malignancies. *Leukemia*. 2017; 31(6): 1259-1268.
 41. Hassani SN, Rezaeeyan H, Ghodsi A, Saki N. Restoration of natural killer cell cytotoxicity in the suppressive tumor microenvironment: novel approaches to treat AML. *J Hematopathol*. 2017; 10(3-4): 109-116.
 42. Deng W, Gowen BG, Zhang L, Wang L, Lau S, Iannello A, et al. Antitumor immunity. A shed NKG2D ligand that promotes natural killer cell activation and tumor rejection. *Science*. 2015; 348(6230): 136-139.
 43. Szczepanski MJ, Szajnik M, Welsh A, Whiteside TL, Boyiadzis M. Blast-derived microvesicles in sera from patients with acute myeloid leukemia suppress natural killer cell function via membrane-associated transforming growth factor- β 1. *Haematologica*. 2011; 96(9): 1302-1309.
 44. Morbach H, Schickel JN, Cunningham-Rundles C, Conley ME, Reisli I, Franco JL, et al. CD19 controls Toll-like receptor 9 responses in human B cells. *J Allergy Clin Immunol*. 2016; 137(3): 889-98. e6.
 45. Zhao X, Lapalombella R, Joshi T, Cheney C, Gowda A, Hayden-Ledbetter MS, et al. Targeting CD37-positive lymphoid malignancies with a novel engineered small modular immunopharmaceutical. *Blood*. 2007; 110(7): 2569-2577.
 46. Manshoury T, Do KA, Wang X, Giles FJ, O'Brien SM, Saffer H, et al. Circulating CD20 is detectable in the plasma of patients with chronic lymphocytic leukemia and is of prognostic significance. *Blood*. 2003; 101(7): 2507-2513.
 47. Caivano A, Laurenzana I, De Luca L, La Rocca F, Simeon V, Trino S, et al. High serum levels of extracellular vesicles expressing malignancy-related markers are released in patients with various types of hematological neoplastic disorders. *Tumour Biol*. 2015; 36(12): 9739-9752.
 48. Vahdat L, Maslak P, Miller WH Jr, Eardley A, Heller G, Scheinberg DA, et al. Early mortality and the retinoic acid syndrome in acute promyelocytic leukemia: impact of leukocytosis, low-dose chemotherapy, PMN/RAR-alpha isoform, and CD13 expression in patients treated with all-trans retinoic acid. *Blood*. 1994; 84(11): 3843-3849.
 49. Ehninger A, Kramer M, Röhlig C, Thiede C, Bornhäuser M, von Bonin M, et al. Distribution and levels of cell surface expression of CD33 and CD123 in acute myeloid leukemia. *Blood Cancer J*. 2014; 4: e218.
 50. Wells SJ, Bray RA, Stempora LL, Farhi DC. CD117/CD34 expression in leukemic blasts. *Am J Clin Pathol*. 1996; 106(2): 192-195.
 51. Lemoli RM, Salvestrini V, Bianchi E, Bertolini F, Fogli M, Amabile M, et al. Molecular and functional analysis of the stem cell compartment of chronic myelogenous leukemia reveals the presence of a CD34⁻ cell population with intrinsic resistance to imatinib. *Blood*. 2009; 114(25): 5191-5200.
 52. Tzoran I, Rebibo-Sabbah A, Brenner B, Aharon A. Disease dynamics in patients with acute myeloid leukemia: new biomarkers. *Exp Hematol*. 2015; 43(11): 936-943.
 53. Ramirez PA, Macanas P, Navarrete L, Quezada T, Broekhuizen R, Nervi B. The MCP-1/CCR2 axis in the biology of acute myeloid leukemia: possible role in blast cell migration. *Am Soc Hematology*. 2012; 120(21): 1439.
 54. de Jonge HJ, Valk PJ, de Bont ES, Schuringa JJ, Ossenkoppele G, Vellenga E, et al. Prognostic impact of white blood cell count in intermediate risk acute myeloid leukemia: relevance of mutated NPM1 and FLT3-ITD. *Haematologica*. 2011; 96(9): 1310-1317.
 55. Taverna S, Flugy A, Saieva L, Kohn EC, Santoro A, Meraviglia S, et al. Role of exosomes released by chronic myelogenous leukemia cells in angiogenesis. *Int J Cancer*. 2012; 130(9): 2033-2043.
 56. Shirzad R, Shahrabi S, Ahmadzadeh A, Kampen KR, Shahjahani M, Saki N. Signaling and molecular basis of bone mar-

- row niche angiogenesis in leukemia. *Clin Transl Oncol*. 2016; 18(10): 957-971.
57. Zhou Q, Gallagher R, Ufret-Vincenty R, Li X, Olson EN, Wang S. Regulation of angiogenesis and choroidal neovascularization by members of microRNA-23~27~24 clusters. *Proc Natl Acad Sci USA*. 2011; 108(20): 8287-8292.
 58. Tadokoro H, Umezumi T, Ohyashiki K, Hirano T, Ohyashiki JH. Exosomes derived from hypoxic leukemia cells enhance tube formation in endothelial cells. *J Biol Chem*. 2013; 288(48): 34343-34351.
 59. Chen L, Wang J, Wang B, Yang J, Gong Z, Zhao X, et al. MiR-126 inhibits vascular endothelial cell apoptosis through targeting PI3K/Akt signaling. *Ann Hematol*. 2016; 95(3): 365-374.
 60. Zhang HM, Li Q, Zhu X, Liu W, Hu H, Liu T, et al. miR-146b-5p within BCR-ABL1-positive microvesicles promotes leukemic transformation of hematopoietic cells. *Cancer Res*. 2016; 76(10): 2901-2911.
 61. Ito T, Kwon HY, Zimdahl B, Congdon KL, Blum J, Lento WE, et al. Regulation of myeloid leukaemia by the cell-fate determinant Musashi. *Nature*. 2010; 466(7307): 765-768.
 62. Pardanani A, Tefferi A, Hanson C, Brooks C, Finke C, Chen D, et al. Aberrant expression of CD123 (interleukin-3 receptor- α) on neoplastic mast cells. *Leukemia*. 2015; 29(7): 1605-1608.
 63. Testa U, Pelosi E, Frankel A. CD 123 is a membrane biomarker and a therapeutic target in hematologic malignancies. *Biomarker Res*. 2014; 2(1): 4.
 64. Forrest AR, Kanamori-Katayama M, Tomaru Y, Lassmann T, Ni-nomiya N, Takahashi Y, et al. Induction of microRNAs, mir-155, mir-222, mir-424 and mir-503, promotes monocytic differentiation through combinatorial regulation. *Leukemia*. 2010; 24(2): 460-466.
 65. Guo CJ, Pan Q, Li DG, Sun H, Liu BW. miR-15b and miR-16 are implicated in activation of the rat hepatic stellate cell: An essential role for apoptosis. *J Hepatol*. 2009; 50(4): 766-778.
 66. Chim CS, Wong KY, Qi Y, Loong F, Lam WL, Wong LG, et al. Epigenetic inactivation of the miR-34a in hematological malignancies. *Carcinogenesis*. 2010; 31(4): 745-750.
-

Histone Modification Marks Strongly Regulate *CDH1* Promoter in Prostospheres as A Model of Prostate Cancer Stem Like Cells

Fatemeh Shokraii, M.Sc.^{1,2#}, Maryam Moharrami, M.Sc.^{3#}, Nasrin Motamed, Ph.D.^{3*}, Maryam Shahhoseini, Ph.D.^{4,5}, Mehdi Totonchi, Ph.D.⁵, Vahid Ezzatizadeh, Ph.D.^{2,6}, Javad Firouzi, M.Sc.², Pardis Khosravani, M.Sc.², Marzieh Ebrahimi, Ph.D.^{2*}

1. Department of Developmental Biology, University of Science and Culture, ACECR, Tehran, Iran

2. Department of Stem Cells and Developmental Biology, Cell Science Research Center, Royan Institute for Stem Cell Biology and Technology, ACECR, Tehran, Iran

3. School of Biology, College of Science, University of Tehran, Tehran, Iran

4. Department of Epidemiology and Reproductive Health, Reproductive Epidemiology Research Center, Royan Institute for Reproductive Biomedicine, ACECR, Tehran, Iran

5. Department of Genetics, Reproductive Biomedicine Research Center, Royan Institute for Reproductive Biomedicine, ACECR, Tehran, Iran

6. Department of Medical Genetics, Royesh Medical Laboratory Centre, Tehran, Iran

#The first two authors equally contributed to this work.

*Corresponding Addresses: P.O.Box: 14155-6455, School of Biology, College of Science, University of Tehran, Tehran, Iran
P.O.Box: 16635-148, Department of Stem Cells and Developmental Biology, Cell Science Research Center, Royan Institute for Stem Cell Biology and Technology, ACECR, Tehran, Iran
Emails: motamed2@khayam.ut.ac.ir, mebrahimi@royaninstitute.org

Received: 15/January/2018, Accepted: 2/October/2018

Abstract

Objective: Cadherin-1 (*CDH1*) plays an important role in the metastasis, while expression of this protein is under control of epigenetic changes on its gene promoter. Therefore we evaluated both DNA methylation (DNAm_{et}) and histone modification marks of *CDH1* in prostate cancer stem like cells (PCSLCs).

Materials and Methods: In this experimental study, we isolated PCSLCs using cell surface marker and prostaspheroid formation, respectively. The cells isolated from both methods were characterized and then the levels of H3K4me₂, H3K27me₃, H3K9me_{2/3} and H3K9ac as well as DNAm_{et} were assessed in *CDH1* promoter of the isolated cells.

Results: The CD44⁺ CD49^{hi} cells were not validated as PCSLCs. However, prostaspheres overexpressed stemness related genes and had higher ability of invasion potential, associated with reduction in *CDH1* expression. Epigenetic status analysis showed that *CDH1* promoter was hypo-methylated. Histone modifications of H3K9ac and H3K4me₃ were significantly reduced, in parallel with an increased level of H3K27me₃.

Conclusion: Our results suggest that slight decrease of DNAm_{et} of the CpG island in *CDH1* promoter does not significantly contribute to the change of *CDH1* expression. Therefore, histone modifications are responsible in repressing *CDH1* in PCSLCs.

Keywords: Cancer Stem Cells, *CDH1*, Histone Modification, Methylation, Prostate Cancer

Cell Journal (Yakhteh), Vol 21, No 2, July-September (Summer) 2019, Pages: 124-134

Citation: Shokraii F, Moharrami M, Motamed N, Shahhoseini M, Totonchi M, Ezzatizadeh V, Firouzi J, Khosravani P, Ebrahimi M. Histone modification marks strongly regulate *CDH1* promoter in prostospheres as a model of prostate cancer stem like cells. Cell J. 2019; 21(2): 124-134. doi: 10.22074/cellj.2019.5702.

Introduction

Great advances in basic cancer research have demonstrated presence of the rare cell population (1-2%) with the ability of self-renewal, multi-potency, tumor initiation, tumor growth/re-growth, drug resistance and metastasis (1, 2). These cells, named tumor initiating cells or cancer stem cells (CSCs), could generally be identified based on the expression of a variety of cell surface markers such as CD24, CD44, CD133, CD166, Trop-1 and EpCAM (3, 4). They are able to form spheres or colonies in defined cultures (3, 5) as well as efflux of certain DNA dyes (6). Several studies have reported that prostate cancer arises from normal epithelial tissue based on genetic changes and chromosomal abnormalities, both of which are responsible for cell transformation, tumor initiation and progression (7). In addition, recent studies have indicated the crucial role of epigenetic regulatory elements in etiology of prostate cancer (8). In this regard, DNA methylation (DNAm_{et}) and post-translational modifications of histones play pivotal role in regulating gene expression and chromatin

remodeling (9) involved in tumor initiation and progression (8). Epigenetic alterations could aberrantly render repression or expression of particular genes involved in malignancy, facilitating carcinogenesis and/or human cancers progression. Thus, disruption of either of these processes is strongly observed in almost all human malignancies, including prostate, breast, ovarian, pancreatic and esophageal cancers (8, 10, 11).

It has been demonstrated that alteration of DNAm_{et} as well as histone modification status, in prostate cancer, influences an extensive number of genes involved in cell migration, polarity and metastasis (11, 12). Cluster of differentiation H1 gene cadherin 1 (*CDH1*), as a hallmark of epithelial-mesenchymal transition (EMT) event, is mostly repressed by various epigenetic mechanisms. This phenomenon causes a shift from epithelial to mesenchymal phenotype in tumor cells with high potential of invasion and metastasis (13). Thus far, several studies have been performed on the epigenetic

status of particular EMT involved genes, including *CDH1* in prostate cancer cell lines, patients' sample tissues and prostate cancer stem cells (PCSCs) individually (14). However, most of them just focused in one aspect of epigenetic regulation; DNAmethyl or histone modifications. Therefore, more studies are needed to better understand the effect of both DNAmethyl and histone modifications in *CDH1* gene, as an important factor for EMT, in PCSCs or prostate cancer stem like cells (PCSLCs).

In the present study, we enriched the PCSLCs from prostate cancer cell lines using two different methods: particular cell surface markers as well as sphere formation. After characterization of PCSLCs and confirmation of the potency of invasion in PCSLCs, level of DNAmethyl as well as some remarkable histone modification marks was assessed in *CDH1* promoter region.

Materials and Methods

Cell culture

Two human prostate cancer cell lines "prostate stem cell carcinoma (PC3), and human prostate adenocarcinoma cells (LNCaP)" were obtained from National Cell Bank of Iran (NCBI), Pasture Institute, Tehran, Iran. Roswell Park Memorial Institute 1640 (RPMI 1640) and Dulbecco's Modified Eagle Medium (DMEM, both purchased from Gibco, Germany) were used to culture human prostate cell lines. Both media were supplemented with 2 mM glutamine (Gibco, Germany), 100 U/mL of penicillin and 100 µg/mL streptomycin (Gibco, Germany) and 10% fetal bovine serum (FBS, Gibco, Germany). The cells were preserved in 5% CO₂ humidified air and 37°C cell culture incubator.

For sphere culture, 10⁵ cells were plated in T25 flask coated with 12 mg/mL of 2-hydroxyethyl methacrylate (poly-HEMA, Sigma, USA) in 95% ethanol, while the flasks were washed once with phosphate buffer saline (PBS) before cell seeding. The cells were cultured in serum-free medium supplemented with 20 ng/mL epidermal growth factor (EGF) and basic fibroblast growth factor (bFGF, both from Royan Biotech, Iran) for four days. Next, prostate spheres were enzymatically dissociated by Trypsin-EDTA (Invitrogen, USA) and maintained at -70°C for future molecular assessments.

Flowcytometry and cell sorting

Expression of some stem cell related markers, including CD133, CD44, CD49b, CD29 and CD24 (Table S1) (See Supplementary Online Information at www.celljournal.org), were assessed using BD FACS Aria II (Beckman Dickinson, USA) on the indicated prostate cancer cell lines. To minimize non-specific binding, single cell suspensions were treated with blocking solution before staining (30 minutes on ice). To sort the cells, about 5×10⁶ LNCaP or PC3 cells were stained and sorted in RPMI-1640 medium containing 30% FBS. Post-sorting analysis was performed to ensure the purity of sorted sub-populations.

Cell doubling time assessment

PC3, LNCaP and isolated sub-populations were seeded at the concentration of 3×10³ cells/well in the 12-well plates. Quantity of the cells was subsequently counted after 72, 120 and 168 hours. Doubling time was calculated based on " $(T2-T1)/3.32 \times (\log n2 - \log n1)$ ", where T2 is the harvesting time; T1 is seeding time; n2 is the number at harvesting and n1 is the number at seeding time.

Colony formation assay

Briefly, 40 cells of different groups were seeded in each well of 6-well plates. After two weeks culture in the complete RPMI-1640 medium supplemented with 2 mM glutamine (Gibco, Germany), 100 U/mL of penicillin and 100 µg/mL streptomycin (Gibco, Germany) and 10% FBS, number of colonies was counted under the phase-contrast microscope.

Spheroid formation assay

5×10³ cells/well from prostate cancer cell lines and sorted cells were seeded into 6-well ultra-low attachment plates, in serum-free media supplemented with 20 ng/mL EGF and bFGF. The sphere quantity was subsequently counted after 14 days of growth, using phase contrast microscope.

Quantitative reverse transcription polymerase chain reaction analysis

The expression of stemness related genes (*OCT4*, *SOX2*, *NANOG*, *c-MYC* and *KLF4*) as well as metastasis related genes (*CDH1* and *CDH2*) were assessed by quantitative reverse transcription polymerase chain reaction (qRT-PCR) in the sorted sub-populations, spheres and parental cells. Briefly, total mRNA was extracted from 2×10⁵ cells with RNeasy Mini Kit (Qiagen, Germany) according to the manufacturer's instruction. Next, 1 µg of total RNA was reverse transcribed by RevertAid™ H Minus First Strand cDNA Synthesis Kit (Fermentase, USA). Relative qRT-PCR was performed applying cDNA, Power SYBR Green mastermix (Applied Biosystems, USA) and related primers in a 7500 Real-Time PCR System (Applied Biosystems, USA). Glyceraldehyde-3-phosphatedehydrogenase (*GAPDH*) specific primers were applied as internal control, in this experiment. The sequences of forward and reverse primers as well as annealing temperatures are listed in Table S2 (See Supplementary Online Information at www.celljournal.org). qRT-PCR was performed triplicate for each biological experiment (n=3). Relative quantification levels were evaluated by 2^{-ΔΔCt}.

Chromatin Immunoprecipitation

Histone modifications of H3K9ac, H3K9me2/3, H3K4me2 and H3K27me3 were analyzed on the regulatory region of *CDH1*, in prostaspheres and parental cells, using chromatin immunoprecipitation quantitative PCR (ChIP-qPCR) technique. In this regards, Orange ChIP kit (Diagenode, Belgium) was used according to

the manufacturer's instruction. Briefly, chromatin derived from 1×10^5 cells was used for each immunoprecipitation reaction. PCR amplification was performed on the DNA recovered from the ChIP samples as well as the respective total chromatin input by using primers listed in Table S2 (See Supplementary Online Information at www.celljournal.org). Next, immunoprecipitated DNA was quantified by real-time PCR, in a 7500 Real-Time PCR system. The data were expressed as a percentage of input DNA associated with the immunoprecipitated DNA relative to a 1/100 dilution of input chromatin.

DNA methylation assay

Bisulfite modification of genomic DNA was performed using EpiTect Bisulfite kit (Qiagen, Germany) according to manufacturer's protocol. Briefly, a total volume of 140 μ L mastermix was made using 1 μ g DNA, 35 μ L DNA protect buffer and 85 μ L bisulfite mixture reagent. The mastermix was respectively incubated at 99°C for 5 minutes, 60°C for 25 minutes, 99°C for 5 minutes, 60°C for 85 minutes, 99°C for 5 minutes and ultimately 60°C for 175 minutes.

Next, methylation status of 17 CpG sites was evaluated in a 210 bp *CDH1* regulatory region, using the following primers:

F: 5'-TTTTAGGTTAGAGGGTTATT-3'

R: 5'-CTCACAAATACTTTACAATTCC-3'

Bisulfite sequencing PCR (BSP) was performed in a total volume of 20 μ L, composed of 57- μ L of converted DNA, 10 pmol of each forward and reverse primers, 1.5 U AmpliTaq Gold Polymerase, 10x PCR reaction buffer (containing 15 mM MgCl₂ and 0.2 mM of each dNTP), using an initial denaturation at 95°C for 10 minutes, followed by six cycles of 95°C for 1 minute, 57°C for 1 minute, 72°C for 1 minute and 34 cycles of 95°C for 45 seconds, 53°C for 30 seconds, 72°C for 40 seconds, terminated by incubation at 72°C for 10 minutes. The PCR products were analyzed in a 2% agarose gel, and the desired size was purified. The fragment was subsequently cloned in Top-10 using InsTA Clone PCR Cloning Kit (Thermo Fisher Scientific, USA). 12 positive clones per sample were selected and prepared for colony-PCR using general M13 primers. The purified products were ultimately sequenced with M13 primers in an ABI 3130-Avant automated sequencer (Applied Biosystems, USA), followed by alignment and analysis in Chromas (Technelysium Pty Ltd, Australia).

Statistical analysis

Data were analyzed by one-way ANOVA using SPSS software. The data are presented as mean \pm SD of three different replicates. A threshold of $P < 0.05$ were considered statistically significant different.

Results

Enrichment and characterization of PCSLCs derived from PC3 and LNCaP

To enrich cancer stem-like cells, protein expression of the identified markers for PCSCs "CD44, CD133, CD29, CD49b and CD24" were firstly examined by FACS in both

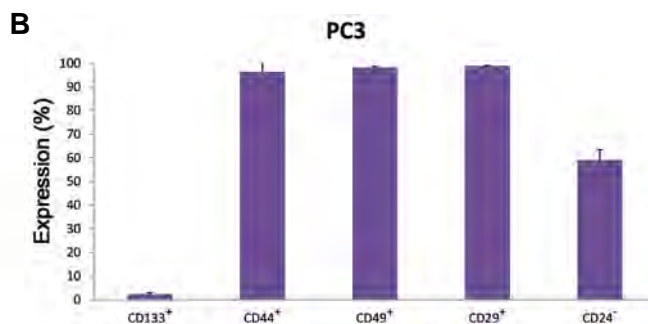
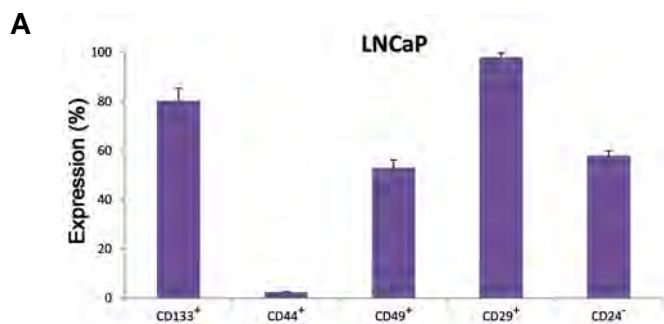
PC3 and LNCaP cell lines. We found that 80% of LNCaP cells expressed CD133, while only 3% of them were positive for CD44 (Fig.1A). In contrast, almost all (about 100%) of the PC3 cells were positive for CD44 as well as CD49b, and only about 3% of them expressed CD133 (Fig.1B). Both lines were positive for CD29 and about 60% of these cells were negative for CD24. With regards to expression of the aforementioned surface markers (Fig.1C, D), LNCaP was sorted upon co-expression of CD133 and CD49b in four different groups: CD133⁺/CD49b⁺, CD133⁺/CD49b⁻, CD133⁻/CD49b⁺ and CD133⁻/CD49b⁻, none of which had difference in doubling time and cell growth (Data are not shown). They were subsequently sorted only according to expression of CD133 (Fig.1E). PC3 cells were also sorted based on co-expression of CD44 and CD49b in two different groups: CD44⁺/CD49b^{high} and CD44⁺/CD49b^{low} (Fig.1F). Purity of the isolated populations was generally more than 90% in each group.

To characterize the sorted cells, obtained from LNCaP and PC3, cell growth as well as colony (under diluted conditions) and spheroid (in serum-free medium under low attachment culture conditions) formation capacities were tested. Our findings demonstrated no significant difference in the cell growth and sphere formation ability in unsorted, CD133⁺ and CD133⁻ cells isolated from LNCaP (doubling time: 22.6, 22.37 and 22.09 hours, respectively, $P \geq 0.05$, Fig.2A, C). However, these abilities were higher in CD44⁺/CD49b^{high} and PC3 unsorted cells, compared to CD44⁺/CD49b^{low} (doubling time in unsorted and CD44⁺/CD49b^{high} cells was 32.025 and 29.685 hours, respectively, $P < 0.004$). Meanwhile, unsorted cells and CD44⁺/CD49b^{high} showed approximately 12.6 ± 1.1 fold increase in spheroid formation than CD44⁺/CD49b^{dim} ($P < 0.05$, Fig.2B, D).

Morphologically spheroids derived from LNCaP were large, round shape and tightly packed (Fig.2E), whereas the PC3 spheroids were grapes-like, loosely packed containing fewer cells (Fig.2F).

The results of colony formation assay revealed that LNCaP, PC3 and their relevant sorted groups yielded a mixture of colony morphologies after 6-7 days of culture, classified as holoclones, meroclones and paraclones. The holoclones were round shape and large in size with tightly packed small cells, whereas paraclones had irregular shape and comprised of loosely packed flattened and scattered cells. Meroclones were intermediate in terms of the size and number, while they were mixture of holoclones and paraclones (Fig.3A). There was no significant difference in colony forming efficiency between unsorted, CD133⁺ and CD133⁻ LNCaP cells (Fig.3B). In PC3, the CD44⁺/CD49b^{high} cells were more capable to form holoclones (30.3%) and meroclones (21.95%), compared to CD44⁺/CD49b^{low} (with a respective rate of 0.27 and 2.81%) as well as unsorted PC3 cells with a range of 2.87 and 11.25%, respectively (Fig.3C).

Taken together, these data demonstrated that CD133 was not specific marker for identification of PCSCs in LNCaP line. While the PC3 CD44⁺/CD49b^{high} sub-population revealed cancer stem-like properties. Therefore, we selected PC3 cells for further analysis from molecular aspect.



C

Expression	% (Mean ± SD)
CD133 ⁺ /49b ⁻	44.88 ± 2.55
CD133 ⁺ /49b ⁺	49.74 ± 3.96
CD133 ⁻ /49b ⁻	4.9 ± 1.38
CD133 ⁻ /49b ⁺	9.4 ± 4.69
CD133 ⁺ /29 ⁺	20.08 ± 2.10
CD133 ⁺ /29 ⁻	78.99 ± 1.83
CD133 ⁻ /29 ⁻	0.42 ± 0.23
CD133 ⁻ /29 ⁺	0.47 ± 0.33
CD133 ⁺ /24 ⁻	54.34 ± 1.33
CD133 ⁺ /24 ⁺	25.15 ± 0.39
CD133 ⁻ /24 ⁻	7.48 ± 0.46
CD133 ⁻ /24 ⁺	13.02 ± 0.48
CD133 ⁺ /44 ⁺	0.42 ± 0.4
CD133 ⁺ /44 ⁻	1.38 ± 0.37
CD133 ⁻ /44 ⁻	23.27 ± 2.49
CD133 ⁻ /44 ⁺	75.60 ± 5.03

Expression	% (Mean ± SD)
CD44 ⁺ /49b ⁻	1.93 ± 0
CD44 ⁺ /49b ⁺	2.01 ± 0.91
CD44 ⁻ /49b ⁻	38.03 ± 7.84
CD44 ⁻ /49b ⁺	58.67 ± 9.73
CD44 ⁺ /29 ⁺	95.55 ± 3.23
CD44 ⁺ /29 ⁻	1.54 ± 0.31
CD44 ⁻ /29 ⁻	1.12 ± 0.71
CD44 ⁻ /29 ⁺	0.07 ± 0.098
CD44 ⁺ /24 ⁻	0.39 ± 0.007
CD44 ⁺ /24 ⁺	2.95 ± 1.32
CD44 ⁻ /24 ⁻	52.67 ± 6.7
CD44 ⁻ /24 ⁺	42.88 ± 3.81
CD29 ⁺ /49b ⁻	51.17 ± 1.95
CD29 ⁺ /49b ⁺	47.71 ± 2.75
CD29 ⁻ /49b ⁻	1.08 ± 0.77
CD29 ⁻ /49b ⁺	0.03 ± 0.028

D

Expression	% (Mean ± SD)
CD133 ⁺ /49b ⁻	0.05 ± 0.07
CD133 ⁺ /49b ⁺	1.75 ± 1.06
CD133 ⁻ /49b ⁻	1.75 ± 0.07
CD133 ⁻ /49b ⁺	96.5 ± 0.99
CD133 ⁺ /29 ⁺	96.85 ± 1.20
CD133 ⁺ /29 ⁻	3 ± 1.34
CD133 ⁻ /29 ⁻	0.125 ± 0.17
CD133 ⁻ /29 ⁺	-
CD133 ⁺ /24 ⁻	0.69 ± 0.73
CD133 ⁺ /24 ⁺	1.57 ± 0.73
CD133 ⁻ /24 ⁻	58.2 ± 1.74
CD133 ⁻ /24 ⁺	39.54 ± 3.20
CD133 ⁺ /44 ⁺	97.15 ± 0.28
CD133 ⁺ /44 ⁻	2.575 ± 0.53
CD133 ⁻ /44 ⁻	0.25 ± 0.28
CD133 ⁻ /44 ⁺	-

Expression	% (Mean ± SD)
CD44 ⁺ /49b ⁻	0.57 ± 0.44
CD44 ⁺ /49b ⁺	90.73 ± 6.2
CD44 ⁻ /49b ⁻	1.78 ± 2.5
CD44 ⁻ /49b ⁺	8.4 ± 4.18
CD44 ⁺ /29 ⁺	0.1 ± 0.14
CD44 ⁺ /29 ⁻	99.75 ± 0.28
CD44 ⁻ /29 ⁻	0.05 ± 0.07
CD44 ⁻ /29 ⁺	0.125 ± 0.17
CD44 ⁺ /24 ⁻	58.8 ± 2.43
CD44 ⁺ /24 ⁺	41.11 ± 2.47
CD44 ⁻ /24 ⁻	0.09 ± 0.04
CD44 ⁻ /24 ⁺	-
CD29 ⁺ /49b ⁻	2.5 ± 1.55
CD29 ⁺ /49b ⁺	97.4 ± 1.41
CD29 ⁻ /49b ⁻	0.15 ± 0.21
CD29 ⁻ /49b ⁺	-

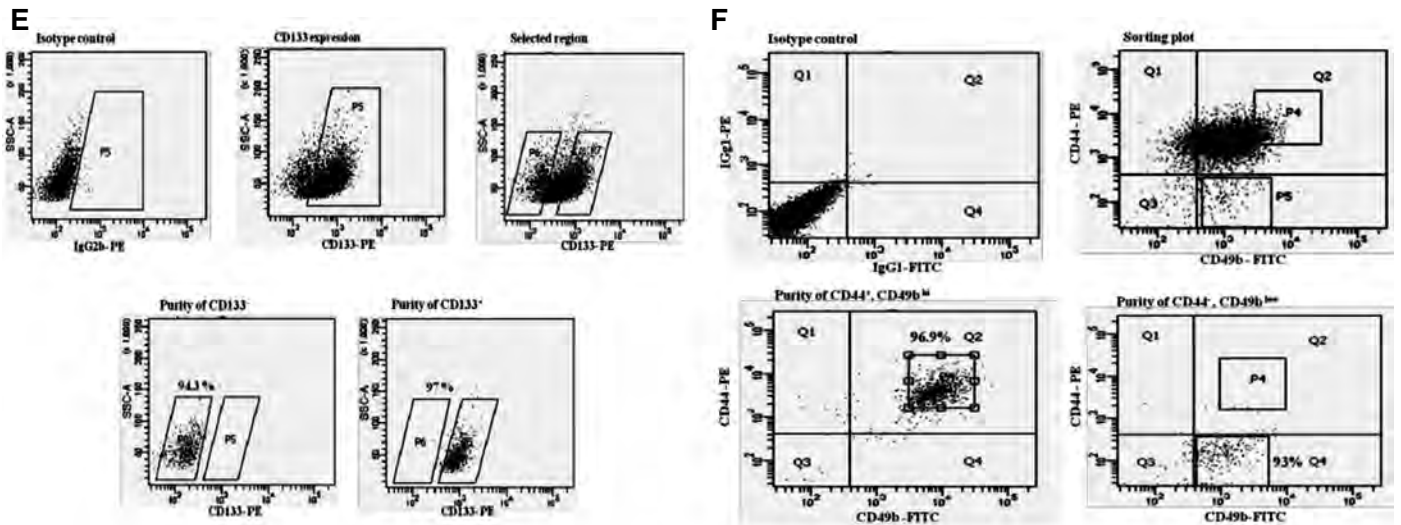
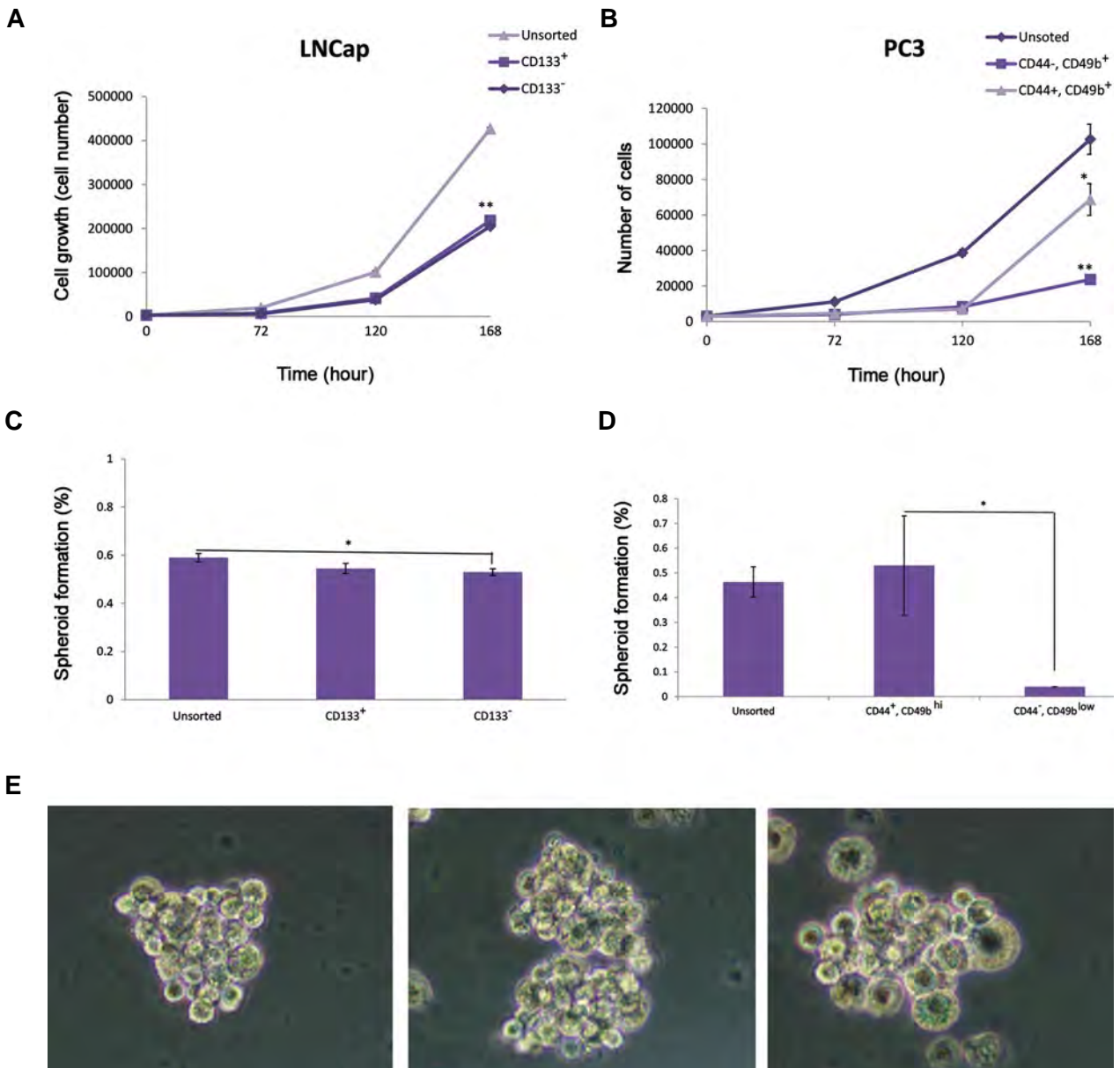


Fig.1: Characterization of prostate cancer stem like cells (PCSLCs). Co-expression of putative stem cell markers in **A, C.** LNCap and **B, D.** PC3 prostate cancer lines. Putative cell surface markers for PCSCs were quantified by immuno-fluorescent cell analysis, using FACS machine, **E.** LNCap cells were sorted based on the expression of CD133 and categorized in two CD133⁺ and CD133⁻ sub-populations, **F.** PC3 cells were sorted according to co-expression of CD44 and CD49b, led to classification of them in two different groups: CD44⁺/CD49b^{high} and CD44⁺/CD49b^{low}.



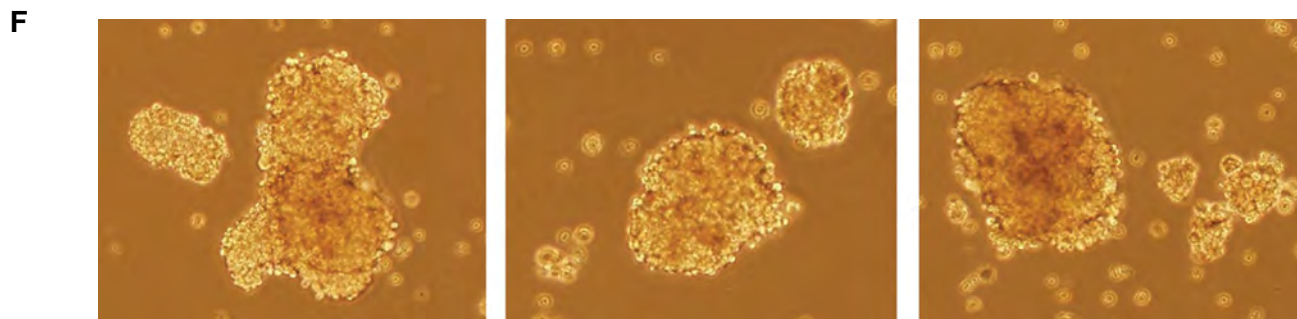


Fig.2: Characterization of the sorted cancer cells based on proliferation rate and ability to form spheres. Cell viability was assessed in **A**. CD133⁺ and CD133⁻ LNCaP cells, **B**. CD44⁺/CD49b^{high} and CD44⁺/CD49b^{low} PC3 cells, compared to unsorted cells by MTT assay during 168 hours of culture. Sphere formation capacity were evaluated on serum free medium supplemented with basic fibroblast growth factor (bFGF), epidermal growth factor (EGF) and B27 in low attach culture dishes in **C**. LNCaP sorted cells, **D**. PC3 cells (n=3, *, P<0.05, **, P<0.01). Morphology of spheroids derived from **E**. LNCaP (scale bar: 50 μm), and **F**. PC3 sorted cells and parental cells (scale bar: 50 μm).

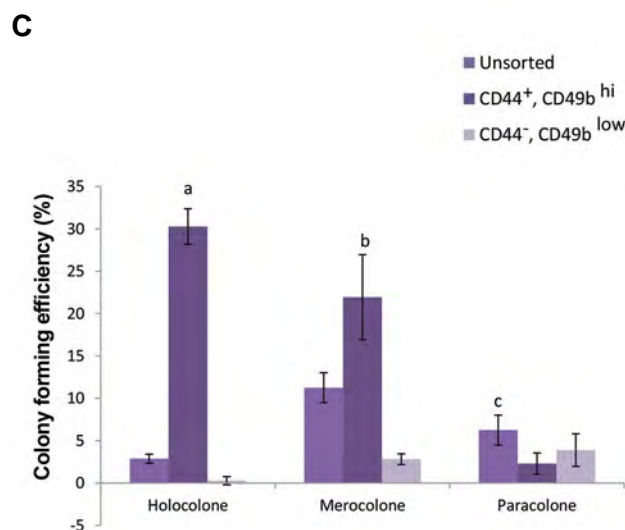
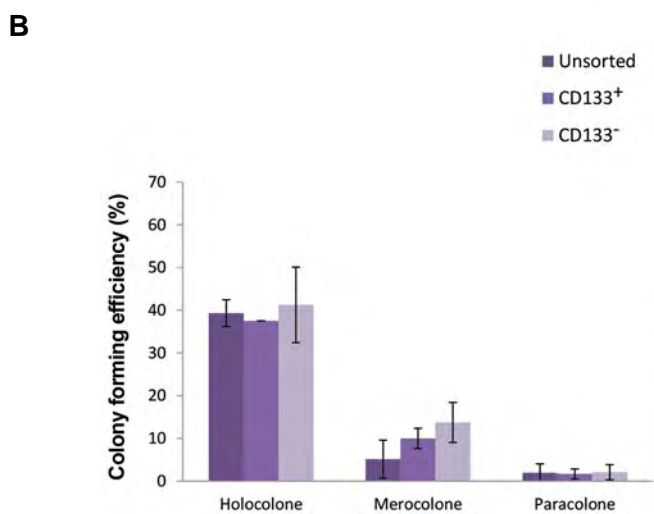
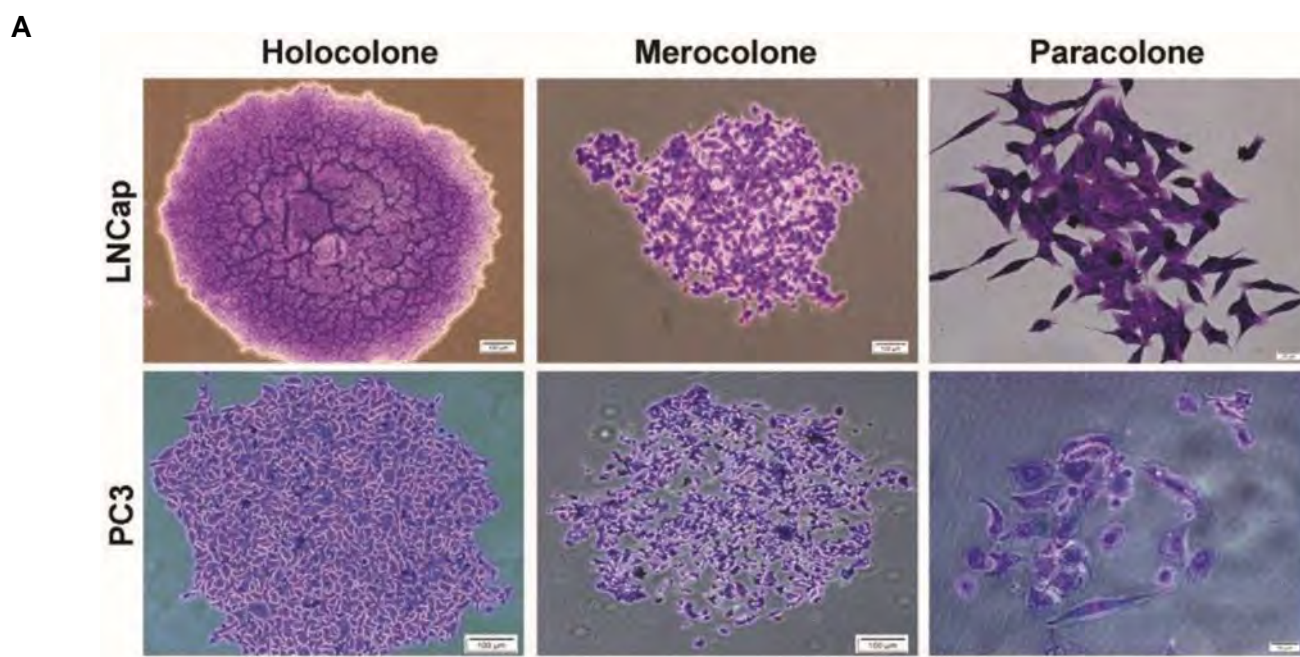


Fig.3: Colony forming efficiency of PC3 and LNCaP sorted cells. **A**. Images show phase-contrast micrographs of the stained colonies with crystal violet, **B**. Graphs represent the frequency of holocolones, merocolones and paracolones in LNCaP, and **C**. PC3 and their sorted groups after 14 days of culture. The frequency of each type of colonies was determined in three replicate (mean ± SD). a; P<0.001 vs. all, b; P<0.01 vs. all, and c; P<0.05 vs. CD44⁺/CD49b^{high}.

Stemness and EMT related gene expressions in CD44⁺/CD49b^{high} and prostaspheres

The expression of *OCT4*, *SOX2*, *NANOG*, *c-MYC*, *KLF4*, as stemness related genes, as well as *CDH1* and *CDH2*, as EMT related genes, were analyzed in the sorted cells and prostaspheres derived from PC3. All stemness related genes except *c-MYC* were significantly over-expressed in prostaspheres (Fig.4A, P<0.05). Conversely, expression of *c-MYC* was significantly down-regulated

(P=0.007). Most of the stemness related genes were not increased or even contrarily were down-regulated in both sorted cells obtained from PC3 cells (Fig.4A). *CDH1* was strongly down-regulated in PC3-prostaspheres, while their invasion and migration potentials were significantly increased (Fig.4B-E). Interestingly, *CDH1* was over-expressed in CD44⁺/CD49b^{high}, while the respective change was not significant in the counterpart sorted cells (Fig.4B). The changes in N-cadherin gene (*CDH2*) were not significant in neither groups (Fig.4B, P>0.05).

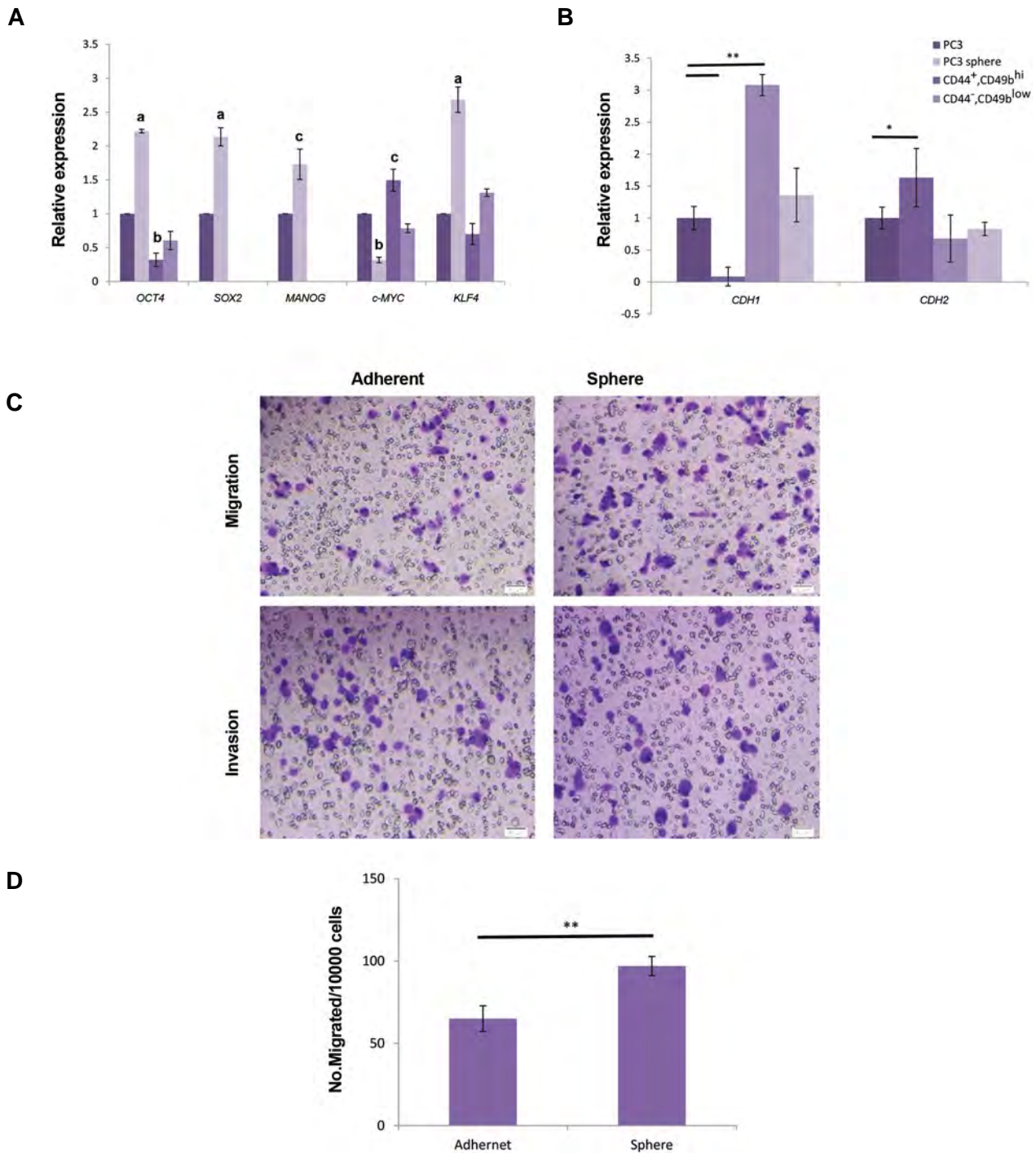


Fig.4: PC3 cancer stem cells (CSC) characterization. **A.** The expression level of stemness related genes, **B.** Important metastasis related genes were assessed by quantitative reverse transcription polymerase chain reaction (qRT-PCR) in PC3 and the respective sub-populations. Expression levels were normalized to Glycerinaldehyde-3-phosphatedehydrogenase (*GAPDH*). a; P≤0.001 vs. all, b; P≤0.01 vs. all, c; P≤0.05 vs. PC3, **, P≤0.01, and *, P≤0.05, **C.** Morphology of the migrated and invaded cells. Quantification of **D.** Migrated, and **E.** Invaded cells (n=3, mean ± SD, **, P≤0.01).

Differential DNA methylation and histone modifications of the *CDH1* promoter in prostaspheres and parental cells

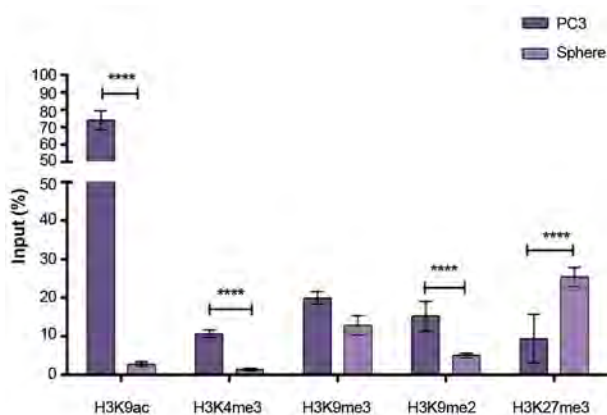
The main purpose of this study was to understand the epigenetic alterations of H3K9ac, H3K9me2/3, H3K4me3 and H3K27me3, as well as DNAm of the *CDH1* regulatory region in the PCSLCs. A significant hyper-acetylation of lysine 9 of histone 3 was observed in the *CDH1* promoter of PC3 cells (Fig.5A). However, this was reduced 40 fold in PC3 spheres. In addition, methylation of histone 3 at lysine 4, representing an open and euchromatin form of the *CDH1* regulatory region, was reduced 10 fold in the PC3 spheres. In contrast, the repressive mark of H3K27me3 was increased 2.5 fold in the spheres ($P < 0.05$). Among the repressive markers of H3K9me2/3, H3K9me2 was reduced significantly ($P < 0.05$), but the change of H3k9me3 was not significant in the PC3 spheres.

The prostaspheres were more hypo-methylated than parental cells, especially in the -83, -103, -105 and -122 bp regions of *CDH1* (Fig.5B, Table 1). Thus, we determined that the latter four CpG regions had maximum effect on the regulation of *CDH1*.

Table 1: Rang of *CDH1* promoter CpG methylation (%) in PC3 spheroids, sorted cells and the parental cells

Group	-122 bp	-105 bp	-103 bp	-83 bp
PC3 Cells	33	58	41	58
CD44 ⁺ /CD49b ⁺	11	22	22	11
CD44 ⁺ /CD49b ⁺	11	22	22	11
Spheroids	0	25	25	8

A



B

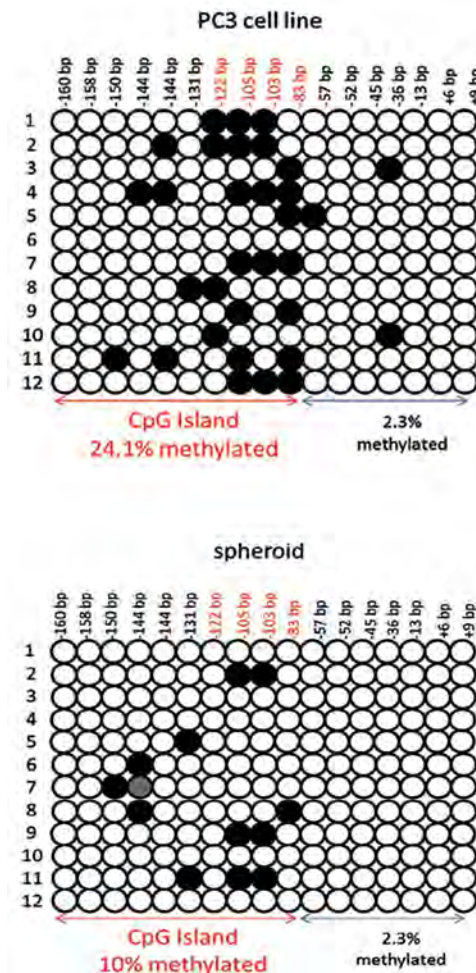


Fig.5: Epigenetic characterization of PC3 cancer stem cells (CSC). **A.** ChIP analysis of histone modifications on the regulatory region of *CDH1* in PC3 spheroids and the respective parental cells. The results are expressed according to a 1/100 dilution of input chromatin and **B.** DNA methylation level of *CDH1* promoter in the PC3 spheroids and its parental cells. Polymerase chain reaction (PCR) was carried out for a CpG island within the promoter. All of the epigenetic data are reported as the mean \pm SD ($n=3$), ****; $P < 0.0001$, and ***; $P < 0.001$.

Discussion

This is the first study on simultaneous evaluation of histone and DNAm for the regulatory region of *CDH1* gene in the PCSLCs. In the first step, we attempted to isolate PCSLCs based on the previously reported stem cell surface markers; however, it was not successful. In fact, the CD133⁺ and CD133⁻ sorted LNCap cells (non-metastatic line) had no significant difference in terms of colony and spheroid formation abilities. Moreover, isolation of CSCs based on the co-expression of CD44 and CD49b in PC3 cells (metastatic line), resulted in more clonogenic with higher number of spheroids in CD44⁺/CD49b^{high} cells. Nevertheless, no difference on the ability of colony and sphere formations as well as stemness related gene expressions were determined between CD44⁺/CD49b^{high} and parental cells.

Although, since 2005, many reports have shown that CD133 alone or in combination with CD44 and/or a2b1

integrin is a stem like population marker and it is used for isolation of PCSCs (15, 16), some experimental models have shown that cells expressing those markers are not appropriately enriched in stem cell population of prostate cancer (17, 18). Therefore, we suggest that determining only cell surface markers could not be an authentic method for isolating CSCs from prostate cancer lines. This is indeed consistent with previous reports in the other cancer types (19). It has been reported that cell surface markers could easily be changed based on cell density, number of passages, pH of the culture medium and length of culture. Thus, in long term passaging some of the cell surface markers are diminished (20). Isolation of CSCs, using cell surface marker, might be favorable in patient's tumor biopsies or tumor primary cultures.

The other approach to enrich CSCs from cell lines or tumor biopsies is sphere formation. CSCs are the only cells with an ability of proliferation in serum free culture and non-anchorage dependent way (21). Our preliminary results revealed that PC3-spheres are clonogenic and able to migrate as well as extravasate from matrigel layer *in vitro*.

In advanced human prostate tumors, expression of *CDH1* is strongly reduced. The initial evidences indicated that DNA hyper-methylation could inactivate *CDH1* (22, 23). Curiously, other study later demonstrated that changes in histone modifications, rather than DNAmeth, may be the predominant factor in reactivation of *CDH1* expression (23, 24) in cancers. Moreover, genome wide mapping of DNAmeth demonstrated that most robust CpG island promoters are unmethylated, even in the gene inactive status. In contrast, low CpG content promoters are largely methylated, while this methylation does not prevent gene expression (25). All of these findings provide that notion of epigenetic regulation complexity based on histone modification and DNAmeth is far from what yet understood. Thus far, no study has been performed in the context of both histone modification and DNAmeth, in regulatory site of *CDH1* in PCSCs. In line with previous studies, our results demonstrated that upon CSC enrichment, the expression of *CDH1* was reduced and these isolated cells represented more aggressive fate, resulted in higher potential of migration and invasion *in vitro*. DNAmeth analysis showed significant hypo-methylation of *CDH1* promoter CpG site. Among chromatin remodeling factors, reduction in the canonical epigenetic marks of transcription initiation (H3K4me3 and H3K9me3) and enhancement in the repressive mark H3K27me3 was observed in prostaspheres derived from PC3 cells. Although, DNA promoter hyper-methylation was previously reported as the principle epigenetic cause of silencing *CDH1* (22, 26, 27), other studies highlight that H3K27me3 activity plays more important role in *CDH1* repression (28). Considering that DNAmeth event generally

happens in the repressed gene promoter regions of normal cells, Ke et al. (24) reported low correlation between DNAmeth and gene silencing of EMT related genes in prostate cancer.

In this context, several possible mechanisms might be involved for *CDH1* gene silencing of prostaspheres. Firstly, methylation could gradually be lost over the sphere formation, as CSLCs in culture grow earlier than methylation and it can be copied from the replicating parental DNA, resulting in progressive loss of DNAmeth (29-32). Secondly, *CDH1* gene silencing is influenced by both DNAmeth and chromatin remodeling factors, with an attention toward the latter factors. Thus, the effect of H3K9ac and H3K4me3, as two activating markers, and H3K27me3, as repressing marker, is stronger than DNA hypo/hyper-methylation in gene expression. It is proposed that DNAmeth is a strong silencing mark, while the genes are modified by only DNA methyl transferases (DNMTs), without concomitant of H3K4me3. In this respect, it appears that DNAmeth of promoters could just slightly contribute in gene repression. Thirdly, it is proposed that both DNAmeth and H3K4me3 have similar complementary effect on some gene expressions. Consistent with this, several studies have demonstrated that individual activity of DNAmeth, in absence of H3K4me3, suppressed gene transcription, while this effect was slightly reduced in combination of DNA and H3K4 methylations (24, 33). In addition, investigations revealed that increased H3K4me3 caused several gene up-regulations during EMT, while they were down-regulated with H3K4me3 reduction. Controversy effect of H3K27me3 is observed in gene regulation; whereby most of the genes with increased H3K27me3 were under-expressed through EMT process, while genes with decreased H3K27me3 were up-regulated. However, no significant correlation was observed between DNAmeth and gene expression levels throughout EMT (24). Previously, genome-wide analyses of H3K4me3 and H3K27me3 showed a strong correlation between H3K4me3 gene expression, in addition to the correlation of H3K27me3 activity, and gene repression in embryonic stem cells (34-37), T-cells (38) hematopoietic stem cells/progenitor cells (39) as well as prostate cancer cells (40). Fourthly, it has been hypothesized that bivalent H3K4me3/K27me3 is a repressive mark and H3K4me3/DNAmeth is an activation mark in prostate cells. Interestingly, investigations implicated that the marked genes with H3K4me3/DNAmeth are preferentially active (24) which suggests a misleading conclusion in the case of predicting gene expression based only on the activity of DNA methylated without considering H3K4me3 modification.

Conclusion

These findings indicate the complicated epigenetic regulation of the *CDH1* promoter at prostaspheres,

as a model of PCSLCs. In *CDHI* promoter region of these spheres, H3K27me₃ was enhanced. In contrast, three histone modification marks (H3K9ac, H3K4me₃, H3K9me₂) and DNAm_{et} were reduced, despite down-regulation of the respective gene. This finding correlated with enhancement of metastasis potential and accumulation of malignant features. In this model, we suggested that slight decrease of DNAm_{et} of the CpG island in *CDHI* promoter does not significantly contribute to the change of *CDHI* expression. Therefore, histone modifications are responsible in repressing *CDHI* expression in PCSLCs.

Authors' Contributions

F.Sh., M.M., P.Kh., J.F.; Performed the experiments, participated in data collection and evaluation. M.Sh., M.E., N.M., M.T.; Participated in study design, contributed extensively in interpretation of the data and the conclusion. V.E.; Made discussions and participated in writing and editing the manuscript. All authors read and approved the final manuscript.

Acknowledgements

This study was funded by Royan Institute (Grant No. 90221800 and 9022070). We thank the collaboration and valuable help of Azam Samadian as molecular laboratory technician and Atefeh Safarpour for completing some experiments. None of the authors have any financial, consultant, institutional and other relationship that might lead to bias or conflict of interest for the information contained on the present manuscript.

References

- Chen K, Huang YH, Chen JL. Understanding and targeting cancer stem cells: therapeutic implications and challenges. *Acta Pharmacol Sin.* 2013; 34(6): 732-740.
- Doherty MR, Smigiel JM, Junk DJ, Jackson MW. Cancer stem cell plasticity drives therapeutic resistance. *Cancers (Basel)*. 2016; 8(1). pii: E8.
- Portillo-Lara R, Alvarez MM. Enrichment of the cancer stem phenotype in sphere cultures of prostate cancer cell lines occurs through activation of developmental pathways mediated by the transcriptional regulator Δ Np63 α . *PLoS One.* 2015; 10(6): e0130118.
- Leon G, MacDonagh L, Finn SP, Cuffe S, Barr MP. Cancer stem cells in drug resistant lung cancer: Targeting cell surface markers and signaling pathways. *Pharmacol Ther.* 2016; 158: 71-90.
- Cao L, Zhou Y, Zhai B, Liao J, Xu W, Zhang R, et al. Sphere-forming cell subpopulations with cancer stem cell properties in human hepatoma cell lines. *BMC Gastroenterol.* 2011; 11: 71.
- Gangavarpu KJ, Huss WJ. Isolation and applications of prostate side population cells based on dye cycle violet efflux. *Curr Protoc Toxicol.* 2011; Chapter 22: Unit 22.2.
- Garnis C, Buys TP, Lam WL. Genetic alteration and gene expression modulation during cancer progression. *Mol Cancer.* 2004; 3: 9.
- Sharma S, Kelly TK, Jones PA. Epigenetics in cancer. *Carcinogenesis.* 2010; 31(1): 27-36.
- Handy DE, Castro R, Loscalzo J. Epigenetic modifications: basic mechanisms and role in cardiovascular disease. *Circulation.* 2011; 123(19): 2145-2156.
- Baylin SB, Ohm JE. Epigenetic gene silencing in cancer - a mechanism for early oncogenic pathway addiction? *Nat Rev Cancer.* 2006; 6(2): 107-116.
- Ngollo M, Dagdemir A, Karsli-Cepioglu S, Judes G, Pajon A, Penault-Llorca F, et al. Epigenetic modifications in prostate cancer. *Epigenomics.* 2014; 6(4): 415-426.
- Muñoz P, Iliou MS, Esteller M. Epigenetic alterations involved in cancer stem cell reprogramming. *Mol Oncol.* 2012; 6(6): 620-636.
- Berx G, van Roy F. Involvement of members of the cadherin superfamily in cancer. *Cold Spring Harb Perspect Biol.* 2009; 1(6): a003129.
- Liang L, Sun H, Zhang W, Zhang M, Yang X, Kuang R, et al. Meta-analysis of EMT datasets reveals different types of EMT. *PLoS One.* 2016; 11(6): e0156839.
- Jaworska D, Król W, Szliszka E. Prostate cancer stem cells: research advances. *Int J Mol Sci.* 2015; 16(11): 27433-27449.
- Miki J, Furusato B, Li H, Gu Y, Takahashi H, Egawa S, et al. Identification of putative stem cell markers, CD133 and CXCR4, in hTERT-immortalized primary nonmalignant and malignant tumor-derived human prostate epithelial cell lines and in prostate cancer specimens. *Cancer Res.* 2007; 67(7): 3153-3161.
- Wei X, Orjalo AV, Xin L. CD133 does not enrich for the stem cell activity in vivo in adult mouse prostates. *Stem Cell Res.* 2016; 16(3): 597-606.
- Harris KS, Kerr BA. Prostate Cancer Stem Cell Markers Drive Progression, Therapeutic Resistance, and Bone Metastasis. *Stem Cells Int.* 2017; 2017: 8629234.
- Roudi R, Madjd Z, Ebrahimi M, Samani FS, Samadikuchak-saraei A. CD44 and CD24 cannot act as cancer stem cell markers in human lung adenocarcinoma cell line A549. *Cell Mol Biol Lett.* 2014; 19(1): 23-36.
- Pellacani D, Packer RJ, Frame FM, Oldridge EE, Berry PA, Labarthe MC, et al. Regulation of the stem cell marker CD133 is independent of promoter hypermethylation in human epithelial differentiation and cancer. *Mol Cancer.* 2011; 10: 94.
- Fan X, Liu S, Su F, Pan Q, Lin T. Effective enrichment of prostate cancer stem cells from spheres in a suspension culture system. *Urol Oncol.* 2012; 30(3): 314-318.
- Yoshiura K, Kanai Y, Ochiai A, Shimoyama Y, Sugimura T, Hirohashi S. Silencing of the E-cadherin invasion-suppressor gene by CpG methylation in human carcinomas. *Proc Natl Acad Sci USA.* 1995; 92(16): 7416-7419.
- Li LC, Carroll PR, Dahiya R. Epigenetic changes in prostate cancer: implication for diagnosis and treatment. *J Natl Cancer Inst.* 2005; 97(2): 103-115.
- Ke XS, Qu Y, Cheng Y, Li WC, Rotter V, Øyan AM, et al. Global profiling of histone and DNA methylation reveals epigenetic-based regulation of gene expression during epithelial to mesenchymal transition in prostate cells. *BMC Genomics.* 2010; 11: 669.
- Weber M, Hellmann I, Stadler MB, Ramos L, Paabo S, Rebhan M, et al. Distribution, silencing potential and evolutionary impact of promoter DNA methylation in the human genome. *Nat Genet.* 2007; 39(4): 457-466.
- Cedar H, Bergman Y. Linking DNA methylation and histone modification: patterns and paradigms. *Nat Rev Genet.* 2009; 10(5): 295-304.
- Esteller M. Cancer epigenomics: DNA methylomes and histone-modification maps. *Nat Rev Genet.* 2007; 8(4): 286-298.
- Cao Q, Yu J, Dhanasekaran SM, Kim JH, Mani RS, Tomlins SA, et al. Repression of E-cadherin by the polycomb group protein EZH2 in cancer. *Oncogene.* 2008; 27(58): 7274-7284.
- Santourlidis S, Florl A, Ackermann R, Wirtz HC, Schulz WA. High frequency of alterations in DNA methylation in adenocarcinoma of the prostate. *Prostate.* 1999; 39(3): 166-174.
- Menendez L, Benigno BB, McDonald JF. L1 and HERV-W retrotransposons are hypomethylated in human ovarian carcinomas. *Mol Cancer.* 2004; 3: 12.
- Schulz WA, Hatina J. Epigenetics of prostate cancer: beyond DNA methylation. *J Cell Mol Med.* 2006; 10(1): 100-125.
- Ting DT, Lipson D, Paul S, Brannigan BW, Akhavanfard S, Coffman EJ, et al. Aberrant overexpression of satellite repeats in pancreatic and other epithelial cancers. *Science.* 2011; 331(6017): 593-596.
- Li X, Wang X, He K, Ma Y, Su N, He H, et al. High-resolution mapping of epigenetic modifications of the rice genome uncovers interplay between DNA methylation, histone methylation, and gene expression. *Plant Cell.* 2008; 20(2): 259-276.
- Bernstein BE, Mikkelsen TS, Xie X, Kamal M, Huebert DJ, Cuff

- J, et al. A bivalent chromatin structure marks key developmental genes in embryonic stem cells. *Cell*. 2006; 125(2): 315-326.
35. Mikkelsen TS, Ku M, Jaffe DB, Issac B, Lieberman E, Giannoukos G, et al. Genome-wide maps of chromatin state in pluripotent and lineage-committed cells. *Nature*. 2007; 448(7153): 553-560.
36. Zhao XD, Han X, Chew JL, Liu J, Chiu KP, Choo A, et al. Whole-genome mapping of histone H3 Lys4 and 27 trimethylations reveals distinct genomic compartments in human embryonic stem cells. *Cell Stem Cell*. 2007; 1(3): 286-298.
37. Dahl JA, Reiner AH, Klungland A, Wakayama T, Collas P. Histone H3 lysine 27 methylation asymmetry on developmentally-regulated promoters distinguish the first two lineages in mouse preimplantation embryos. *PLoS One*. 2010; 5(2): e9150.
38. Wei G, Wei L, Zhu J, Zang C, Hu-Li J, Yao Z, et al. Global mapping of H3K4me3 and H3K27me3 reveals specificity and plasticity in lineage fate determination of differentiating CD4+ T cells. *Immunity*. 2009; 30(1): 155-167.
39. Cui K, Zang C, Roh TY, Schones DE, Childs RW, Peng W, et al. Chromatin signatures in multipotent human hematopoietic stem cells indicate the fate of bivalent genes during differentiation. *Cell Stem Cell*. 2009; 4(1): 80-93.
40. Ke XS, Qu Y, Rostad K, Li WC, Lin B, Halvorsen OJ, et al. Genome-wide profiling of histone h3 lysine 4 and lysine 27 trimethylation reveals an epigenetic signature in prostate carcinogenesis. *PLoS One*. 2009; 4(3): e4687.
-

Preparation and Evaluation of A Novel Liposomal Nano-Formulation in Metastatic Cancer Treatment Studies

Fatemeh Barzegari Firouzabadi, Ph.D.^{1,2*}, Shahrbanoo Oryan, Ph.D.¹, Mohammad Hasan Sheikhha, Ph.D.³,
Seyed Mehdi Kalantar, Ph.D.³, Ameneh Javed, Ph.D.⁴

1. Department of Animal Biology, Faculty of Biological Science, Kharazmi University, Tehran, Iran

2. Departeman of Biology, College of Science, Payame Noor University, Yazd, Iran

3. Reproductive and Genetic Unit, Research and Clinical Center for Infertility, Shahid Sadoughi University of Medical Sciences, Yazd, Iran

4. Department of Biology, Faculty of Science, Science and Art University, Yazd, Iran

*Corresponding Address: P.O.Box: 15719-14911, Department of Animal Biology, Faculty of Biological Science, Kharazmi University, Tehran, Iran
Email: f.barzegary@gmail.com

Received: 6/May/2018, Accepted: 15/August/2018

Abstract

Objective: Today, in clinical trials, we suffer from the lack of effective methods with minimal side effects to deliver medication. Thus, efforts to identify better conditions for delivery of biomedical drugs seem necessary. The purpose of this study was to design a new liposomal formula for transportation of microRNA in osteosarcoma.

Materials and Methods: In this experimental study, several liposomal formulations were synthesized. Physical and chemical parameters, including size, zeta potential, polydispersity index, long-term stability of the liposomal-microRNA complex and the amount of *miR-143* loading in liposome based nano-vesicles were optimized using different techniques. Similarly, the effect of free and encapsulated microRNA toxicity were investigated and compared in a human bone osteosarcoma cell line, named SaOs-2.

Results: In this study, we could produce a novel and optimized formulation of cationic PEGylated liposomal microRNA for gene delivery. The present synthesized microRNA lipoplex system was non-agglomerated. The system remained stable after four months and *miR-143* leakage was not observed by performing gel electrophoresis. The microRNA lipoplex could enhance conduction of the loaded *miR-143*, and it also showed good biocompatibility to the healthy cells.

Conclusion: The PEGylated microRNA lipoplex system had a high potential for the systematic migration of *miR-143* and it could improve intracellular stability of the released microRNA.

Keywords: Cell Survival, Liposome, microRNA, Osteosarcoma

Cell Journal (Yakhteh), Vol 21, No 2, July-September (Summer) 2019, Pages: 135-142

Citation: Barzegari Firouzabadi F, Oryan Sh, Sheikhha MH, Kalantar SM, Javed A. Preparation and evaluation of a novel liposomal nano-formulation in metastatic cancer treatment studies. Cell J. 2019; 21(2): 135-142. doi: 10.22074/cellj.2019.6008.

Introduction

Cancer is a disease in which the cells begin to grow and divide due to the various causes and continuously produce abnormal cells (1). Despite the endless efforts of scientists to treat cancer, there is no therapeutic system yet for the successful treatment of cancer, thus making this disease one of the leading causes of mortality worldwide. Although many molecular factors of this disease have been discovered, it is still very difficult to detect many indirect and direct factors in the development of cancer, and in many cases, providing physicians unable to cure this disease (2, 3).

Several systemic and topical malformations related to bone have turned it into a crucial subject to study. From higher to lower degree, bones could contribute to different diseases, caused by genetic or environmental factors. Bone cancer is a type of malignancy spreading to bone from another cancerous tissue (4, 5). Compared to the metastatic bone cancer, more commonly observed in adolescent, osteosarcoma is a malignant tumor, with childhood and adulthood onset. So that 75% of the patients are less than 20 years old (6, 7). Since osteosarcoma is involved in the community of children and adult

population, it is important to study different treatment approaches for this disease.

Gene therapy is a biological method for treatment of disease through repairing and eliminating gene defects. Gene therapy strives to treat abnormal cells by inserting oligo- or poly-nucleotide fragments. In gene therapy, selecting an appropriate carrier with high transfection efficiency and minimal toxicity is very important. In past, viral carriers were used for gene transfer. Although, viral vectors have high efficiency for gene transfer, potential of oncogenesis ability, high cost and limitations in transported DNA size are some disadvantages of their application. At present, researchers are paying more attention to non-viral polymeric carriers, including liposomes. These carriers have higher biocompatibility than viral types, while they have low level of gene expression (8, 9).

Liposomes are bilayer polymeric vesicles that can be used for loading different biological molecules, including microRNAs. In case of utilizing cationic lipids, the resultant particle would have a positive charge net and the negative charge of the nucleic acids is compensated facilitating cellular absorption. This strategy is used

with high success rate probability for microRNAs, as therapeutic agents for cancer treatment (10). microRNAs include short non-coding RNAs (about 21-25 nucleotides) that are commonly used as inhibitor of target gene mRNAs. This procedure is mainly performed by influencing the stability and translation of mRNAs at post-transcriptional levels. During the past few years, study of microRNAs in human cancers has revealed that many of them act as tumor suppressors (11, 12). *miR-143* is a well-known tumor suppressor that neutralizes tumor progression by regulating a number of oncogenes. It has been shown that *miR-143* prevents tumorigenicity by targeting the *N-RAS* gene in glandular cancer (13) and *COX2* gene in intestinal cancer (14). In the present study, *miR-143* (cancer inhibitor) loaded liposomal system (microRNA lipoplex) was designed and targeted against human bone sarcoma SaOs-2 cell line, in order to obtain a targeted drug delivery system and to reduce the harmful effects of chemotherapeutics.

Materials and Methods

Cell line

Human bone sarcoma SaOs-2 cell line was obtained from the National Cell Bank of Iran (NCBI), Pasteur Institute, Tehran, Iran. Human primary osteoblast (Hum-63 cell line), as short-term culture, were kindly provided by Shahid Sadoughi University of Medical Sciences, Yazd, Iran. Cells were incubated (Matter, Germany) at 37°C and 5% CO₂ in the Dulbecco's Modified Eagle's medium (DMEM, Gibco Invitrogen, Germany), containing fetal bovine serum (FBS, Sigma, USA), augmented with penicillin and streptomycin (both from sigma, USA). After three successive passages, the cells were treated with microRNA lipoplex system. In this research, ethical considerations are approved based on the International Campus of Yazd University of Medical Sciences, Yazd, Iran.

Chemicals

Cholesterol, 1,2-dioleoyl-3-trimethylammonium-propane (DOTAP), 4% paraffinic acid solution and fluorescent label (Dil) were respectively purchased from Sigma-Aldrich and Avanti Polar Lipids (both from USA). Polyethylene glycol (PEG) and dipalmitoyl phosphatidylcholine (DPPC) were purchased from Lipoid (GmbH, Germany). The 4, 6 diamidino-2-phenylindole (DAPI) was purchased from Thermo Fisher, USA. All other chemicals and solvents, used in this study, were of the highest purity and analytical grade. microRNA mimic, *hsa-miR-143* and CY-5 *miR-143* (microRNA conjugate with red fluorescent dye) was purchased from Sigma-Aldrich, USA.

Synthesis of uniform nano-liposomal formulation

Preparation of thin lipid film

In this experimental study, lipid phase consisting of PEG, cholesterol (Chol), DOTAP, DPPC, DSPE-mPEG (2000) and different DOTAP concentrations (0, 30, 40

and 50%), dissolved in chloroform. DOTAP is a cationic phospholipid used in this liposome formulation to generate positive bands in the system. Then, the organic phase of solution was removed using a rotary evaporator and a thin lipid film was formed on the balloon wall. To ensure complete solvent removal, the thin lipid film was aerated for several minutes with nitrogen gas and placed at 4°C for 24 hours.

Hydration of lipid film and reducing the size of liposomal products

The liquid phase for hydration of the thin film was composed of phosphate buffered saline (PBS) with pH=7.4. Immediately after addition of PBS, a milky fluid was formed, which was identical to the multilamellar vesicles (MLV) liposomes. To reduce the size of MLV and small unilamellar vesicles (SUV), the resultant samples were sonicated. To prevent unwanted rise in temperature during sonication, the balloons containing nano-liposomes were placed in an ice container under 60% amplitude for 20 minutes (7 seconds ON and 10 seconds OFF).

Determination of physico-chemical characteristics of nano-liposomes

Determination of particle size distribution

To measure size of the nano-liposomal specimens and liposome-gene complex, the samples were first diluted twice with distilled water (DW). To measure liposomal size, final concentration of the samples was 0.225 mg/ml. Thus at this concentration, liposomal size was not affected by their concentration. In contrast, an error was observed at higher or lower concentrations, due to inaccurate calculation. For that, dilution was performed before size analysis. Hydrodynamic diameter and polydispersity index (PDI) of the specimens was determined by Dynamic Light Scattering (DLS, Brookhaven Corp, USA) at room temperature. All measurements were repeated four times.

Zeta potential measurements

The surface charge and Zeta potential of nano-liposomes was measured using a Zeta Sizer (Brookhaven Instruments, USA) at 25°C. To determine surface charge, 1500 µl samples were used with 0.1 µg/ml concentration. Each parameter was measured thrice.

Morphological evaluations

Shape and surface morphology of the synthesized nano-liposome system were evaluated by Field Emission Scanning Electron Microscopy (FESEM, KYKY-EM3200-30KV, China).

Formulation of microRNA containing lipoplex

For microRNA loading into the cationic nano-liposomes, different ratios of SUV liposome to microRNA were incubated at ambient temperature for 30 minutes. To increase stability time and uniformity of the products, cationic nano-liposomes were filtered five times with the extruder before incubation.

Optimization of microRNA loading into nano-liposomes with agarose gel electrophoresis

To determine optimal dosage of loading microRNA into nano-liposomes, various microRNA and liposomal ratios were casted onto the agarose gel (2%) electrophoresis with ethidium bromide (30 minutes electrophoresis at 80 volts). Briefly, 5 µl of a suspension containing liposome-*miR-143* complex, was combined with 1 µl of loading buffer (Biolabs, UK). Different concentrations of microRNA and liposome were analyzed to determine the most appropriate liposomal concentration for microRNA loading. After completion of agarose electrophoresis, the gel was transferred to gel documentation system (UVP, UK) and the results were analyzed.

Physical stability of lipoplex

Leakage stability

Ability of the lipoplex system to preserve *miR-143* was monitored for 4 months at 4°C, and microRNA leakage from lipoplex was evaluated by electrophoresis.

Stability in mouse serum

To study stability of the designed nano-systems in conditioned *in vitro* environment, the lipoplex was kept in mouse serum (at 37°C) for different time periods (one, two and four hours), then put into 6-well cell culture plates containing SaOs-2 cell line, and placed in the humidified 37°C incubator under 5% CO₂ for 1 hour. The cells were then washed 3 times with PBS and fixed with 4% paraformaldehyde solution (Thermo Fisher Scientific, USA) for 15 minutes. Fluorescence microscope (Olympus, Japan) was employed to observe the samples.

Investigation of cytotoxicity after nano-liposome administration

Hum-63 cells were cultured in 96-well microplates, containing DMEM, modified with 10% FBS, 1% penicillin/streptomycin (Gibco Invitrogen, USA) at 37°C and 5% CO₂. Repeatability, accuracy and sensitivity of the tests were high. MTT assay was used to determine cytotoxicity after 48 and 72 hours of Hum-63 cell treatment with different concentrations of empty liposomes. Plates were placed in incubator for 24, 48 and 72 hours. After each incubation period, the cells were washed twice with PBS and 20 µl of 5 mg/ml MTT (diluted with PBS) and they were added to each well and the plates were incubated for four hours to allow the formazan crystal formation. After completion of four hours incubation, the internal solution of each well was completely removed and 200 µl dimethyl sulfoxide (DMSO) was added to dissolve the crystals. The resultant samples were studied with microplate ELISA reader (Biotek Instruments Inc, USA), and the cell viability percentage was calculated

using the following formula:

$$\% \text{ Viable cells} = \frac{\text{Mean optical absorption in the test group} - \text{Average light absorption in culture medium}}{\text{Mean optical absorption in the control group} - \text{Average light absorption in culture medium}} \times 100$$

Comparative study of the lipoplex system effect

SaOs-2 cells were seeded in 96-well plates for 24 hours to adhere to the plate bottom. The medium was next replaced with fresh culture medium (in control), or treated with a lipoplex complex, free microRNA and empty liposomes. After 72 hours MTT analysis was performed, as stated above and the resultant absorption was recorded at 570 and 630 nm wavelengths.

Investigation of microRNA delivery into bone cancer cells through lipoplex system

Bone cancer SaOs-2 cell line was used to study lipoplex transfection. Firstly, sterile glass lamella was placed inside the wells of a 6-well plate, and the cells were counted and added at the concentration of 5×10^5 cells/well. After 24 hours, the culture medium was drained and the cells were exposed to liposomal CY-5 microRNA, diluted with culture medium. The cells were incubated for 3 hours at 37°C and they were then washed thrice with cold PBS and fixed with paraformaldehyde solution. DAPI solution (125 µg/ml) was used for 15 minutes to stain the cell nuclei. The efficacy of microRNA cell transfection was evaluated using a fluorescence microscope (Olympus, Japan).

Statistical analysis

For statistical analysis of the data, SPSS for Windows was used and the paired t test was used to compare different groups, where $P < 0.05$ was considered statistically significant.

Results

Zeta potential and particle size analysis

Liposomes were prepared with DPPC, cholesterol, DOTAP and DSPE-mPEG. Table 1 shows characteristics of the various formulations, synthesized for carrying microRNA. In addition, Figure 1A shows DLS analysis of optimal formula. According to the results, with increasing DOTAP concentration, surface charge of liposomes is also increased. DOTAP molecule with a positive agent group produced a positive charge in the liposomal structure. In all cases, dispersion index was less than 0.3 which indicates no agglomeration in liposomal particles, and zeta potential was positive, while it was reduced after incubation with microRNA (15-17). PEGylation reduced PDI of liposomes, due to the increase in repulsive force of particles with a positive charge. Additionally, spatial blocking prevented accumulation of the particles (18).

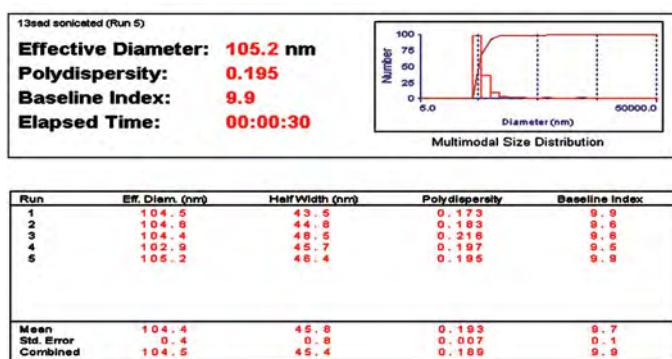
Electron micrograph of nano-liposomes is shown in Figure 1B. SEM micrograph confirmed the size and spherical shape of the newly nano-formulated system.

Table 1: Characterization of liposomal formulations

Code	DPPC (g)	Chol (g)	DOTAP (g)	PEG (g)	Zeta potential (mv)	Size (nm)	PDI	Total volume (ml)
F1	0.0102	0.0023	0	0	-24.33 ± 0.83	148.4 ± 2.4	0.297 ± 0.01	1
F2	0	0.0038	0.0071	0	+38.23 ± 0.33	125.22 ± 2.3	0.230 ± 0.024	1
F3	0.0061	0.0013	0.0061	0	+34.21 ± 0.23	130 ± 1.3	0.202 ± 0.02	1
F4	0.0071	0.0016	0.0046	0	+21.87 ± 1.43	114.67 ± 1.60	0.128 ± 0.01	1
F5	0.0066	0.0015	0.0046	0.0028	+29.32 ± 1.02	119.52 ± 0.8	0.107 ± 0.01	1
F6	0.0068	0.0015	0.0046	0.0016	+27.24 ± 0.21	105.23 ± 0.36	0.109 ± 0.03	1
F6 with microRNA	0.0068	0.0015	0.0046	0.0016	+13.61 ± 0.33	137.45 ± 0.51	0.110 ± 0.02	1

DPPC; 1,2- Dipalmitoyl-sn-glycero-3 phosphocholine, DOTAP; 1,2-dioleoyl-3-trimethylammonium-propane, PEG; DistearoylPhosphoethanolamine (PE 18:0/ 18:0 -PEG2000, DSPE-mPEG 2000), and PDI; Dispersion index.

A



optimal formula. PEG binds to the phospholipid chains and improves liposomal absorption and transportation (19-21). Surface modification of liposomes with PEG also improved biocompatibility and intracellular oligonucleotide stability (21). The length of PEG chain should be optimized to overcome the problems associated with entering as well as escaping the liposomal formulations from endosomal tract, to create a PEG shield. PEGylation process increased the size of nano-liposomal products. Consequently, the presence of PEG in the structure of nano-liposomes was optimal and the PEGylation was kept to 3%.

B

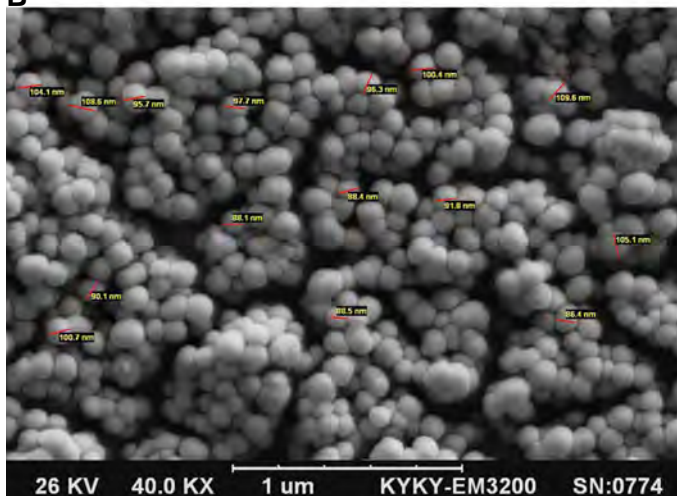


Fig.1: Particle size and SEM microscope analysis. **A.** DLS analysis of optimal formula and **B.** SEM micrograph of the newly formulated nano-liposomes. SEM; Scanning electron microscope and DLS; Dynamic light scattering.

Optimization of microRNA loaded into nano-liposomes with agarose electrophoresis gel

As shown, all of the lipoplex particles with lower than 180/1 µg/µg (liposome/microRNA) concentration had moved along the gel. The concentration of 1 µg microRNA per 180 µg of the loaded liposomes was the highest concentration, remaining in the well and had no movement within the gel (Fig.2B).

Physical stability of nano-lipoplex containing microRNA

To determine the stability of nano-lipoplex containing *miR-143*, amount of leakage and release of microRNA from the nano-vesicles, the complex was stored for four months at -4°C temperature. Within a certain time range, the system containing microRNA was sampled and microRNA leakage was monitored by agarose gel electrophoresis. As shown, the system remained stable after four months, and microRNA leakage was not observed by the gel electrophoresis (Fig.3A).

The stability of nano-lipoplex containing microRNA was studied at various time intervals (one, two and four hours) by subjecting it to mouse plasma, to evaluate the ability of formulated liposome in protecting *miR-143* against degradation (Fig.3B). After one, two and four hours contact with plasma, the nano-lipoplex containing microRNA could successfully be absorbed by SaOs-2 cells. Analysis of fluorescence confirms no significant change in the uptake of microRNA with passage of time.

Investigation of cell survival after liposomal treatment

Cytotoxicity of the various formulations in Hum-63 cells was investigated (Fig.2A). As the results show toxicity was elevated with increasing DOTAP concentration in nano-liposomes. These properties have also been approved within 72 hours of treatment. According to these results, F2 formula has a very good positive charge, while it has a very high toxicity effect on the tested cells; so the formula is not satisfactory. In contrast, F6 formula has both positive charge and low toxicity. Therefore, it was selected as the

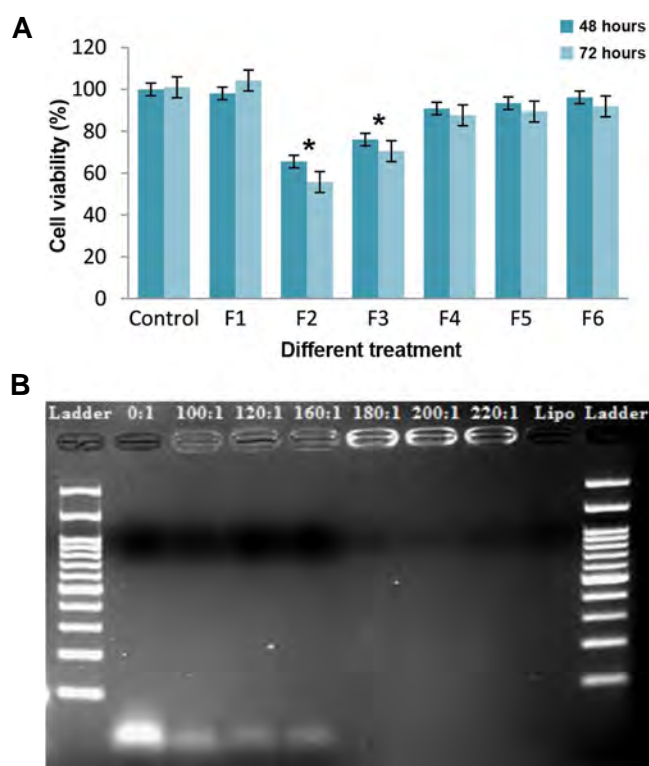


Fig.2: Investigation of cell survival after liposomal treatment and optimization of microRNA loaded into nano-liposomes. **A.** Comparison of the toxicity impact of various empty liposome formulations after 48 and 72 hours in hum-63 cells and **B.** Optimization of loading microRNA into nano-liposomes with agarose gel electrophoresis to determine the maximum effective concentration of liposome (μg)/microRNA (μg). *; $P < 0.05$.

Study the effect of lipoplex containing microRNA system

The toxicity rate of Hum-63 and SaOs-2 cell lines at 72 hour is shown in Figure 4A. The empty nano-liposomes, as shown by the previous cell test, are non-toxic. According to the results, microRNA, either free or encapsulated in the liposome, reduced cell growth, while the liposomal formulation had shown more toxicity, especially in SaOs-2 cells compared to Hum-63 cell. Viability and shape *In vitro* of SaOs-2 bone cancer cells treated with free microRNA or encapsulated microRNA after 72 hours is shown in Figure 4B.

Nano-liposomal microRNA localization assay

Cellular uptake of SaOs-2 cells, treated with free microRNA and liposomal *miR-143*, was studied by fluorescence microscopy. As shown in Figure 5, the cells treated with entrapped microRNA showed greater “red color” intensity compared to treated cells with free microRNA. It is well-known that entrapped microRNA (at nano-scale) could penetrate the cells by endocytosis, whereas the free microRNA molecules (at angstrom-scale) were moved by diffusion mechanism. Results showed that SaOs-2 cell line successfully absorbed the entrapped microRNA.

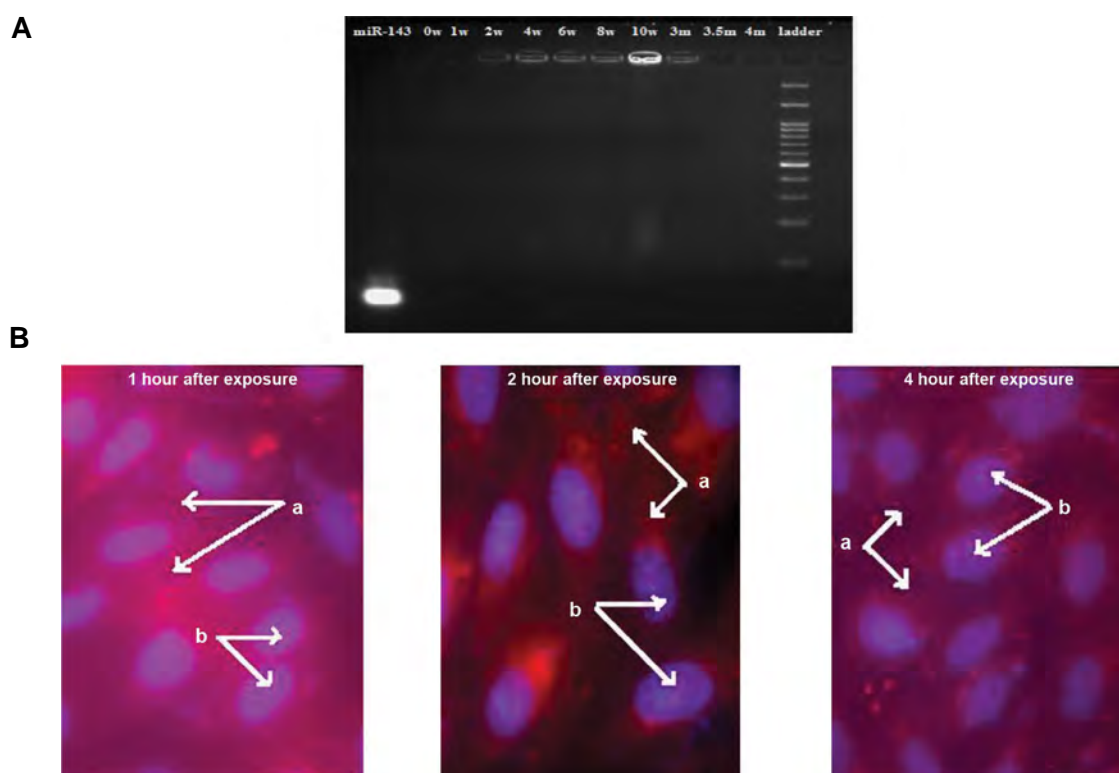


Fig.3: Analysis of the stability test of free microRNA as well as microRNA loaded into lipoplex vesicles and stability of the nano-lipoplex containing microRNA in plasma. **A.** (Right to left): row 1; free microRNA, row 2; lipoplex -immediately after formation, row 3; lipoplex -after one week, row 4; lipoplex -after two weeks, row 5; lipoplex -after four weeks, row 6; lipoplex -after six weeks, row 7; lipoplex -after eight weeks, row 8; lipoplex -after ten weeks, row 9; lipoplex -after three months, row 10; lipoplex -after three and half months, row 11; lipoplex -after four months, row 12; Ladder. w; Week. m; Month and **B.** Nano-lipoplex vesicles were mixed with mouse plasma for one, two and four hours. After this period the SaOs-2 cells were treated with the prepared liposome suspension for one hour at 37°C . *miR-143* was labeled with CY-5 (red) and nucleus was counterstained with DAPI (blue); their merge created a turquoise blue color. a; Liposomal *miR-143* accumulation in the cytoplasm and b; Nuclei stained with DAPI prior to analysis (magnification: $\times 60$).

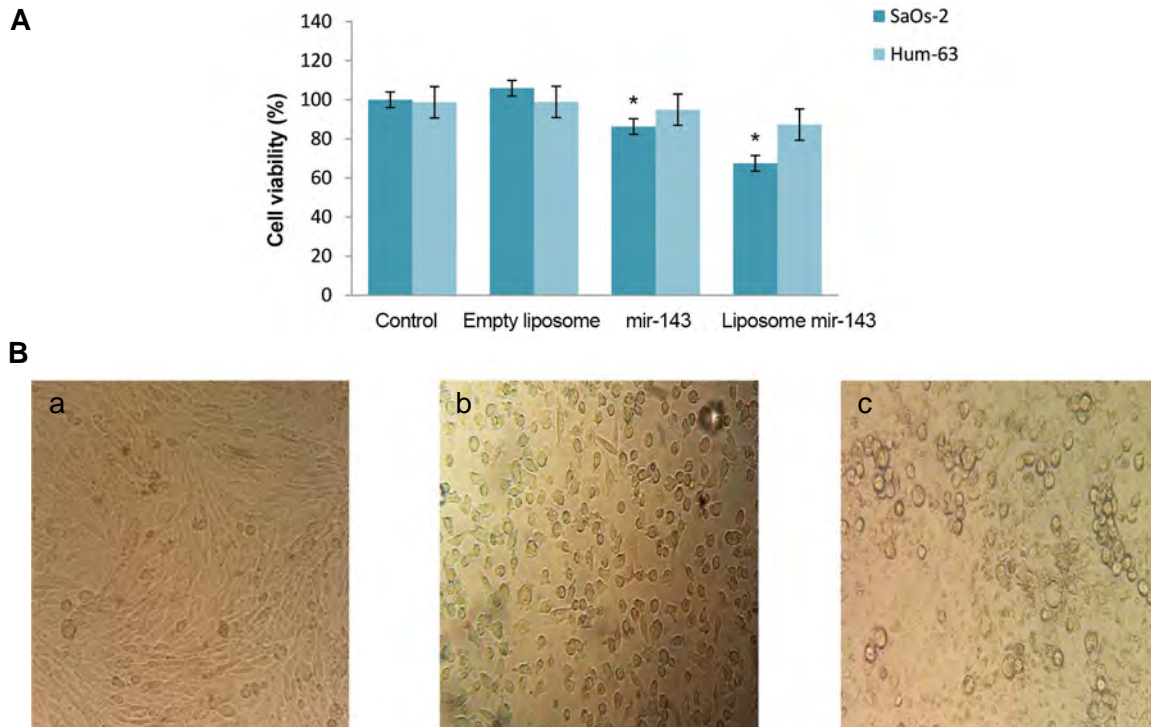


Fig.4: Investigation of lipoplex containing microRNA system effect. **A.** Comparison of free and encapsulated microRNA toxicity after 72 hours, in SaOs-2 and Hum-63 cell lines and **B.** *In vitro* analysis of viability and shape of SaOs-2 cell line. a; With no treatment, b; Treated with free microRNA, and c. Treated with liposomal *miR-143* after 72 hours. *; $P < 0.05$.

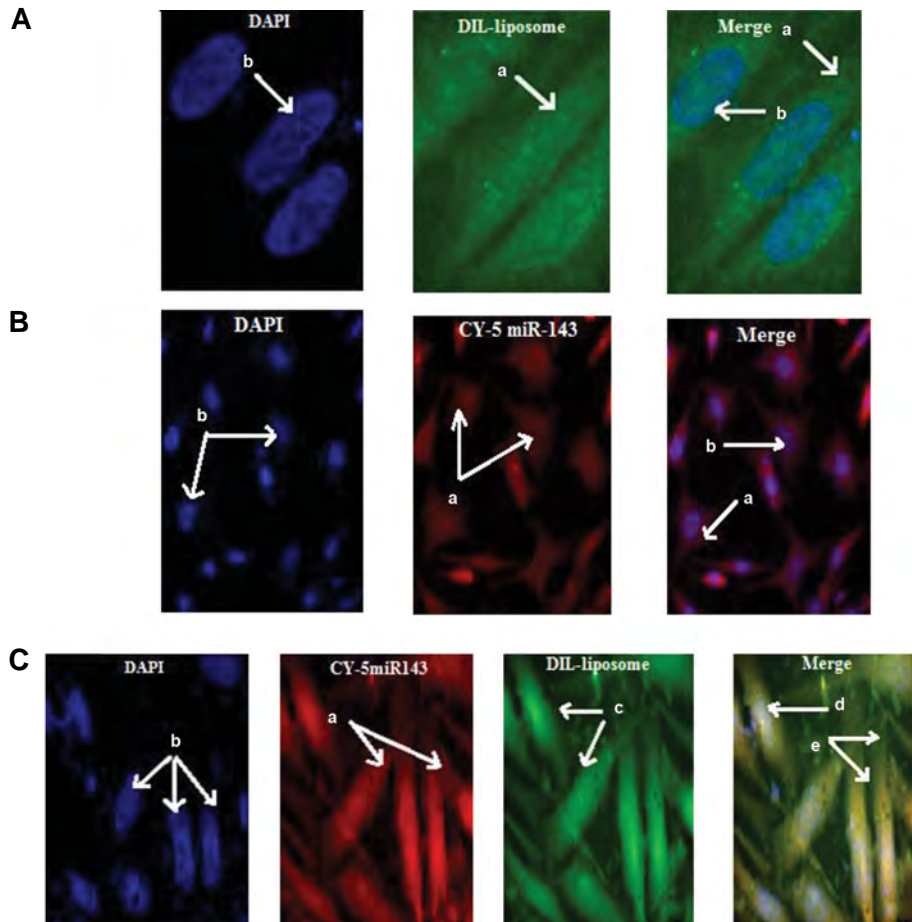


Fig.5: Fluorescence micrographs of cellular uptake, in SaOs-2 cells after three hours treatment. **A.** Empty liposome: a; Accumulation of empty liposomes in the cytoplasm, b; Nuclei stained with DAPI prior to analysis (blue), **B.** Free microRNA: a; Accumulation of the free *miR-143* in the cytoplasm, b; Nuclei stained with DAPI prior to analysis (blue), and **C.** Liposomal microRNA: a; *miR-143* accumulation in the cytoplasm, b, d; Nuclei stained with DAPI prior to analysis (blue), c; Liposome accumulation in the cytoplasm, and e: liposomal *miR-143* accumulation in the cytoplasm (magnification: $\times 60$).

Discussion

Cancer happens when abnormal cells divide in an uncontrolled way. Osteosarcoma is a cancerous tumor in bone. Osteosarcoma is more common in children and adolescents. Gene therapy is a progressive pathway for transferring genetic material to some cells to correct and manipulate the genome for treatment of various diseases (1, 5, 7, 8, 22). The concept underlying gene therapy is accessible via exogenous DNA, microRNA, short interfering RNA (siRNA) and short hairpin RNA (shRNA). Delivery of free genetic material into the cell generally faces with numerous obstacles. To solve this problem, we tried to design a non-toxic and functional vehicle with high gene loading capacity to provide a specific dose of therapeutic genetic material to target cells. In this regard, optimization and control of the drug agent is important in terms of timing, targeting, dose and maintenance of the therapeutic properties (9, 11, 23).

Several reports indicate *miR-143* is one of the down-regulated microRNAs in different types of cancers, while low levels of *miR-143* have been recognized in many malignant tumors. So, genomic loss of *miR-143* can promote advanced proliferation in cancerous cells (13, 14). In this study, for the first time, we tried to design a cationic liposomal system to transfer *miR-143* into osteosarcoma.

In this study, we evaluated a new formulation of microRNA-cationic transmission system. The liposome structure is based on different values of DPPC, DOTAP, CHOL and DSPE mPEG2000. The new liposomal formulation is stable and prolonged (15). The importance of the compounds used in this formulation has been confirmed in previous reports (16, 17, 24). The particles size in this study was less than 140 nm with and without *miR-143* which is consistent to the reports of Zhang et al. (18) and Nourbakhsh et al. (19).

As a result, PEGylation could improve zeta potential and retained particles at low agglomeration levels. PEGylation also created a shield against cationic scavenging by the macrophage system, thus preventing them to be removed from body's internal environment (20, 21). It can also partially affect lack of motion of the lipoplex microRNA along the gel.

The positive charge effect of cationic liposomes inures physical linkage between the gene and liposome. The cationic and neutral properties of liposomes depend on the presence of DOTAP phospholipid. Toxicity of the systems depends on the presence of this phospholipid (17, 18, 25). Cationic lipids are toxic, but in the developed formula in this study, due to its combination with other compounds, such as DPPC, toxicity is diminished (12, 26-29). Similar reports were previously reported by Haghirsadat et al. (21) and Rehman et al. (30).

Gel electrophoresis confirmed the stability of lipocomplex in environment, by subjecting it to mouse plasma. Additionally, observed fluorescence confirms

that no significant change has occurred in the uptake of microRNA with passage of time.

In study the effect of microRNA containing lipoplex system on SaOs-2 cell line, liposomal formulation had shown more toxicity in comparison with free *miR-143*. This is due to the slow releasing behavior of microRNA containing lipoplex, leading to more toxicity for cancer cells as well as a reduction in the use of microRNA and its targeting. Large concentrations of free microRNA small molecules entered into the cells through membrane. However, immediate entry of large volumes of free microRNA into a portion of cell may result in prevention of further import of microRNA from other cellular sites. In the form of nano-lipoplex, microRNA release was limited by slow liberation of nano-liposomal system. As a result, microRNA was gradually introduced to the cell membrane, where it caused uniformity in microRNA absorption into the cell for long-term use (17, 28). This fact help reduce microRNA dosage, due to accumulation at the site. This reduces the amount of drug, needed to treat cancer and increases the therapeutic index along with improvement of cellular toxicity in the SaOS-2 cells. Although application of DOTAP in the formulations leads to a slight reduction of formula biocompatibility, development of these formulations requires preparation of a positive charge formulation for microRNA transport. By optimizing the amount of phospholipid in the formulations, this can be also applied to improve the biocompatibility factor and achieve cationic properties.

The prepared liposomal microRNA formulation could effectively enter the cancerous cells, mostly into the nucleus, whereas free microRNA was predominately distributed in the cytoplasmic region. Accumulation of the *miR-143* in nucleus could induce apoptosis and inhibit DNA replication (29, 30). Concentrating *miR-143* within cancerous cells via carrier system effectively enhanced their anti-cancer activity (31, 32). On the contrary, our results have shown high drug accumulation after three hours treatment. This may be due to smaller size of nanoparticles utilized in our study, leading to increase of diffusion.

Conclusion

This study suggests a novel and optimized formulation of cationic PEGylated liposomal microRNA for gene delivery. We used small molecule microRNA for evaluating the ability of gene encapsulation, as a delivery system. Cytotoxicity assay showed that toxicity of microRNA, loaded into the liposomes in SaOs-2 cells, was higher than the free form of microRNA, due to the presence of positive surface charge. Cationic liposomes had an ability to interact electrostatically with cell membrane with a negative charge. Hence, these structures could easily pass through cell membrane. It is important to increase microRNA efficiency by improving delivery system design. To solve this problem, we developed and characterized various polypeptide-containing formulations and evaluated them for four months

stability parameters, size, zeta potential and gene loading efficiency. Thus, we were able to produce a high-loading microRNA-lipoplex system, not agglomerated, capable of being stored at 4°C for four months without significant leakage of microRNA. Transmission of microRNA into the cell was elevated through the lipoplex system, while it had a good biocompatibility against healthy cells. Consequently, the PEGylated nano-liposomal formulation had a high potential for the systematic migration of microRNA and it could improve the intracellular stability of free microRNA. In general, this study suggested a PEGylated nano-liposomal formulation slowly released, while it had nano-scale size, in the range of 100–200 nm, in the form of mono-dispersed particles.

Authors' Contributions

F.B.F., S.O., M.H.S.; Contributed to concept and design of project. F.B.F; Participated in molecular experiments, data collection, statistical analysis, and participated in the finalization of the manuscript. S.M.K., A.J.; Contributed to statistical analysis, and interpretation of data. F.B.F., A.J.; Contributed to writing and editing manuscript. All authors read and approved the final manuscript.

Acknowledgements

This study was conducted at the International Center for Bioethical Research of Shahid Sadoughi University of Medical Sciences, Yazd, Iran. This research did not receive any specific grant from funding agencies in the public, commercial, or not-for-profit sectors. There is no conflict of interest in this study.

References

- Torre LA, Bray F, Siegel RL, Ferlay J, Lortet-Tieulent J, Jemal A. Global cancer statistics, 2012. *CA Cancer J Clin*. 2015; 65(2): 87-108.
- Bou Kheir T, Futoma-Kazmierczak E, Jacobsen A, Krogh A, Bardram L, Hother C, et al. miR-449 inhibits cell proliferation and is down-regulated in gastric cancer. *Mol Cancer*. 2011; 10: 29.
- Naderinezhad S, Amoabediny G, Haghirsadat F. Co-delivery of hydrophilic and hydrophobic anticancer drugs using biocompatible pH-sensitive lipid-based nano-carriers for multidrug-resistant cancers. *RSC Adv*. 2017; 7(48): 30008-30019.
- Jeon SY, Park JS, Yang HN, Woo DG, Park KH. Co-delivery of SOX9 genes and anti-Cbfa-1 siRNA coated onto PLGA nanoparticles for chondrogenesis of human MSCs. *Biomaterials*. 2012; 33(17): 4413-4423.
- Kupcsik L, Stoddart MJ, Li Z, Benneker LM, Alini M. Improving chondrogenesis: potential and limitations of SOX9 gene transfer and mechanical stimulation for cartilage tissue engineering. *Tissue Eng Part A*. 2010; 16(6): 1845-1855.
- Santos JL, Pandita D, Rodrigues J, Pêgo AP, Granja PL, Tomás H. Non-viral gene delivery to mesenchymal stem cells: methods, strategies and application in bone tissue engineering and regeneration. *Curr Gene Ther*. 2011; 11(1): 46-57.
- Oliveira AC, Ferraz MP, Monteiro FJ, Simões S. Cationic liposome-DNA complexes as gene delivery vectors: development and behaviour towards bone-like cells. *Acta Biomater*. 2009; 5(6): 2142-2151.
- Tamaki H, Harashima N, Hiraki M, Arichi N, Nishimura N, Shiina H, et al. Bcl-2 family inhibition sensitizes human prostate cancer cells to docetaxel and promotes unexpected apoptosis under caspase-9 inhibition. *Oncotarget*. 2014; 5(22): 1139-1412.
- Scholz C, Wagner E. Therapeutic plasmid DNA versus siRNA delivery: common and different tasks for synthetic carriers. *J Control Release*. 2012; 161(2): 554-565.
- van Kouwenhove M, Kedde M, Agami R. MicroRNA regulation by RNA-binding proteins and its implications for cancer. *Nat Rev Cancer*. 2011; 11(9): 644-656.
- Soriano A, Jubierre L, Almazán-Moga A, Molist C, Roma J, de Toledo JS, et al. microRNAs as pharmacological targets in cancer. *Pharmacol Res*. 2013; 75: 3-14.
- Gui T, Shen K. miRNA-101: a potential target for tumor therapy. *Cancer Epidemiol*. 2012; 36(6): 537-540.
- Wang L, Shi ZM, Jiang CF, Liu X, Chen QD, Qian X, et al. MiR-143 acts as a tumor suppressor by targeting N-RAS and enhances temozolomide-induced apoptosis in glioma. *Oncotarget*. 2014; 5(14): 5416-5427.
- Wu XL, Cheng B, Li PY, Huang HJ, Zhao Q, Dan ZL, et al. MicroRNA-143 suppresses gastric cancer cell growth and induces apoptosis by targeting COX-2. *World J Gastroenterol*. 2013; 19(43): 7758-7765.
- Soema PC, Willems GJ, Jiskoot W, Amorij JP, Kersten GF. Predicting the influence of liposomal lipid composition on liposome size, zeta potential and liposome-induced dendritic cell maturation using a design of experiments approach. *Eur J Pharm Biopharm*. 2015; 94: 427-435.
- Bao Y, Jin Y, Chivukula P, Zhang J, Liu Y, Liu J, et al. Effect of PEGylation on biodistribution and gene silencing of siRNA/lipid nanoparticle complexes. *Pharm Res*. 2013; 30(2): 342-351.
- Haghirsadat F, Amoabediny G, Helder MN, Naderinezhad S, Sheikha MH, Forouzanfar T, et al. A comprehensive mathematical model of drug release kinetics from nano-liposomes, derived from optimization studies of cationic PEGylated liposomal doxorubicin formulations for drug-gene delivery. *Artif Cells Nanomed Biotechnol*. 2018; 46(1): 169-177.
- Zhang W, Peng F, Zhou T, Huang Y, Zhang L, Ye P, et al. Targeted delivery of chemically modified anti-miR-221 to hepatocellular carcinoma with negatively charged liposomes. *Int J Nanomedicine*. 2015; 10: 4825-4836.
- Nourbakhsh M, Behravan J, Lage H, Abnous K, Mosaffa F, Badiie A, et al. Nanoliposomes-mediated MDR1 siRNA delivery: preparation, characterization and cellular uptake. *Nanomed J*. 2015; 2(1): 39-45.
- Huang Y, Chen J, Chen X, Gao J, Liang W. PEGylated synthetic surfactant vesicles (Niosomes): novel carriers for oligonucleotides. *J Mater Sci Mater Med*. 2008; 19(2): 607-614.
- Haghirsadat F, Amoabediny G, Sheikha MH, Zandieh-Doulabi B, Naderinezhad S, Helder MN, et al. New liposomal doxorubicin nanoformulation for osteosarcoma: drug release kinetic study based on thermo and pH sensitivity. *Chem Biol Drug Des*. 2017; 90(3): 368-379.
- Mitra AK, Agrahari V, Mandal A, Cholkar K, Natarajan C, Shah S, et al. Novel delivery approaches for cancer therapeutics. *J Control Release*. 2015; 219: 248-268.
- Sun NF, Liu ZA, Huang WB, Tian AL, Hu SY. The research of nanoparticles as gene vector for tumor gene therapy. *Crit Rev Oncol Hematol*. 2014; 89(3): 352-357.
- Saenz del Burgo L, Pedraz JL, Orive G. Advanced nanovehicles for cancer management. *Drug Discov Today*. 2014; 19(10): 1659-1670.
- Bose RJ, Arai Y, Ahn JC, Park H, Lee SH. Influence of cationic lipid concentration on properties of lipid-polymer hybrid nanospheres for gene delivery. *Int J Nanomedicine*. 2015; 10: 5367-5382.
- Cui S, Wang B, Zhao Y, Chen H, Ding H, Zhi D, et al. Transmembrane routes of cationic liposome-mediated gene delivery using human throat epidermis cancer cells. *Biotechnol Lett*. 2014; 36(1): 1-7.
- Filion MC, Phillips NC. Toxicity and immunomodulatory activity of liposomal vectors formulated with cationic lipids toward immune effector cells. *Biochim Biophys Acta*. 1997; 1329(2): 345-356.
- Tivnan A, Orr WS, Gubala V, Nooney R, Williams DE, McDonagh C, et al. Inhibition of neuroblastoma tumor growth by targeted delivery of microRNA-34a using anti-disialoganglioside GD2 coated nanoparticles. *PLoS One*. 2012; 7(5): e38129.
- Haghirsadat F, Amoabediny G, Naderinezhad S, Forouzanfar T, Helder MN, Zandieh-Doulabi B. Preparation of PEGylated cationic nanoliposome-siRNA complexes for cancer therapy. *Artif Cells Nanomed Biotechnol*. 2018: 1-9.
- Rehman Zu, Zuhorn IS, Hoekstra D. How cationic lipids transfer nucleic acids into cells and across cellular membranes: recent advances. *J Control Release*. 2013; 166(1): 46-56.
- Khatiri N, Baradia D, Vhora I, Rathi M, Misra A. Development and characterization of siRNA lipoplexes: effect of different lipids, in vitro evaluation in cancerous cell lines and in vivo toxicity study. *AAPS PharmSciTech*. 2014; 15(6): 1630-1643.
- Kibria G, Hatakeyama H, Sato Y, Harashima H. Anti-tumor effect via passive anti-angiogenesis of PEGylated liposomes encapsulating doxorubicin in drug resistant tumors. *Int J Pharm*. 2016; 509(1-2): 178-187.

Effectiveness of Plasmocure™ in Elimination of *Mycoplasma* Species from Contaminated Cell Cultures: A Comparative Study versus Other Antibiotics

Vahid Molla Kazemiha, M.Sc.¹, Shahram Azari, Ph.D.¹, Mahdi Habibi-Anbouhi, Ph.D.¹, Amir Amanzadeh, Ph.D.¹, Shahin Bonakdar, Ph.D.¹, Mohammad Ali Shokrgozar, Ph.D.^{1*}, Reza Mahdian, M.D., Ph.D.^{2*}

1. National Cell Bank of Iran, Pasteur Institute of Iran, Tehran, Iran
2. Department of Molecular Medicine, Pasteur Institute of Iran, Tehran, Iran

*Corresponding Addresses: P.O.Box: 1316943551, National Cell Bank of Iran, Pasteur Institute of Iran, Tehran, Iran
P.O.Box: 1316943551, Department of Molecular Medicine, Pasteur Institute of Iran, Tehran, Iran
Emails: mashokrgozar@pasteur.ac.ir, dr.reza.mahdian@gmail.com

Received: 24/April/2018, Accepted: 26/August/2018

Abstract

Objective: *Mycoplasmas* spp. is among major contaminants of eukaryotic cell cultures. They cause a wide range of problems associated with cell culture in biology research centers or biotechnological companies. *Mycoplasmas* are also resistant to several antibiotics. Plasmocin™ has been used to treat cell lines but Plasmocin™-resistant strains have been reported. InvivoGen has developed a new anti-*Mycoplasma* agent called Plasmocure™ in order to eliminate resistant *Mycoplasma* contamination. The aim of this study was the selection of the best antibiotics for treatment of *mycoplasma* in cell cultures.

Materials and Methods: In this experimental study, a total of 100 different mammalian cell lines contaminated with different *Mycoplasma* species were evaluated by microbiological culture (as the gold standard method), indirect DNA fluorochrome staining, enzymatic (MycoAlert™), and universal or species-specific polymerase chain reaction (PCR) detection methods. In this study, animal and human cell lines available in National Cell Bank of Iran, were treated with Plasmocure™. The treatment efficacy and cytotoxicity of Plasmocure™ were compared with those of commonly used antibiotics such as BM-cyclin, Plasmocin™, MycoRAZOR™, sparfloracin and enrofloxacin.

Results: Plasmocure™ is comprised of two antibiotics that act through various mechanisms of action than those in Plasmocin™. Two-week treatment with Plasmocure™ was enough to completely eliminate *Mycoplasma* spp. A moderate toxicity was observed during *Mycoplasma* treatment with plasmocure™; But, after elimination of *Mycoplasma*, cells were fully recovered. *Mycoplasma* infections were eliminated by Plasmocure™, BM-cyclin, Plasmocin™, MycoRAZOR™, sparfloracin and enrofloxacin. However, the outcome of the treatment process (i.e. the frequency of complete cure, regrowth or cell death) varied among different antibiotics.

Conclusion: The highest number of cured cell lines was achieved by using Plasmocure™ which also had the lowest regrowth rate after a period of four months. As a conclusion; Plasmocure™ might be considered an effective antibiotic to treat *Mycoplasma* infections in mammalian cell cultures especially for precious or vulnerable cells.

Keywords: Cell Culture, Cytotoxicity, *Mycoplasma*, Treatment

Cell Journal (Yakhteh), Vol 21, No 2, July-September (Summer) 2019, Pages: 143-149

Citation: Molla Kazemiha V, Azari Sh, Habibi-Anbouhi M, Amanzadeh A, Bonakdar Sh, Shokrgozar MA, Mahdian R. Effectiveness of plasmocure™ in elimination of *Mycoplasma* species from contaminated cell cultures: A comparative study versus other antibiotics. Cell J. 2019; 21(2): 143-149. doi: 10.22074/cellj.2019.5996.

Introduction

Mycoplasma spp. contaminations cause a wide range of economical and biotechnical troubles in cell cultures in biological research laboratories as well as biotechnology companies (1, 2). In 1956, *Mycoplasma* was described as one of the most important contaminants of cell cultures (3). Most of the *Mycoplasma* species are known as saprophytic and commensal microbes in eukaryotes (4, 5). They are the smallest and simplest self-replicating bacteria lacking cell wall properties. The cell membrane of *Mycoplasma* is made of triple-layers of cholesterol. Previous studies indicated that 5-87% of cell lines in different cell banks are infected with *Mycoplasma* strains. Among more than 200 species of known mollicutes, 20 of them have been isolated from infected cell cultures. Eight species of *Mycoplasmas* including *M.arginini*, *M.fermentans*, *M. orale*, *M. hyorhinis*, *M. hominis*, *M. salivarium*, *M. pirum* and *Acholeplasma laidlawii* are responsible for more than 95% of *Mycoplasma*-related cell

culture contaminations (6). *Mycoplasma* contaminations can affect the proliferation, the morphology, as well as the metabolic properties of the infected cells. *Mycoplasma* infections may also alter the genome, transcriptome, and proteome properties of the host cells and alter their plasma membrane antigens (1, 4).

Methods for eliminating *Mycoplasmas* from cell cultures include physical, chemical, immunological, and antibiotic-based approaches. Nevertheless, the methods of *Mycoplasma* elimination should ideally be simple, rapid, efficient, reliable, and inexpensive. They should also have minimal effects on cultured eukaryotic cells (7, 8). Three groups of antibiotics namely, tetracyclines, macrolides and fluoroquinolones, have been shown to be highly effective against *Mycoplasmas* in patients or in cell culture. Since each antibiotic has a specific activity and might not completely eliminate all the *Mycoplasmas* present in a culture, using a combination

of antibiotics has been frequently implemented (9, 10). The InvivoGen Company has introduced several antibiotics with different mechanisms of action to treat *Mycoplasma*-contaminated cell cultures. In particular, Plasmocin™ (InvivoGen, USA, Cat No. ant-mpt version 16F09-MM) is used to treat cell lines infected by *Mycoplasmas* and related cell wall-less bacteria. Plasmocin™ can also be used as prophylaxis for *Mycoplasma* and other bacterial contaminations. However, some *Mycoplasmas* have been reported to be resistant to Plasmocin™ (8, 11). To eradicate these *Mycoplasmas*, InvivoGen has developed a new anti-mycoplasma agent called Plasmocure™ (Alternative *Mycoplasma* Removal Agent, InvivoGen, USA, Cat No. ant-pc version 16F09-MM). Plasmocure™ is comprised of two antibiotics that act through mechanisms different from those of Plasmocin™. Two-week treatment with Plasmocure™ is enough to completely eradicate *Mycoplasmas* (12). In the present study, we aimed to compare the efficacy and cytotoxicity of Plasmocure™ versus five other available antibiotics namely, Plasmocin™, BM-cyclin (Roche), MycoRAZOR™, sparfloxacin and enrofloxacin. To this end, we evaluated the effectiveness of these antibiotics in elimination of different *Mycoplasma* species contaminating various mammalian cell lines, at National Cell Bank of Iran (NCBI).

Materials and Methods

Cell cultures

In this experimental study, 100 different animal and human cell lines available at NCBI were randomly selected (Table S1) (See Supplementary Online Information at www.celljournal.org). All cell lines were analyzed by indirect DNA fluorochrome staining (DAPI, Roche, Germany), mycoplasma enzymatic detection kit (MycoAlert™, Lonza, Switzerland), universal or species-specific polymerase chain reaction (PCR) detection technique and microbiological culture as the reference method. During the experiments, the cells were incubated at 37°C in 88% humidified air containing 5% CO₂ and cultured in medium including 10-20% fetal bovine serum (FBS, Gibco®-Invitrogen, USA) (13, 14). In addition, specific media were used for growth factors-dependent cell lines. The following reagents and antibiotics were used in this study:

Reagents (cell culture media, growth factors, supplements and antibiotics)

Dulbecco's modified eagle medium high glucose (DMEM, Gibco®-Invitrogen, USA), Roswell Park Memorial Institute medium 1640 (RPMI 1640, Gibco®-Invitrogen, UK), F12 nutrient mixture (Hams'F12, Gibco®-Invitrogen, USA), McCoy's 5A medium (ATCC®, USA), eagle's minimum essential medium (EMEM, ATCC®, USA), Leibovitz's L-15 medium (ATCC®, USA), earle's balanced salt solution (EBSS,

Gibco®-Invitrogen, USA), horse serum (Gibco®-Invitrogen, NewZealand), Trypsin-EDTA (Gibco®, USA), fischer's medium (Gibco®-Invitrogen, USA), penicillin/streptomycin (Gibco®-Invitrogen, USA), non-essential amino acid (NEAA, Gibco®-Invitrogen MEM, USA), oxalate, pyruvate, and insulin (OPI, Sigma-Aldrich®, Germany), human insulin (Sis), bovine insulin (Sigma-Aldrich®, Germany), human endothelial cell growth factor (Sigma-Aldrich®, Germany), MEBM/MEGM (mammary epithelial cell growth) (MEGM™, Lonza, Switzerland) medium, fibroblast growth factor-basic from bovine pituitary (bFGF, Sigma-Aldrich®, Germany), 200 mM L-glutamine (Gibco®-Invitrogen, USA), 100 mM sodium pyruvate (Gibco®-Invitrogen, USA), oxalate, sodium bicarbonate (Sigma Aldrich®, Germany), 2-mercaptoethanol (0.05 mM 2ME, Sigma-Aldrich®, Germany), hypoxanthine (Sigma Aldrich®, USA), thymidine (Sigma-Aldrich®, Germany), epidermal growth factor (EGF, Sigma-Aldrich®, Germany), granulocyte macrophage colony-stimulating factor (GM-CSF) recombinant human protein (Gibco®-Invitrogen, USA). At the beginning, culture media, FBS, trypsin and phosphate-buffered saline (PBS, Sigma-Aldrich®, Germany) were analyzed and checked for *Mycoplasma* contamination by above-mentioned methods. For every harvested cell line, *Mycoplasma* contamination was evaluated after 3-5 days of culture in an antibiotic-free medium. In order to confirm the absence of contamination with other microorganisms, cell lines were examined through the quality control of microbiological culture (14, 15). Cells were treated with antibiotics including Plasmocure™ (InvivoGen, USA), BM-cyclin (Roche, Germany), Plasmocin™ (InvivoGen, USA), MycoRAZOR™ (Biontex, Cambio Ltd), sparfloxacin (Zagam®) (Sigma-Aldrich®, Biochemica, Germany) and enrofloxacin (Baytril®) (Sigma-Aldrich®, Biochemica, Germany). The Plasmocure™ cytotoxicity and efficacy for eradication of *Mycoplasma* contamination, as well as the frequency of *Mycoplasma* regrowth were compared with those of the above-mentioned antibiotics (Table 1).

The working concentrations of Plasmocure™, BM-cyclin (Roche), Plasmocin™ and MycoRAZOR™ were chosen according to the manufacturer's instructions. Furthermore, sparfloxacin and enrofloxacin working concentrations were determined according to previously published reports (7, 12, 16-18). Following treatment with these reagents, the cells were cultured without penicillin, streptomycin or other commonly-used antibiotics (i.e. under antibiotic-free conditions) for at least another 1-2 weeks prior to testing for residual *Mycoplasma* contamination. All the cured cultures were re-examined for regrowth of *Mycoplasmas* for 4 months following the treatment (10).

Table 1: Protocols suggested for elimination of *Mycoplasma* contamination using different antibiotics, including treatment periods and final concentration of each antibiotic

Brand name	Reagent (category)	Mode of action (inhibition of)	Effect on bacteria	Treatment period	Final concentration (µg/ml)
Plasmocure™	ND	Protein synthesis	Unpublished	14 days	50
Plasmocin™	ND	Protein synthesis, DNA replication	Unpublished	14 days	25
BM-cyclin	I=tiamulin (macrolid) , II=minocycline (tetracycline)	Protein synthesis, Protein synthesis	Bacteriostatic, Bacteriostatic	3×3 days 3×4 days	10 (4 µl/ml), 5 (4 µl/ml)
MycoRAZOR™	Antibiotic mixture in PBS	Protein synthesis	Unpublished	3-5 passes	10 (20 µl/ml)
Zagam®	Sparfloxacin (quinolone)	DNA and RNA synthesis	Bactericidal	7 days	10 (1 µl/ml)
Baytril®	Enrofloxacin (quinolone)	Nucleic acid synthesis	Bactericidal	7 days	25 (25 µl/ml)

ND; Not defined and PBS; Phosphate-buffered saline.

Detection of mollicutes

Detection of *Mycoplasma* contamination by microbiological culture

The suspended cells (1 ml) were added to 10 ml of Pleuropneumonia-Like Organisms (PPLO) broth medium (BD Difco™, USA) supplemented with 10% horse serum (Gibco®, New Zealand), 1% yeast extract agar (Sigma-Aldrich®, Germany), L-arginine (Sigma-Aldrich®, Germany), D-glucose (Dextrose, Gibco®, USA) and cultured at 37°C for 48-72 hours. In the next step, PPLO medium was vigorously stirred to observe monotonous turbidity. After centrifugation at 1500 rpm for 15 minutes, the precipitate (100 µl) was transferred to a solid PPLO agar (BD Difco™, USA) culture plate and incubated at 37°C for 4-6 weeks. Microscopy observation was used to investigate the formation of non-typical colonies or egg form of *Mycoplasma* colonies, every 3-4 days (1).

Detection of *Mycoplasma* contamination by indirect DNA DAPI staining

This experiment was performed according to previous published reports (21, 22). Briefly, cells were cultured on cover slips and stained with 4', 6-diamidino-2'-phenylindole-dihydrochloride (DAPI, Roche, Germany) working solution in methanol (1 µg/ml) at 37°C for 15 minutes. *Mycoplasma* bodies were detected as polymorphous particles with blue fluorescence. For indirect staining, the supernatants of cell cultures that were suspected to be contaminated with *Mycoplasma*, were added to the *Mycoplasma*-free Vero cell line (NCBI C101b, National Cell Bank of Iran) (19, 20).

Detection of *Mycoplasma* contamination by MycoAlert™ *Mycoplasma* detection kit

The enzymatic MycoAlert™ *Mycoplasma* detection kit was used according to the manufacturer's instruction. Briefly, the ratio of the ATPs level in each sample before (Reading A) and after (Reading B) the addition of MycoAlert™ substrate, was considered an indicator for the presence of *Mycoplasma* contamination. The presence

of contamination was proved if the Reading B/Reading A ratio was greater than 1 (1, 21, 22).

Mycoplasma detection using universal and specific polymerase chain reaction method

The *Mycoplasma* contamination status in 100 cell lines (Table S1) (See Supplementary Online Information at www.celljournal.org) was also determined using PCR-based method as described previously (9, 20). In addition to universal primer pair, 11 species-specific primer pairs were designed based on the 16SrRNA of mollicutes (Fig.1). Sequences of all primers were previously published (20, 21).

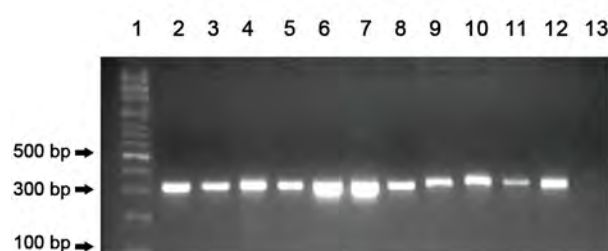


Fig.1: Polymerase chain reaction (PCR) gel electrophoresis of different *Mycoplasma* DNA strains with *Mycoplasma* species-specific primers. Lane 1 DNA size marker (100 bp DNA Ladder, Roche XIV), lane 2 *U.urealyticum* (amplicon size 323 bp), lane 3 *M.fermentans* (amplicon size 324 bp), lane 4 *M.oral* (amplicon size 325 bp), lane 5 *M.salivarium* (amplicon size 324 bp), lane 6 *M.hominis* (amplicon size 301 bp), lane 7 *A.laidlawii* (amplicon size 300 bp), lane 8 *M.pirum* (amplicon size 324 bp), lane 9 *M.pneumoniae* (amplicon size 329 bp), lane 10 *M.genitalium* (amplicon size 335 bp), lane 11 *M.hyorhinis* (amplicon size 334 bp), lane 12 *M.arginini* (amplicon size 326 bp), lane 13 DNA-free water (negative control).

Determination of *Mycoplasma* contamination status in control cell lines

The control cell lines of the study were assessed for *Mycoplasma* contamination using microbiological culture (as the reference standard test), indirect DNA DAPI staining, enzymatic MycoAlert™ and PCR detection (with universal and specific primers) methods. Vero cell line (NCBI C101a) contaminated with several *Mycoplasma* species, and

Mycoplasma-free Vero cell line (NCBI C101b) distinct from different sources, were prepared and *Mycoplasma*-free NSO (NCBI C142) cell line were evaluated by above-mentioned methods and confirmed as positive and negative controls, respectively. Three different *Mycoplasma* strains including *M.hyorhinitis*, *M.arginini* and *M.fermentans* were detected and identified in the positive control cells (Vero cell line contaminated with *Mycoplasma* (NCBI C101a) by species-specific PCR primers) (20, 21).

Statistical analysis

Statistical analysis was performed using SPSS 24.0 software (IBM® SPSS® Statistics, USA). Non-parametric Chi-square test (χ^2) was used for comparisons of two-by-two in six groups. In Chi-square tests, the difference among the antibiotics for the treatment of *Mycoplasma*-infected cell lines was analyzed and interpreted. Differences with a $P < 0.05$ were considered statistically significant.

Results

Characteristics, frequency and treatment of *Mycoplasma* contaminations

In this study, 100 different human and animal cell lines were randomly selected and assessed for mycoplasma contamination. The type of mollicutes in each cell line determined by PCR-based method indicating that 65/100 (65%) of the infected cell cultures was contaminated by one *Mycoplasma* species. Moreover, 19/100 (19%) samples were contaminated with two species and 16/100 (16%) were contaminated with three different species (Table S1) (See Supplementary Online Information at www.celljournal.org). *M.hyorhinitis* was detected in 46/100 (46%) of the studied samples, *M.arginini* in 40/100 (40%), *M.fermentans* in 32/100 (32%), *M. orale* in 12/100 (12%), *A.laidlawii* in 6/100 (6%), *M.salivarium* in 4/100 (4%), *M.pirum* in 3/100 (3%), and *M.hominis*, *M.genitalium*, *U.urealyticum* and *M.pneumoniae* in 2/100 (2%).

Eradication of *Mycoplasma* contaminations

The results obtained from *Mycoplasma* treatment process are summarized in Table S1 (See Supplementary Online Information at www.celljournal.org) and Figure 2. *Mycoplasma* infections were eliminated by Plasmocure™, BM-cyclin (Roche), Plasmocin™, MycoRAZOR™, sparfloxacin and enrofloxacin in 91, 70, 66, 55, 33 and 15% of the contaminated cell cultures, respectively. Furthermore, decontamination was confirmed by PCR, as no *Mycoplasma* was detected in cured cell cultures 14 days after the completion of the treatment period. *Mycoplasma* regrowth (re-infection or recurrent infection) was observed in 3, 12, 17, 42, 62 and 83% of the cured cell lines four months after treatment with Plasmocure™, Plasmocin™, BM-cyclin (Roche), MycoRAZOR™, sparfloxacin and enrofloxacin, respectively. According to the obtained results, the highest level (22%) of cell cytotoxicity (culture death) was observed among Plasmocin-treated cell lines. While, BM-cyclin (Roche), Plasmocure™, sparfloxacin, MycoRAZOR™ and enrofloxacin were cytotoxic to up to 13, 6, 5, 3 and 2% of the studied cell lines, respectively (Table S1 [See Supplementary Online Information at www.celljournal.org], Fig.2). The outcome in the 6 groups of antibiotics showed a significant difference in two-by-two comparison antibiotics in reciprocal case (Table 2). There were significant differences between Plasmocure™ and other antibiotics ($P=0.001$) with regard to treatment of contaminated cell cultures (Table 2, Fig.2).

However, there was no significant difference between Plasmocin™ and BM-cyclin in the comparison of the treatment outcome ($P=0.193$). Overall, results reported on antibiotic treatments of cell cultures by different studies are summarized in Table 3.

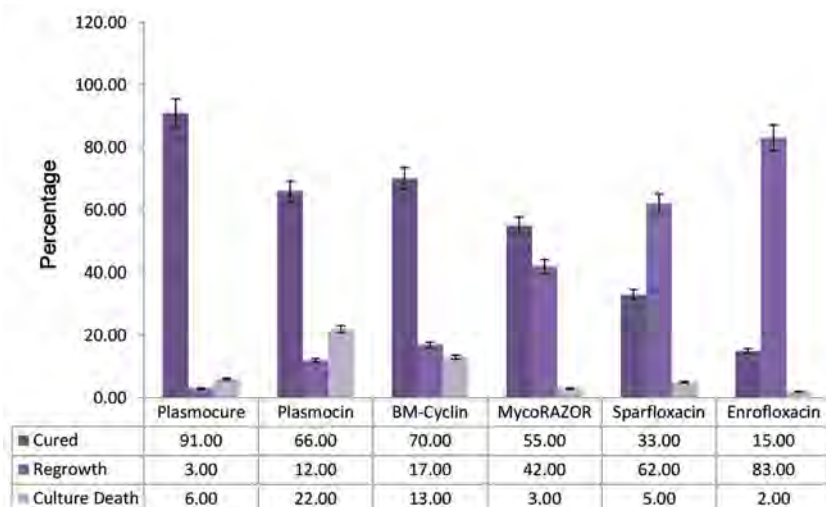


Fig.2: Overall results of the treatment of *Mycoplasma*-positive cell cultures with six antibiotics including Plasmocure™, Plasmocin™, BM-cyclin (Roche), MycoRAZOR™, Sparfloxacin and Enrofloxacin.

Table 2: Two-by-two comparison between the antibiotics evaluated in current study with respect to effectiveness in elimination of *Mycoplasma*

Row	Antibiotic	Number of cured	Number of regrowth	Number of culture death	Antibiotic	P value
1	Plasmocure™	91	3	6	Plasmocin™	0.001*
					BM-cyclin	0.001*
					MycOAZOR™	0.001*
					Sparfloxacin	0.001*
					Enrofloxacin	0.001*
2	Plasmocin™	66	12	22	BM-cyclin	0.193
					MycOAZOR™	0.001*
					Sparfloxacin	0.001*
					Enrofloxacin	0.001*
3	BM-cyclin	70	17	13	MycOAZOR™	0.001*
					Sparfloxacin	0.001*
					Enrofloxacin	0.001*
4	MycOAZOR™	55	42	3	Sparfloxacin	0.007*
					Enrofloxacin	0.001*
5	Sparfloxacin	33	62	5	Enrofloxacin	0.004*
6	Enrofloxacin	15	83	2	-	-

*; P<0.05.

Table 3: The results of different studies reported antibiotic treatment of *Mycoplasmas*-contaminated cell cultures

Antibiotics	Plasmocure™			Plasmocin™			BM-cyclin (Roche)			MRA			MycOAZOR™			Ciprofloxacin			Sparfloxacin			Enrofloxacin		
	C	R	D	C	R	D	C	R	D	C	R	D	C	R	D	C	R	D	C	R	D	C	R	D
Molla Kazemiha et al. (10)	-	-	-	65	10	25	66.25	16.25	17.50	31.25	58.75	10	-	-	-	20	80	0	-	-	-	-	-	-
Molla Kazemiha et al. (9)	-	-	-	-	-	-	100	12.5	17.5	70	62.5	12.5	-	-	-	42.5	82.5	0	-	-	-	-	-	-
Uphoff et al. (12)	-	-	-	84.5	10.3	5.2	86.4	6.8	6.8	-	-	-	-	-	-	-	-	-	-	-	-	73.8	23.8	2.4
Uphoff and Drexler (16)	-	-	-	-	-	-	82	7	11	66	24	10	-	-	-	77	17	6	85	12	3	73	19	8
Fleckenstein and Drexler (35)	-	-	-	-	-	-	84	5	11	64	22	13	-	-	-	77	14	9	-	-	-	-	-	-
Current study	91	3	6	66	12	22	70	17	13	-	-	-	55	42	3	-	-	-	33	62	5	15	83	2

The data present the outcome of the experiments for the cell lines treated. The values indicate the frequency of each outcome as a percentage for each antibiotic. MRA; Mycoplasma removal agent, C; Cure, R; Regrowth, D; Death of culture, and -; Not tested.

Discussion

Mycoplasma contamination remains one of the major problems in cell culture laboratories. *Mycoplasmas* can cause significant biological changes in cultured mammalian cells. In fact, consequences of *Mycoplasma* contamination are unpredictable and may affect molecular

and cellular properties of the infected cells (7, 23, 24). In particular, *Mycoplasma* contamination can lead to attenuation of cell proliferation, unreliable experimental results, and potentially unsafe biological products (1, 25). *Mycoplasmas* are resistant to many antibiotics which are commonly used in cell culture. This problem

has become more widespread since the introduction of more sensitive, rapid, and efficient methods of detection of *Mycoplasmas* in cell culture. Recent reports have estimated that *Mycoplasma* contamination may affect up to 83% of cell cultures worldwide (2, 4, 6, 10). Administration of antibiotics is the most reliable and efficient approach to combat *Mycoplasma* contamination. However, it is important to determine the efficacy and potential side-effects of the antibiotics on the eukaryotic cells in culture. For treatment of irreplaceable, valuable and expensive cell lines, the safety of the antibiotics used against *Mycoplasma* contamination, is particularly important (2, 4, 8). In addition, some cell types may be infected with different *Mycoplasma* species making it difficult to draw an accurate conclusion on choosing an antibiotic (7, 26, 27). In our experience, Plasmocure™ was able to cure 91 out of 100 cell lines (91%), with 3 cases of regrowth (3%) and 6 of cell death (6%). Plasmocure™ is comprised of two bactericidal components belonging to different antibiotic families. They both act by inhibiting protein synthesis but through distinct mechanisms. One of these antibiotic binds to the 50s subunit of the bacterial ribosome and blocks the peptidyltransferase activity. The other antibiotic which binds to isoleucyl-tRNA synthetase prevents the addition of isoleucine to bacterial proteins (28-30).

Remarkably, the problem of regrowth in Plasmocure™-treated cell lines was resolved by using Plasmocin™ or BM-cyclin (Roche), and *vice versa*. In case of cytotoxicity and cell death, especially in severe and intensive contaminations with multiple *Mycoplasma* strains, BM-cyclin (Roche) and Plasmocin™ were used successfully. In case of mild contaminations, particularly for vulnerable or precious cells such as myeloma, lymphoma, hybridoma or primary cultures, MycoRAZOR™ along with fluoroquinolones (sparfloxacin and enrofloxacin) can be used as alternative antibiotics. Plasmocin™ (comprised of a macrolide and a quinolone) acts on the protein machinery and DNA replication by interfering with ribosomal translation and replication fork, respectively. BM-cyclin (Roche) binds to the 30S and 50S ribosomal subunits and inhibits protein synthesis. According to the manufacturer's information, the bacteriostatic components of BM-cyclin (Roche) are pleuromutilin and tetracycline whereas Plasmocin™ is composed of a macrolide and a quinolone (10-12, 31, 32). MycoRAZOR™ is an effective antibiotic against *Mycoplasma*, which is active at low concentrations against various *Mycoplasma* species. It diminishes *Mycoplasmas* protein biosynthesis by interfering with their ribosome function as well as DNA transcription. MycoRAZOR™ has no undesired impact on the eukaryotic cells in the culture. On the other hand, sparfloxacin and enrofloxacin as members of the fluoroquinolone family, inhibit bacterial DNA gyrase and DNA replication (33).

Zakharova et al. (32) showed that Plasmocin™ can effectively treat chronic *Mycoplasma* infections. Similarly, Molla Kazemiha et al. (10) observed that *Mycoplasma* infections were eradicated by Plasmocin™, BM-cyclin

(Roche), ciprofloxacin and MRA (Mycoplasma Removal Agent, AbDSerotec, UK), in 65, 66.25, 20 and 31.25% of the cell lines, respectively. In addition, cytotoxicity was reported in 0, 10, 17.5 and 25% of the cell lines treated with ciprofloxacin, MRA, BM-cyclin (Roche) and Plasmocin™, respectively. Nevertheless, recurrent *Mycoplasmas* infection was observed in 10 to 80% of the studied cell lines after four months. In another study done by Molla Kazemiha et al. (9), *Mycoplasma* infections were eradicated in 100, 70 and 42% of the infected cell lines treated with BM-cyclin (Roche), MRA and ciprofloxacin, respectively. It is noteworthy that, the risk of cell culture loss was 0, 12.5 and 17.5% for ciprofloxacin, MRA and BM-cyclin (Roche), respectively. However, 82.5 (for ciprofloxacin), 62.5 (for MRA) and 12% (BM-cyclin) of the treated cell lines showed *Mycoplasma* regrowth (9, 18).

In this study, we observed high frequency of *Mycoplasma* resistance/regrowth following treatment with enrofloxacin (83%), sparfloxacin (62%) or MycoRAZOR™ (42%). Plasmocure™, BM-cyclin (Roche) and Plasmocin™ were effective especially in elimination of *M.hyorhinae*, *M.arginini*, *M.fermentans* and *M. orale* which were resistant to the other antibiotics used in this study. Plasmocure™ showed the lowest frequency (3%) of regrowth in our experiments while regrowth was observed in 17 and 12% of cell lines treated with BM-cyclin (Roche) and Plasmocin™, respectively. Plasmocure™, BM-cyclin (Roche), Plasmocin™ and MycoRAZOR™ effectively eradicated mollicutes and cured 91, 70, 66 and 55% of the cell lines, respectively. However, sparfloxacin and enrofloxacin were considerably less efficient as they cured only 33 and 15% of the cell lines, respectively.

Plasmocin™ caused the highest rate of culture death (22%), although, it targets the prokaryotic DNA replication and protein synthesis machineries which are different from those of eukaryotic cells. In addition, MycoRAZOR™ showed lower cytotoxicity on the studied cell lines (culture death of 3%), which might reduce the risk of culture loss. Therefore, it may be recommended as the first-line alternative especially in case of expensive or hard-to-obtain cell lines (9, 10, 34). Moreover, quinolones and fluoroquinolones such as ciprofloxacin, enrofloxacin or sparfloxacin were used along with MycoRAZOR™ without increased cytotoxicity (35).

Finally, we observed that the combination of two or more antibiotic with different mechanisms of action makes the interpretation of the results more complicated. Based on our experiments, this might increase the risk of culture death or antibiotic resistance of *Mycoplasmas*. Thus, we suggest using two or more antibiotics in alternating periods for a successful treatment or eradication of *Mycoplasma* contamination. For example, BM-cyclin (Roche) or MycoRAZOR™ (inhibitors of protein synthesis) can be used alternately along with ciprofloxacin, enrofloxacin or sparfloxacin (inhibitors of DNA gyrase activity and DNA replication) with specified intervals during the treatment period.

Conclusion

This report suggests Plasmocure™ as a reliable anti-*Mycoplasma* agent in comparison with other antibiotics for elimination of *Mycoplasma* contamination in cultured cells. As a conclusion, we recommend Plasmocure™ as an effective antibiotic for the treatment of *Mycoplasma* infections in mammalian cell cultures especially for precious or vulnerable cells. These findings may also help researchers at biotechnology laboratories for selection of appropriate antibiotics for treatment of *Mycoplasma* contamination in cell cultures.

Acknowledgements

This work was financially supported by a research grant from Pasteur Institute of Iran (grant No. 869, 2017). The authors would like to thank Ms. N. Ahmadi and Ms. L. Ghazizadeh at National Cell Bank of Iran (NCBI) for their technical assistance. There is no conflict of interest in this study.

Authors' Contributions

V.M.K.; Participated in the study design, experimental work, data collection and evaluation, statistical analysis and writing the draft of the manuscript. S.A., A.A., S.B.; Contributed to the experimental works, interpretation of data, and statistical analysis. R.M., M.A.S., M.H.-A.; Participated in data interpretation and the revising of the manuscript. All authors read and approved the final manuscript.

References

- Volokhov DV, Graham LJ, Brorson KA, Chizhikov VE. Mycoplasma testing of cell substrates and biologics: Review of alternative non-microbiological techniques. *Mol Cell Probes*. 2011; 25(2-3): 69-77.
- Drexler HG, Dirks WG, MacLeod RA, Uphoff CC. False and mycoplasma-contaminated leukemia-lymphoma cell lines: time for a reappraisal. *Int J Cancer*. 2017; 140(5): 1209-1214.
- Cheong KA, Agrawal SR, Lee AY. Validation of nested PCR and a selective biochemical method as alternatives for mycoplasma detection. *J Basic Microbiol*. 2011; 51(2): 215-219.
- Nikfarjam L, Farzaneh P. Prevention and detection of Mycoplasma contamination in cell culture. *Cell J*. 2012; 13(4): 203-212.
- Uphoff CC, Drexler HG. Detection of mycoplasma contamination in cell cultures. *Curr Protoc Mol Biol*. 2014; 106: 28.4.1-14.
- Chernov VM, Chernova OA, Sanchez-Vega JT, Kolpakov AI, Ilin-skaya ON. Mycoplasma Contamination of cell cultures: vesicular traffic in bacteria and control over infectious agents. *Acta Naturae*. 2014; 6(3): 41-51.
- Drexler HG, Uphoff CC. Mycoplasma contamination of cell cultures: Incidence, sources, effects, detection, elimination, prevention. *Cytotechnology*. 2002; 39(2): 75-90.
- Baronti C, Pastorino B, Charrel R, de Lamballerie X. Mycoplasma removal: Simple curative methods for viral supernatants. *J Virol Methods*. 2013; 187(2): 234-237.
- Molla Kazemiha V, Shokrgozar MA, Arabestani MR, Shojaei Moghadam M, Azari S, Maleki S, et al. PCR-based detection and eradication of mycoplasma infections from various mammalian cell lines: a local experience. *Cytotechnology*. 2009; 61(3): 117-124.
- Molla Kazemiha V, Azari S, Amanzadeh A, Bonakdar S, Shojaei Moghadam M, Habibi Anbouhi M, et al. Efficiency of Plasmocin™ on various mammalian cell lines infected by mollicutes in comparison with commonly used antibiotics in cell culture: a local experience. *Cytotechnology*. 2011; 63(6): 609-620.
- Romorini L, Riva DA, Blüguermann C, Videla Richardson GA, Scassa ME, Sevlever GE, et al. Effect of Antibiotics against mycoplasma sp. on human embryonic stem cells undifferentiated status, pluripotency, cell viability and growth. *PLoS One*. 2013; 8(7): e70267.
- Uphoff CC, Denkmann SA, Drexler HG. Treatment of mycoplasma contamination in cell cultures with plasmocin. *J Biomed Biotechnol*. 2012; 2012: 267678.
- Drexler HG, Uphoff CC, Dirks WG, MacLeod RA. Mix-ups and mycoplasmas: the enemies within. *Leuk Res*. 2002; 26(4): 329-333.
- Phelan K, May KM. Mammalian cell tissue culture techniques. *Curr Protoc Mol Biol*. 2017; 117: A.3F.1-A.3F.23.
- Rose S, Black T, Ramakrishnan D. Mammalian cell culture. In: Victor AV, Sarad RP, editors. *Handbook of industrial cell culture*. New Delhi, India: Springer; 2003; 69-103.
- Uphoff CC, Drexler HG. Comparative antibiotic eradication of mycoplasma infections from continuous cell lines. *In Vitro Cell Dev Biol Anim*. 2002; 38(2): 86-89.
- Uphoff CC, Drexler HG. Eradication of mycoplasma contaminations. *Methods Mol Biol*. 2013; 946: 15-26.
- Soltanian B, Irani S, Hashemi S, Mozghani SHR, Ajorloo M, Cheraghi Y, et al. Mycoplasma contamination in cell cultures treated with ciprofloxacin and enrofloxacin: brief report. *Tehran Univ Med J*. 2015; 72(11): 794-798.
- Andrade NM, Arismendi NL. DAPI staining and fluorescence microscopy techniques for phytoplasmas. *Methods Mol Biol*. 2013; 938: 115-121.
- Molla Kazemiha V, Bonakdar S, Amanzadeh A, Azari S, Memarnejadian A, Shahbazi S, et al. Real-time PCR assay is superior to other methods for the detection of mycoplasma contamination in the cell lines of the National Cell Bank of Iran. *Cytotechnology*. 2016; 68(4): 1063-1080.
- Molla Kazemiha V, Amanzadeh A, Memarnejadian A, Azari S, Shokrgozar MA, Mahdian R, et al. Sensitivity of biochemical test in comparison with other methods for the detection of mycoplasma contamination in human and animal cell lines stored in the National Cell Bank of Iran. *Cytotechnology*. 2014; 66(5): 861-873.
- Falagan-Lotsch P, Lopes TS, Ferreira N, Balthazar N, Monteiro AM, Borojevic R, et al. Performance of PCR-based and Bioluminescent assays for mycoplasma detection. *J Microbiol Methods*. 2015; 118: 31-36.
- Souza FT, Souza Sostruznik L, Casagrande Scolari R, Maciel de Castro KJ, Giugliani R, Coelho JC. Comparison of the measurement of lysosomal hydrolase activity in mycoplasma-contaminated and non-contaminated human fibroblast cultures treated with mycoplasma removal agent. *Clin Biochem*. 2007; 40(8): 521-525.
- Uphoff CC, Drexler HG. Detection of mycoplasma contaminations. *Methods Mol Biol*. 2013; 946: 1-13.
- Gedye C, Cardwell T, Dimopoulos N, Tan BS, Jackson H, Svobodová S, et al. Mycoplasma Infection Alters Cancer Stem Cell Properties in Vitro. *Stem Cell Rev*. 2016; 12(1): 156-161.
- Uphoff CC, Drexler HG. Elimination of Mycoplasmas from Infected Cell Lines Using Antibiotics. *Methods Mol Biol*. 2011; 731: 105-114.
- Boslett B, Nag S, Resnick A. Detection and antibiotic treatment of mycoplasma arginini contamination in a mouse epithelial cell line restore normal cell physiology. *Biomed Res Int*. 2014; 2014: 532105.
- Lee H, Kang S, Kim W. Drug repositioning for cancer therapy based on large-scale drug-induced transcriptional signatures. *PLoS One*. 2016; 11(3): e0150460.
- Jia B, Wee TL, Boudreau CG, Berard DJ, Mallik A, Juncker D, et al. Parallelized cytoindentation using convex micropatterned surfaces. *Biotechniques*. 2016; 61(2): 73-82.
- Jayakar SK, Loudig O, Brandwein-Gensler M, Kim RS, Ow TJ, Ustun B, et al. Apolipoprotein E Promotes invasion in oral squamous cell carcinoma. *Am J Pathol*. 2017; 187(10): 2259-2272.
- Singh S, Puri SK, Srivastava K. Treatment and control of mycoplasma contamination in Plasmodium falciparum culture. *Parasitol Res*. 2008; 104(1): 181-184.
- Zakharova E, Grandhi J, Wewers MD, Gavrillin MA. Mycoplasma suppression of THP-1 cell TLR Responses is corrected with antibiotics. *PLoS One*. 2010; 5(3): e9900.
- Li L, Shen W, Zhang K, Tang X, Guo N, Shen F, et al. In-vitro Antimycoplasmal Activity of Triclosan in Combination with Fluoroquinolones against Five mycoplasma Species. *Iran J Pharm Res*. 2012; 11(4): 1111-1119.
- Kloskowski T, Olkowska J, Nazlica A, Drewa T. The influence of ciprofloxacin on hamster ovarian cancer cell line CHO A48. *Acta Pol Pharm*. 2010; 67(4): 345-349.
- Fleckenstein E, Drexler HG. Elimination of mycoplasma contamination in cell cultures. *Biochemica*. 1996; 1(1): 48-51.

In Vitro and *In Vivo* Comparison of Different Types of Rabbit Mesenchymal Stem Cells for Cartilage Repair

Mohammad Ali Khalilifar, M.Sc.^{1,2}, Mohamadreza Baghaban Eslaminejad, Ph.D.^{1*}, Mohammad Ghasemzadeh, Ph.D.³, Samaneh Hosseini, Ph.D.¹, Hossein Baharvand, Ph.D.^{1,2}

1. Department of Stem Cells and Developmental Biology, Cell Science Research Center, Royan Institute for Stem Cell Biology and Technology, ACECR, Tehran, Iran
2. Department of Developmental Biology, University of Science and Culture, Tehran, Iran
3. Infertility and Reproductive Health Research Center, Health Research Institute, Babol University of Medical Sciences, Babol, Iran

*Corresponding Address: P.O.Box: 16635-148, Department of Stem Cells and Developmental Biology, Cell Science Research Center, Royan Institute for Stem Cell Biology and Technology, ACECR, Tehran, Iran
Email: eslami@royaninstitute.org

Received: 3/July/2018,, Accepted: 8/September/2018

Abstract

Objective: Systematic studies indicate a growing number of clinical studies that use mesenchymal stem cells (MSCs) for the treatment of cartilage lesions. The current experimental and preclinical study aims to comparatively evaluate the potential of MSCs from a variety of tissues for the treatment of cartilage defect in rabbit's knee which has not previously been reported.

Materials and Methods: In this experimental study, MSCs isolated from bone marrow (BMMSCs), adipose (AMSCs), and ears (EMSCs) of rabbits and expanded under *in vitro* culture. The growth rate and differentiation ability of MSCs into chondrocyte and the formation of cartilage pellet were investigated by drawing the growth curve and real-time polymerase chain reaction (RT-PCR), respectively. Then, the critical cartilage defect was created on the articular cartilage (AC) of the rabbit distal femur, and MSCs in collagen carrier were transplanted. The studied groups were as the control (only defect), sham (defect with scaffold), BMMSCs in the scaffold, EMSCs in the scaffold, and EMSCs in the scaffold with cartilage pellets. Histological and the gene expression analysis were performed following the transplantation.

Results: Based on our comparative *in vitro* investigation, AMSCs possessed the highest growth rate, as well as the lowest chondrogenic differentiation potential. In this context, MSCs of the ear showed a significantly higher growth rate and cartilage differentiation potential than those of bone marrow tissue ($P < 0.05$). According to our *in vivo* assessments, BMMSC- and EMSC-seeded scaffolds efficiently improved the cartilage defect 4 weeks post-transplantation, while no improvement was observed in the group contained the cartilage pellets.

Conclusion: It seems that the ear contains MSCs that promote cartilage regeneration as much as the conventional MSCs from the bone marrow. Considering a high proliferation rate and easy harvesting of MSCs of the ear, this finding could be of value for the regenerative medicine.

Keywords: Articular Cartilage, Mesenchymal Stem Cells, Rabbit, Transplantation

Cell Journal (Yakhteh), Vol 21, No 2, July-September (Summer) 2019, Pages: 150-160

Citation: Khalilifar MA, Baghaban Eslaminejad MR, Ghasemzadeh M, Hosseini S, Baharvand H. *In vitro* and *in vivo* comparison of different types of rabbit mesenchymal stem cells for cartilage repair. Cell J. 2019; 21(2): 150-160. doi: 10.22074/cellj.2019.6149.

Introduction

The treatment of articular cartilage (AC) injuries is one of the major challenges in orthopedics. Despite encouraging results of the current approaches in the elimination of symptoms of cartilage lesions, the newly-formed tissue is not similar to normal hyaline cartilage in terms of biomechanical properties and the long-term durability. Therefore, it is necessary to develop a biological solution to achieve maximum quality of new AC with the long-term effect (1).

AC is structurally composed of four areas: the superficial area, middle area, deep area, and calcified area (1). The extracellular matrix feature, chondrocyte phenotype, and the cell shape vary among the different areas (2). AC is referred to the as hyaline cartilage that covers the end of bones and forms diarthrodial joints acting as a shock reducer and a lubricant. AC is a kind of tissue where the cellular matrix shows a collapsed structure lacking lymphatic, blood, and nerve supply, and contains a minimum number of chondrocytes (3). Thus,

it has limited the intrinsic regeneration capacity (4). Accordingly, the untreated defects lead to osteoarthritis (OA) and joint degeneration. OA causes the disruption of the collagen networks and proteoglycan depletion of AC. In addition to AC, OA involves in the other joint tissues such as the synovium, meniscus, and subchondral bone (5). Therefore, successful treatment of cartilage defect is essential to prevent the progression of cartilage destruction.

There are different strategies for cartilage defect treatment, yet each procedure possesses several limitations. Debridement and lavage are appropriate for the chondral lesions smaller than 2 cm in diameter. Microfracture is used for the cases with small chondral lesions (smaller than 2-3 cm in diameter), but the newly-formed tissue is fibrocartilage (6). Donor limitation and donor site morbidity are the limitations with respect to the use of autografts or mosaicplasty. This technique could cover maximum 3-4 cm of a defect. Osteochondral allograft transplantation is commonly used for the extended

osteocondral defects; however, the tissue adaptability and limited availability are the most restrictions of this method. In 1987, Brittberg introduced the autologous chondrocyte implantation (ACI) for the treatment of full-thickness defect (7). Recent studies have reported the advantages of ACI versus microfracture, but, in spite of using third-generation of ACI, it has own drawbacks. The requirement for a two-stage surgery, expansion under *in vitro* culture, dedifferentiation after implantation and inability to treat large chondral defects due to donor site deficit and morbidity are some of the drawbacks for the use of chondrocytes related to ACI (8). To overcome the limitations of current approaches, tissue engineering with three basic parts, cells, scaffolds, and biological signaling molecules have emerged as an alternative strategy to repair cartilage efficiently (9). Furthermore, multiple studies have so far been conducted to improve the AC injuries, using a variety of cells worldwide (4).

A proper cell source should meet several criteria such as easy accessibility, expansion, differentiation capacity, and the lack of tumorigenic and immunogenic properties. Embryonic stem cells (ESCs), induced pluripotent stem cells (iPSCs), committed chondrocytes, and adult stem cells are the candidate cell sources for clinical application. ESCs and iPSCs are associated with the ethical and tumor formation concern. Chondrocytes have limited redifferentiation capability, while the adult stem cells which can be obtained from different adult tissues would be a promising cell source (10). The ease of separation and expansion, multipotency and capability to differentiate into mesodermal and nonmesodermal lineages, low immunogenicity, and secretion of trophic factors by MSCs have attracted great attention for the future cell-based approaches (11-14). Studies of cartilage repair using MSCs have mainly focused on the application of bone marrow mesenchymal stem cells (BMMSCs). It has been shown that differentiation into chondrocyte is induced by some growth factors (15-17). Numerous clinical studies have demonstrated the positive effect of BMMSCs in AC regeneration (18). In recent years, MSCs isolated from adipose tissue (AMSCs) have been considered a potent alternative due to their availability and minimal donor tissue morbidity (9). AMSCs have been applied to regenerate cartilage defects (19), and comparison between BMMSC and AMSC in differentiation potential to chondrocyte was also investigated (9, 20). Moreover, ear-derived MSCs (EMSCs) showed the differentiation capability into osteocytes, chondrocytes, and adipocytes (21).

Seeding of MSCs onto diverse scaffolds such as collagen is an effective method used to deliver MSCs into cartilage defects. The ideal scaffold, in addition to keeping implanted MSCs inside cartilage lesions, should provide the bioactive compounds necessary for the induction of differentiation and maturation of MSCs (22). In this study, for the first time, an attempt was made to compare the differentiation ability, and regenerative potential of MSCs derived from bone marrow, adipose, and the ear

to chondrocytes *in vitro*. Furthermore, we evaluated the regenerative potential of a construct comprised of commercially-available collagen type I (as a scaffold) loaded with MSCs from bone marrow and the ear (as a cellular component), and cartilage pellets (as a biological signal) in rabbit's AC defects.

Material and methods

Rabbits

In this experimental study, skeletally matured New Zealand white rabbits (*Oryctolagus cuniculus*) were provided by the animal house of Royan Institute, Tehran, Iran. The Rabbits were used in the experiments weighing approximately 2.7 kg (ranging from 2.1 to 3.1 Kg). The animal care was done in accordance with the animal house guidelines and approval from the Ethics Committee of the Royan Institute. Eighteen white rabbits were generally anesthetized by one dose of an intramuscular injection of 35 mg/kg ketamine and 10 mg/kg xylazine mix (ketamine HCL 100 mg/ml and xylazine HCL 20 mg/ml, Alfasan, Holland). The animals were kept in one cage while they were free to move.

Isolation and culture of rabbit's ear mesenchymal stem cells

A small piece of the ear (1 cm diameter) without large blood vessels was punched under anesthesia. The wound area was disinfected with oxytetracycline spray after punching, and because of the high intrinsic regeneration potential of rabbit ear, the healing occurred after 8 weeks (Fig.S1) (See Supplementary Online Information at www.celljournal.org). The outer layers of the skin and connective tissues were removed, and the remaining cartilage was washed with PBS, and then, chopped. Cartilage was digested with 5 mg/ml collagenase type I (Sigma-Aldrich, USA) in phosphate buffered saline (PBS) at 37°C for three hours. The isolated cells were cultured in Dulbecco's Modified Eagle Medium (DMEM, +4500 mg/L Glucose, Gibco, USA) supplemented with 10% fetal bovine serum (FBS, Gibco, USA) and Pen/Strep (50 U/ml penicillin+50 µg/ml streptomycin, Pen/Strep (Gibco, USA) and incubated at 37°C with humidified 5% CO₂. The medium was changed after 48 hours to remove non-adherent cells. Adherent cells were cultured till reached 80% confluent (23). The cells were removed by trypsin-EDTA (0.05% trypsin-EDTA, Gibco, USA) and passaged to a 75-cm² flask (TPP, Switzerland). The cells proliferated until passage three.

Isolation and culture of bone-marrow mesenchymal stem cells of rabbits

The knees of anesthetized rabbits were shaved and disinfected with Savlon surgical scrub. Bone marrow was harvested under aseptic conditions from the tibia. Specimens were cultured in a 25 cm² culture flask that contained 4 ml DMEM low glucose with 10% FBS and

Pen/Strep (50 unit/ml penicillin+50 µg/ml streptomycin). The flask was incubated at 37°C with humidified 5% CO₂. After 2 days, the medium was changed to remove non-adherent cells, and the adherent cells were cultured till reached 80% confluent. The culture medium was changed every two days, and the cells proliferated until passage three.

Isolation and culture of adipose mesenchymal stem cells of rabbits

We obtained the adipose tissue from the fat pad located subcutaneously between the scapulae of rabbit and chopped well as previously described (24). The tissue was digested in 5 mg/ml collagenase for three hours at 37°C under constant agitation. The digested tissue passed through 70-micron nylon filter mesh followed by centrifugation at 1500 rpm. The cell pellet was cultured in DMEM culture medium. After 48 hours, the medium was changed to discard non-adherent cells; the adherent cells were cultured for the next seven days by changing the medium twice weekly. The cells proliferated until passage three.

Tri-lineage cell differentiation

To prove the mesenchymal phenotype of the isolated cells, passage-3 cells were differentiated into adipogenic, chondrogenic, and osteogenic lineages. 0.3×10^6 cells were seeded per well of a 6-well culture plate. For osteogenic differentiation, the medium was replaced by osteogenic medium-DMEM supplemented with 50 mg/ml ascorbic acid 2-phosphate (Sigma, USA), 10 mM β glycerol phosphate (Sigma, USA) and 10 nM dexamethasone (Sigma, USA). After two weeks, the medium was discarded and cell monolayers were fixed with methanol, and then, stained with alizarin red.

To induce adipogenesis, the adipogenic medium that contained 100nM dexamethasone (Sigma, USA) and 50 mg/ml indomethacin (Sigma, USA), 100 µM L-Ascorbic acid (Sigma, USA) was added to each well. At day 21, the culture medium was removed and the cells were fixed with 4% formalin at room temperature for 1 hour, and then, stained with oil red solution in isopropanol 99% for 15 minutes. The light microscope was used to visualize the adipose droplets.

A micro-mass culture system was used to induce chondrogenic differentiation of MSCs. Briefly, 2.5×10^5 passaged-3 cells were pelleted under 400 g for 10 minutes and cultured in chondrogenic medium (high glucose DMEM supplemented by 10 ng/ml transforming growth factor-β3 (TGF-β3, Sigma, Germany), 10 ng/ml bone morphogenetic protein-6 (BMP6, Sigma, Germany), 1:100 diluted insulin transferrin selenium+premix (Sigma, Germany, 6.25 µg/ml insulin, 6.25 µg/ml transferrin, 6.25 ng/ml selenious acid, 1.25 mg/ml bovine serum albumin, and 5.35 mg/ml linoleic acid, and 10% FBS) for 21 days at 37°C, 5% CO₂; with medium change twice weekly. Chondrogenic differentiation was assessed by both

toluidine blue and Verhoeff-van Gieson staining of pellet sections. The sections were hydrated and stained, using toluidine blue for 30 seconds at room temperature for showing proteoglycan subunits in the extracellular matrix which is one of the characteristics of hyaline cartilage. The pellet sections were also stained with Verhoeff-van Gieson that is useful in demonstrating of elastic fibers which are abundant in elastic cartilage such as the ear and invisible in hyaline cartilage.

For the cartilage production as previously reported (25), third passaged cells were suspended in the chondrogenic medium at 2×10^7 cells/ml. Droplets (12.5 µl) were carefully placed at the bottom of each well of a 96-well plate. Cells were allowed to adhere at 37°C for 2 hours, followed by the addition of 200 µl chondrogenic medium incubated at 37°C with 5% CO₂ and 80% humidity. After 24 hours, the cells of the droplets joined together and became spherical. The medium was changed every 3 days, and micro masses were harvested on days 21, for transplantation in defects.

Growth rate and proliferation

To study the growth rate and proliferation velocity of MSCs from three different tissues, the growth curves for these cells were plotted. 10^4 passaged-3 cells of each group were seeded per well of a 24-well plate. Every day, the cells from two wells were harvested and singled with trypsin/EDTA, treated with diluted trypan blue and counted unstained cells with Neubauer slide under a light microscope until day 12. The culture medium was DMEM with 10% FBS and 100 U/ml pen/strep that was changed every two days. We calculated the population doubling time (PDT) using the following formula: $DT = T \ln 2 / \ln (X_e / X_b)$.

Quantitative real-time polymerase chain reaction analysis

The expression levels of chondrogenic [*SOX9*, *COL2a1*, and *AGGRICAN (ACAN)*], adipogenic [lipoprotein lipase (*LPL*), adiponectin (*ADIPOQ*) and *PPARG*], and osteogenic markers (*OCN*, *OPN*, *ALP*, and *COL1a1*) were evaluated using quantitative polymerase chain reaction (qPCR) (23). The list and sequences of primer pairs are provided in Appendix Table S1 (See Supplementary Online Information at www.celljournal.org). Trizol reagent was used for total RNA extraction according to the manufacturer's instructions (Sigma, USA). cDNA was synthesized (Eppendorf mastercycler gradient, Germany) according to the cDNA Reverse Transcription Kit protocol (Sina Clone, Iran). The PCR was performed with SYBR Green universal PCR Master Mix (Applied Biosystems StepOnePlus™ Real-time PCR System, USA) with a real-time PCR system (Applied Biosystems Life Technologies, Inc., ABi StepOnePlus) and analyzed with Step One software (Applied Biosystems, version 2.1).

Glyceraldehyde-3-phosphate dehydrogenase (*GAPDH*)

primers were utilized as an internal control. To calculate the fold change, the $\Delta\Delta CT$ method was used, and all values were normalized against undifferentiated MSCs.

Animal studies

The rabbits were generally anesthetized and legs prepared as described previously (26). Briefly, a 4cm medial parapatellar incision was made over the knees, and the patella retracted. We used a hand drill (trephine drill, 369.05, A. TITAN, USA) to create a critical defect (4.5 mm in diameter and depth of 1 mm) on the AC of the patellar groove of the distal femur (27) (Fig.S2) (See Supplementary Online Information at www.celljournal.org). Collagen type 1 scaffold that was used in this study was commercially-available and purchased from Koken Cellgen, Collagen solutions for tissue culture, Japan. The rabbits were divided into different groups including the negative control (defect without any treatment), sham group (defects filled with only collagen type 1 scaffold), the group that was transplanted with 10^6 BMMSCs in scaffold, the group that was received 10^6 EMSCs in scaffold, and the group that was implanted with 10^6 EMSCs in scaffold along with several cartilage pellets. The animals were anesthetized 4 and 8 weeks post-surgery with an intramuscular injection of 35 mg/kg ketamine and 3 mg/kg xylazine and then euthanized with saturated KCl heart injection. Rabbit knees were removed and prepared for macroscopic and microscopic evaluations.

To detect MSCs in recovered defects, BMMSCs were labeled with PKH26 red fluorescent cell membrane linker, a vital dye for *in vivo* cell tracking studies (MINI26, Sigma-Aldrich, Germany)

Macroscopic and microscopic evaluations

Macroscopic evaluation: the removed knees were numbered in a histological laboratory on a clean cloth and photographed. The filling rate, color, and surface mode of the repaired defect of the knees were scored blindly according to the scoring system identified by Rudert et al. (28) (Table S2) (See Supplementary Online Information at www.celljournal.org).

Microscopic evaluation: to histologically evaluate the degree of regeneration in damaged cartilage, all femoral condyles were trimmed and fixed in 10% buffered formalin for 48 hours. The tissues were decalcified using 5% formic acid in distilled water for 7 days. The decalcified tissue was dehydrated with 60-100% ethanol, immersed in xylene, and finally embedded in paraffin. At two different levels, from anterior to posterior, 5 μ m thick paraffin sections were cut from transverse femoral condyle and stained with toluidine blue and hematoxylin-eosin (H&E). These sections were scored by two pathologists using the criteria reported by Wakitani et al. (29) containing matrix-staining, surface regularity, cell morphology, the thickness of cartilage (%), and integration with adjacent cartilage (Table S3) (See Supplementary Online Information at www.celljournal.org).

Statistical analysis

Data analysis was performed using one-way analysis of variance (one-way ANOVA) for the comparison of pellet cartilage diameters and Mann-Whitney U for macroscopic and microscopic improvement evaluations by means of the SPSS software version 16 (IBM, USA). The $P < 0.05$ was statistically considered significant.

Results

Isolation and characterization of mesenchymal stem cells

We isolated MSCs from the ear, adipose, bone marrow tissues, and expanded plastic adherent cells. The cells were spindle-shaped, fibroblast-like, and formed colonies. The differentiation of MSCs into adipocytes and osteoblast cell types was assessed by oil red and alizarin red (Fig.1A-L) staining, as well as qRT-PCR. The oil droplets existed in the culture plates indicated the adipogenesis (Fig.1D-F). As shown in Figure 1J-L, the mineral deposition occurred in all groups.

Since the purpose of this study was to produce the cartilage tissue in a laboratory for transplantation, the cell growth rate was an important factor for saving time and cost. As shown in Figure 1M and PDT calculation, AMSCs had the highest rate of growth and proliferation, whereas the lower growth belonged to EMSCs and BMMSCs (34 hours versus 43 and 51 hours, respectively).

The expression profile of the gene markers of osteoblast, adipose, and cartilage tissues was investigated using RT-PCR. The results confirmed the expression of specific differentiation markers in these tissues (Fig.2). The expression of adipose differential markers by differentiated AMSCs showed a significant difference in *LPL*, *ADIPOQ*, and *PGAMA* gene expression. AMSCs also showed a significant difference in osteogenic gene expression namely *OCN*, *COL1a1*, *OPN*, and *ALP* after differentiation into the osteoblast. The differentiated AMSCs into chondrocytes only showed a significant difference in *SOX9* and *COL2a1* expression, but *ACAN* gene expression was not increased. Investigation of the gene expression in differentiated BMMSCs showed a significant difference in *OCN*, *COL1a1*, *OPN*, and *ALP* in differentiated osteoblast. *PPARG*, *ADIPOQ*, and *LPL* expressions also showed a significant difference in adipocytes which differentiate from BMMSCs. Differentiated chondrocytes from BMMSCs showed a significant difference in *ACAN* and *COL2a1* gene expression, but not in *SOX9*. The analysis of the gene expression in differentiated EMSCs showed a significant difference in *PPARG*, *ADIPOQ*, and *LPL* in differentiated adipocytes. *OCN*, *COL1a1*, *OPN* and *ALP* gene expression in osteoblast originated from EMSCs showed a significant increase. *SOX9*, *COL2a1*, and to a lesser extent *ACAN* were significantly increased in chondrocytes which differentiate from EMSCs.

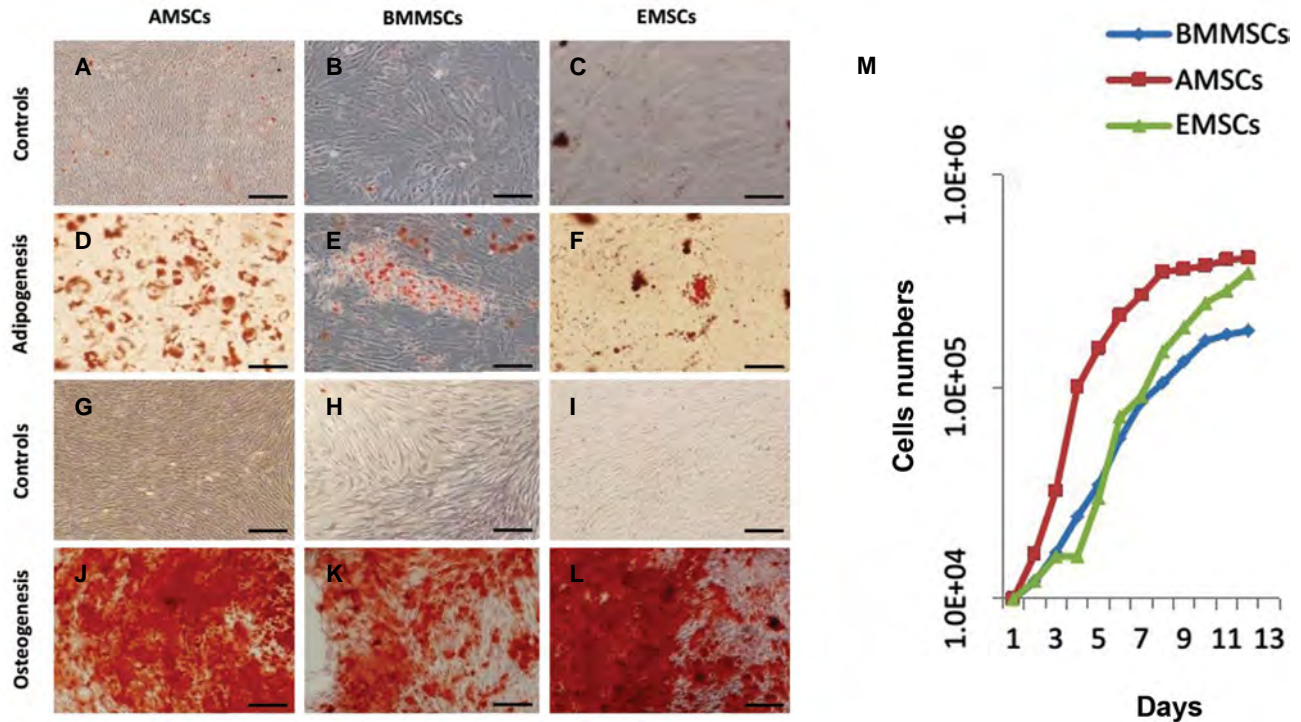


Fig.1: Evaluation of differentiation potential and growth rate of MSCs which were derived from adipose, the ears and bone marrow. **A-F.** Differentiation of extracted MSCs into adipocytes after oil-red staining (differentiation controls are shown on the top of the images, respectively) (scale bar: A: 200 μ m, B: 100 μ m, C: 50 μ m, D: 100 μ m, E: 50 μ m, F: 50 μ m), **G-L.** Differentiation of extracted MSCs into osteoblast cells after alizarin red staining (differentiation controls are shown on the top of the images, respectively) (scale bar: G-L: 200 μ m), and **M.** The growth rate curve of the three MSCs which were derived from adipose, the ear, and bone marrow were illustrated (cell counting using improved Neubauer Hemocytometer).
MSC; Mesenchymal stem cells, AMSC; Adipose MSC, BMMSC; Bone marrow MSC, and EMSC; Ear MSC.

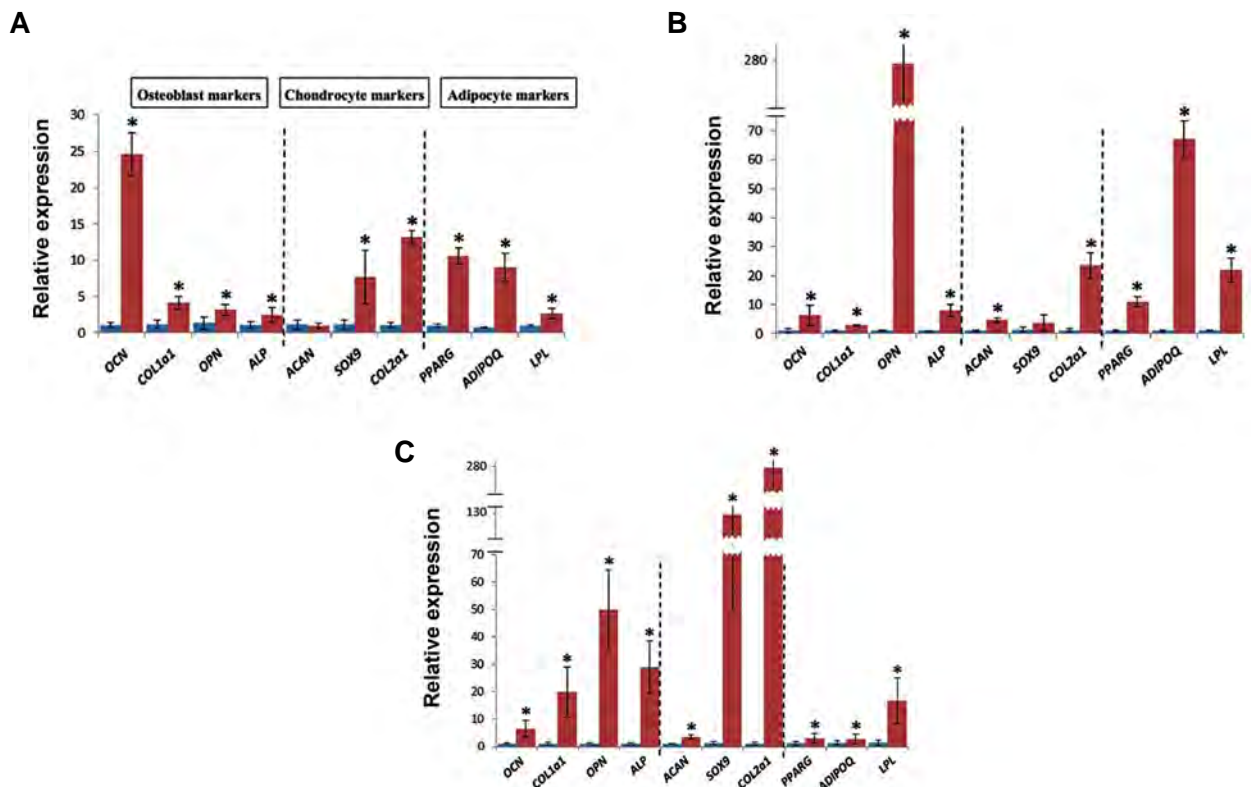


Fig.2: The expression profile of differential markers in differentiated versus undifferentiated cells. Expression analysis of **A.** AMSCs, **B.** BMMSCs, and **C.** EMSCs by real-time polymerase chain reaction. These results indicated the expression of differentiated genes compared to the undifferentiated cells. Adipocyte markers: *OCN*, *COL1a1*, *OPN*, and *ALP*. Chondrocyte markers: *ACAN*, *SOX9*, and *COL2a1*. Osteoblast markers: *PPARG*, *ADIPOQ*, and *LPL*.
*; $P < 0.05$ versus undifferentiated cells, error bar: means \pm SD, n=5, AMSC; Adipose mesenchymal stem cell, BMMSC; Bone marrow MSC, and EMSC; Ear mesenchymal stem cell.

Comparison of cartilage differentiation capacity among isolated mesenchymal stem cells

All three cell lines underwent differentiation into chondrocyte lineage using the micro mass culture system. Figure 3A shows the size of produced cartilage from different MSCs. The average sizes of produced pellet cartilages were 0.683, 0.573, and 1.847 mm for BMMSCs, AMSCs, and EMSCs, respectively. The statistical analysis showed significant differences between groups in terms

of the size. The microscopic structure of differentiated cartilage from three types of MSCs was investigated using toluidine blue staining, in which acidic proteoglycans (AGGRICANS) showed purple color (Fig.3B-D). Due to the small size of AMSCs pellet cartilage, it was excluded from the experimental groups. To analyze elastin fiber formation in produced pellet cartilages, Verhoff staining was performed (Fig.3E-L). No elastin strands were found in differentiated cartilages, and they were structurally similar to knee cartilage, which is a hyaline type.

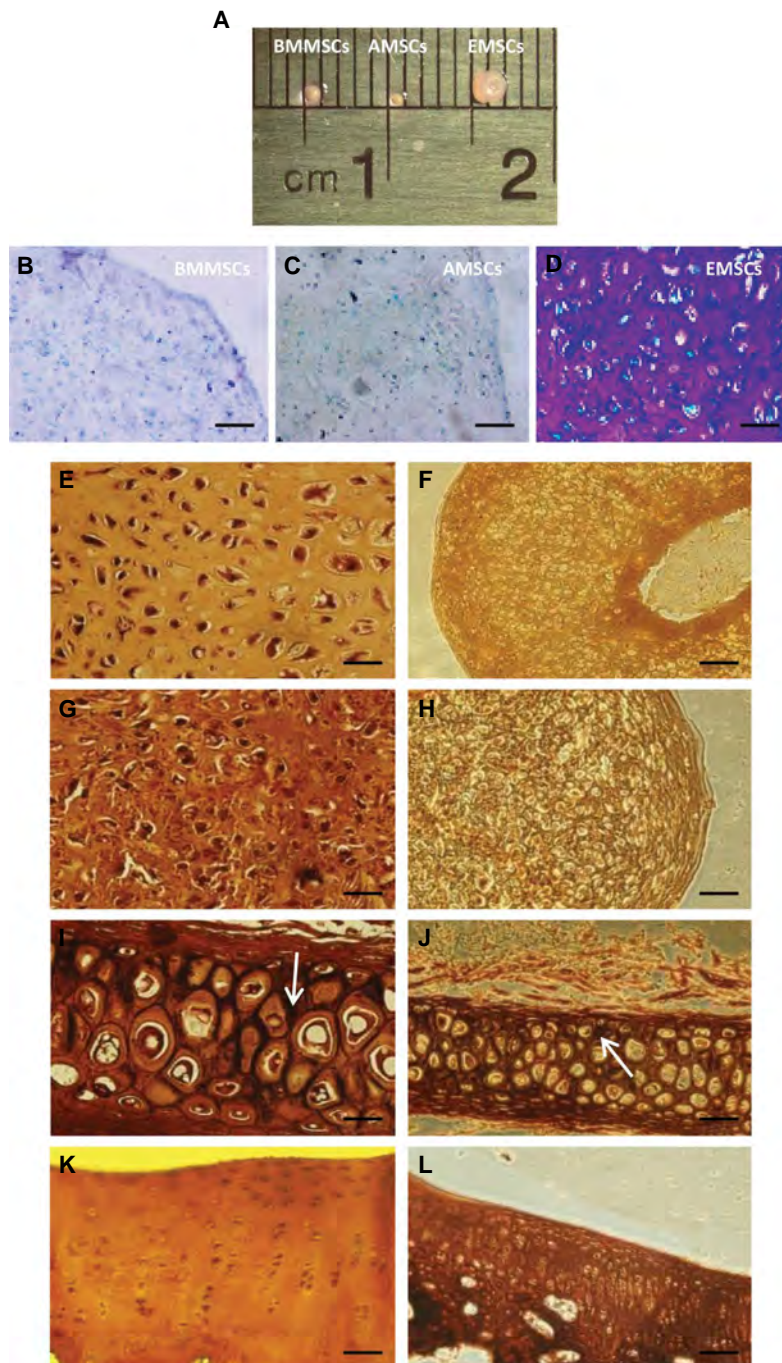


Fig.3: Size and microscopic structure of differentiated cartilage from three MSCs derived cells. **A.** Comparison the size of cartilage produced from BMMSCs, AMSCs, and EMSCs. EMSCs derived cartilage was significantly larger than other ones, **B-D.** Microscopic structure of cartilages following staining with toluidine blue. In EMSCs cartilage, more AGGRECAN production is obvious (scale bar: **B, C:** 100 μ m, **D:** 50 μ m), and **E-L.** Verhoff staining of elastin strands in differentiated cartilage tissues from the EMSCs (**E, F**), BMMSCs (**G, H**), rabbit's ear (**I, J.** as positive controls) where elastin fibers are well seen (white arrows) and the rabbit's knee cartilage (**K, L.** as negative controls) in which elastin strands are not visible as well as E-H images. The arrows indicate the MSC; Mesenchymal stem cell, AMSC; Adipose MSC, BMMSC; Bone marrow MSC, and EMSC; Ear MSC.

Macroscopic and microscopic assessments in different groups

For transplantation of cells and produced cartilages for the defect sites in rabbits, collagen type I was used as a scaffold. Cross-sections of the MSC-seeded scaffold (collagen I) that were stained with PKH26 dye revealed a relatively uniform distribution of MSCs throughout a gel (Fig.4A-C).

After transplantation, knees were removed and decalcified. The knee sections showed smoothness of grafting surface and the adhesion of the grafting tissue to adjacent tissues (Fig.4D-I). The macroscopic evaluation indicated that all studied groups were improved compared to the control group 4 weeks post-transplantation. However, only BMMSCs/scaffold and EMSCs/scaffold showed a significant difference

in terms of filling, color, and smoothness in the macroscopic scoring evaluation. The groups received MSCs/scaffold showed a significant difference in improvement of score compared to both the control and sham groups after 8-week (Fig.5).

Based on microscopic scores, after 4 weeks post-implantation, the knees that received EMSCs/scaffold and BMMSCs/scaffold had higher scores than the other groups. This difference is significant when compared to the negative control (only defect). Also, in 8 weeks groups, there was a significant difference between the groups receiving EMSCs/scaffold and the control. On the other hands, there was no significant difference among the 8 weeks post-implantation groups (Fig.5).

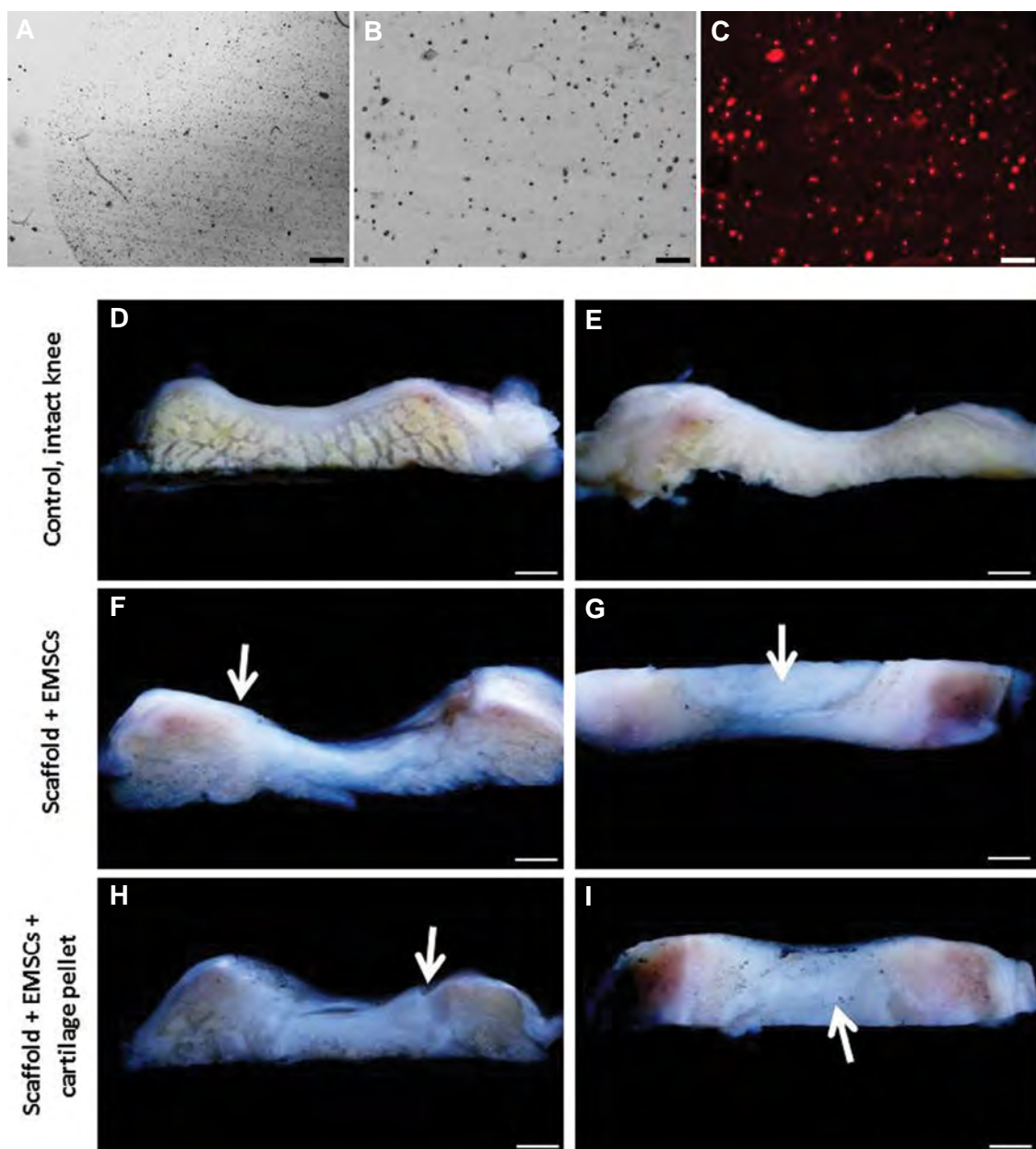


Fig.4: Distribution of MSCs in the scaffold and cross-sectional features of the trimmed knees. **A.** Microscopic view of cross-sections of the scaffold containing BMMSCs, in which a uniform distribution of cells is observed in scaffold (scale bar: 500 μm), **B, C.** The scaffold cross-section containing the stained cells with PKH26 (scale bar: 100 μm), **D, E.** Cross-sectional and upper facial features of the trimmed knees in the control (healthy knee), **F, G.** Knees receiving EMSCs/Scaffold, and **H, I.** Knees receiving EMSCs/Scaffold along with cartilage pellet. The arrows indicate the smoothness level of grafting surface (G and I) and the adhesion of the grafting tissue to adjacent tissues (F and H). (D-I: scale bars: 1 mm). MSC; Mesenchymal stem cell, BMMSC; Bone marrow MSC, and EMSC; Ear MSC.

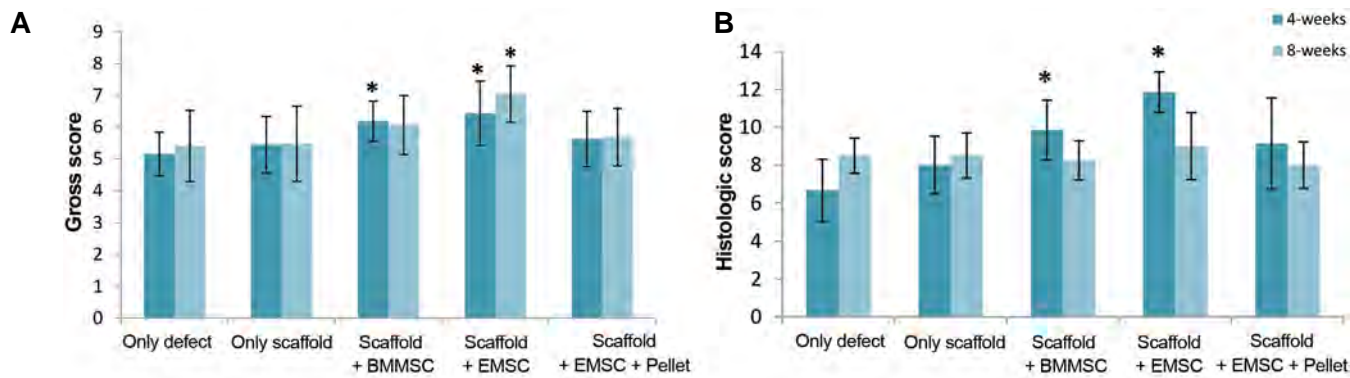


Fig.5: The results of the assessment forms and improvement score charts for the different groups in 4- and 8-week samples. **A.** The results of the assessment forms (n=18 each) showed a significant difference in scaffold+BMMSC or EMSC in 4-week groups and a significant difference in scaffold+EMSC in 8-week group and **B.** The histologic score of the different groups (n=6 each) showed a significant difference in scaffold+BMMSC or EMSC only in 4-week groups. A significant difference in the groups was shown with the only defect group. *; P<0.05 versus only defect group, BMMSC; Bone marrow mesenchymal stem cells, and EMSC; Ear MSC.

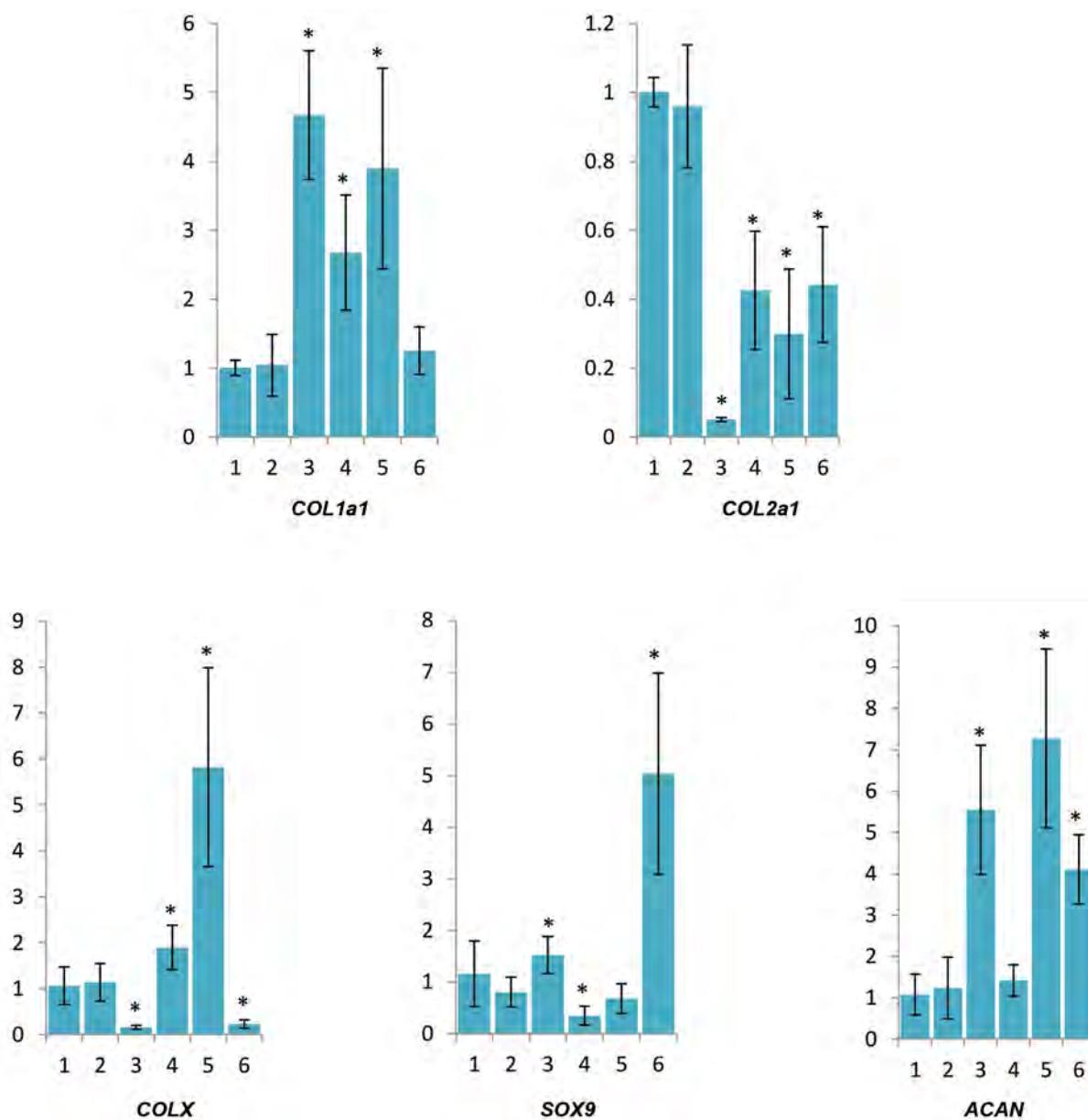


Fig.6: The evaluation of the expression of cartilage marker genes *in vivo* samples after 8 weeks in different groups. A significant difference in the groups was shown with the only defect group. *; P<0.05 versus only defect group, 1; Only defect, 2; Only scaffold, 3; Scaffold+BMMSCs, 4. Scaffold+EMSCs, 5; Sca+EMSC+pallet, and 6; Intact knee cartilage.

Gene expression analysis

The expression profile of cartilage marker was analyzed 8 weeks post-implantation (Fig.6). The results indicated that there were no significant differences in all analyzed genes between the defect and scaffold alone samples. The expression level of *COL1a1* was up-regulated in all groups that received MSCs compared to intact cartilage, sham, and negative control. There was no significant difference between healthy knee, defect (negative control), and sham.

The expression level of *COL2a1* was significantly increased in the negative control and sham groups compared to the other groups. The groups receiving EMSC/scaffold and EMSC/scaffold with cartilage pellet did not show any significant difference in the expression of *COL2a1*. In contrast, the expression of *COL2a1* was substantially decreased in the BMMSC/scaffold.

The gene expression of *COLX* was significantly down-regulated in the BMMSCs/scaffold and intact groups compared to both control and sham groups. However, the groups that received EMSCs/scaffold with and without cartilage pellet had a significant increase compared to the negative control.

The higher expression level of *SOX9* was detected in BMMSCs/scaffold in comparison with the negative control. The EMSCs/scaffold showed a significant reduction in the expression level of *SOX9*. With respect to the positive control, all groups showed a significant decrease in the expression of *SOX9*.

A significant increase in *ACAN* expression level was detected in BMMSCs/scaffold, EMSCs/Scaffold with cartilage pellet, and an intact knee compared to the other groups.

Discussion

Nowadays, one of the major challenges in orthopedics is the treatment of AC injuries and mesenchymal stem cells are a promising cell source in regenerative medicine of the cartilage repair. Despite growing interest in the use of MSCs in preclinical research for AC regeneration, the translation into clinical settings is not satisfying. Although cell-based therapy is apparently simple in cartilage tissue due to the absence of an intrinsic capillary network and low density of one cell type, mechanical properties, and pre-stressed matrix make the cartilage more complicated (3). Previous systematic studies indicated the clinical benefit of MSCs therapies in most studies with no major adverse effects in the treatment or cell harvest (30, 31). However, several factors such as MSCs extraction technique, manipulation, and the release of the cells, as well as the optimization of cellular dose are the challenges ahead. On the other hand, the heterogeneity and lack of defined standards in studies caused using various strategies. Therefore, specific studies to find the best cell source and how to manage the manipulation of the cells, as well as the release techniques and the indication of pathology are

necessary in order to achieve an effective treatment.

Our results showed that all three types of the isolated MSCs were differentiated into bone, adipose, and cartilage that confirmed the mesenchymal phenotype of the extracted cells. The cell growth rate is of great importance in tissue engineering in order to shorten the process time and decrease the expenses. The comparative curve of the cell growth and its doubling time indicated that AMSCs grew faster than BMMSCs and EMSCs. Therefore, these cells could be suitable candidates for cartilage tissue engineering. In addition to the growth rate, differentiation potential into chondrocytes and chondrogenic gene expressions are the other determinative factors. EMSCs and BMMSCs produce bigger pellets in comparison with AMSCs, which are in agreement with the previous studies. The results of qPCR showed that the expression of *ACAN* in AMSC and *SOX9* in BMMSC did not show any significant differences. Significant differences were found in the expression of *SOX9*, *ACAN*, and *COL2a1* in EMSCs, confirming the higher capability of EMSCs for chondrogenic differentiation. Thus, AMSCs, in spite of their simple harvesting and rapid growth, could not be a proper cell source in this study according to the results of the differentiation of these cells into pellets cartilage. The ability of AMSCs for differentiation into chondrocyte is supposedly improved by the alteration of the induction medium composition (32). Interestingly, depending on the extraction and differentiation methods, EMSCs seem to have a better potential for the differentiation into cartilage.

The differentiation of MSCs into the cells of tissues that they are originated from is one of the main concerns in tissue engineering. Interestingly, Verhoeff-van Gieson staining confirmed the absence of elastin strands in the differentiated cartilage obtained from EMSCs and BMMSCs. Elastic fibers are abundant in the elastic cartilage of the ear and invisible in hyaline cartilage. It appears that ear-derived MSCs can effectively differentiate into hyaline cartilage, as Mizuno et al. reported the potential of the ear-derived cartilage progenitor cells in the reconstruction of joint hyaline cartilage (33).

In cell-based cartilage therapy, some issues such as the safety of MSCs and viability of the cells before transplantation should be considered. Although, techniques are being developed throughout the world and the safety of MSCs has been proven in ongoing clinical trials, but, basic studies seeking suitable cell source and approving a valid methodology and regenerative intervention can reduce many concerns. We sought to address the chondrogenic potential of the isolated cells in cartilage defects. Macroscopic evaluation of the defect site indicated that all cell/scaffold groups led to cartilage regeneration, though the EMSCs/scaffold improved the lesion more quickly 4 weeks post-transplantation. Eight weeks after transplantation, there was no significant improvement which might be related to the inherent regeneration ability. Indeed, cartilage in rabbits, unlike human, has an inherent repair ability that affects many

analyses (34). The histological analysis revealed a higher degree of defect regeneration in all cell/scaffold groups than the only defect group 4 weeks post-transplantation. These results confirmed the macroscopic results, while in microscopic scoring the 8-week groups, there was no significant difference between the groups and the control group. Of note, the addition of a pellet to cell/scaffold not only did not improve the outcomes but also had a negative effect on EMSCs/scaffold. Previous experiments have shown the positive effects of cartilage fragment in cartilage regeneration (35). Our findings are not in agreement with this notion. This difference could be due to different materials (cartilage fragment versus MSCs palette) used in these studies. Based on these results, it is concluded that the use of the rabbit's knee is a convenient model for the short-term (first four weeks) *in vivo* studies, and after that, the inherent regeneration system would repair the cartilage defect.

The *SOX9* gene, a master transcription factor, is the main enhancer of specific cartilage genes such as *COL2a1*, *COL1A1*, *COL1A2*, *ACAN*, cartilage binding protein, and *COMP* (36). Downregulation of *SOX9* in our results may be related to the expression of inflammatory factors such as interleukin-1 β and TNF- α in the defect site, as the expression of these factors has a negative effect on the expression of the *SOX9* (37) and *COL2a1*. Aggrecan is the main proteoglycan of the cartilage extracellular matrix which could indicate a severe chondrogenesis activity (38) in scaffold/BMMSC and scaffold/EMSC/pellet groups. Although *SOX9* is the upstream regulator of *ACAN*, there are additional pathways and transcription factors that regulate *ACAN* expression (39). Collagen X is a marker of cartilage cells present in hypertrophic stage and leads to the bone formation (40), which could indicate hypertrophy of cartilage cell in scaffold/EMSC and scaffold/EMSC/pellet groups. However, here, we used collagen type I as a scaffold that exists in bone tissue, skin, and tendon. The expression of collagen type I gene and *COL2a1* in cartilage-transplanted tissues could represent the fibrosis of these structures and cross-talk of the ECM and transplanted cells. Taken together, in our *in vivo* gene expression analyses, we should consider the expression time and complex signaling crosstalk in chondrogenesis.

Conclusion

Despite the improvements in regenerative medicine, the application of cell-based cartilage therapy in clinic remains complex. Here, we compared chondrogenesis potential of bone marrow-, adipose-, and the ear-derived MSCs *in vitro* and *in vivo*, and showed the different characteristics and regeneration capacity of these cell sources. AMSCs have the highest proliferation rate, but lowest differentiation potential to cartilage compared with EMSCs and BMMSCs. Furthermore, EMSCs showed the highest chondrogenic potential as shown in the gene expression and histologic assessments. These results confirmed the importance of cell source selection with respect to *in vivo* cartilage regeneration. In line with this,

EMSCs would be an appropriate option for promoting cartilage reconstruction. Moreover, since the ear tissue could be easily harvested from a cadaver, it would be a valuable substitute for MSCs from bone marrow tissue. Overall, these findings could be used to improve the strategies in cell-based cartilage therapy.

Acknowledgments

The authors would like to acknowledge Mostafa Najar-Asl for his help in histological assessments, Foroughazam Sayahpour for molecular analyses, Dr. Niloofar Sodeifi and Dr. Amir Kamali for histologic scoring and Dr. Ehsan Ranaei Pirmardan for the edition of the manuscript, tables, and pictures. The present study was financially supported by Royan Institute (code: 90223502). The authors declare no conflict of interest.

Authors' Contributions

M.A.Kh; Contributed to all experimental work, statistical analysis, interpretation of data, and drafted the manuscript. S.H.; Contributed to interpretation of data and revised manuscript. H.B.; Advised on the project and participated in study design, data collection and evaluation. M.Gh.; Conducted the surgery. M.R.B.E.; Was responsible for the overall supervision, participated in study design, data collection and evaluation. All authors performed editing and approving the final version of this manuscript for submission, also participated in the finalization of the manuscript and approved the final draft.

References

1. Johnstone B, Alini M, Cucchiari M, Dodge GR, Eglin D, Guilak F, et al. Tissue engineering for articular cartilage repair--the state of the art. *Eur Cell Mater*. 2013; 25: 248-267.
2. Nakagawa Y, Muneta T, Otabe K, Ozeki N, Mizuno M, Udo M, et al. Cartilage derived from bone marrow mesenchymal stem cells expresses lubricin *in vitro* and *in vivo*. *PLoS One*. 2016; 11(2): e0148777.
3. Bernhard JC, Vunjak-Novakovic G. Should we use cells, biomaterials, or tissue engineering for cartilage regeneration? *Stem Cell Res Ther*. 2016; 7(1): 56.
4. Yamasaki S, Mera H, Itokazu M, Hashimoto Y, Wakitani S. Cartilage repair with autologous bone marrow mesenchymal stem cell transplantation: review of preclinical and clinical studies. *Cartilage*. 2014; 5(4): 196-202.
5. Mandelbaum B, Waddell D. Etiology and pathophysiology of osteoarthritis. *Orthopedics*. 2005; 28(2 Suppl): S207-S214.
6. Steadman JR, Rodkey WG, Rodrigo JJ. Microfracture: surgical technique and rehabilitation to treat chondral defects. *Clin Orthop Relat Res*. 2001; (391 Suppl): S362-S369.
7. Brittberg M, Lindahl A, Nilsson A, Ohlsson C, Isaksson O, Peterson L. Treatment of deep cartilage defects in the knee with autologous chondrocyte transplantation. *N Engl J Med*. 1994; 331(14): 889-895.
8. Matsiko A, Levingstone TJ, O'Brien FJ. Advanced Strategies for articular cartilage defect repair. *Materials (Basel)*. 2013; 6(2): 637-668.
9. Xie X, Wang Y, Zhao C, Guo S, Liu S, Jia W, et al. Comparative evaluation of MSCs from bone marrow and adipose tissue seeded in PRP-derived scaffold for cartilage regeneration. *Biomaterials*. 2012; 33(29): 7008-7018.
10. Seo S, Na K. Mesenchymal stem cell-based tissue engineering for chondrogenesis. *J Biomed Biotechnol*. 2011; 2011: 1-8.
11. Nadri S, Kazemi B, Eslaminejad MB, Yazdani S, Soleimani M. High yield of cells committed to the photoreceptor-like cells from conjunctiva mesenchymal stem cells on nanofibrous scaffolds. *Mol Biol Rep*. 2013; 40(6): 3883-3890.
12. Nadri S, Yazdani S, Arefian E, Gohari Z, Eslaminejad MB, Kazemi B, et al. Mesenchymal stem cells from trabecular meshwork be-

- come photoreceptor-like cells on amniotic membrane. *Neurosci Lett*. 2013; 541: 43-48.
13. Alizadeh E, Eslaminejad MB, Akbarzadeh A, Sadeghi Z, Abasi M, Herizchi R, et al. Upregulation of MiR-122 via trichostatin A treatments in hepatocyte-like cells derived from mesenchymal stem cells. *Chem Biol Drug Des*. 2016; 87(2): 296-305.
 14. Faghihi F, Baghaban Eslaminejad M, Nekookar A, Najar M, Salekdeh GH. The effect of purmorphamine and sirolimus on osteogenic differentiation of human bone marrow-derived mesenchymal stem cells. *Biomed Pharmacother*. 2013; 67(1): 31-38.
 15. Baghaban Eslaminejad M, Malakooty Poor E. Mesenchymal stem cells as a potent cell source for articular cartilage regeneration. *World J Stem Cells*. 2014; 6(3): 344-354.
 16. Koga H, Engebretsen L, Brinchmann JE, Muneta T, Sekiya I. Mesenchymal stem cell-based therapy for cartilage repair: a review. *Knee Surg Sports Traumatol Arthrosc*. 2009; 17(11): 1289-1297.
 17. Emadedin M, Ghorbani Liastani M, Fazeli R, Mohseni F, Moghadasali R, Mardpour S, et al. Long-term follow-up of intra-articular injection of autologous mesenchymal stem cells in patients with knee, ankle, or hip osteoarthritis. *Arch Iran Med*. 2015; 18(6): 336-344.
 18. Bornes TD, Adesida AB, Jomha NM. Mesenchymal stem cells in the treatment of traumatic articular cartilage defects: a comprehensive review. *Arthritis Res Ther*. 2014; 16(5): 432.
 19. Lee JM, Im GI. SOX trio-co-transduced adipose stem cells in fibrin gel to enhance cartilage repair and delay the progression of osteoarthritis in the rat. *Biomaterials*. 2012; 33(7): 2016-2024.
 20. Hildner F, Albrecht C, Gabriel C, Redl H, van Griensven M. State of the art and future perspectives of articular cartilage regeneration: a focus on adipose-derived stem cells and platelet-derived products. *J Tissue Eng Regen Med*. 2011; 5(4): e36-e51.
 21. Sart S, Schneider YJ, Agathos SN. Ear mesenchymal stem cells: an efficient adult multipotent cell population fit for rapid and scalable expansion. *J Biotechnol*. 2009; 139(4): 291-299.
 22. Kazemi D, Shams Asenjan K, Dehdilani N, Parsa H. Canine articular cartilage regeneration using mesenchymal stem cells seeded on platelet rich fibrin: Macroscopic and histological assessments. *Bone Joint Res*. 2017; 6(2): 98-107.
 23. Baghaban Eslaminejad M, Bordbar S. Isolation and characterization of the progenitor cells from the blastema tissue formed at experimentally-created rabbit ear hole. *Iran J Basic Med Sci*. 2013; 16(2): 109-115.
 24. Zhu Y, Liu T, Song K, Fan X, Ma X, Cui Z. Adipose-derived stem cell: a better stem cell than BMSC. *Cell Biochem Funct*. 2008; 26(6): 664-675.
 25. Zhang L, Su P, Xu C, Yang J, Yu W, Huang D. Chondrogenic differentiation of human mesenchymal stem cells: a comparison between micromass and pellet culture systems. *Biotechnol Lett*. 2010; 32(9): 1339-1346.
 26. Im GI, Kim DY, Shin JH, Hyun CW, Cho WH. Repair of cartilage defect in the rabbit with cultured mesenchymal stem cells from bone marrow. *J Bone Joint Surg Br*. 2001; 83(2): 289-294.
 27. Chu CR, Szczodry M, Bruno S. Animal models for cartilage regeneration and repair. *Tissue Eng Part B Rev*. 2010; 16(1): 105-115.
 28. Rudert M, Wilms U, Hoberg M, Wirth CJ. Cell-based treatment of osteochondral defects in the rabbit knee with natural and synthetic matrices: cellular seeding determines the outcome. *Arch Orthop Trauma Surg*. 2005; 125(9): 598-608.
 29. Wakitani S, Goto T, Pineda SJ, Young RG, Mansour JM, Caplan AI, et al. Mesenchymal cell-based repair of large, full-thickness defects of articular cartilage. *J Bone Joint Surg Am*. 1994; 76(4): 579-592.
 30. Filardo G, Perdisa F, Roffi A, Marcacci M, Kon E. Stem cells in articular cartilage regeneration. *J Orthop Surg Res*. 2016; 11: 42.
 31. Deng Z, Jin J, Zhao J, Xu H. Cartilage defect treatments: with or without cells? Mesenchymal Stem cells or chondrocytes? Traditional or matrix-assisted? A systematic review and meta-analyses. *Stem Cells Int*. 2016; 2016: 9201492.
 32. Diekman BO, Rowland CR, Lennon DP, Caplan AI, Guilak F. Chondrogenesis of adult stem cells from adipose tissue and bone marrow: induction by growth factors and cartilage-derived matrix. *Tissue Eng Part A*. 2010; 16(2): 523-533.
 33. Mizuno M, Kobayashi S, Takebe T, Kan H, Yabuki Y, Matsuzaki T, et al. Brief report: reconstruction of joint hyaline cartilage by autologous progenitor cells derived from ear elastic cartilage. *Stem cells*. 2014; 32(3): 816-821.
 34. Ahern BJ, Parvizi J, Boston R, Schaer TP. Preclinical animal models in single site cartilage defect testing: a systematic review. *Osteoarthritis Cartilage*. 2009; 17(6): 705-713.
 35. Bonasia DE, Marmotti A, Rosso F, Collo G, Rossi R. Use of chondral fragments for one stage cartilage repair: a systematic review. *World J Orthop*. 2015; 6(11): 1006-1011.
 36. Henrotin Y, Kurz B, Aigner T. Oxygen and reactive oxygen species in cartilage degradation: friends or foes? *Osteoarthritis Cartilage*. 2005; 13(8): 643-654.
 37. Orriols M, Varona S, Aguiló S, Galán M, Martínez González J, Rodríguez C. Inflammation inhibits vascular fibulin-5 expression: involvement of transcription factor SOX9. *Clin Investig Arterioscler*. 2016; 28(6): 271-280.
 38. Lauing KL, Cortes M, Domowicz MS, Henry JG, Baria AT, Schwartz NB. Aggrecan is required for growth plate cytoarchitecture and differentiation. *Dev Biol*. 2014; 396(2): 224-236.
 39. Hu G, Codina M, Fisher S. Multiple enhancers associated with ACAN suggest highly redundant transcriptional regulation in cartilage. *Matrix Biol*. 2012; 31(6): 328-337.
 40. Zhong L, Huang X, Karperien M, Post JN. The regulatory role of signaling crosstalk in hypertrophy of mscs and human articular chondrocytes. *Int J Mol Sci*. 2015; 16(8): 19225-19247.

Generation and Characterization of Induced Pluripotent Stem Cells from Mononuclear Cells in Schizophrenic Patients

Qing Liu, M.D.^{1,2,3#}, Jiang Du, Ph.D.^{1,4#}, Jinyu Fan, Ph.D.^{1,2}, Wenqiang Li, Ph.D.^{1,3}, Weiyun Guo, M.D.²,
Huigen Feng, Ph.D.^{1,2*}, Juntang Lin, Ph.D.^{1,4*}

1. Stem Cell and Biotherapy Engineering Research Center of Henan, Xinxiang Medical University, Xinxiang, China
2. College of Life Science and Technology, Xinxiang Medical University, Xinxiang, China
3. Henan Key Lab of Biological Psychiatry, The Second Affiliated Hospital of Xinxiang Medical University, Xinxiang, China
4. College of Biomedical Engineering, Xinxiang Medical University, Xinxiang, China

The first two authors contributed equally to this work.

*Corresponding Address: Stem Cell and Biotherapy Engineering Research Center of Henan, Xinxiang Medical University, Xinxiang, China
Emails: fenghuigen@xxmu.edu.cn, linjtlin@126.com

Received: 9/March/2018, Accepted: 1/July/2018

Abstract

Objective: Schizophrenia (SZ) is a mental disorder in which psychotic symptoms are the main problem. The pathogenesis of SZ is not fully understood, partly because of limitations in current disease models and technology. The development of induced pluripotent stem cell (iPSC) technology has opened up the possibility of elucidating disease mechanisms in neurodegenerative diseases. Here, we aimed to obtain iPSCs from peripheral blood mononuclear cells (PBMCs) of normal and schizophrenic individuals and analyze the inflammatory response in these iPSCs.

Materials and Methods: In this experimental study, we isolated PBMCs from whole blood of healthy individuals and SZ patients and reprogrammed them into iPSCs by transfection of recombinant lentiviruses that contained Yamanaka factors (Oct4, Sox2, Klf4 and c-Myc). We calculated the numbers of iPSC clones and stained them with alkaline phosphatase (ALP), Nanog, SSEA4, Nestin, Vimentin, and AFP to confirm their efficiency and pluripotency. The iPSCs were analyzed by real-time quantitative polymerase chain reaction (qRT-PCR) for the expressions of inflammatory factors.

Results: iPSCs from schizophrenic patients (SZ-iPSCs) exhibited typical morphology and highly expressed pluripotent markers. These iPSCs retained their normal karyotype and differentiated *in vitro* to form embryoid bodies (EBs) that expressed markers of all 3 germ layers. However, iPSCs from the SZ-iPSCs group had a weak capacity to differentiate into ectoderm compared to the normal iPSCs (Con-iPSC). An elevated, stronger inflammatory response existed in iPSCs from schizophrenic individuals.

Conclusion: We successfully obtained iPSCs from PBMCs of schizophrenic patients without genetic operation and analyzed the expressions of pluripotent markers and inflammatory factors between the Con-iPSC and SZ-iPSC groups. Taken together, our results may assist to explain the pathogenesis of SZ and develop new strategies for clinical diagnosis and treatment.

Keywords: Induced Pluripotent Stem Cell, Peripheral Blood Mononuclear Cells, Pluripotency, Reprogramming, Schizophrenia

Cell Journal (Yakhteh), Vol 21, No 2, July-September (Summer) 2019, Pages: 161-168

Citation: Liu Q, Du J, Fan J, Li W, Guo W, Feng H, Lin J. Generation and characterization of induced pluripotents. stem cells from mononuclear cells in schizophrenic patients. Cell J. 2019; 21(2): 161-168. doi: 10.22074/cellj.2019.5871.

Introduction

Somatic cell reprogramming into a pluripotent state by induced pluripotent stem cell (iPSC) technology not only paves the way for organ regeneration but also provides a powerful tool for studying pathological processes (1, 2). In 2006, Takahashi and Yamanaka (3) were the first to successfully reprogram mouse fibroblasts into iPSCs using retroviral vectors to introduce 4 genes that encode transcription factors (*Oct4*, *Sox2*, *Klf4*, and *c-Myc*). iPSCs, like embryonic stem cells (ESCs), can give rise to every other cell type in the body, such as neuron, heart, pancreatic, and liver cells (4). Therefore, iPSCs technology is considered a powerful tool to study the pathological processes of diseases and clinical treatment due to its pluripotency (5). Recently, generation of iPSCs from somatic cells

in disease models has become an important method for basic research of pathogenesis (6, 7).

Schizophrenia (SZ), common mental disorder that usually appears in late adolescence or early adulthood (8), is mainly defined by psychiatric signs that include disorders of delusions, hallucinations, cognition, and emotion (9). SZ has a heavy burden for family and society because of the risk of suicide, lack of medical care, and a higher risk of delusion in schizophrenic patients (10). The pathogenesis of SZ is unclear due to the limitations of current disease models, technology, and clinical approach (11-13).

Recently, researchers generated iPSCs from human fibroblasts of SZ patients and further induced these

iPSCs to form neuron cells. The iPSCs derived neuron cells from SZ patients had lower protein levels of PSD95 compared with the neurons from normal iPSCs, as well as incomplete neuronal development and less junctions (14). Another paper reported that neuron cells from iPSCs that had the *DISC1* mutation, an identified genetic risk factor for SZ, showed defective neuronal synapses and abnormal neuronal gene expression in contrast to normal neurons (15, 16). Hence, iPSCs technology has played an important role in the study and clinical application of SZ (17, 18). In this study, we generated iPSCs from peripheral blood mononuclear cells (PBMCs) of schizophrenic patients and analyzed the morphology, pluripotency, and capacity for differentiation, which would provide choices for the establishment of an SZ model *in vitro*.

Materials and Methods

Isolate and culture of peripheral blood mononuclear cells

The PBMCs were prepared by density gradient centrifugation at room temperature using fresh whole blood both from healthy participants and SZ patients. Then cells were cultured in X-VIVO™ 15 medium (Lonza, Switzerland) supplemented with 1% penicillin/streptomycin. Healthy participants and the family member/legal guardian of SZ patients provided informed consent. This study was approved by the Ethics Review Board at Xinxiang Medical University.

Generation of induced pluripotent stem cells from peripheral blood mononuclear cells

In this experimental study, we generated human iPSCs from PBMCs by using retroviruses as described previously with some modifications (19). Briefly, after the PBMCs were introduced with Oct4, Sox2, Klf4 and c-Myc, the cells were transferred into a 3 cm² dish covered with Matrigel (BD Biosciences, USA) in X-VIVO™ 15 medium. After 2 days, the cells were reseeded onto dishes with standard iPSC medium, Knockout™ DMEM, that consisted of 20% knockout serum replacement, 1% L-glutamine, 1% nonessential amino acids, 0.1 mM β-mercaptoethanol, 1% penicillin/streptomycin, and 10 ng/ml fibroblast growth factor 2 (bFGF, BD Biosciences, USA). We changed the medium every other day until iPSC colonies formed. All cells were cultured in a humidified atmosphere that contained 5% CO₂ at 37°C.

Alkaline phosphatase staining

After infection of the PBMCs, we could observe the iPSC colonies under a fluorescent microscope. To detect alkaline phosphatase (ALP) activity, a cytochemical assay was performed using a Leukocyte Alkaline Phosphatase Kit (Yeasen, China) according

to the manufacturer's protocol.

Karyotype analysis

iPSCs were treated for about 45 minutes with Karyo MAX Colcemid (Gibco, USA), harvested, and fixed with methanol:acetic acid (3:1). The cell pellet was washed, resuspended, dropped on a slide, and dried on a hotplate. Cells were stained with Giemsa and the metaphase chromosome number from individual nuclei were counted microscopically (Olympus BX51, Japan, 100X), imaged by CytoVision software, and subjected for G-band karyotyping at Xinxiang Medical University. Karyotypes were described according to the International System for Human Cytogenetic Nomenclature (ISCN) (19).

Immunofluorescence staining

Cells placed on the chamber slides were fixed in 4% paraformaldehyde (PFA, Boster, China) for 15 minutes at room temperature, washed with PBS, and permeabilized with 0.2% Triton X-100 (Sigma, USA) in PBS (PBS-T) for 20 minutes. Cells were incubated overnight in blocking buffer that contained the following primary antibodies: Nanog (1:200; Abcam, USA), SSEA4 (1:200; Abcam, USA), Nestin (1:200; Proteintech, USA), Vimentin (1:200; Abcam, USA), and AFP (1:200; Proteintech, USA) after blocking with 5% fetal bovine serum for 1 hour. Cells were rinsed and primary antibodies detected with appropriate secondary antibodies for 1-2 hours at room temperature in the dark. Then nuclei were counterstained with DAPI. Images were acquired using the Nikon fluorescence microscope and Adobe Photoshop (Adobe Systems) software.

Reverse transcription polymerase chain reaction

Total RNA was isolated from cultured cells with the RNeasy Micro Kit (Qiagen, Germany) and reverse transcribed according to the SuperScript III Reverse Transcriptase protocol (Thermo Fisher Scientific). The reverse transcription polymerase chain reaction (RT-PCR) was performed using PrimeSTAR® MAX DNA Polymerase (Takara, Japan).

In vitro differentiation

The iPSCs were plated in ultra-low adhered six-well plates with DMEM/F12 medium that contained 20% Knockout™ serum replacement, 1% L-glutamine, 1% nonessential amino acids, 0.1 mM β-mercaptoethanol, and 1% penicillin/streptomycin. After 7 days, we transferred the resultant embryoid bodies (EB) into six-well plates coated with Matrigel (8 EB per well) in differentiation medium that consisted of DMEM, 20% fetal bovine serum (FBS, Gibco, USA), 1% MEM non-essential amino acid solution, and 1% penicillin/streptomycin. The medium was changed every other day.

Real-time quantitative polymerase chain reaction

We performed real-time quantitative polymerase chain reaction (qRT-PCR) with a SYBR® Premix Ex Taq™ II Kit and Applied Biosystems 7500. Primers for *GAPDH*, *IL-1 β* , *IL-6*, *IL-8*, and *CCL2* were as previously reported (20). Relative transcription levels were determined using the $2^{-\Delta\Delta CT}$ analysis method.

Results

Isolation of peripheral blood mononuclear cells

PBMCs were purified from 7.5 mL of human whole circulating blood obtained from normal and SZ individuals by density centrifugation using a Ficoll gradient. This centrifugation separated the lymphocytes, monocytes, and plasma (Fig.1A). The PBMC layers were carefully transferred to a new tube and washed twice with 1X PBS. After centrifugation, the cells were resuspended in the appropriate volume of culture medium. Further, flow cytometry analysis showed that isolated PBMCs were mainly a subset of CD45⁺ or CD14⁺ monocyte cells (Fig.1B). The human PBMCs were then recovered with a final centrifugation

and stored at -80°C.

Generation of induced pluripotent stem cells from peripheral blood mononuclear cells

Lentiviral vectors played a major role in the historical development of iPSC technology due to their ability to efficiently transduce murine cells for lasting expression of transgenes. The isolated PBMCs were transduced with a lentiviral plasmid that encoded OSKM factors (Fig.2A) and mCherry fluorescent protein at day 4. The OSKM factors in these PBMCs could be activated after they were infected by the virus. The cells were subsequently transferred to Matrigel and cultured with Knockout™ DMEM medium. The iPSC-like colonies started to form 2 weeks later from the infected PBMCs that grew on the Matrigel (Fig.2B). We picked the colonies that displayed a typical morphology of iPSCs and mCherry protein expression from normal people and SZ patients (Fig.2C).

ALP enzymatic activity represents ESC pluripotency. We performed ALP staining and the results showed that the iPSC clones were ALP positive in both normal and SZ individuals (Fig.2C). These data showed that we could successfully establish iPSC clones with fewer transformed cells from the PBMCs in SZ patients.

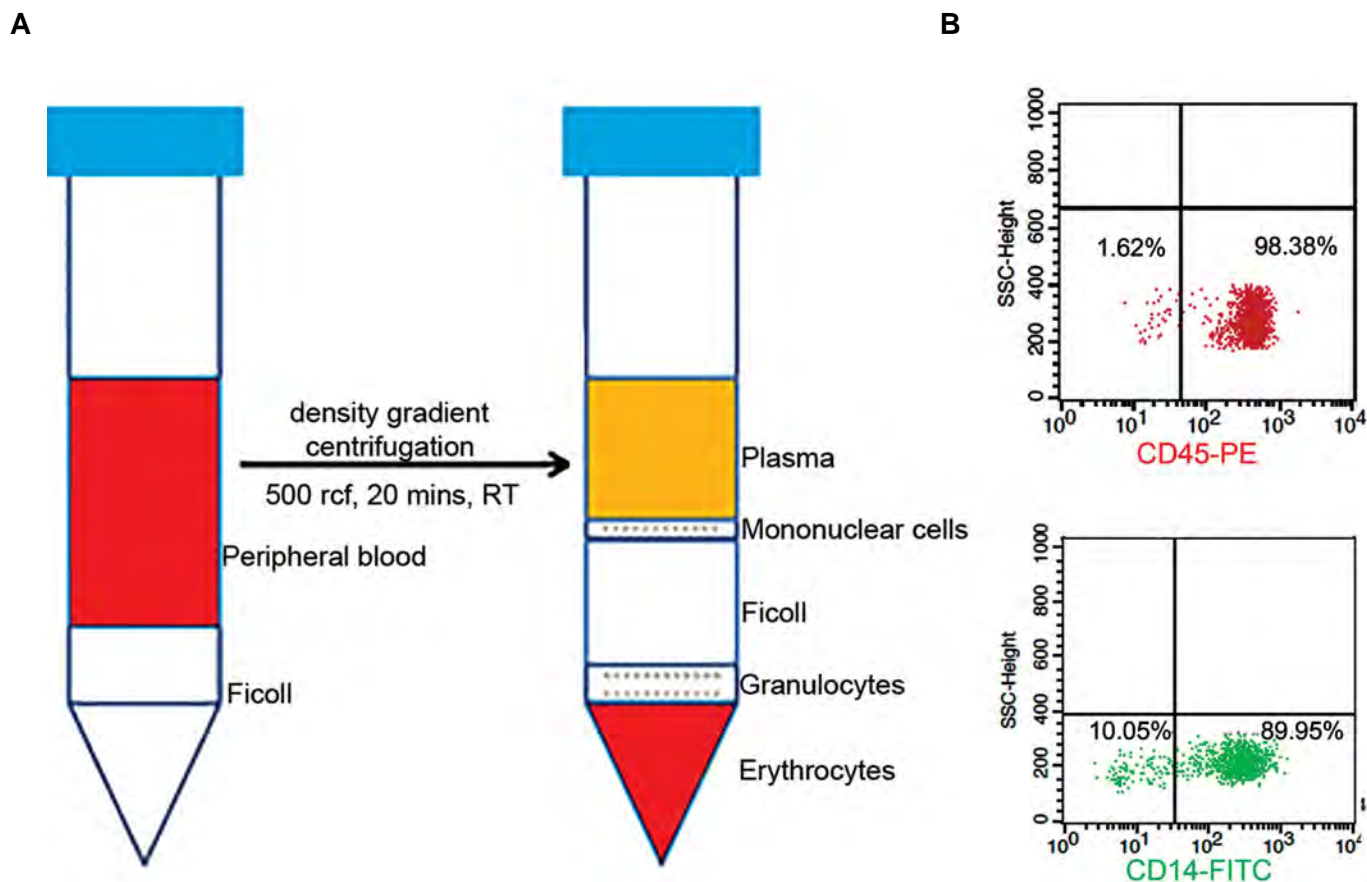


Fig.1: Experimental protocol for isolation of human peripheral blood mononuclear cells (PBMCs) from whole blood. **A.** Steps for isolation of human PBMCs from whole circulating blood by density gradient centrifugation and **B.** Flow cytometry analysis showed that the PBMCs significantly expressed the CD45⁺ or CD14⁺ genotypes.

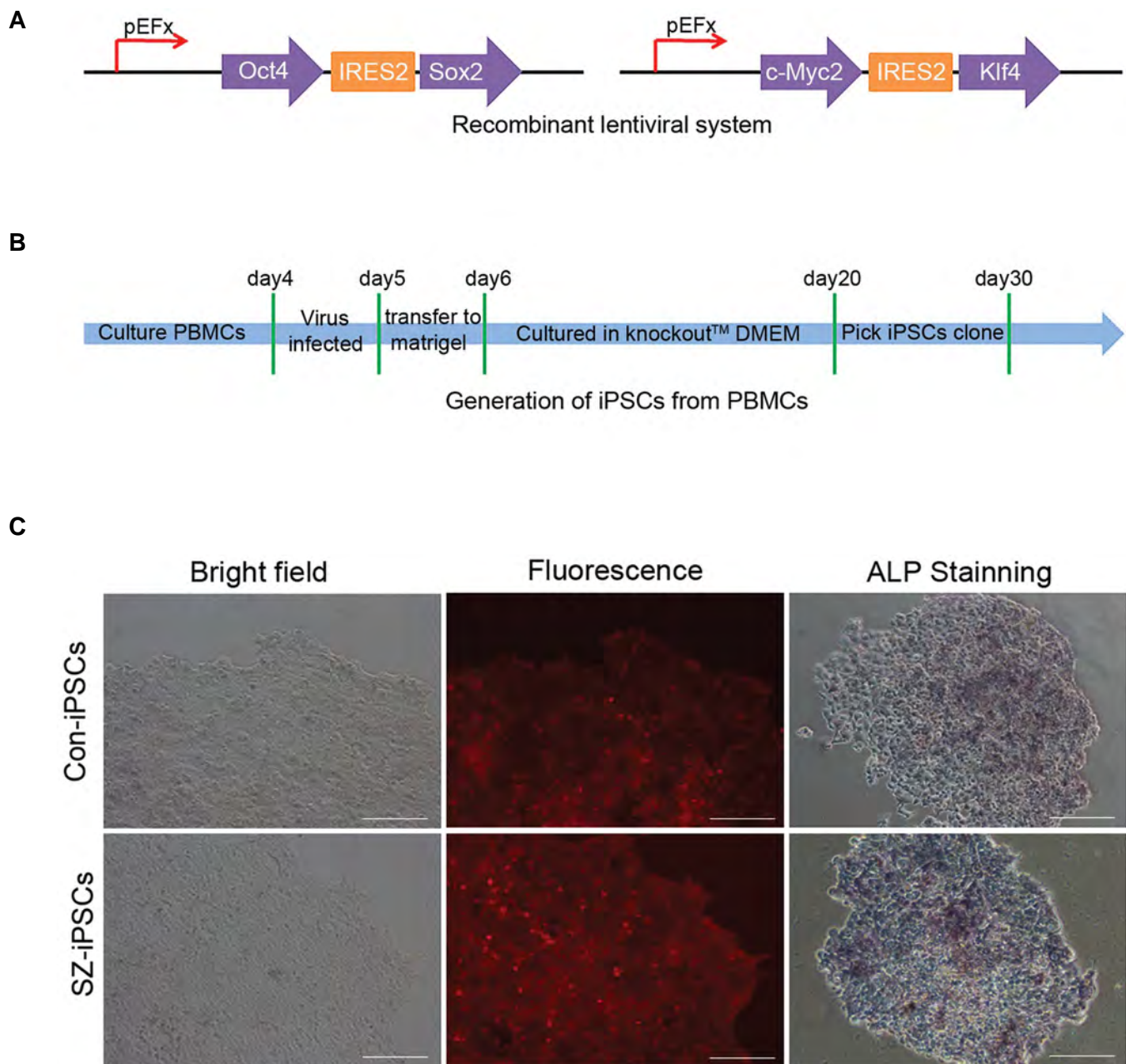


Fig.2: Generation of induced pluripotent stem cells (iPSCs) from peripheral blood mononuclear cells (PBMCs) using a recombinant lentivirus system. **A.** Recombinant lentivirus vectors that contained transcription factors Oct4, Sox2, Klf4, and c-Myc, **B.** Diagram of generation of iPSCs from PBMCs, and **C.** The morphology and alkaline phosphatase (ALP) staining of generated iPSCs from PBMCs in normal people and schizophrenia (SZ) individuals (scale bar: 50 μ m).

Characterization of induced pluripotent stem cells from peripheral blood mononuclear cells

We sought to assess whether the PBMCs from SZ patients could be reprogrammed into iPSCs. We selected the clones and re-plated them into six-well plates coated with Matrigel. We analyzed expressions of the pluripotency markers (*Nanog*, *Oct4*, *Rex1*, *Sox2*) in iPSCs and PBMCs by RT-PCR (Fig.3A). Karyotyping analysis showed that the iPSCs from SZ patients had normal karyotypes according to the standard G-banding technique (Fig.3B). We detected activity of pluripotency markers by immunostaining

and observed relatively high expression levels of Nanog and SSEA4 in the generated iPSCs (Fig.3C). In addition, we analyzed the numbers of iPSC clones per cm^2 and fluorescent cells in immunofluorescence staining (Fig.3D). There was no significant difference in iPSCs formed between normal people and SZ patients. These results indicated that the generated iPSCs from PBMCs displayed pluripotency as well as ESCs and other iPSCs.

To further determine the pluripotency of iPSCs, we cultured undifferentiated EBs (Fig.4A) with differential

medium and then determined the differentiation potential of iPSCs by RT-PCR. The results showed both differentiated iPSCs from normal people (Con-iPSCs) and SZ patients (SZ-iPSCs) expressed ectoderm (Pax6, Nestin), mesoderm (Kdr1, α -cardiac actin) and endoderm (Afp, Gata4) markers (Fig.4B). In addition, we performed *in vitro* differentiation assays and found that the iPSCs had the ability to differentiate into 3 germ layer-derived cell types. The assay used Nestin as a marker for ectoderm differentiation, Vimentin to mark mesoderm differentiation, and alpha fetoprotein (AFP) for endoderm differentiation (Fig.4C). However, a study of the fluorescent positive cells of Nestin, AFP, and Vimentin staining showed that the iPSCs had a weak capacity to differentiate into ectoderm and strong ability to differentiate into endoderm and mesoderm in SZ patients compared to normal people (Fig.4D). Taken together, the PMBCs of normal people and SZ patients had a similar ability to generate iPSCs. Nevertheless, it seemed that the iPSCs from SZ patients might have some defect for differentiating into ectoderm cells compared to those from normal people.

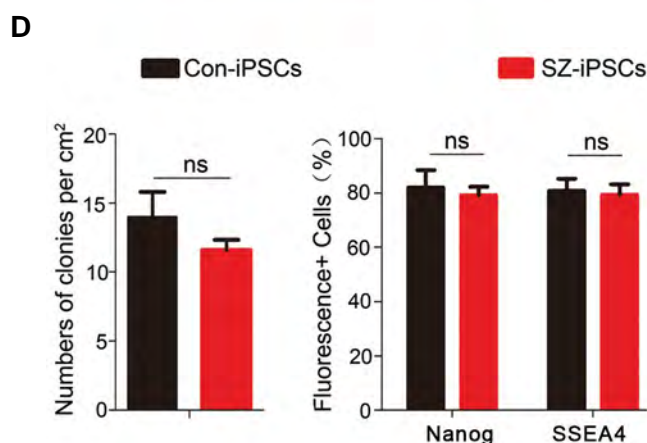
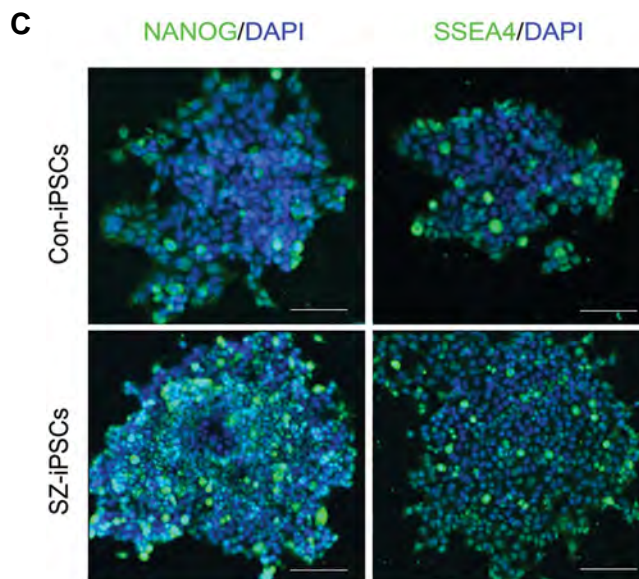
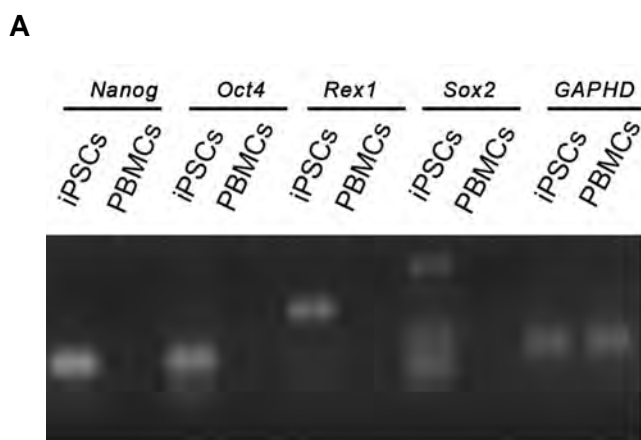


Fig.3: Characterization of induced pluripotent stem cells (iPSCs) from peripheral blood mononuclear cells (PBMCs). **A.** Reverse transcription polymerase chain reaction (RT-PCR) shows the different expressions of *Nanog*, *Oct4*, *Rex1*, and *Sox2* between iPSCs and PBMCs, **B.** Images for karyotyping of the schizophrenia (SZ)-iPSC line, **C.** Immunofluorescence staining of pluripotency markers Nanog and SSEA4 of expanded iPSCs from PBMCs in normal individuals and SZ patients (scale bar: 50 μ m), and **D.** Analysis of the numbers of iPSC clones per cm² and fluorescent positive cells by immunofluorescence staining. P values were determined by the student's t test. ns; Not significant. Error bars indicate SEM.

Expression of inflammatory factors in induced pluripotent stem cells of normal individuals and schizophrenia patients

There is ample evidence that inflammation/immune system can influence and shape the development of the CNS and behavior. The importance of this information as a factor in the etiology of SZ has been strongly emphasized by different laboratories that have investigated the effects of inflammation (21, 22). We detected the expression of inflammatory factors in iPSCs derived from normal and SZ patients when compared by qRT-PCR analysis. The results showed that the expression levels of *Il1b*, *Il6*, *Il8*, and *CCL2* in iPSCs from the SZ-iPSC group were much higher than the Con-iPSC group (Fig.5). This assay showed that the inflammation/immune system might play an important role in the etiology of SZ disorders.

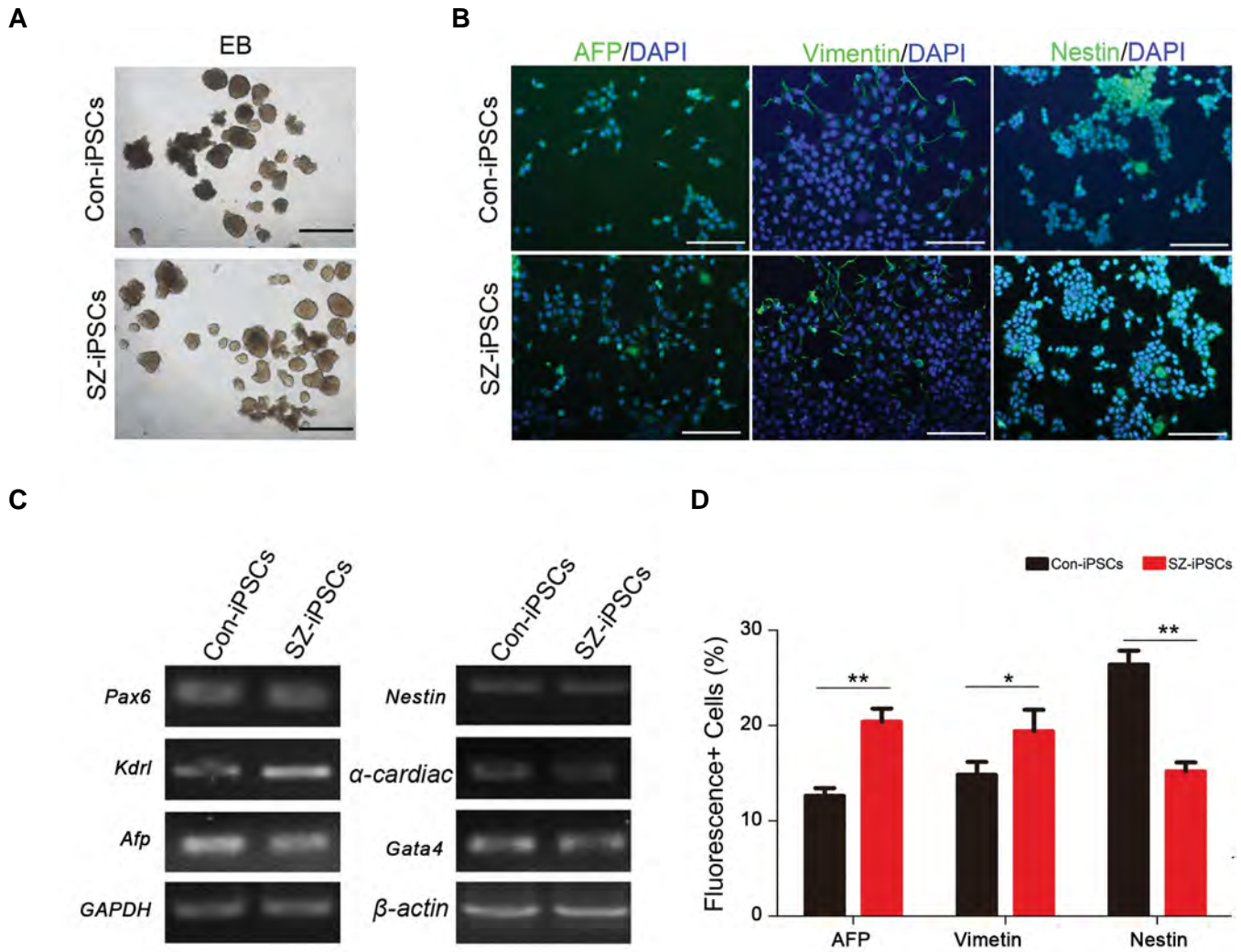


Fig.4: *In vitro* differentiation of schizophrenia induced pluripotent stem cells (SZ-iPSCs) from peripheral blood mononuclear cells (PBMCs). **A.** Embryoid body (EB) formation assay after 4 days of suspension culture, **B.** Reverse transcription polymerase chain reaction (RT-PCR) shows analogous expression levels of transcripts for the 3 germ-layers, **C.** Day 14 cultures contain cells immunoreactive for ectodermal (Nestin), mesodermal (Vimentin) and endodermal (AFP) germ layer markers (scale bar: 50 μ m), and **D.** Analysis of fluorescent positive cells by immunofluorescence staining. P values are determined by the student's t test. Error bars indicate SEM. *; P<0.05 and **; P<0.005.

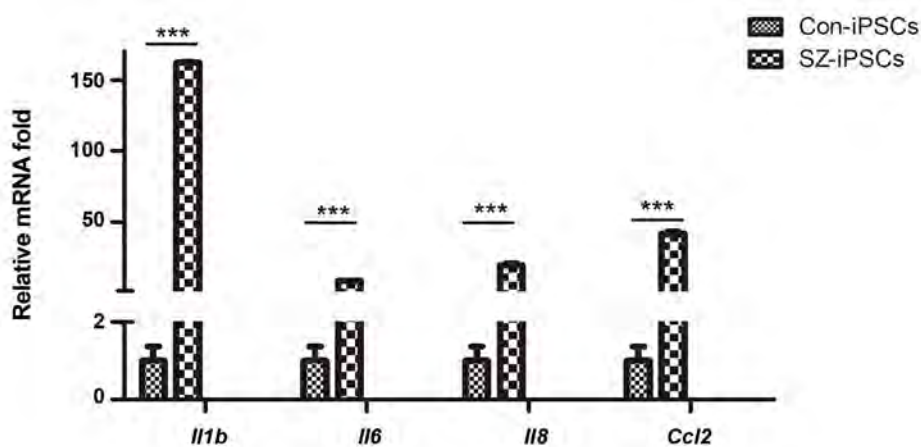


Fig.5: Expression of inflammatory factors between normal induced pluripotent stem cells (Con-iPSCs) and schizophrenia induced pluripotent stem cells (SZ-iPSCs). Real-time quantitative polymerase chain reaction (qRT-PCR) shows analogous expression levels of transcripts for IL-1b, IL-6, IL-8, and CCL2 between Con-iPSCs and SZ-iPSCs. P values are determined by the student's t test. Error bars indicate SEM. ***; P<0.005.

Discussion

The appearance of human ESCs was believed to be beneficial in cell therapy and other medical applications (23). iPSCs, because of their similar characteristics to ESCs, became a novel alternative in stem cell biology. After the discovery of iPSCs, numerous scientists have established iPSCs from various somatic cell types, especially fibroblasts. Unlike fibroblasts, which are difficult to obtain, peripheral blood cells can be easily procured without the need for surgery (24). The biggest difference between fibroblasts and PBMCs is that the PBMCs first need to transform into an attached form during reprogramming. In our study, we have used Matrigel to help the floating cells attach and improve adherence and reprogramming. Then, the settled cells could expand into reprogrammed iPSCs. The pluripotency of the PBMC-derived iPSCs generated by our study could be used in therapeutic cell research and disease modeling.

SZ is a severe neurodevelopmental disorder that results from genetic and environmental factors. The pathogenesis of SZ is not fully understood, in part due to the limitations of current disease models and technology. In recent years, numerous researchers have focused on the establishment of an SZ disease model. The emergence of iPSC technology provides a new strategy to study SZ. Our study has demonstrated that PBMCs in SZ patients can be successfully reprogrammed into iPSCs without feeder layer cells, which are indispensable for reprogramming of fibroblasts. We can study the pathology and the mechanism of action of SZ using the SZ-iPSCs model *in vitro*.

Inflammatory factors play an important role in infection and inflammation and are crucial mediators of the cross-talk between the brain and the immune system. SZ may be associated with an imbalance in inflammatory cytokines. Degradation products of inflammatory substances have been described in schizophrenic brain tissue (25). In terms of the cytokine pattern in SZ, interferon (IFN)-gamma, interleukin (IL)-2, soluble IL-2 receptors, IL-6, and IL-10 have been frequently observed in unmedicated SZ patients (26). However, expression of the inflammatory factors of iPSCs from SZ patients remains unclear. Our findings from iPSC technology provide evidence of the establishment of an inflammatory syndrome in SZ.

Conclusion

We successfully derived iPSCs from PBMCs of schizophrenic patients and showed that schizophrenic patients had a higher, stronger inflammatory response in iPSCs. Our results might lead to the development of new strategies for clinical diagnosis and treatment of SZ.

Acknowledgments

This work was supported by the Natural Science

Foundation of China (81771226), Henan Province Natural Science Foundation (162102310488, 142300410192), Xinxiang City Foundation (CXRC16003, ZD17008), Scientific Research Foundation of Xinxiang Medical University (YJSCX201603Z), and Xinxiang Medical University Foundation (20172DCG-03). There is no conflict of interest in this study.

Authors' Contributions

H.F., J.L.; Contributed to conception and design. Q.L., J.D., J.F., J.L.; Contributed to all of the experimental work, data and statistical analysis, and interpretation of data. W.L., W.G.; Contributed extensively in interpretation of the data and the conclusion. All authors read and approved the final manuscript.

References

- Okita K, Ichisaka T, Yamanaka S. Generation of germline-competent induced pluripotent stem cells. *Nature*. 2007; 448(7151): 313-317.
- Takahashi K, Tanabe K, Ohnuki M, Narita M, Ichisaka T, Tomoda K, et al. Induction of pluripotent stem cells from adult human fibroblasts by defined factors. *Cell*. 2007; 131(5): 861-872.
- Takahashi K, Yamanaka S. Induction of pluripotent stem cells from mouse embryonic and adult fibroblast cultures by defined factors. *Cell*. 2006; 126(4): 663-676.
- Wernig M, Meissner A, Foreman R, Brambrink T, Ku M, Hochedlinger K, et al. In vitro reprogramming of fibroblasts into a pluripotent ES-cell-like state. *Nature*. 2007; 448(7151): 318-324.
- Okano H, Yamanaka S. iPS cell technologies: significance and applications to CNS regeneration and disease. *Mol Brain*. 2014; 7: 22.
- Kamao H, Mandai M, Okamoto S, Sakai N, Suga A, Sugita S, et al. Characterization of human induced pluripotent stem cell-derived retinal pigment epithelium cell sheets aiming for clinical application. *Stem Cell Reports*. 2014; 2(2): 205-218.
- Kikuchi T, Morizane A, Doi D, Onoe H, Hayashi T, Kawasaki T, et al. Survival of human induced pluripotent stem cell-derived midbrain dopaminergic neurons in the brain of a primate model of Parkinson's disease. *J Parkinsons Dis*. 2011; 1(4): 395-412.
- Insel TR. Rethinking schizophrenia. *Nature*. 2010; 468(7321): 187-193.
- Naismith SL, Norrie LM, Mowszowski L, Hickie IB. The neurobiology of depression in later-life: clinical, neuropsychological, neuroimaging and pathophysiological features. *Prog Neurobiol*. 2012; 98(1): 99-143.
- van Os J, Kapur S. Schizophrenia. *Lancet*. 2009; 374(9690): 635-645.
- Kálmán S, Garbett KA, Janka Z, Mirnics K. Human dermal fibroblasts in psychiatry research. *Neuroscience*. 2016; 320: 105-121.
- Saini C, Brown SA, Dibner C. Human peripheral clocks: applications for studying circadian phenotypes in physiology and pathophysiology. *Front Neurol*. 2015; 6, 95.
- Schmidt MJ, Horvath S, Ebert P, Norris JL, Seeley EH, Brown J, et al. Modulation of behavioral networks by selective interneuronal inactivation. *Mol Psychiatry*. 2014; 19(5): 580-587.
- Lau CI, Wang HC, Hsu JL, Liu ME. Does the dopamine hypothesis explain schizophrenia? *Rev Neurosci*. 2013; 24(4): 389-400.
- Chiang CH, Su Y, Wen Z, Yoritomo N, Ross CA, Margolis RL, et al. Integration-free induced pluripotent stem cells derived from schizophrenia patients with a DISC1 mutation. *Mol Psychiatry*. 2011; 16(4): 358-360.
- Wen Z, Nguyen HN, Guo Z, Lalli MA, Wang X, Su Y, et al. Synaptic dysregulation in a human iPSC cell model of mental disorders. *Nature*. 2014; 515(7527): 414-418.
- Jacobs BM. A dangerous method? The use of induced pluripotent stem cells as a model for schizophrenia. *Schizophr Res*. 2015; 168(1-2): 563-568.
- Kennedy A, Cribbs AP. Production and concentration of lentivirus for transduction of primary human t cells. *Methods Mol Biol*. 2016; 1448: 85-93.
- Loh YH, Agarwal S, Park IH, Urbach A, Huo H, Heffner GC, et al. Generation of induced pluripotent stem cells from human blood.

- Blood. 2009; 113(22): 5476-5479.
20. Zhao GN, Zhang P, Gong J, Zhang XJ, Wang PX, Yin M, et al. Tmbim1 is a multivesicular body regulator that protects against non-alcoholic fatty liver disease in mice and monkeys by targeting the lysosomal degradation of Tlr4. *Nat Med.* 2017; 23(6): 742-752.
 21. Bauer S, Kerr BJ, Patterson PH. The neuropoietic cytokine family in development, plasticity, disease and injury. *Nat Rev Neurosci.* 2007; 8(3): 221-232.
 22. Bilbo SD, Schwarz JM. The immune system and developmental programming of brain and behavior. *Front Neuroendocrinol.* 2012; 33(3): 267-286.
 23. Zhang XB. Cellular reprogramming of human peripheral blood cells. *Genomics, Proteomics Bioinformatics.* 2013; 11(5): 264-274.
 24. Staerk J, Dawlaty MM, Gao Q, Maetzel D, Hanna J, Sommer CA, et al. Reprogramming of human peripheral blood cells to induced pluripotent stem cells. *Cell Stem Cell.* 2010; 7(1): 20-24.
 25. Körschenhausen DA, Hampel HJ, Ackenheil M, Penning R, Müller N. Fibrin degradation products in post mortem brain tissue of schizophrenics: a possible marker for underlying inflammatory processes. *Schizophr Res.* 1996; 19(2-3): 103-109.
 26. Müller N, Schwarz MJ. Neuroimmune-endocrine crosstalk in schizophrenia and mood disorders. *Expert Rev Neurother.* 2006; 6(7): 1017-1038.
-

***MafA* Overexpression: A New Efficient Protocol for *In Vitro* Differentiation of Adipose-Derived Mesenchymal Stem Cells into Functional Insulin-Producing Cells**

Dian Dayer, Ph.D.^{1*}, Mohammad Reza Tabandeh, Ph.D.^{2,3}, Eskandar Moghimipour, Ph.D.^{1,4}, Mahmood Hashemi Tabar, Ph.D.^{1,5}, Ata.A Ghadiri, Ph.D.^{1,6}, Elham Allah Bakhshi, Ph.D.¹, Mahmoud Orazizadeh, Ph.D.^{1,5}, Mohammad Ali Ghafari, Ph.D.^{1,7}

1. Cellular and Molecular Research Center, Ahvaz Jundishapur University of Medical Sciences, Ahvaz, Iran
2. Department of Biochemistry and Molecular Biology, Faculty of Veterinary Medicine, Shahid Chamran University of Ahvaz, Ahvaz, Iran
3. Stem Cells and Transgenic Technology Research Center, Shahid Chamran University of Ahvaz, Ahvaz, Iran
4. Department of Pharmaceutics, Faculty of Pharmacy, Ahvaz Jundishapur University of Medical Sciences, Ahvaz, Iran
5. Department of Anatomy, Faculty of Medicine, Ahvaz Jundishapur University of Medical Sciences, Ahvaz, Iran
6. Department of Immunology, Faculty of Medicine, Ahvaz Jundishapur University of Medical Sciences, Ahvaz, Iran
7. Department of Biochemistry, Faculty of Medicine, Ahvaz Jundishapur University of Medical Sciences, Ahvaz, Iran

*Corresponding Address: P.O.Box: 61357-15794, Cellular and Molecular Research Center, Ahvaz Jundishapur University of Medical Sciences, Ahvaz, Iran
Email: dayer86@gmail.com

Received: 13/December/2017, Accepted: 7/August/2018

Abstract

Objective: We proposed a novel differentiation method for the efficient differentiation of adipose-derived mesenchymal stem cells (ADMSCs) into functional insulin-producing cells (IPCs) based on *MafA* overexpression.

Materials and Methods: In this experimental study, a eukaryotic expression vector containing *MafA* [*MafA*/pcDNA3.1(+)] was constructed and purified. ADMSCs were differentiated into IPCs. ADMSCs were assigned in two groups including control (C), and the *MafA* overexpressed (*MafA*+) groups. The ADMSCs were transfected by *MafA*/pcDNA 3.1(+) at day 10 of the differentiation. Differentiated cells were analyzed for the expression of multiple β cell specific genes (*Nkx2.2*, *Ngn3*, *Isl-1*, *Pdx1*, *MafA*, *Nkx6.1*, and *Insulin*) using real-time polymerase chain reaction (PCR). The insulin secretion potency of the differentiated cells in response to glucose exposure was also determined using an enzyme-linked immunosorbent assay (ELISA) method and Dithizone (DTZ) staining. The IPCs from the control manipulated group, and un-differentiated ADMSCs group were transplanted to streptozotocin (STZ)-diabetic rats. Rats were monitored for blood glucose and insulin concentration.

Results: The results revealed that ADMSCs were successfully differentiated into IPCs through the 14 day differentiation protocol. The expression of β -cell specific genes in *MafA*+ IPCs was higher than in control cells. Glucose-induced insulin secretion after the exposure of IPCs to glucose was higher in *MafA*+ group than the control group. The STZ-diabetic rats showed an ability to secrete insulin and apparent hyperglycemic condition adjustment after transplantation of the control IPCs. The mean insulin concentration of diabetic rats that were transplanted by manipulated IPCs was significantly higher than ADMSCs-transplanted rats; however, no effect was observed in the concentration of blood glucose.

Conclusion: The overexpression of *MafA* can be used as a novel promising approach for the efficient production of IPCs from ADMSCs *in vitro*. However, the future therapeutic use of the *MafA*+ IPCs in diabetic animals needs further investigations.

Keywords: Adipose Tissue, Insulin-Producing Cells, *MafA*, Mesenchymal Stem Cells

Cell Journal (Yakhteh), Vol 21, No 2, July-September (Summer) 2019, Pages: 169-178

Citation: Dayer D, Tabandeh MR, Moghimipour E, Hashemi Tabar M, Ghadiri A, Allah Bakhshi E, Orazizadeh M, Ghafari MA. *MafA* overexpression: a new efficient protocol for *in vitro* differentiation of adipose-derived mesenchymal stem cells into functional insulin-producing cells. Cell J. 2019; 21(2): 169-178. doi: 10.22074/cellj.2019.5669.

Introduction

Diabetes mellitus is the most common metabolic disorder worldwide. With regard to the significant increase in the number of diabetic patients and diabetic complications, much of the latest scientific research is focused on the design of a reliable plan for the treatment of diabetes mellitus (1). In diabetes mellitus type 1 (T1DM) the autoimmune destruction of pancreatic beta cells results in insufficient insulin secretion (2). Stem cell therapy can be regarded as one of the most interesting methods of the production of functional pancreatic beta cells (3). Some limitations of this approach are the generation of cells with immature or abnormal appearance and the lack of

insulin secretion ability (4). In this view, the optimization of differentiation protocols is inevitable. Recently, several genetic manipulations have been developed in order to generate the functional artificial pancreatic beta cells (5-7). *MafA* is a transcription factor with a b-zip design which belongs to *MafA* family. *MafA* protein binds to the insulin enhancer element, RIPE3b, of the insulin gene promoter and activates the insulin gene expression (8).

Synergistic cooperation of *MafA* with *NeuroD* and *Pdx1* increases the insulin synthesis and secretion. Moreover, *MafA* coordinates with *MafB* to induce pancreatic β cells generation and differentiation (9). *MafA* regulates the

glucose and energy balance in different tissues such as adipose tissue, pancreas, and muscle, and its deficiency in mice leads to diabetes and diabetic nephropathy (10). Some studies emphasized the eventual role of *MafA* in the differentiation of adipocytes and adipose tissue sensitivity to insulin (11-13). Given these findings, it has been suggested that *MafA* can be used as an effective factor for the renewal of pancreatic β cells and the induction of differentiation of stem cells into insulin-producing cells (IPCs) (14). The study by Chiou et al. (15) showed that *MafA* promotes the reprogramming of placenta-derived multipotent stem cells into pancreatic islets-like cells. With regard to the significant role of *MafA* in the production and maintenance of mature beta cells, we designed a novel protocol for the differentiation of adipose-derived mesenchymal stem cells (ADMSc) into functional IPCs by the overexpression of *MafA*.

Materials and methods

Cloning of *MafA* into a pcDNA3.1+ plasmid vector

In this experimental study, the RNXTM reagent (Sinaclon, Iran) was used for the isolation of the total RNA as recommended by the manufacturer. The purity of isolated RNA was assessed using a Nanodrop spectrophotometer (Nanodrop 2000 TM, Thermo, Canada). The reaction of cDNA synthesis was carried out using a CycleScript RT PreMix cDNA synthesis kit (Bioneer, South Korea) in a total volume of 20 μ L according to the manufacturer's recommendation. The PCR reaction was performed utilizing Taq DNA Polymerase 2X Master Mix Red (Ampliqon, Denmark) in a total amount of 20 μ L. MgCl₂ and each of the primer concentrations were modified to 1.5 mM and 250 nM, respectively. The primers (Bioneer, South Korea) which were designed for the generation of full-length *MafA* gene were as follow: 5'-ATATAAGCTTAATATGGCCGCGGAGCTGGC-3' and 5'-ATCGGGATCCTCACAGAAAGAAGTCG-3'.

The Primer Premier 5 software (Premier Biosoft International, USA) was used for the design of particular primers with restriction sites at the 5' (HindIII) (Vivantis Malaysia) and 3' ends (EcoRI) (Vivantis Malaysia). Polymerase chain reaction (PCR) was performed using a Thermal Cycler (Eppendorf Mastercycler, Germany). The thermal cycle included 35 cycles as follows: 5 minutes at 95°C for the initial denaturation, 1 minute at 94°C for denaturation, 1 minute at 58°C for annealing, 1 minute at 72°C for the extension and a final extension at 72°C for 5 minutes. The amplified PCR products were visualized by 1% agarose gel electrophoresis in TAE buffer stained with DNA Safe stain (Merck, Germany) under ultraviolet (UV) light (Mabna Tajhiz, Iran). The *MafA* PCR product was purified from the agarose gel using a Gel DNA Recovery Kit (SinaClon BioSciences, Iran) according to the manufacturer's recommendation. Double digestion of PCR products and pcDNA3.1+ vector (ThermoFisher Scientific, USA) were performed utilizing EcoRI and the Hind III restriction enzymes at 37°C for 2 hours. The digested fragments were visualized using agarose gel

electrophoresis. The fragments were purified by a Gel DNA Recovery Kit (Bioneer, South Korea) according to the manufacturer's recommendation. The obtained purification linear vector and insert were ligated to each other using T4 DNA ligase (Fermentas, USA). The reaction was deactivated by the incubation for 15 minutes at 65°C. The competent cells were prepared from *E. coli* Top10F' cell (Clontech Laboratories, Inc USA) using the calcium chloride method. The obtained competent cells were transformed with 2 μ L of the ligation product. The positive transformed bacterial cells were picked up on LB medium agar plates containing ampicillin (100 μ g/ml, Sigma, USA). Some of the colonies were confirmed by colony PCR using universal T7 and BGH primers (Bioneer, South Korea). After the selection of the positive recombinant clones, the plasmid DNA was extracted from the cells cultured overnight using a Miniprep plasmid isolation kit (SinaClon, Biosciences, Iran) and confirmed by PCR, restriction enzyme digestion, followed by DNA sequencing using T7 and BGH primers. The plasmid was purified using an AccuPrep Nano Plus Plasmid Mini Extraction Kit (Bioneer, Korea) and sequenced using a Big Dye terminator V.3.1 Cycle Sequencing Kit in an ABI 3130 Genetic analyzer (Applied Biosystems, USA).

Preparation of tissues

Normal Sprague Dawley male rats (n=5) with an age range of 2-3 months were chosen for the experiment. All animals used were housed in accordance to the Guide for the Care and Use of Laboratory Animals by the National Academy of Sciences (National Institutes of Health Publication No. 86-23). The animal experiment was approved by the Animal Experiments Committee of the Ahvaz Jundishapur University of Medical Sciences (AJUMS.REC.1393.100). Rats were anesthetized with a mixture of 100 mg/kg ketamine (Sigma, USA) and 10 mg/kg xylazine (Sigma, USA). Pancreatic tissue and adipose tissue from splanchnic region isolated in a sterile condition. The tissues were washed three times with sterile PBS that contained 3% Pen /Strep (Gibco, UK).

Isolation of rat of adipose-derived mesenchymal stem cells

The isolated splanchnic adipose tissue was chopped into very small pieces. The explants were placed in the 25 cm² culture flask. Three milliliters of Dulbecco's Modified Eagle's Medium-high glucose (DMEM-HG, Gibco, Netherlands) containing 15% fasting blood glucose (FBS, Sigma, USA) and 1% Pen/Strep was gently added to each flask. Flasks were placed in a 37°C incubator with 5% CO₂. After 4 days, the culture medium was replaced by DMEM-HG containing 10% FBS and 1% Pen/Strep. When the adherent cells reached confluence, the explants were removed. The culture medium was replaced every 3 days.

Characterization of adipose-derived mesenchymal stem cells

The expression of cell surface biomarkers named

clusters of differentiation (CD) including CD34, CD45, CD90, and CD105 was determined using flow cytometry method, as described previously. The osteogenic and adipogenic differentiation potency of ADMSCs were assessed using the osteogenic and adipogenic mediums, as described previously (16, 17).

The protocol for differentiation of adipose-derived mesenchymal stem cells into insulin producing cells

The isolated cells were pooled, counted, and randomly divided into 2 groups based on the modification of the basic differentiation protocol. The experimental groups included the control group and the *MafA* overexpressed (*MafA*⁺) groups. All experiments were done in triplicates (three flasks for each differentiation protocol). In the control group, the basic differentiation protocol was performed. The basic differentiation protocol consisted of 3 main stages. In stage 1, cells (1×10^6 /ml) were cultured in a medium containing DMEM-LG (Gibco, Netherland), 10% FBS, and 1% Pen/Strep until the cells reached 80% confluency. In stage 2, the differentiation medium contained DMEM-low glucose (DMEM-LG), 20 μ M nicotinamide (Sigma, USA), 5% FBS, and 1% Pen/Strep for 7 days. In stage 3, cells were cultured in a medium of stage 2 plus 10 μ M Exendix-4 (Sigma, USA) for 7 days (16). In the *MafA*⁺ group, cells were differentiated through basic differentiation protocol, and then, transfected with a recombinant *MafA*/ pCDNA3.1(+) vector at day 3 of stage 3.

Transfection of differentiated adipose-derived mesenchymal stem cells by the recombinant vector

Differentiated ADMSCs were trypsinized and seeded in 25 ml flasks 24 hours before the transfection. At day 10 of differentiation, cells were washed three times with phosphate buffered saline (PBS, Calbiochem, Iran), trypsinized, counted, and suspended at a density of 10^6 /ml in serum-free DMEM-HG. Then, 100 μ l of cells were mixed with 5 μ g of suitable vector pCDNA(3.1+) in control group and recombinant *MafA*/pCDNA 3.1(+) in the experimental group in 0.4 ml electroporation cuvette (Biorad, USA), and gently mixed by pipetting. The mixture was placed in an electroporation system (GenePulser system II, Biorad, USA) and one pulse of 140V was delivered for 15 milliseconds. Following the electroporation, cells were plated onto a 25 ml flask that contained a differentiation medium and was incubated at 37°C and 5% CO₂. After 24 hours, Gentamicin (350 μ g/ml, Sigma, USA) was added to the growth media for the positive selection of antibiotic-resistant ADMSCs. The media were changed every 3 days, and Gentamicin selection was maintained for 7 days. Antibiotic-resistant ADMSCs were split to be grown for the differentiation.

Detection of *MafA* expression in transfected cells

In order to confirm the overexpression of *MafA* in *MafA*/pCDNA 3.1(+) transfected cells, dot blot analysis, indirect enzyme-linked immunosorbent assay (ELISA), and real-time PCR were performed. Gentamicin resistant

ADMSCs were split to grow for 24 hours at 37°C. Cells were trypsinized and centrifuged at 1200 \times rpm for 8 minutes; then washed with PBS. Cell lysis was done using radio immune precipitation assay (RIPA) buffer consisted of 50 mM HCl, 150 mM NaCl, 0.1% Triton X-100, 0.1% sodium dodecyl sulfate (SDS), 1mM EDTA, 1 mM NaF, and 1 mM phenyl methyl sulfonyl fluoride (PMSF) in ddH₂O. Samples were centrifuged at 10000 \times rpm for 10 minutes, and the supernatants were separated for further analysis. Protein concentration was determined by the Bradford method using 1 mg/ml bovine serum albumin as a standard.

Dot blot analysis

A nitrocellulose membrane (Millipore, USA) was pre-wetted for 5 minutes in a mixture of tris-buffered saline and Tween 20 (TBS-T) (20 mM Tris, 150 mM NaCl, 0.05% Tween 20, pH=7.5), and then, soaked in distilled water for 2 minutes. The lysate of control and *MafA*/pCDNA 3.1(+) transfected cells (~10 μ g protein) was dotted on nitrocellulose membrane. Non-specific binding sites were then blocked using TBS-T containing 5% skim milk (Merck, Germany) for 30 minutes at room temperature, rinsed three times with TBS-T, and incubated for 30 minutes with 1:1000 dilution of specific antibody against rat *MafA* protein (Santa Cruz Biotechnology, USA, Art No:sc-390491). This antibody was a mouse monoclonal antibody specific for an epitope mapping between amino acids 330-341 which are near the C-terminus of *MafA*, recommended for the detection of *MafA* of the mouse, rat, and human origin. The membrane was incubated for 30 minutes with rabbit anti-rat HRP-conjugated IgG antibody (Santa Cruz Biotechnology, USA, Art No: SC-2786) with a dilution of 1:1000. Following three washes with PBS buffer, the substrate [50 mM Tris buffer, pH=7.8, containing 6 mg 3'-Diaminobenzidine (DAB), 10 μ L H₂O₂] was used for the detection.

Indirect ELISA for the detection of *MafA* expression in transfected cells

Microwell plates (Nunc, Denmark) were coated with 100 μ l per well of the *MafA* antibody (Santa Cruz Biotechnology, USA, Art No: sc-390491) (500 ng), diluted in coating buffer (0.2 M sodium carbonate/bicarbonate, pH=9.4), and incubated overnight at room temperature. After washing the plates three times with PBST (PBS with 0.05% v/v Tween 20), the unbound sites were blocked with 200 μ l of blocking solution at 37°C for 1 hour. Then, the plates were washed three times with PBST. After that, 100 μ l of cell lysates were added into each well and incubated at room temperature for 1 hour. After the plates were washed three times with washing solution, 100 μ l of the *MafA* antibody (500 ng) diluted in coating buffer was pipetted into each well and incubated for 1 hour at room temperature. Then, the plates were washed three times with washing buffer and 100 μ l of rabbit anti-rat horseradish peroxidase (HRP)-conjugated IgG antibody (Santa Cruz Biotechnology, USA, Art No: SC-2786, 1:1000) diluted in PBST was added and

incubated for 1 hour at room temperature. The plates were washed five times, and 150 μ l of substrate solution (0.1 mg/ml 3,3',5,5'-Tetramethylbenzidine (TMB) in 0.1 M citrate-phosphate buffer, pH=5.0 containing 0.03% hydrogen peroxide) was added into each well. The reaction was stopped after 30 minutes by adding 50 μ l of 1.25 M sulfuric acid, and the absorbance was read in a microplate reader (BioTek, USA) in a dual wavelength mode (450-630 nm). Lysis buffer was used as a blank control. The validation of the antibody was performed using mouse eye extract as a positive control (Santa Cruz Biotechnology, USA, Art No: sc-364241). All assays were performed in triplicate. Data was reported by the unit of OD450 nm/ mg protein.

Real time polymerase chain reaction

The gene expression pattern between the control and experimental groups was compared. The details are available in "the evaluation of IPCs functionality *in vitro*" section.

The evaluation of insulin producing cells functionality *in vitro*

Dithizone staining

At the end of the differentiation protocol, DTZ (Sigma Aldrich, USA) solution (100 ng/ml) was dissolved in dimethyl sulfoxide (Sigma Aldrich, USA). After filtrating through a 0.2 μ m filter, DTZ solution was added to each 25

cm² flask at the volume of 3 ml. Cells were incubated at 37°C for 30 minutes and washed three times with PBS. Cells were analyzed using an inverted microscope (Olympus, Japan) for the detection of Crimson red-stained clusters.

Real-time polymerase chain reaction analysis

At the end of the experiment, the two obtained groups of differentiated cells were analyzed for the gene expression through real-time PCR. At day 14 of differentiation, differentiated cells isolated. The RNA extraction was performed by the use of RNXTM reagent (CinaClon, Iran) according to the manufacturer's recommendation. One μ g of produced RNA was used for cDNA synthesis by utilization of a CycleScript cDNA synthesis kit (CycleScript RT PreMix Bioneer, South Korea) based on the manufacturer's recommendation. The real-time PCR reaction was carried out by means of an Ampliqon RealQ Plus Master kit for SYBR Green I[®] (Ampliqon, Denmark) on a Lightcycler[®] Detection System (Roche, USA), as described previously (17, 18). Table 1 shows the list of the genes and primers used for real-time PCR. The negative controls consisted of two distinct reactions without cDNA or RNA. The 2^{- $\Delta\Delta$ Ct} method was performed to compare the gene expression between different groups (19). All qPCR analyses were performed according to the Minimum Information for Publication of Quantitative Real-Time PCR Experiments (MIQE) guideline (20).

Table 1: Characteristics of primers used in real-time polymerase chain reaction

Gene name	Sequence (5'-3')	length (bp)	Accession number
<i>GAPDH</i>	F: TG GTATCGTGGAAAGGACTC R: CCTGCTTCACCACCTTCTTG	290	NM_002046/6
<i>Pdx1</i>	F: GGAGGGTTTGGAAAACCACT R: ACAAACATAACCCGAGCACA	131	NM_022852.3
<i>Nkx2.2</i>	F: AAACCGTCCCAGCGTTAAT R: TGCTTTAGAAGACGGCTGAC	126	NM_001191904.1
<i>Nkx6.1</i>	F: ACACACGAGACCCACTTTTT R: TTCTGGAACCAGACCTTGAC	147	NNM_031737.1
<i>Isl-1</i>	F: GCTTTTCAGCAACTGGTCA R: AATAGGACTGGCTACCATGC	123	NM_017339.3
<i>Insulin</i>	F: ATCTTCAGACCTTGGCACTG R: ATCTTCAGACCTTGGCACTG	141	NM_019129.3
<i>MafA</i>	F: CTGCTGTCCTACTATGCTCA R: TGTATTTCCTCCAGGAGTTACAG	137	XM_006241903.2
<i>Ngn-3</i>	F: CTATTCTTTTGCCTGGTAC R: CTGACGGTCACTTGGCAG	128	NM_021700.1

Insulin secretion assay

The ability of different IPCs for the synthesis and secretion of insulin was compared through the insulin secretion assay, as described previously. The insulin concentration was determined using a rat-specific insulin ELISA kit (RayBiotech, USA) based on a protocol recommended by the manufacturer, as described previously (17). The concentration of insulin was reported as $\mu\text{IU/ml}$.

Transplantation of insulin-producing cells and evaluation of insulin-producing cells functionality *in vivo*

The study group consisted of 15 normal male Sprague Dawley rats with 8 weeks age and 180-200 g weight. The experimental diabetes mellitus condition was induced using 50 mg/kg of Streptozotocin (STZ, Sigma Aldrich, USA) in citrate buffer. Rats possessed three blood glucose above 500 mg/ml (at least three measurements) were chosen as diabetic. The diabetic rats were studied in three groups. Group 1 (n=5) was injected with undifferentiated ADMSCs, the control group (n=5) received un-manipulated IPCs. The remained group (n=5) was injected with manipulated IPCs. At day 14 of differentiation, the differentiated IPCs of all three experimental groups were detached by trypsinization. After washing three times with PBS, 1×10^6 of isolated cells were suspended in 200 μl of DMEM-HG. Rats were anesthetized using 100 mg/kg ketamine and 10 mg/kg xylazine as a mixture. The differentiated cells were injected through the tail vein into rats (19). The blood glucose concentration was determined once a week by utilizing a glucometer (EasyGluco, South Korea). After six weeks, a 25 mM glucose solution was injected into rats. After 10 minutes, rats were anesthetized using 100 mg/Kg ketamine and 10 mg/Kg xylazine as a mixture, and 2 ml of whole blood was acquired. After 5 minutes, the serum was obtained by centrifugation at 2000 rpm. The insulin concentration in serums was measured by an ELISA method.

Statistical analyses

Data analyses were done using the SPSS 18.0 software package (SPSS Inc., Chicago, IL, USA). All analyses were done in triplicate. One-way ANOVA followed by *Tukey* post-hoc analysis was used to test differences between various means including the expression level of different genes and insulin concentration. The difference between two independent groups was determined using *t* test. All experimental data were presented as the mean \pm SEM. The level of significance for all tests was set at $P < 0.05$.

Results

Characteristics of *MafA*-pCDNA3.1(+) vector

According to the applied primers in RT-PCR step, colony PCR, restriction site digestion, and DNA sequencing, the accuracy of *MafA* cloning into pCDNA3.1(+) plasmid was confirmed (Fig.1). Dot blot analysis, ELISA, and Real-time quantitative PCR were performed on selected

Gentecin resistant ADMSCs clones in order to determine the expression of *MafA* in transfected cells. Dot blot results showed a low level of *MafA* protein in ADMSCs cells transfected with pCDNA3.1(+) and a high level of *MafA* protein in *MafA*/ pCDNA 3.1(+) transfected cells (Fig.2A). The ELISA and Real-time PCR analysis of Gentecin resistant ADMSCs clones showed a significant increase in *MafA* expression compared with the control cells (Fig.2B, C).

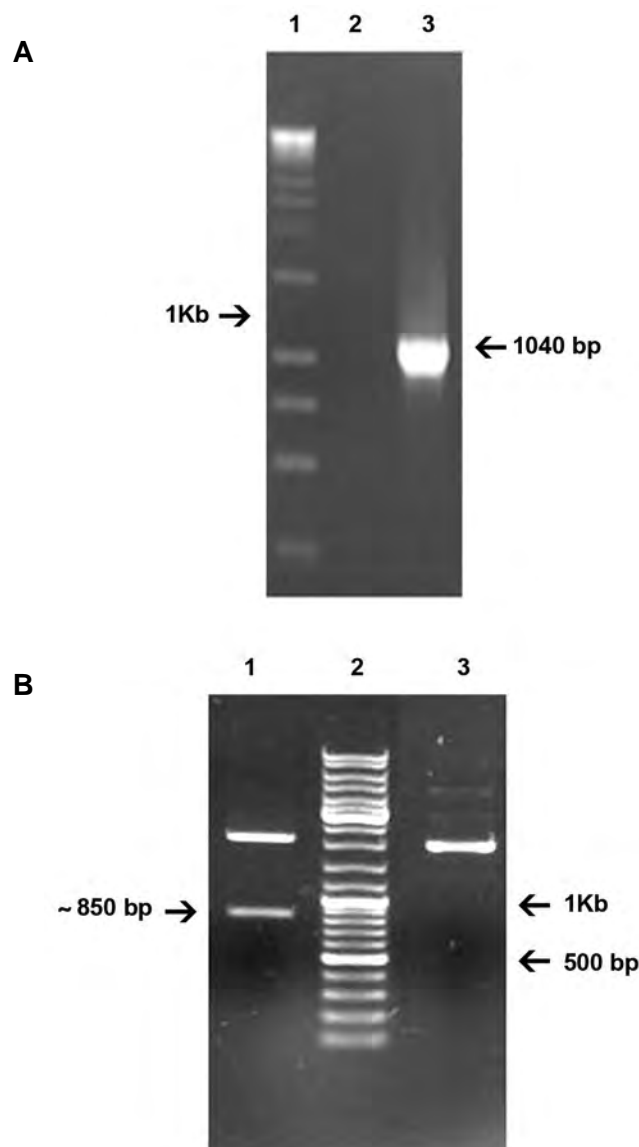


Fig.1: Polymerase chain reaction screening of positive clone of *E. coli* Top10F' containing *MafA*/pCDNA3.1(+) vector using universal primer (T7 promoter and BGH reverse primers) on 1% agarose gel electrophoresis. **A.** Lane 1; 1 kb DNA ladder, Lane 2; Negative control, and Lane 3; A 1040 bp band corresponding to 870 bp *MafA* gene and 170 bp flanking regions of plasmid and **B.** The analysis of the enzyme digestion for the recombinant *MafA*/pCDNA 3.1(+) vector. Lane 1; A 870 bp *MafA* gene separated from the recombinant vector after digestion using *EcoRI* and *HindIII* enzymes, Lane 2; 100 bp DNA ladder, and Lane 3; Recombinant *MafA*/pCDNA 3.1(+) before the digestion.

Characterization of adipose-derived mesenchymal stem cells

In vitro differentiation of adipose-derived mesenchymal stem cells into adipocytes and osteocytes

In order to confirm the multipotent ability of ADMSCs,

after the third passage, cells were cultured in the adipogenic or osteogenic mediums. The results confirmed the differentiation of ADMSc into osteocytes and adipocytes. The deposits of calcium were visualized by Alizarin red staining showing the osteocytes formation (results are not shown). The vacuoles of lipids were also exhibited by oil red o staining identified the adipocytes formation (17) (results are not shown).

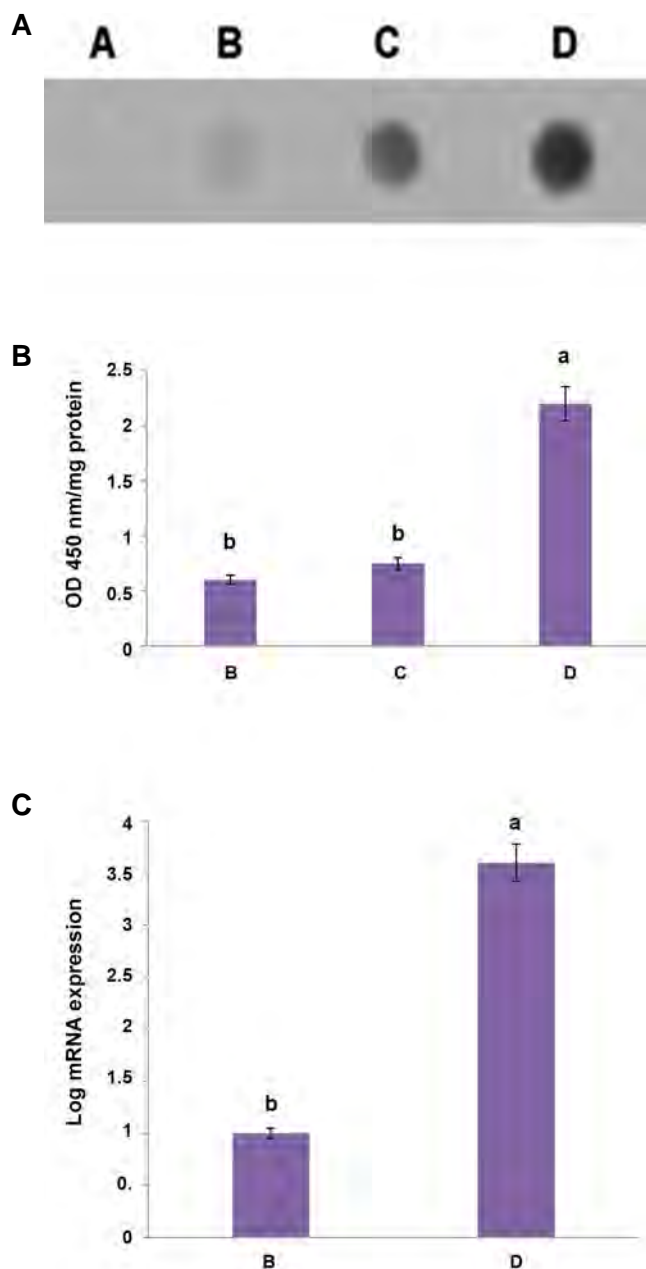


Fig.2: Protein and mRNA expression analysis of *MafA* in transfected adipose-derived mesenchymal stem cells (ADMScs). **A.** Dot blot, **B.** ELISA, and **C.** Real-time polymerase chain reaction (PCR) analysis of *MafA* expression in ADMScs after the transfection with pCDNA 3.1+ or *MafA*/pCDNA 3.1(+) plasmids. **A.** Blank (cell lysis buffer), **B.** ADMScs transfected with pCDNA 3.1+, **C.** Mouse eye extract (positive control) (Santa Cruz Biotechnology, USA, Art No: sc-364241), and **D.** ADMScs transfected with *MafA*/pCDNA 3.1(+) recombinant vector. *GAPDH* was used as a calibrator for real-time PCR analysis. Data are expressed as the mean \pm SE. The statistical significance difference at $P < 0.05$ is represented by different letters.

The identification of adipose derived mesenchymal stem cells surface glycoproteins

ADMScs were evaluated for the expression of specialized surface cell markers of mesenchymal stem cells by flow cytometry. The results showed 99% positive expression of CD90 and 98% positive expression of CD105. ADMScs were negative for CD34 and CD45 antigens (17) (results are not shown).

Evaluation of differentiation stages

The morphology of differentiated cells

In passage 3, all ADMScs were mesenchymal stem cells with the fibroblast-like shape. Changes in ADMScs appearance during the 14 days of differentiation are shown in Figure 3. Spindle-like ADMScs were gently changed to round epithelial-like cells during the stage 2 of differentiation. By the progression of differentiation, cells began to shortening slowly and were gathered together. In stage 3 of differentiation, the morphology of cells changed to spheroid-like shape with similarity to pancreatic islets. The differentiated cells were stained as Crimson red with DTZ (Fig.3).

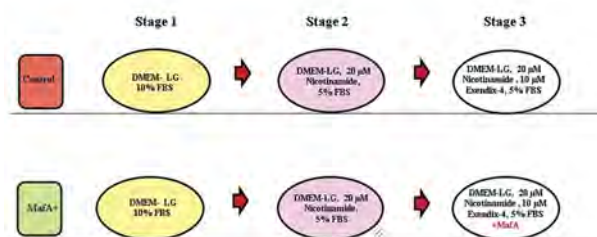


Fig.3: Differentiation protocol of ADMScs into IPCs. ADMScs in control group were differentiated into IPCs using the three stages basic protocol. Cells in MafA+ group were transfected with *MafA*/pCDNA 3.1(+) recombinant plasmid. Undifferentiated ADMScs showed spindle-like shape at the beginning of differentiation. The number of cells with epithelial-like shape was increased at day 7 of differentiation. IPCs that were distinctly stained as crimson red with DTZ became apparent at the final step of differentiation. ADMScs; Adipose derived mesenchymal stem cells, IPCs; Insulin producing cells, DTZ; Dithizone, and DMEM-LG; Dulbecco's Modified Eagle's Medium-low glucose.

Evaluation of insulin-producing cells functionality in vitro

The expression of critical pancreas-related genes after the MafA overexpression

Comparison between the different groups of differentiated cells in the expression of specific genes involved in pancreatic islets formation and insulin synthesis showed that the expression of *Nkx2.2*, *Ngn3*, *Isl1*, *Pdx1*, *MafA*, *Nkx6.1*, and insulin was significantly higher in the manipulated group compared with the control group (Fig.4).

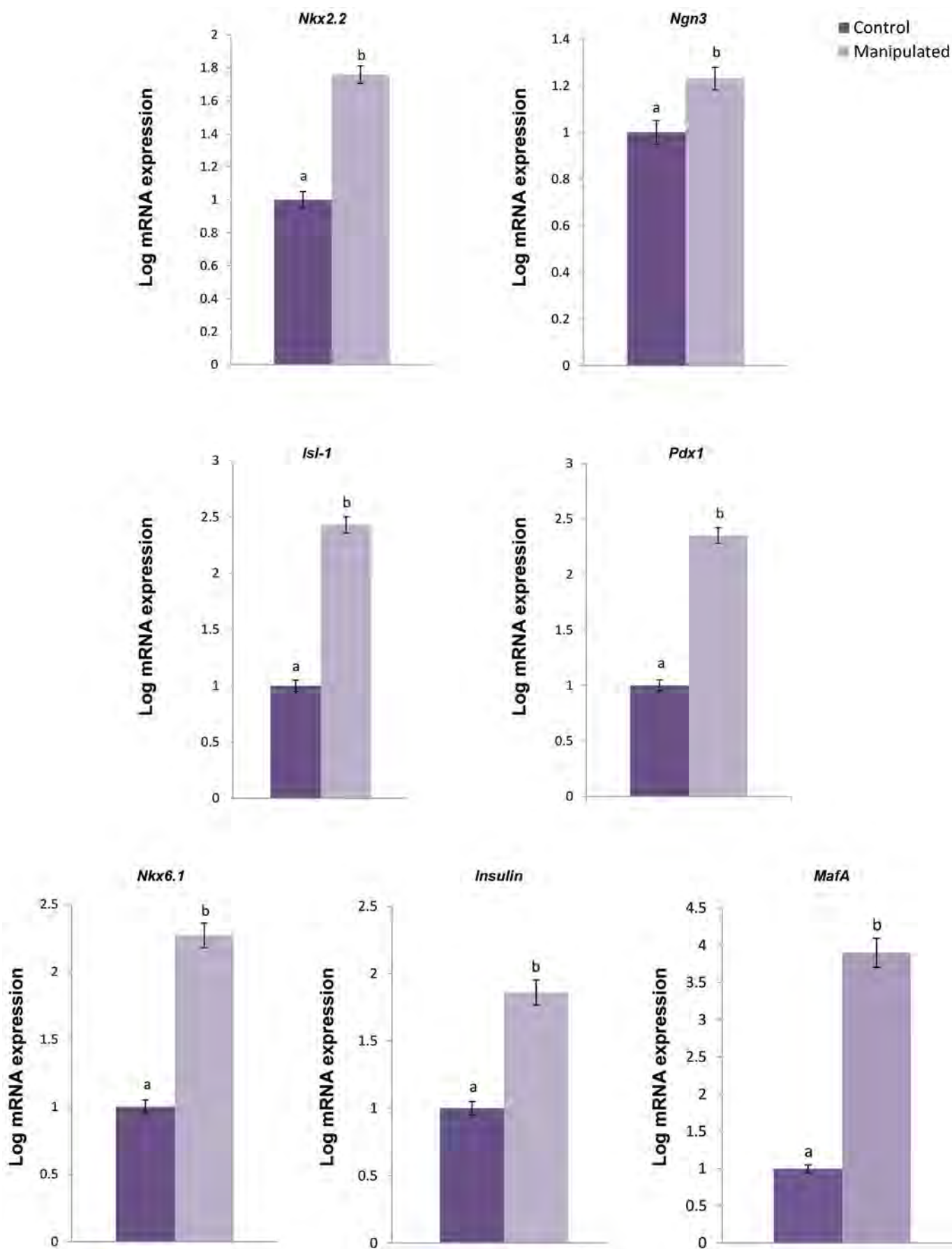


Fig.4: The expression of pancreas-related genes after the *MafA* overexpression. The over-expression of *MafA* had high stimulatory effect on the expression of *Pdx1*, *MafA*, *Nkx2.2*, *Nkx6.1*, *Ngn3*, *Isl1*, and *Insulin* ($P < 0.05$). *GAPDH* was used as a calibrator for real-time polymerase chain reaction (PCR) analysis. Data are expressed as the mean \pm SE. The statistical significance difference at $P < 0.05$ is represented by different letters.

Insulin secretion assay

The manipulated group exhibited a significantly higher insulin secretion ability in response to glucose compared with the control group (Fig.5A).

Evaluation of insulin-producing cells functionality *in vivo*

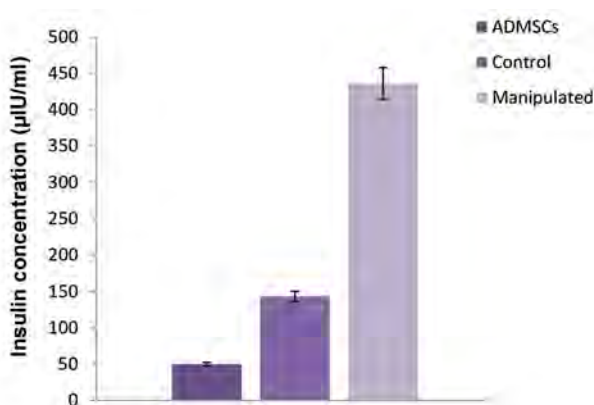
Insulin secretion assay

The measurement of blood insulin concentrations six weeks after transplantation showed significantly higher amounts of the mean rats' insulin concentration receiving the control and manipulated IPCs compared to rats which received un-differentiated ADMSCs. However, rats receiving the control IPCs secreted the higher amounts of insulin compared to those with manipulated IPCs (Fig.5B).

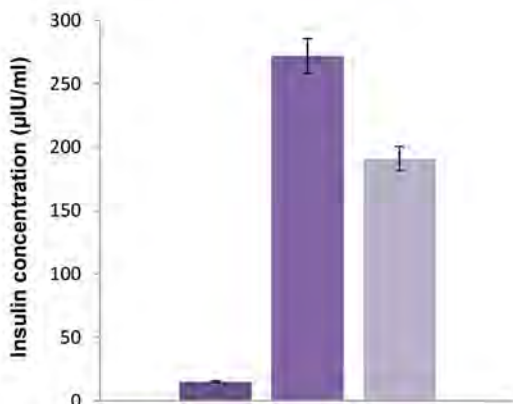
Monitoring of blood glucose concentration

There was no noticeable difference in the concentration of blood glucose of the STZ-diabetic rats which received un-differentiated ADMSCs during the sixth-week monitoring. When the control IPCs were transplanted to STZ-diabetic rats, a remarkable reduction in the mean blood glucose concentration was observed within 3 weeks. Then, the mean value of blood glucose concentration was gradually elevated. Afterward, the mean value of glucose concentration did not reach the normal glycemic condition until the end of the sixth week after transplantation. There was no obvious reduction in the mean blood glucose concentration in STZ-diabetic rats which were injected by the manipulated IPCs (Fig.5C).

A



B



C

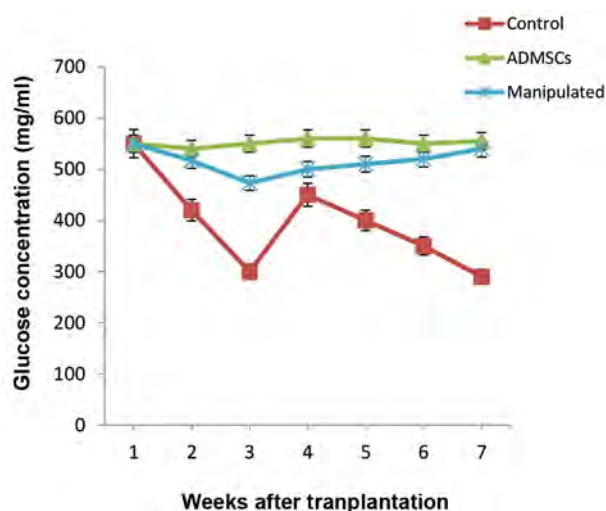


Fig.5: Insulin secretion assay results. **A.** Insulin secretion assay in IPCs before the transplantation. MafA+IPC showed obviously a higher ability of insulin secretion in comparison to the control IPCs ($P < 0.05$). **B.** Insulin secretion assay in IPCs after the transplantation. The diabetic rats which received the control or MafA+ IPCs showed obviously a higher insulin secretion ability in comparison to un-differentiated ADMSCs ($P < 0.05$), and **C.** The monitoring of the blood glucose concentration after the transplantation of IPCs. Diabetic rats that received un-differentiated ADMSCs showed no detectable change in the blood glucose concentration. Rats receiving the positive control IPCs, showed a sharp reduction in the blood glucose concentration within 3 weeks after the transplantation. After that, the mean blood glucose concentration raised to 450 mg/dl. Next, the blood glucose concentration was reduced gradually. At sixth week after the transplantation the average amount of glucose concentration reached 290 mg/dl. Diabetic rats receiving the manipulated IPCs or undifferentiated IPCs, showed no detectable ability to control the hyperglycemic condition. IPC; Insulin producing cells and ADMSCs; adipose derived mesenchymal stem cells.

Discussion

Recent studies have demonstrated the feasibility of transplanting functional insulin-producing cells which are derived from various sources such as ADMSCs (12, 13, 21). However, some obstacles, such as failure to generate functional IPCs and instability of differentiated cells remain. These problems impede the application of stem cells in the clinical settings (22).

Treatment with the guidance of homing factors in differentiation of stem cells into IPCs is a suitable way to improve differentiation protocols (23). In this survey, we defined a new protocol for the differentiation of ADMSCs into IPCs using the *MafA* overexpression. In accordance with the previous study, our results showed a successful differentiation of ADMSCs into IPCs (16, 17). The artificial IPCs which were produced in the present study expressed various genes which were related to pancreatic beta cell maturation, maintenance, and insulin secretion including *Nkx2.2*, *Nkx6.1*, *Isl-1*, *Pdx1*, and *Ngn3* (24). Differentiated IPCs exhibited general pancreatic islet cells appearance and ability to secrete insulin in response to glucose exposure (16-18). Then, we overexpressed *MafA* to determine whether this manipulation is capable of promoting the reprogramming potential and insulin production for pancreatic lineage and islet-like characteristics of ADMSCs.

Considering the essential role of *MafA* in the

reprogramming of stem cells into pancreatic cells, the maturation of beta cells and maintenance of insulin secretion ability, Matsuoka et al. (25) reported a marked increase in the insulin promoter activity after the overexpression of *MafA*. The main reason for this effect is that *MafA* acts as a transcription factor that binds to a 340 bp promoter region upstream of the transcription start site of the insulin gene (26).

Therefore, we studied the effect of *MafA* overexpression on the functionality of obtained IPCs. The outcome was an obvious elevation of *Nkx2.2*, *Ngn3*, *Isl-1*, *Pdx1*, and *Nkx6.1* mRNAs expression compared with the control and other experimental groups. Moreover, the insulin expression and secretion were significantly higher in *MafA*+cells than the control cells. These findings were in accordance with the previous report by Chiou et al. (15) demonstrating that *MafA* promotes the reprogramming of placenta-derived multipotent stem cells into pancreatic islets-like and insulin+ cells. It was also reported that the adenoviral *MafA* overexpression, together with *Pdx-1* and *Ngn3*, were markedly induced insulin-producing surrogate cells in pancreatic exocrine cells in adult mice (26). The recent work by Vargas et al. also showed that in the mouse embryo, *MafA* is required at a later time point for the pancreas function and development (27). Taken together, these results revealed a potential for the *MafA* overexpression for the efficient differentiation of stem cells into IPCs *in vitro*. However, the obtained IPCs were able to secrete insulin, they showed no ability to reduce the blood glucose concentration in diabetic rats (28-30). On the other hand, the amount of secreted insulin was not enough to control the hyperglycemic condition.

Conclusion

We have shown that ADMSCs can be effectively differentiated into IPCs through the overexpression of *MafA*. The IPCs obtained via the novel protocol, exhibited the gene expression pattern that mimics pancreatic development, suggesting this *in vitro* model may be a useful method to induce or increase pancreatic endocrine cell differentiation and may have the potential to be a novel approach for producing β -islet cells for the cell-based diabetes therapy. The inability of transplanted IPCs in the reduction of hyperglycemia in diabetic rats may originate from an insufficient number of transplanted IPCs or the short-term survival time of the differentiated cells *in vivo*. Further examinations are required to determine the mechanism by which *MafA* may directly regulate ADMSCs differentiation into IPCs and insulin gene expression.

Acknowledgments

This work was financially supported by grant: CMRC-120 from vice-chancellor for research affairs of Ahvaz Jundishapur University of Medical Sciences. The authors also thank the Cellular and Molecular Research Center of AJUMS experienced personnel. There is no conflict of interest in this study.

Authors' Contributions

D.D., M.H.T., E.M., M.R.T.; Designed the study. D.D., M.R.T.; Performed the study, researched the data, analyzed the results, wrote the manuscript and revising the manuscript critically for important intellectual content. E.A.B., M.H.T., A.A.G., M.A.G., M.O.; Analyzed the data, drafted and revised the manuscript. D.D.; Is the guarantor of this work and, as such, had full access to all the data in the study and takes responsibility for the integrity of the data and the accuracy of the data analysis. All authors read and approved the final manuscript.

References

- Piero MN, Nzaro GM, Njagi JM. Diabetes mellitus a devastating metabolic disorder. *Asian J Biomed Pharm Sci*. 2014; 4 (40): 1-7.
- Colagiuri S. Diabetes: therapeutic options. *Diabetes Obes Metab*. 2010; 12(6): 463-473.
- Xin Y, Jiang X, Wang Y, Su X, Sun M, Zhang L, et al. Insulin-producing cells differentiated from human bone marrow mesenchymal stem cells *in vitro* ameliorate streptozotocin-induced diabetic hyperglycemia. *PLoS One*. 2016; 11(11): e0145838.
- Borisov MA, Petrakova OS, Gvazava IG, Kalistratova EN, Vasiliev AV. Stem cells in the treatment of insulin-dependent diabetes mellitus. *Acta Naturae*. 2016; 8(3): 31-43.
- Borowiak M. The new generation of beta-cells: replication, stem cell differentiation, and the role of small molecules. *Rev Diabet Stud*. 2010; 7(2): 93-104.
- Wang H, Brun T, Kataoka K, Sharma AJ, Wollheim CB. *MafA* controls genes implicated in insulin biosynthesis and secretion. *Diabetologia*. 2007; 50(2): 348-358.
- Aguayo-Mazzucato C, Koh A, El Khattabi I, Li WC, Toschi E, Jermendy A, et al. *MafA* expression enhances glucose-responsive insulin secretion in neonatal rat beta cells. *Diabetologia*. 2011; 54(3): 583-593.
- Ye DZ, Tai MH, Linning KD, Szabo C, Olson LK. *MafA* expression and insulin promoter activity are induced by nicotinamide and related compounds in INS-1 pancreatic beta-cells. *Diabetes*. 2006; 55(3): 742-750.
- Kaneto H, Matsuoka TA, Katakami N, Matsuhisa M. Combination of *MafA*, *PDX-1* and *NeuroD* is a useful tool to efficiently induce insulin-producing surrogate beta-cells. *Curr Med Chem*. 2009; 16(24): 3144-3151.
- Tsuchiya M, Tsuchiya K, Yasuda K, Fujita M, Takinishi A, Furukawa M, et al. *MafA* is a key molecule in glucose and energy balance in the central nervous system and peripheral organs. *Int J Biomed Sci*. 2011; 7(1): 19-26.
- Nishimura W, Takahashi S, Yasuda K. *MafA* is critical for maintenance of the mature beta cell phenotype in mice. *Diabetologia*. 2015; 58(3): 566-574.
- Guo QS, Zhu MY, Wang L, Fan XJ, Lu YH, Wang ZW, et al. Combined transfection of the three transcriptional factors, *PDX-1*, *NeuroD1*, and *MafA*, causes differentiation of bone marrow mesenchymal stem cells into insulin-producing cells. *Exp Diabetes Res*. 2012; 2012: 672013.
- Wang H, Yang Y, Ho G, Lin X, Wu W, Li W, et al. Programming of human umbilical cord mesenchymal stem cells *in vitro* to promote pancreatic gene expression. *Mol Med Rep*. 2013; 8(3): 769-774.
- Tsuchiya M, Misaka R, Nitta K, Tsuchiya K. Transcriptional factors, *Mafs* and their biological roles. *World J Diabetes*. 2015; 6(1): 175-183.
- Chiou SH, Chen SJ, Chang YL, Chen YC, Li HY, Chen DT, et al. *MafA* promotes the reprogramming of placenta-derived multipotent stem cells into pancreatic islets-like and insulin+ cells. *J Cel Mol Med*. 2011; 15(3): 612-624.
- Kim B, Yoon BS, Moon JH, Kim J, Jun EK, Lee JH, et al. Differentiation of human labia minora dermis-derived fibroblasts into insulin-producing cells. *Exp Mol Med*. 2012; 44(1): 26-35.
- Dayer D, Tabar MH, Moghimipour E, Tabandeh MR, Ghadiri AA, Bakhshi EA, et al. Sonic hedgehog pathway suppression and re-activation accelerates differentiation of rat adipose-derived mesenchymal stromal cells toward insulin-producing cells. *Cytherapy*. 2017; 19(8): 937-946.
- Xin Y, Jiang X, Wang Y, Su X, Sun M, Zhang L, et al. Insulin-pro-

- ducing cells differentiated from human bone marrow mesenchymal stem cells in vitro ameliorate streptozotocin-induced diabetic hyperglycemia. *PLoS One*. 2016; 11(1): e0145838.
19. Tabandeh MR, Golestani N, Kafi M, Hosseinic A, Saeb M, Sarkoohi P. Gene expression pattern of adiponectin and adiponectin receptors in dominant and atretic follicles and oocytes screened based on brilliant cresyl blue staining. *Anim Reprod Sci*. 2012; 131(1-2): 30-40.
 20. Bustin SA, Benes V, Garson JA, Hellemans J, Huggett J, Kubista M, et al. The MIQE guidelines: minimum information for publication of quantitative real-time PCR experiments. *Clin Chem*. 2009; 55(4): 611-622.
 21. Thakkar UG, Vanikar AV, Trivedi HL. Should we practice stem cell therapy for type 1 diabetes mellitus as precision medicine. *Cytotherapy*. 2017; 19(5): 574-576.
 22. Roche E, Reig JA, Campos A, Paredes B, Isaac JR, Lim S, et al. Insulin-secreting cells derived from stem cells: clinical perspectives, hopes and hopes. *Transpl Immunol*. 2005; 15(2): 113-129.
 23. Ghorbani A, Naderi-Meshkin H. The endocrine regulation of stem cells: physiological importance and pharmacological potentials for cell-based therapy. *Curr Stem Cell Res Ther*. 2016; 11(1): 19-34.
 24. Khorsandi L, Khodadadi A, Nejad-Dehbashi F, Saremy S. Three-dimensional differentiation of adipose-derived mesenchymal stem cells into insulin-producing cells. *Cell Tissue Res*. 2015; 361(3): 745-753.
 25. Matsuoka TA, Kaneto H, Miyatsuka T, Yamamoto T, Yamamoto K, Kato K, et al. Regulation of MafA expression in pancreatic beta-cells in db/db mice with diabetes. *Diabetes*. 2010; 59(7): 1709-1720.
 26. Zhang C, Moriguchi T, Kajihara M, Esaki R, Harada A, Shimohata H, et al. MafA is a key regulator of glucose-stimulated insulin secretion. *Mol Cell Biol* 2005; 25(12): 4969-4976.
 27. Vargas N, Alvarez-Cubela S, Giraldo JA, Nieto M, Fort NM, Cechin S, et al. TAT-Mediated Transduction of MafA Protein In Utero Results in Enhanced Pancreatic Insulin Expression and Changes in Islet Morphology. *PLoS One*. 2011; 6(8): e22364.
 28. Janus A, Holz GG, Theise ND, Hussain MA. In vivo derivation of glucose-competent pancreatic endocrine cells from bone marrow without evidence of cell fusion. *J Clin Investig*. 2003; 111(6): 843-850.
 29. Lechner A, Yang YG, Blacken RA, Wang L, Nolan AL, Habener JF. No evidence for significant trans-differentiation of bone marrow into pancreatic beta-cells in vivo. *Diabetes*. 2004; 53(3): 616-623.
 30. Choi JB, Uchino H, Azuma K, Iwashita N, Tanaka Y, Mochizuki H, et al. Little evidence of transdifferentiation of bone marrow-derived cells into pancreatic beta cells. *Diabetologia*. 2003; 46(10): 1366-1374.
-

Endometriotic Mesenchymal Stem Cells Epigenetic Pathogenesis: Deregulation of *miR-200b*, *miR-145*, and *let7b* in A Functional Imbalanced Epigenetic Disease

Parisa Mashayekhi, M.D.¹, Mehrdad Noruzinia, M.D., Ph.D.^{1*}, Sirous Zeinali, Ph.D.², Sepideh Khodaverdi, M.D.³

1. Department of Medical Genetics, Faculty of Medical Sciences, Tarbiat Modares University, Tehran, Iran

2. Biotechnology Research Center, Pasteur Institute of Iran, Tehran, Iran

3. Endometriosis Research Center, Iran University of Medical Science, Tehran, Iran

*Corresponding Address: P.O.Box: 14115-111, Department of Medical Genetics, Faculty of Medical Sciences, Tarbiat Modares University, Tehran, Iran

Email: noruzinia@modares.ac.ir

Received: 13/March/2018, Accepted: 17/July/2018

Abstract

Objective: Stem cell issue is a strong theory in endometriosis pathogenesis. It seems that endometriotic mesenchymal stem cells (MSCs) show different characteristics compared to the normal MSCs. Determined high proliferation and low differentiation/decidualization potential of endometriotic MSCs could be accompanied by their microRNAs deregulation influencing their fate and function. In this study for the first time, we evaluated the expression of *miR-200b*, *miR-145*, and *let-7b* in endometriotic compared to non-endometriotic MSCs. These microRNAs are involved in biological pathways related to proliferation and differentiation of stem cells. Their aberrant expressions can disturb the proliferation/ differentiation balance in stem cells, altering their function and causing various diseases, like endometriosis.

Materials and Methods: In this experimental study, MSCs were isolated from three endometriotic and three non-endometriotic eutopic endometrium, followed by their characterization and culture. Expression of *miR-200b*, *miR-145*, and *let-7b* was ultimately analyzed by quantitative reverse transcription polymerase chain reaction (qRT-PCR).

Results: We found that the expression of *miR-200b* was up-regulated ($P < 0.0001$) whereas the expression of *miR-145* and *let-7b* was down-regulated ($P < 0.0001$) in endometriotic MSCs in comparison with non-endometriotic normal controls.

Conclusion: Proliferation and differentiation are important dynamic balanced biological processes, while in equilibrium, they determine a healthy stem cell fate. It seems that they are deregulated in endometriotic MSCs and change their function. *miR-200b*, *miR-145*, and *let-7b* are deregulated during endometriosis and they have pivotal roles in the modulating proliferation and differentiation of stem cells. We found up-regulation of *miR-200b* and down-regulation of *miR-145* and *let-7b* in endometriotic MSCs. These changes can increase self-renewal and migration, while decreasing differentiation of endometriotic MSCs. Our achievements emphasize previous findings on the importance of proliferation/ differentiation balance in MSCs and clarify the role of microRNAs as main players in faulty endometriotic stem cells development.

Keywords: Cell Differentiation, Cell Self-Renewal, Mesenchymal Stromal Cells, microRNAs

Cell Journal (Yakhteh), Vol 21, No 2, July-September (Summer) 2019, Pages: 179-185

Citation: Mashayekhi P, Noruzinia M, Zeinali S, Khodaverdi S. Endometriotic mesenchymal stem cells epigenetic pathogenesis: deregulation of *miR-200b*, *miR-145*, and *let7b* in a functional imbalanced epigenetic disease. Cell J. 2019; 21(2): 179-185. doi: 10.22074/cellj.2019.5903.

Introduction

Endometriosis is a common, benign gynecologic disorder recognized by the presence of the endometrial tissue out of the uterus, especially on pelvic organs and peritoneum. The most clinical presentation is pelvic pain worsen during menstruation, painful intercourse and infertility. Endometriosis affects approximately 10% of women in reproductive age and it may occur in about 50% of those with pelvic pain, infertility or both (1).

Several theories have thus far been proposed including retrograde menstruation, coelomic metaplasia, steroid hormones, oxidative stress, impaired immune function, decreased apoptosis, genetics, epigenetics, and stem cells, while evidences show each of these factors has partially been involved in endometriosis pathogenesis (2).

During each menses, almost all of the functional layer and small amount of the basalis layer containing a lot of stem cells shed in the uterus (3). They can migrate out of

the uterus through retrograde menstruation, seed there and establish endometriotic lesions. However, the presence of endometriosis in 10% of women despite the presence of retrograde menstruation in over 90% of them seems intriguing. Several evidences show that the stem cells generating endometriotic lesions are characteristically different from the normal stem cells. They have a higher ability to proliferate and a lower capacity for differentiation and decidualization (4). It appears to us that impaired proliferation/differentiation and decidualization balance can changes stem cell character and function, while this makes them susceptible to develop endometriosis.

Several studies investigated genetic contribution in endometriosis, most of which failed to determine any significant correlation. Some studies demonstrated that epigenetic deregulation is, in fact, the underlying pathogenic mechanism of endometriosis (5) and it alters gene expression in response to hormonal and environmental factors (i.e., through dynamic changes of

the environment).

Epigenetic changes play an important role in the pathogenesis of various diseases, including cancers, and they are used as biomarkers for early diagnosis (6). Epigenetics is longtime proved concept, involved in stem cell regulation (7). microRNAs (miRs) are short non-coding RNA molecules with critical roles in post-transcriptional regulation of different genes (8) and, as epigenetic regulators, they are key molecules involved in the determination of stem cell fate by regulation of the self-renewal and differentiation-related pathways (9). Their aberrant expression can change stem cell functions and cause the differences between endometriotic and normal stem cells (10). Thus far, deregulation of microRNAs has been confirmed to contribute to endometriosis and infertility (11).

In this study, we chose three microRNAs (*miR-200b*, *miR-145* and *let-7b*) dysregulated during endometriosis (12) and their expressions were evaluated in endometriotic mesenchymal stem cells (MSCs).

Aberrant expression of *miR-200b* has been reported in many cancers (13). Up-regulation of this microRNA promotes cell proliferation in cervical cancer (14). Transfection of endometriotic stem cells with *miR-200b* increases cell proliferation and side population phenotype through enhancing expression of *KLF4*, *SOX2*, *OCT4* and *c-MYC*, in addition to transforming mature cells into pluripotent cells (15). *miR-200c* overexpression in human embryonic stem cells (hESCs) up-regulates *NANOG* expression and decreases apoptosis, resulting in maintenance of their self-renewal ability and proliferation (16). *miR-200* family helps transition of human fibroblasts to pluripotent stem cells by *ZEB2* suppression and mesenchymal-epithelial transition (MET) induction in cooperation with *OCT4* and *SOX2* (17).

Overexpression of *miR-145* inhibits cell proliferation and migration by suppressing the *TGF-β1* expression in breast cancer cells (18). This microRNA induces differentiation of cervical cancer stem cells (CSCs) by suppressing the stem cell transcription factors involved in maintaining CSCs self-renewal (19). *miR-145* acts as a tumor suppressor molecule in a lot of cancers (20). *miR-145* inhibits endometriotic cell proliferation, and self-renewal via targeting *OCT4*, *KLF4*, and *SOX2* and induces hESC and CSCs differentiation (21-23). Its expression is down-regulated in hESCs and increased within differentiation.

let-7 is strongly accepted as a tumor suppressor microRNA and expression of its family members are down-regulated in several types of cancer (24). *let-7b* suppresses the expression of *OCT4* as well as *SOX2* and it reprogrammes CSCs into the differentiated cells via a *let-7/LIN28* feedback loop (25). *let-7b* overexpression inhibits proliferation and induces differentiation in adult and CSCs (26).

It seems that *miR-200b*, *miR-145*, and *let-7b* could

be involved in the modulation of self-renewal and differentiation of stem cells, so their role in stem cell dysfunction could be postulated as a plausible theory.

Considering this hypothesis, we compared the expression of these microRNAs (*miR-200b*, *miR-145*, and *let-7b*) in MSCs isolated from three women who had pelvic endometriosis and three women without endometriosis. This comparison shows the aberrant expression of these microRNAs in endometriotic MSCs and supports the presence of proliferation/differentiation imbalance in endometriosis initiating MSCs.

Material and Methods

Ethics statement

This study was approved by the Ethics Committee of Medical Faculty of Tarbiat Modares University (no. 1395.409), Tehran, Iran. Written informed consent was taken from each patient after a standard genetic counselling.

Specimen sources

Human endometrial tissue samples were obtained from three premenopausal women (30-45 years old) undergoing hysterectomy for non-endometrial benign pathological condition and another three patients with endometriosis undergoing laparoscopy for endometriosis in the Rasoul Akram Hospital of Iran Medical University (Tehran, Iran). Eutopic endometrial tissues were obtained from the patients. The patients had not received hormone treatments for at least three months before sample collection. Diagnosis of endometriotic and non-endometriotic collected tissues was validated by histopathological test by two experienced histopathologists.

Isolation and culture of human endometrial mesenchymal stem cells

Tissues were separated and washed in phosphate buffered saline (PBS) then minced into 1-2 mm³ pieces in a medium containing Dulbecco modified Eagle medium/Ham's F-12 (DMEM/F-12, Invitrogen, UK) and 1% penicillin-streptomycin antibiotics solution (Invitrogen, USA). Briefly, cell suspension of endometrial cells was obtained using enzymatic digestion using collagenase type 3 (300 µg/ml, Sigma, Germany) and mechanical procedure at 37°C for 90 minutes, then centrifuged for 5 minutes at 3000 rpm. Cell suspensions were filtered through 150, 100, 40 µm mesh to remove undigested tissues and epithelial components. Endometrial stromal cells were next cultured in DMEM/F-12 containing 1% penicillin-streptomycin solution and 10% fetal bovine serum (FBS, Gibco, USA) at 37°C in 95% air and 5% CO₂ conditions. Endometrial stromal cells in passages 3-4 were used for characterization by flow cytometry analyses.

Endometrial stromal cells flow cytometry analysis

Isolated stromal cells were trypsinized and centrifuged.

The cell pellet was resuspended in PBS supplemented with 5% FBS and incubated with monoclonal antibodies for 30 minutes at 4°C in the dark. Human CD45 (BD Bioscience, USA) and CD34 (IMMUNOSTEP, Spain) antibodies were served as negative controls, while anti-human CD90 (BD Bioscience, USA), CD105 (IMMUNOSTEP, Spain), CD73 (BD Bioscience, USA) and CD146 (BD Bioscience, USA) were used as specific antibodies. Cells were evaluated with a FACS Calibur apparatus (Becton Dickinson, USA). Finally, the analysis was done using FlowJo 7.6 software.

Differentiation of endometrial mesenchymal stem cells

For evaluating the endometrial MSCs differentiation potential, endometrial stromal cells (CD146+, CD90+, CD105+, CD73+ and CD34-, CD45-) were seeded in 24-well plates and cultured in osteogenic and adipogenic differentiation media for 4 weeks, separately. Control cells were also cultured in low serum medium (DMEM/F12 with 1% FBS and 1% penicillin-streptomycin antibiotic solution) for the same incubation time. Control and differentiation media were changed every 2-3 days. Three weeks later, osteogenic and adipogenic differentiations were respectively checked by staining with 4% Alizarin Red (pH=4.1) and 1% Oil Red O (both from Sigma, Germany) (27).

RNA extraction and cDNA synthesis

Total RNA was extracted from the cells using TRIzol reagent (Sigma, Germany). RNA concentration and purity were assessed by Nanodrop (the ratio of absorbance at 260 and 280 nm ≥ 1.8), then we ran the extracted RNA on denaturing agarose gel electrophoresis and the gel was stained with ethidium bromide for evaluating the quality of extracted RNA. cDNA was synthesized using specific stem-loop primers for microRNAs (*miR-200b*, *let-7b*, *miR-145*, and *RNU44*) in a total volume of 20 μ l using the cDNA synthesis kit (Takara Bio, Japan).

Stem-loop RT primers were designed in accordance with the protocol described by Chen et al. (28). Primer

sequences are presented in Table 1.

Quantitative reverse transcription polymerase chain reaction for evaluation of the microRNA expression levels

To determine expression of the microRNAs (*miR-200b*, *miR-145* and *let-7b*) in the cells, we used the Allele ID6 and Oligo7 software for designing the specific forward primers and universal reverse primer. *RNU44* was used as an internal control. Primers were synthesized at Pishgam Co. (Tehran, Iran). We used Syber Green Assay kit (Applied Biosystems, UK) according to the manufacturer's protocol. qRT-PCR reactions were done in 10 μ l of the reaction mixture using AB StepOne Real-Time PCR System (Applied Biosystems, UK). All qRT-PCR experiments were repeated three times. Data were analyzed using Pfaffl method and normalized by *RNU44* expression in each sample.

Statistical analysis

We used student's t test by GraphPad Prism 6 software for statistical analysis and comparison of microRNA expressions between samples. Results were considered significant at $P < 0.05$.

Results

Isolation and characterization of endometrial mesenchymal stem cells

Human MSCs were isolated from the endometrium and they were cultured. Flow cytometry analysis confirmed the expression of MSC markers CD73 (98.5%), CD90 (99.1%), CD105 (96.3%) and CD146 (84.8%). Expression of hematopoietic markers, including CD34 (0.474%) and CD45 (1.99%), were negative (Fig.1A-F). To evaluate differentiation potential of the isolated endometrial MSCs, we induced adipogenic and osteogenic differentiation with specific differentiation media, as specified. Confirmation of differentiation was done through staining of calcium deposits by alizarin red and lipid vacuoles through oil red staining (Fig.1G, H).

Table 1: Sequence of oligonucleotide primers used for quantitative reverse transcription polymerase chain reaction (qRT-PCR) measurements

Primer name	Sequence (5'-3')
<i>let-7b</i> stem-loop primer	GTCGTATCCAGTGCAGGGTCCGAGGTATTCGCACTGGATACGACAACCAC
<i>let-7b</i> forward primer	GCTCTTGAGGTAGTAGGTTGTGTG
<i>miR-200b</i> stem-loop primer	GTCGTATCCAGTGCAGGGTCCGAGGTATTCGCACTGGATACGACTCATCA
<i>miR-200b</i> forward primer	CGCTAATACTGCCTGGTAATGATGA
<i>miR-145</i> stem-loop primer	GTCGTATCCAGTGCAGGGTCCGAGGTATTCGCACTGGATACGACAGGGAT
<i>miR-145</i> forward primer	CATCCGTCCAGTTTTCCAGG
<i>RNU44</i> stem-loop primer	GTCGTATCCAGTGCAGGGTCCGAGGTATTCGCACTGGATACGACAGTCAG
<i>RNU44</i> forward primer	TCACGCCTGGATGATGATAAGC
Universe reverse primer	CAGTGCAGGGTCCGAGGTA

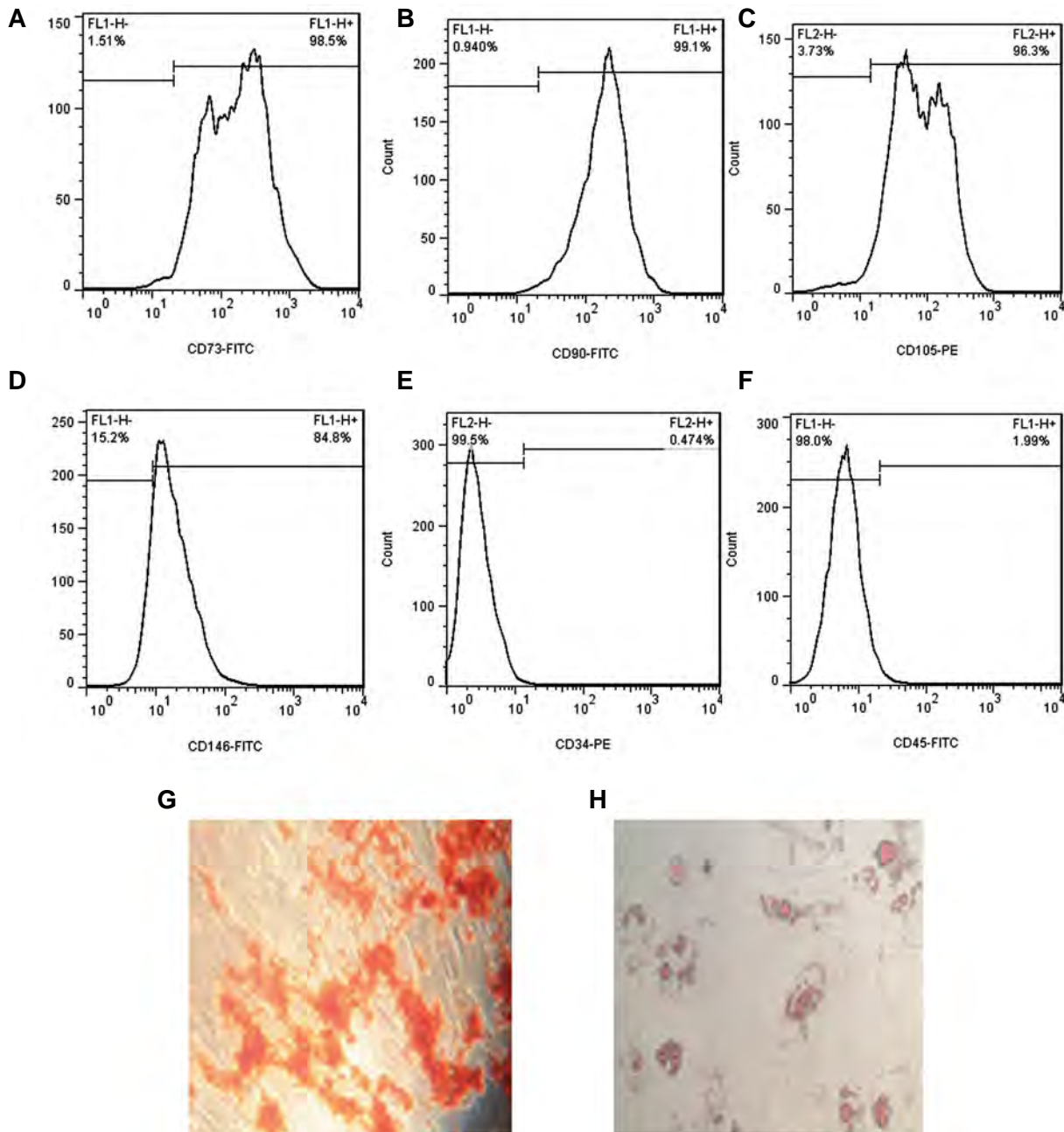


Fig.1: Isolation and characterization of endometrial mesenchymal stem cells (MSCs). Flow cytometry analyses showed that endometrial MSCs positively expressed **A.** CD73 (98.5%), **B.** CD90 (99.1%), **C.** CD105 (96.3%), **D.** CD146 (84.9%) but negatively expressed, **E.** CD34 (0.474%), **F.** CD45 (1.99%), **G.** Osteogenic, and **H.** adipogenic differentiation of the isolated endometrial MSCs.

Quantitative reverse transcription polymerase chain reaction

To explore microRNAs profiling in endometrial MSCs of the endometriotic and non-endometriotic control groups the expression levels of *miR-200b*, *miR-145* and *let-7b* were evaluated by qRT-PCR. The efficiency of qRT-PCR reactions for *miR-200b*, *miR-145* and *let-7b* were measured using LinReg software algorithm (29). Each experiment was repeated three times to eliminate any subjective variation. All reactions were assessed for distinct melting curves, while they showed no nonspecific or primer-dimer peaks.

miR-200b was up-regulated in endometriotic mesenchymal stem cells

Relative expressions of *miR-200b* in the endometriotic MSCs showed up-regulation of this microRNA (4.199 ± 0.6617 , $P < 0.0001$) in comparison with the non-endometriotic control group (Fig.2A).

miR-145 was down-regulated in endometriotic mesenchymal stem cells

Expression of *miR-145* in the endometriotic MSCs was decreased to 0.5467 ± 0.06137 fold ($P < 0.0001$) in comparison with the non-endometriotic control group (Fig.2B).

let-7b was down-regulated in endometriotic mesenchymal stem cells

Expression of *let-7b* in the endometriotic MSCs was 0.3024 ± 0.04454 fold ($P < 0.0001$) less than the non-endometriotic control group (Fig.2C).

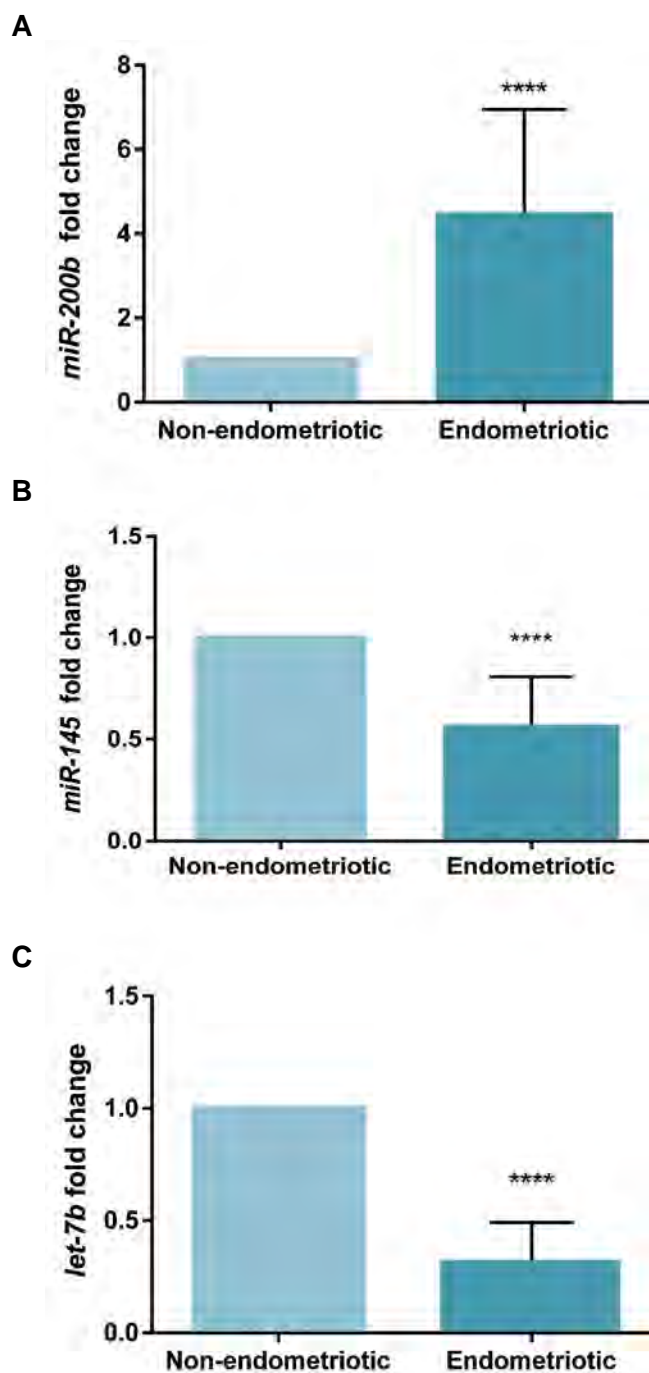


Fig.2: microRNA expression analyses. Relative expressions of *miR-200b*, *miR-145* and *let-7b* in endometrial mesenchymal stem cells (MSCs) of endometriotic patients and non-endometriotic control group, evaluated by quantitative reverse transcription polymerase chain reaction (qRT-PCR). **A.** *miR-200b* expression in endometriotic MSCs was 4.199 ± 0.6617 fold ($P < 0.0001$) higher than non-endometriotic MSCs, **B.** *miR-145* expression in endometriotic MSCs was 0.5467 ± 0.06137 fold ($P < 0.0001$) less than non-endometriotic MSCs, and **C.** Expression of *let-7b* in endometriotic MSCs was 0.3024 ± 0.04454 fold ($P < 0.0001$) less than non-endometriotic MSCs control group. ****; $P < 0.0001$ in comparison to non-endometriotic MSCs.

Discussion

We believe that proliferation/differentiation imbalance plays a pivotal role in the pathogenesis of endometriosis. We evaluated *miR-200b*, *miR-145* and *let-7b* expression as modulators of stem cell proliferation and differentiation (30), in endometriotic and non-endometriotic MSCs. Previous studies have shown that these microRNAs were deregulated in endometriosis while no study evaluated their expression in endometriotic MSCs (31, 32).

Several theories are proposed as the pathogenesis basis of endometriosis. stem cell theory is one main research field in endometriosis. A lot of studies described the role of stem cells in endometriosis development (3). A balance in proliferation/differentiation equilibrium is required for the correct function of stem cells and it seems to us that in several diseases including endometriosis, this balance fails, resulting in altered function of stem cells, and changing their fate. Many studies confirm that endometriotic MSCs are different from non-endometriotic types. They have a higher ability to migrate, attach and proliferate (33, 34), while a lower capacity for differentiation and decidualization is proposed for them, due to the impaired decidualization related pathways (4). We believe that proliferation/differentiation imbalance in endometriotic MSCs is the main underlying cause for endometriosis development and its correlated infertility.

Previous studies have shown that microRNAs are involved in regulation of signaling pathways that control differentiation and proliferation of stem cells during normal development and disease pathogenesis (30).

miR-200b, *miR-145* and *let-7b* are deregulated in several diseases like cancers confirming the aforementioned imbalance. These microRNAs have specific expression profile in endometrial stromal cells during decidualization (35). Deregulation of these microRNAs has been shown in the ectopic and eutopic endometrium of women with endometriosis, but our study is the first to confirm their expressions and roles in endometriotic MSCs. We find that in endometriotic MSCs *miR-200b* is up-regulated significantly as compared to normal control group. Previous studies have shown that *miR-200b* is up-regulated in eutopic endometrium of endometriotic women and involved in endometriosis-associated infertility (31). Overexpression of *miR-200b* increases cell proliferation and MET. It induces generation of pluripotent stem cells in cooperation with transcription factor *SOX2* and *OCT4* (17).

Transfection of endometriotic stem cells with *miR-200b* results in increase side population phenotype through activating *KLF4* and *NANOG* expressions as well as MET, while reducing decidualization. It also enhances metastatic colonization of successfully migrated cells by inhibiting secretion of metastasis inhibitors (15). *miR-200* family members are down-regulated during *in vitro* decidualization (35).

Increased expression of *miR-200b* in endometriotic MSCs, in our study, is in accordance with the findings

of previous studies. It might increase colonization chance of the migrated stem cells, enhance their proliferation and promote their stemness properties by positive regulation of stemness-related genes while decreasing the differentiation potential and decidualization. These changes promote development of endometriosis, disrupt embryo implantation and cause infertility.

Our findings show that *miR-145* is down-regulated in endometriotic MSCs. Previous studies have demonstrated that *miR-145* is down-regulated in the serum of endometriotic patients in comparison with normal control and potentially served as noninvasive biomarkers for endometriosis. Transfection of endometrial stromal cells with *miR-145* inhibits cell proliferation and invasiveness. It also suppresses the stemness by down-regulation of stemness-related genes (36). This microRNA induces differentiation of stem cells through SOX2-LIN28/*let-7* signaling pathway by decreasing SOX2 and LINE-28 protein levels (37). Overexpression of this microRNA in CSCs reduces the expression of stemness-related markers, while it increases cancer cells differentiation (38). In the present study, decreased level of *miR-145* in endometriotic MSCs confirms findings obtained from previous studies. This is consistent with the underlying proposed pathogenesis mechanism to increase stem cell proliferation, decrease their differentiation and facilitate endometriosis risk.

Our results show a down-regulation of *let-7b* in the endometrial MSCs of women with endometriosis. Previous studies have also shown that expression of *let-7* was decreased in the serum of endometriotic patients in comparison with normal control (32).

let-7 is involved in a regulatory feedback loop with *LIN28*, which has a critical role in pluripotency maintenance in collaboration with *NANOG*, *SOX2* and *OCT4* genes. Overexpression of this microRNA in stem cells promotes differentiation, while inhibition of *let-7* results in the proliferation of stem cells and decreases differentiation. Briefly, *let-7b* family members fine-tune the pathways related to self-renewal/differentiation balances (39).

let-7 suppresses the expression of *OCT4* and *SOX2*. It reprogrammes CSCs to differentiate via *let-7/LIN28* feedback loop and its overexpression regulates the stemness by increasing differentiation and decreasing self-renewal in both of the normal and cancer stem cells (26). Reduced level of *let-7* is required for self-renewal and maintenance of the undifferentiated state of embryonic and adult stem cells and its overexpression has opposing effects, reducing their proliferation and leading to their differentiation (39). Overexpression of *let-7b* in neural stem cells inhibits proliferation and promotes differentiation (40).

In this study, *let-7b* down-regulation in endometriotic MSCs consolidates the results of previous studies. *let-7b* is proposed as one of the main players of proliferation/

differentiation imbalance in endometriotic MSCs. In other words, any deregulation of *let-7b* expression alters proliferation/differentiation balance in endometriotic MSCs. *let-7b* deregulation increases the probability of endometriotic lesion formations via enhancing the stem cell proliferation, migration, self-renewal and maintenance of their undifferentiated state. These changes reduce decidualization and increase infertility in patients with endometriosis.

Although the exact underlying pathologic mechanism of endometriosis is yet unclear, current findings discover the strong role of stem cells in endometriosis and confirm their different characteristics and function. Our results consolidate the theory of imbalance between differentiation and proliferation capacity, especially in stem cells of endometriotic patients. This study for the first time evaluates the expression of *miR-200b*, *miR-145* and *let-7b* in endometrial MSCs of women with endometriosis in comparison with normal control, representing that aberrant expression of these microRNAs is present in this pathological condition. These microRNAs contribute to modulating proliferation and/or differentiation of stem cells. This is the first study to evaluate the expression of these microRNAs in endometriotic stem cells. Our findings are in support of a unified differentiation/proliferation imbalance theory.

Conclusion

Endometriosis is a complex and yet unknown gynecological disease in women. Deregulation of microRNAs related to differentiation and proliferation in endometriotic MSCs compared to the normal types confirms the implication of epigenetics and this is in line with many other authors, while supporting the underlying mechanism of endometriosis, as emphasized in this study. We think that impaired balance between differentiation and proliferation in MSCs, which is supported by our study, is essential for endometriosis development.

Acknowledgements

This research was part of Ph.D. thesis which was financially supported by Research Deputy of Tarbiat Modares University, Tehran, Iran. The authors declared no conflict of interests in this research work.

Authors' Contributions

P.M.; Performed the laboratory experiments and wrote the manuscript. M.N.; Designed and supervised the scientific work, analyzed the results and edited the manuscript. S.Kh.; Selected the patients, performed the clinical examination and laparoscopy, collected the endometrial tissue and confirmed the clinical diagnosis. S.Z.; Contributed to the interpretation of the results and conclusion. All authors performed editing and approving the final version of this manuscript for submission, also

participated in the finalization of the manuscript and approved the final draft.

References

- Giudice LC. Clinical practice. Endometriosis. *N Engl J Med*. 2010; 362(25): 2389-2398.
- Sourial S, Tempest N, Hapangama DK. Theories on the pathogenesis of endometriosis. *Int J Reprod Med*. 2014; 2014: 179515.
- Figueira PG, Abrao MS, Krikun G, Taylor HS. Stem cells in endometrium and their role in the pathogenesis of endometriosis. *Ann N Y Acad Sci*. 2011; 1221: 10-17.
- Klemmt PA, Carver JG, Kennedy SH, Koninckx PR, Mardon HJ. Stromal cells from endometriotic lesions and endometrium from women with endometriosis have reduced decidualization capacity. *Fertil Steril*. 2006; 85(3): 564-572.
- Koukoura O, Sifakis S, Spandidos DA. DNA methylation in endometriosis (Review). *Mol Med Rep*. 2016; 13(4): 2939-2948.
- Khakpour G, Pooladi A, Izadi P, Noruzinia M, Tavakkoly Bazzaz J. DNA methylation as a promising landscape: a simple blood test for breast cancer prediction. *Tumour Biol*. 2015; 36(7): 4905-4912.
- Azad M, Kaviani S, Noruzinia M, Mortazavi Y, Mobarra N, Alizadeh S, et al. Gene expression status and methylation pattern in promoter of P15INK4b and P16INK4a in cord blood CD34+ stem cells. *Iran J Basic Med Sci*. 2013; 16(7): 822-828.
- Bartel DP. MicroRNAs: genomics, biogenesis, mechanism, and function. *Cell*. 2004; 116(2): 281-297.
- Guo L, Zhao RC, Wu Y. The role of microRNAs in self-renewal and differentiation of mesenchymal stem cells. *Exp Hematol*. 2011; 39(6): 608-616.
- Hsu CY, Hsieh TH, Tsai CF, Tsai HP, Chen HS, Chang Y, et al. miRNA-199a-5p regulates VEGFA in endometrial mesenchymal stem cells and contributes to the pathogenesis of endometriosis. *J Pathol*. 2014; 232(3): 330-343.
- Yang RQ, Teng H, Xu XH, Liu SY, Wang YH, Guo FJ, et al. Microarray analysis of microRNA deregulation and angiogenesis-related proteins in endometriosis. *Genet Mol Res*. 2016; 15(2).
- Mu P, Zhou J, Ma X, Zhang G, Li Y. Expression, regulation and function of MicroRNAs in endometriosis. *Pharmazie*. 2016; 71(8): 434-438.
- Humphries B, Yang C. The microRNA-200 family: small molecules with novel roles in cancer development, progression and therapy. *Oncotarget*. 2015; 6(9): 6472-6498.
- Zeng F, Xue M, Xiao T, Li Y, Xiao S, Jiang B, et al. MiR-200b promotes the cell proliferation and metastasis of cervical cancer by inhibiting FOXG1. *Biomed Pharmacother*. 2016; 79: 294-301.
- Eggers JC, Martino V, Reinbold R, Schäfer SD, Kiesel L, Starzinski-Powitz A, et al. microRNA miR-200b affects proliferation, invasiveness and stemness of endometriotic cells by targeting ZEB1, ZEB2 and KLF4. *Reprod Biomed Online*. 2016; 32(4): 434-445.
- Huang HN, Chen SY, Hwang SM, Yu CC, Su MW, Mai W, et al. miR-200c and GATA binding protein 4 regulate human embryonic stem cell renewal and differentiation. *Stem Cell Res*. 2014; 12(2): 338-353.
- Wang G, Guo X, Hong W, Liu Q, Wei T, Lu C, et al. Critical regulation of miR-200/ZEB2 pathway in Oct4/Sox2-induced mesenchymal-to-epithelial transition and induced pluripotent stem cell generation. *Proc Natl Acad Sci U S A*. 2013; 110(8): 2858-2863.
- Ding Y, Zhang C, Zhang J, Zhang N, Li T, Fang J, et al. miR-145 inhibits proliferation and migration of breast cancer cells by directly or indirectly regulating TGF-beta1 expression. *Int J Oncol*. 2017; 50(5): 1701-1710.
- Zhou X, Yue Y, Wang R, Gong B, Duan Z. MicroRNA-145 inhibits tumorigenesis and invasion of cervical cancer stem cells. *Int J Oncol*. 2017; 50(3): 853-862.
- Cui SY, Wang R, Chen LB. MicroRNA-145: a potent tumour suppressor that regulates multiple cellular pathways. *J Cell Mol Med*. 2014; 18(10): 1913-1926.
- Xu N, Papagiannakopoulos T, Pan G, Thomson JA, Kosik KS. MicroRNA-145 regulates OCT4, SOX2, and KLF4 and represses pluripotency in human embryonic stem cells. *Cell*. 2009; 137(4): 647-658.
- Adammek M, Greve B, Kässens N, Schneider C, Brüggemann K, Schüring AN, et al. MicroRNA miR-145 inhibits proliferation, invasiveness, and stem cell phenotype of an in vitro endometriosis model by targeting multiple cytoskeletal elements and pluripotency factors. *Fertil Steril*. 2013; 99(5): 1346-1355. e5.
- Yu Y, Nangia-Makker P, Farhana L, G Rajendra S, Levi E, Majumdar AP. miR-21 and miR-145 cooperation in regulation of colon cancer stem cells. *Mol Cancer*. 2015; 14: 98.
- Boyerinas B, Park SM, Hau A, Murmann AE, Peter ME. The role of let-7 in cell differentiation and cancer. *Endocr Relat Cancer*. 2010; 17(1): F19-F36.
- Chien CS, Wang ML, Chu PY, Chang YL, Liu WH, Yu CC, et al. Lin28B/Let-7 regulates expression of Oct4 and Sox2 and reprograms oral squamous cell carcinoma cells to a stem-like state. *Cancer Res*. 2015; 75(12): 2553-2565.
- Büssing I, Slack FJ, Großhans H. let-7 microRNAs in development, stem cells and cancer. *Trends Mol Med*. 2008; 14(9): 400-409.
- Mohammadi Z, Afshari JT, Keramati MR, Alamdari DH, Ganjibakhsh M, Zarmehri AM, et al. Differentiation of adipocytes and osteocytes from human adipose and placental mesenchymal stem cells. *Iran J Basic Med Sci*. 2015; 18(3): 259-266.
- Chen C, Ridzon DA, Broomer AJ, Zhou Z, Lee DH, Nguyen JT, et al. Real-time quantification of microRNAs by stem-loop RT-PCR. *Nucleic Acids Res*. 2005; 33(20): e179.
- Ruijter JM, Ramackers C, Hoogaars WM, Karlen Y, Bakker O, van den Hoff MJ, et al. Amplification efficiency: linking baseline and bias in the analysis of quantitative PCR data. *Nucleic Acids Res*. 2009; 37(6): e45.
- Yao S. MicroRNA biogenesis and their functions in regulating stem cell potency and differentiation. *Biol Proced Online*. 2016; 18: 8.
- Ruan Y, Qian WP, Zhang CH, Zhou L, Hou ZH. Study on microRNA expression in endometrium of luteal phase and its relationship with infertility of endometriosis. *Zhonghua Fu Chan Ke Za Zhi*. 2013; 48(12): 907-910.
- Wang WT, Zhao YN, Han BW, Hong SJ, Chen YQ. Circulating microRNAs identified in a genome-wide serum microRNA expression analysis as noninvasive biomarkers for endometriosis. *J Clin Endocrinol Metab*. 2013; 98(1): 281-289.
- Kao AP, Wang KH, Chang CC, Lee JN, Long CY, Chen HS, et al. Comparative study of human eutopic and ectopic endometrial mesenchymal stem cells and the development of an in vivo endometriotic invasion model. *Fertil Steril*. 2011; 95(4): 1308-1315. e1
- Wingfield M, Macpherson A, Healy DL, Rogers PA. Cell proliferation is increased in the endometrium of women with endometriosis. *Fertil Steril*. 1995; 64(2): 340-346.
- Estella C, Herrero I, Moreno-Moya JM, Quiñonero A, Martínez S, Pellicer A, et al. miRNA signature and Dicer requirement during human endometrial stromal decidualization in vitro. *PLoS One*. 2012; 7(7): e41080.
- Adammek M, Greve B, Kässens N, Schneider C, Brüggemann K, Schüring AN, et al. MicroRNA miR-145 inhibits proliferation, invasiveness, and stem cell phenotype of an in vitro endometriosis model by targeting multiple cytoskeletal elements and pluripotency factors. *Fertil Steril*. 2013; 99(5): 1346-1355. e5.
- Morgado AL, Rodrigues CM, Solá S. MicroRNA-145 regulates neural stem cell differentiation through the Sox2-Lin28/let-7 signaling pathway. *Stem Cells*. 2016; 34(5): 1386-1395.
- Wu Y, Liu S, Xin H, Jiang J, Younglai E, Sun S, et al. Up-regulation of microRNA-145 promotes differentiation by repressing OCT4 in human endometrial adenocarcinoma cells. *Cancer*. 2011; 117(17): 3989-3998.
- Vaz C, Tanavde V. Role of let-7 networks in stem cell maintenance and differentiation. In: Dahiya N, editor. *MicroRNA Let-7*. Hauppauge, NY, 11788 USA; Nova Science Publishers: 2012: 43-56.
- Zhao C, Sun G, Li S, Lang MF, Yang S, Li W, et al. MicroRNA let-7b regulates neural stem cell proliferation and differentiation by targeting nuclear receptor TLX signaling. *Proc Natl Acad Sci USA*. 2010; 107(5): 1876-1881.

Differential Proliferation Effects after Short-Term Cultivation of Mouse Spermatogonial Stem Cells on Different Feeder Layers

Hossein Azizi, Ph.D.^{1*}, Hatef Ghasemi Hamidabadi, Ph.D.^{2,3}, Thomas Skutella, Ph.D.⁴

1. Faculty of Biotechnology, Amol University of Special Modern Technologies, Amol, Iran

2. Department of Anatomy and Cell Biology, Faculty of Medicine, Mazandaran University of Medical Sciences, Sari, Iran

3. Immunogenetic Research Center, Department of Anatomy and Cell Biology, Faculty of Medicine, Mazandaran University of Medical Sciences, Sari, Iran

4. Institute for Anatomy and Cell Biology III, Medical Faculty, Heidelberg University, Im Neuenheimer Feld 307, 69120 Heidelberg, Germany

*Corresponding Address: P.O.Box: 46168-49767, Faculty of Biotechnology, Amol University of Special Modern Technologies, Amol, Iran
Email: h.azizi@ausmt.ac.ir

Received: 21/February/2018, Accepted: 21/August/2018

Abstract

Objective: Spermatogonial stem cells (SSCs) provide the cellular basis for sperm production transforming the male's genetic information to the next generation. We aimed to examine the effect of different feeder layer on proliferation of SSCs.

Materials and Methods: In this experimental study, we compared the *in vitro* effects of the co-culture of mouse SSCs with mouse embryonic fibroblasts (MEFs), sandos inbred mice (SIM) embryo-derived thioguanine- and ouabain-resistant (STO) feeders, and neonate and adult testicular stroma cell (TSC) feeders on the efficiency of mouse SSC proliferation and colony formation. Cells were cultivated on top of MEFs, STO, and neonate and adult TSCs feeder layers for 30 days. The number and diameter of colonies and also the number of cells were evaluated during day 7, 15, 25, and 30 of culture. The mRNA expression of germ cells and somatic cells were analyzed.

Results: In our study, we observed a significant difference in the proliferation rates and colony size of SSCs among the groups, especially for MEFs ($P < 0.05$). SSCs can proliferate on MEFs, but not on STO, neonate or adult TSCs. Using immunocytochemistry by KI67 the proliferative activities of SSC colonies on MEFs were confirmed. The results of Fluidigm real-time polymerase chain reaction (RT-PCR) showed a high expression of the germ cell genes the promyelocytic leukemia zinc finger protein (*PLZF*), deleted in azoospermia-like (*DAZL*), octamer-binding transcription factor 4 (*OCT4*), and DEAD (Asp-Glu-Ala-Asp) box polypeptide 4 (*DDX4* or *VASA*) in SSCs, and a low expression of these genes in the feeder layers. Furthermore, we observed a higher expression of vimentin and integrin-B1 in feeder layers than in SSCs ($P < 0.05$).

Conclusion: Based on the optimal effect of MEFs for better colonization of SSCs, these feeder cells seem to be appropriate candidates for SSC cultures prior to transplantation. Therefore, it is suggested using these feeder cells for SSC cultivation.

Keywords: Feeder Layers, Proliferation, Spermatogonial Stem Cells

Cell Journal (Yakhteh), Vol 21, No 2, July-September (Summer) 2019, Pages: 186-193

Citation: Azizi H, Ghasemi Hamidabadi H, Skutella T. Differential proliferation effects after short-term cultivation of mouse spermatogonial stem cells on different feeder layers. Cell J. 2019; 21(2): 186-193. doi: 10.22074/cellj.2019.5802.

Introduction

The spermatogonial stem cells (SSCs) are located within a stem cell compartment in the basal part of the seminiferous tubules. The testicular tubules are encompassed by peritubular tissue, which consists of a basement membrane located between Sertoli cells of the seminiferous epithelium and myoepithelial cells within the interstitial space (1). Interstitial tissue patches with blood vessels, macrophages, and Leydig cell islands are found around the seminiferous epithelium. Differentiation and self-renewal of SSCs are partially triggered by secretory factors of these types of somatic cells (2). SSC self-renewal and spermatogonial differentiation can be regulated by extrinsic growth factors and cytokines from the somatic environment, and the molecular intrinsic genetic programs within germ cells.

Based on the current knowledge on SSCs, they can be cultivated *in vitro* with specific culture media and feeder layers, as reported in various studies (3-6). Only a few reports exist about SSCs culturing without feeders (7), as the feeder layers are known to be essential factors in SSCs cultivation (8, 9).

At this point, various types of feeder layers are employed in SSC cultivation. Fibroblast cells produce various growth factors, including basic fibroblast growth factor-2 (FGF-2) (10), transforming growth factor- β 2 (11), extracellular matrix proteins (12), activin, *Wnts*, and antagonists of bone morphogenetic proteins (BMPs) (13), which are important in maintenance of stem cells. It is common to utilize primary mouse embryonic fibroblast (MEF) feeders or STO feeder cells for culturing pluripotent stem cells originating from germlines such as embryonic carcinoma (EC) stem cells, embryonic stem (ES) cells, or embryonic germ (EG) cells.

Similar to the feeder supported stem cell cultures mentioned above, nowadays, several SSC studies utilized MEF feeder cells (6, 14, 15). Another well-known mouse cell line was the origin of different kinds of feeder cells, the STO feeder cells, which can substitute MEFs. On STO layers, SSCs were sustained in culture for months, as reported in a study by Nagano et al. (16). Especially, Oatley et al. (17) and Mohamadi et al. (18) used STO feeder cells for *in vitro* SSC cultivation. The proliferation of SSCs was also

described to be enhanced by yolk sac-derived endothelial cell (C166) feeder layers (19). In addition, testicular feeders containing CD34-positive cells have been shown to be useful for the cultivation of GPR125 (an orphan adhesion type G-protein-coupled receptor)-positive SSCs (20).

The goal of this research was to assess the effectiveness of different culture systems (MEF, STO, and neonate and adult TSCs) for *in vitro* mouse SSC germ cell culturing.

Material and Methods

Digestion of testis

Amol University of Special Modern Technologies Ethical Committee (Amol, Iran) approved the animal experiments. Testis cells from 6 days to 6 months-old Oct4-promoter reporter GFP from C57BL/6 transgenic mouse strain were isolated after decapsulation and treatment according to a one-step enzymatic digestion protocol. After removing the tunica albuginea, dissociated testicular tissue was placed in digestion solution, which contained collagenase IV (0.5 mg/ml), DNase (0.5mg/ml) and Dispase (0.5 mg/ml) in HBSS (Hank's Balanced Salt Solution) buffer with Ca⁺⁺ and Mg⁺⁺ (PAA, USA) at 37°C for 8 minutes. Digestion enzymes were purchased from Sigma Aldrich. The digestion enzymes were stopped with 10% ES cell-qualified fetal bovine serum (FBS, Invitrogen, USA) and then pipetted to obtain a single cell suspension. After centrifugation, the specimens were washed with DMEM/F12 (Invitrogen, USA), filtered through a 70 µm strainer and centrifuged for 10 minutes at 1500 rpm (6).

Preparation and culture of the different feeder cells

Sandos inbred mice embryo-derived thioguanine- and ouabain-resistant feeders

STO cell line, which was originally derived by A. Bernstein, Ontario Cancer Institute, Toronto, Canada from a continuous line of SIM mouse embryonic fibroblasts, was ordered commercially from ATCC (STO (ATCC® CRL-1503™)).

For maintenance of STO feeder cells were cultured in T-75 tissue culture flask at 37°C and 5% CO₂ in ATCC-formulated Dulbecco's Modified Eagle's Medium (DMEM, Invitrogen, USA) supplemented with FBS to a final concentration of 10%. The cells were routinely passaged when reaching 90% of confluency. The proliferation of STO cells was inactivated either by γ-irradiation or mitomycin C (10 mg/ml) treatment.

Mouse testicular stromal feeder cells

Testicular stroma cells (TSCs) were prepared both from the testis of neonate and adult mice. After digestion of the testicular tissue, the whole cell fraction was cultured in T-75 tissue culture flask at 37°C and 5% CO₂ on culture media by serially passaging 2-3 times over the span of 2 weeks in DMEM containing 10% FBS. The feeder cells were passaged to a new culture flask when reached 90% confluency. After passage 2-3, TSCs were further treated for mitotic inactivation with mitomycin C (10 mg/ml).

Mouse embryonic feeder cells

For the derivation of MEF cells mouse embryos from E13-E14, pregnant mice were used. After sacrifice of the pregnant females mice with CO₂ asphyxia, the embryos were retrieved by removing the placental and fetal membranes. Afterward, the embryos were washed with Hank's Balanced Salt Solution (HBSS) buffer, followed by excision of the intestinal from the embryos. This was followed by transferring the embryo carcasses to a new plate with HBSS buffer. The tissues were minced by aspiration through a syringe. This was followed by digestion with trypsin or collagenase-dispase (1mg/ml) for 15-20 minutes. The digesting enzymes were inactivated with 15% serum, and the cells were pipetted several times in order to break up the remaining pieces of tissue. For maintenance, MEFs were cultured in DMEM containing 10% FBS in T-75 tissue culture flask at 37°C and 5% CO₂. MEF cells were passaged when the culture cells reached 90% of confluence. In passage 3-4, MEF cells were used for mitotic inactivation with γ-irradiation or mitomycin C treatment.

The culture of testicular cells

The supernatant was removed, and the testicular cell suspension was plated onto 0.2% gelatin-coated culture dishes (approximately 0.2-0.5×10⁵ cells per 3.8 cm² for neonate and 2×10⁵ cells per 3.8 cm² for adult mice) in SSCs medium, which consisted of StemPro-34 medium, 1% N2-supplement (Invitrogen, USA), 6 mg/ml D+glucose (Sigma Aldrich, USA), 5 µg/ml bovine serum albumin (Sigma Aldrich, USA), 1% L-glutamine (PAA, USA), 0,1% β-mercaptoethanol (Invitrogen, USA), 1% penicillin/streptomycin (PAA, USA), 1% MEM vitamins (PAA, USA), 1% non-essential amino acids (PAA, USA), 30 ng/ml estradiol (Sigma Aldrich, USA), 60 ng/ml progesterone (Sigma Aldrich, USA), 20 ng/ml epidermal growth factor (EGF, Sigma Aldrich, USA), 10 ng/ml FGF (Sigma Aldrich, USA), 8 ng/ml GDNF (Sigma Aldrich, USA), 100 U/ml human leukemia inhibitory factor (LIF, Millipore, USA), 1% ES cell qualified FBS, 100 µg/ml ascorbic acid (Sigma Aldrich, USA), 30 µg/ml pyruvic acid (Sigma Aldrich, USA) and 1 µl/ml DL-lactic acid (Sigma Aldrich, USA) at 37°C and 5% CO₂ in air. The molecular and functional characterization of SSCs were established similarly as described in our previous study (6). In the next step, for analyzing the efficiency of mouse SSCs growth and colony formation, about 4000 SSCs were plated on a 24-well plate, in which each well was coated with MEFs from C57BL/6 (C57-MEF), MEFs from CF1 mouse (CF1-MEF), STO, neonate testicular stromal cells (N-TSCs), and adult TSCs (A-TSCs) feeder layers. Afterward, the number and diameter of the colonies, as well as the number of cells were evaluated during day 7, 15, 25, and 30 of culture. The diameter of colonies was measured by the ImageJ software. For the measurement of the number of cells, as we mentioned above, we plated 4000 cells in each well of 24 well plates, and after trypsinization, cells were counted during day 7, 15, 25, and 30.

Gene expression analyses on the Fluidigm Biomark system

Dynamic array chips were employed to measure the expression of the genes by a Fluidigm Real-time polymerase chain reaction (PCR) system (6). All Taqman real-time PCR assays were provided by Thermo Fisher Scientific, for octamer-binding transcription factor 4 (*OCT4*) the assay Mm03053917_g1, deleted in azoospermia-like (*DAZL*) Mm00515630_m1, *VASA* Mm00802445_m1, *INTEGRIN-B1* Mm01200043_m1, zinc finger and BTB domain containing 16 (*PLZF*) Mm01176868_m1, *VIMENTIN* Mm00619195_g1, G-protein coupled receptor 125 (*GPR125*), Tetraspanin-29 (*CD9*) Mm00514275_g1, and the housekeeping gene glyceraldehyde-3-phosphate dehydrogenase (*GAPDH*) Mm99999915_g1, which was used for normalization of the different types of cultured cells. The cultured cells included neonate SSCs (N-SSCs), adult SSCs (A-SSCs), C57-MEF, CF1-MEF, STO, N-TSCs, and A-TSCs. In each sample, about 50 cells were manually selected from the cultures with a micromanipulator, lysed with special lysis buffer containing 9 μ l RT-PreAmp Master Mix (5.0 μ l Cells Direct 2 \times Reaction Mix (Invitrogen, USA), 2.5 μ l 0.2 \times assay pool, 0.2 μ l RT/Taq Superscript III (Invitrogen, USA), and 1.3 μ l TE (Tris-EDTA, Invitrogen, USA) buffer and immediately frozen and stored at -80°C. The number of targeted transcripts was quantified using TaqMan real-time PCR on the BioMark real-time quantitative PCR (qPCR) system (Fluidigm). Every sample was examined in two technical replicates. The Ct values achieved by the BioMark System were analyzed by GenEx software from the MultiD analysis (6).

Immunocytochemical staining

Cells were cultured in 24 well plates and fixed with 4% paraformaldehyde. After rinsing with phosphate buffered solutions (PBS, Invitrogen, USA) the samples were permeabilized with 0.1% Triton (Invitrogen, USA)/PBS and blocked with 1% bovine serum albumin (BSA, Sigma Aldrich)/PBS. After removing the blocking solution, the cells were incubated overnight with the primary Ki67 antibody (Sigma Aldrich, USA). After rinsing, the process was followed by incubation with species-specific secondary antibodies, which were conjugated with fluorochrome; the labeled cells were counterstained with 0.2 μ g/ml 4', 6-diamidino-2-phenylindole (DAPI, DAPI, Sigma Aldrich, USA) for 3 minutes at room temperature and fixed with Mowiol 4-88 reagent (Merck, USA). Labeled cells were examined with a confocal microscope Zeiss LSM 700, and images were taken with a Zeiss LSM-TPMT camera (6).

Statistical analysis

The experiments were replicated at least 3 times. The average for gene expressions in groups was calculated, and the groups were evaluated using one-way analysis of variance (ANOVA) followed by the Tukey's post-hoc tests. The expression of genes was compared with non-parametric Mann-Whitney's test. The variation between groups was considered statistically significant if a value of $P < 0.05$ was obtained.

Results

For analyzing the growth efficiency of mouse SSC on different feeder cells, SSCs were cultivated on C57-MEF, CF1-MEF, STO, N-TSCs, and A-TSCs feeder cover plates. Over time, the microscopic analysis demonstrated that the growth behavior of SSCs on C57-MEF and CF1-MEF was much stronger than on STO, N-TSCs and A-TSCs. A decrease in the number of SSCs growing on STO, N-TSCs, and A-TSCs was observed about 7 days after the initiation of the culture (Fig.1).

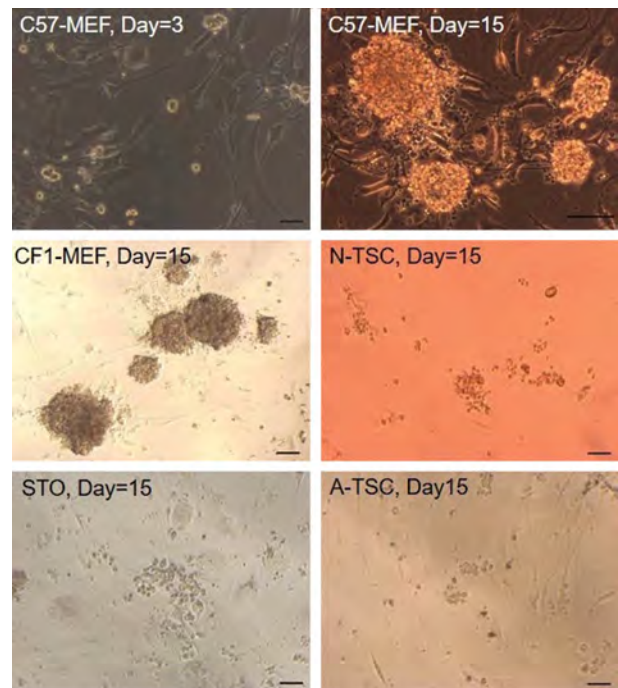


Fig.1: Microscopic observation of SSCs on the different feeder layer. Cultivation of SSCs on C57-MEF (MEF cells isolated from C57BL/6 mouse), CF1-MEF (MEF cells isolated from CF-1 mouse), STO (STO feeder), N-TSCs (TSCs feeder cells isolated from neonate mouse), and A-TSCs (TSCs feeder cells isolated from adult mouse) feeder layers. On day 15 the growth of SSCs was observed on C57-MEF and CF1-MEF feeder layer (scale bar: 100 μ m). SSC; Spermatogonial stem cells, MEF; Mouse embryonic fibroblasts, STO; Sandos inbred mice embryo-derived thioquinine- and ouabain-resistant feeder, and TSC; Testicular stromal cells.

After the transfer of SSCs onto feeders and during the initial phase of the SSC culture, under all conditions, we observed comparable growth behavior and colony formation of SSCs until about day 7. After about 7 days of the initiation of the culture, we observed reduced growing of SSC on STO, NTSC, and ATSC feeder layers, while on C57-MEF and CF1-MEF cells the SSCs continued to proliferate in number and an increase in diameter of colonies and number of SSCs colonies was observed. It should be mentioned that we did not visualize any significant difference between C57-MEF and CF1-MEF feeder layer groups. The changes in SSC number, diameter, and the number of colonies were observed to be significantly higher on days 15 and 25 compared to other time points ($P < 0.05$). Apparently, the maximal growth of SSCs occurred by 25 days after plating the cells on MEF feeders (Fig.2), and the supportive effect of the MEF feeders seemed to diminish after day 25.

Immunofluorescent staining showed that SSC colonies cultured on MEF feeders were strongly positive for the proliferation marker Ki67 in contrast to STO, neonate, and adult TSCs feeder layers (Fig.2). Ki67, a non-histone nuclear protein, is expressed in the course of cell proliferation (21).

To evaluate the expression of germ and somatic cell markers in SSCs and feeder cells, we analyzed the mRNA expression with Fluidigm expression profiling and Taqman assays

of the following genes *PLZF*, *OCT4*, *VASA*, *VIMENTIN*, *DAZL*, *CD9*, *GPR125*, and *INTEGRIN-B1* on neonate and adult SSCs, and on feeder layers C57-MEF, CF1-MEF, STO, NTSCs, and ATSCs. We observed that the expression of *VASA*, *DAZL*, *PLZF*, and *OCT4* in N-SSCs and A-SSCs was significantly higher than in somatic cells ($P < 0.05$). In our analysis, we observed a significantly higher expression of *VIMENTIN* and *INTEGRIN-B1* in somatic cells than N-SSCs and A-SSCs, but not for *CD9* and *GPR125* ($P < 0.05$, Fig.3).

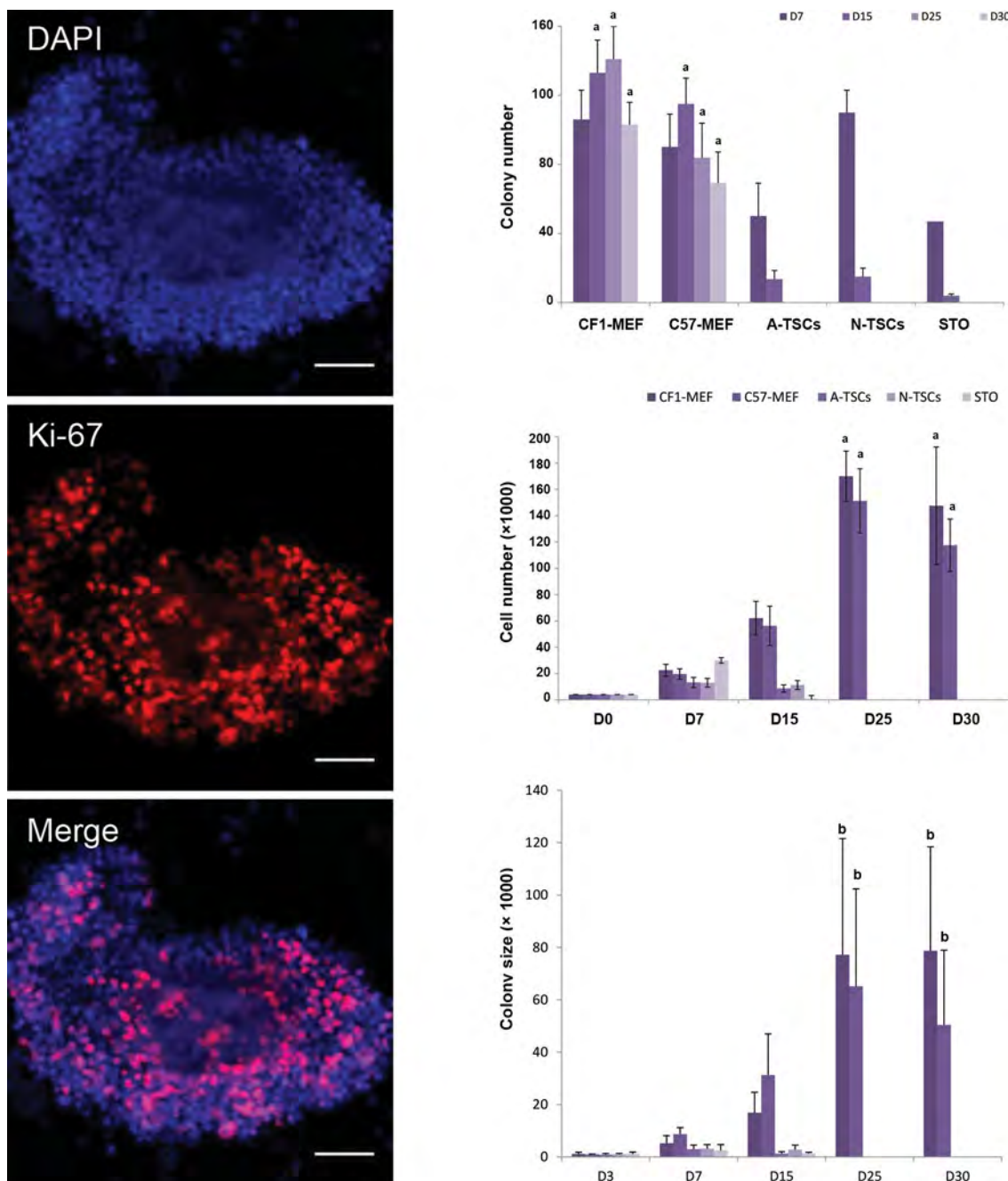


Fig.2: The growth analysis of SSCs on different feeder layer and immunofluorescent staining for Ki67. On C57-MEF (MEF cells isolated from C57BL/6 mouse) and CF1-MEF (MEF cells isolated from CF-1 mouse), feeder layer the number of SSCs, colonies size and colony number were significantly higher in comparison to the other types of feeder cells ($P < 0.05$). a, b; $P < 0.05$ in comparison to other feeder cell groups on the same day. The X-axis shows feeder cells and day. SSCs on MEF feeder layer express Ki67 protein (scale bar: 50 μ m). SSC; Spermatogonial stem cells, MEF; Mouse embryonic fibroblasts, STO; Sandos inbred mice embryo-derived thioguanine- and ouabain-resistant feeder, and TSC; Testicular stromal cells.

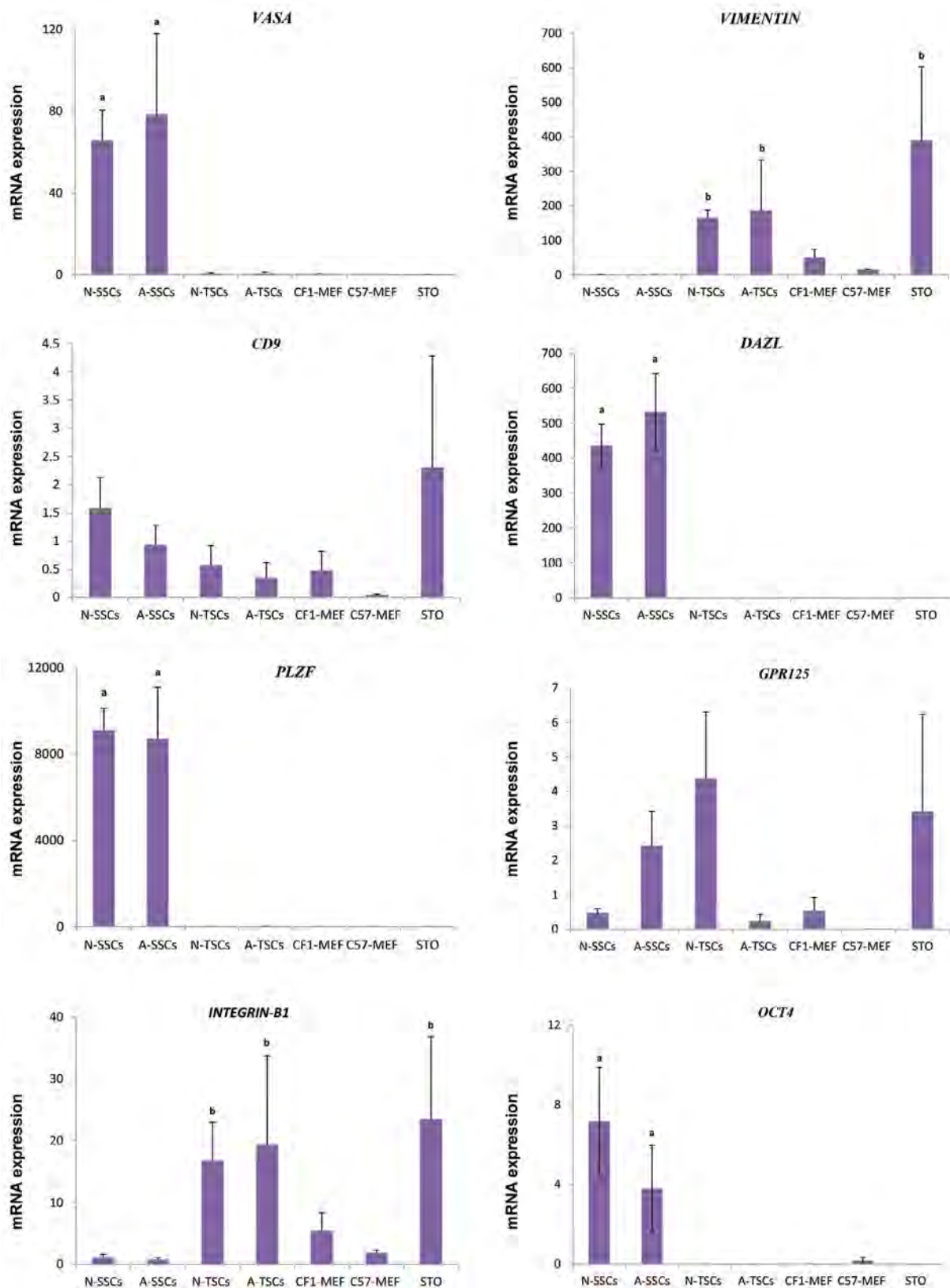


Fig.3: mRNA expression of germ and somatic cell markers in SSCs and feeder cells. The analysis was performed between SSCs and feeders. The significance of the difference between different groups was determined by non-parametric Mann-Whitney’s test. a, b; $P < 0.05$ vs. other feeder cell groups. The expression of *VASA*, *DAZL*, *PLZF*, and *OCT4* in SSCs were significantly ($P < 0.05$) higher than the other groups. The expression of *VIMENTIN* and *INTEGRIN-B1* was significantly higher ($P < 0.05$) in the somatic cells than in SSCs but not *CD9* and *GPR125*. SSC; Spermatogonial stem cells, MEF; Mouse embryonic fibroblasts, STO; Sandos inbred mice embryo-derived thioguanine- and ouabain-resistant feeder, and TSC; Testicular stromal cells.

Discussion

Similar to other adult stem cells, the SSCs pass through several self-renewal and differentiation stages. During proliferation and differentiation, the extrinsic factors originating in the basal and luminal cell niches of the testicular tubules and the intrinsic gene expression pattern influence these processes (22-25). During *in vitro* cultivation, feeder layers should mimic these *in vivo* stem cell niche and might play a crucial role in self-renewal, expansion, and differentiation of SSCs by producing different soluble growth factors and contact-mediated substrates (26). Although the extrinsic factors secreted by feeder layers are only partially known, different feeder layers might cause diverse effects on self-renewal and differentiation of SSCs during cultivation.

In this study, we reported the short-term effect of embryonic and somatic feeder layers on mouse SSC cultivation. SSCs were co-cultured on C57-MEF, CF1-MEF, STO, N-TSCs, and A-TSCs feeder layers for 30 days. Our study demonstrated that the increase in the number of SSCs, the diameter, and the number of SSC colonies on MEF feeder layers was significantly higher than on STO and testicular somatic cells.

We observed by Fluidigm real-time PCR that the expression of the germ cells genes *VASA*, *DAZL*, *PLZF*, and *OCT4* were higher in SSCs than in somatic feeder cells, while the expression of *VIMENTIN* and *INTEGRIN-B1* was higher in somatic cells in comparison to SSCs. It has been demonstrated that CD9 and GPR125 are expressed in germ cells (27), but our data also showed that the expression of these markers in somatic cells. Similarly, Shinohara et al. demonstrated that INTEGRIN-B1 is a surface marker located on SSCs (28) while we observed increased expression of INTEGRIN-B1 in somatic cells. Therefore, it seems that CD9, GPR125, and INTEGRIN-B1 cannot be regarded as specific markers for the identification of SSCs. Our observations are also supported by the data from the Human Protein Atlas (www.proteinatlas.org) which shows that these proteins are also present in somatic cells of the testis.

Similar to our findings, several other groups used MEF feeders for the long-term proliferation of SSCs in culture (6, 14, 29). We proved that somatic TSCs and STO feeder cells could not, or only to a limited degree, support SSC cultures, while several reports demonstrated the beneficial influence of these feeders on the SSC culture (19, 30-33). These various results for the cultivation of SSCs might be caused by differences in species, mouse strains used, and also different populations of SSCs in testis, which all may show different phenotypic characteristics under different culture conditions. The same reasoning can be applied to the different sources of feeder cells used for SSC co-culturing.

In conditions of the short-term culturing, the capability of STO feeders to sustain mouse neonate Thy-1 positive SSCs and bovine testicular germ cells has been reported (34, 35). In contrast to mice, *in vitro* cultivation and the amount of SSCs could be diminished by TM4 or SF7 somatic Sertoli cell lines (36).

The mouse strain from which the harvested feeder cells originated from is another critical factor in SSC cultivation. DBA/2 mice produce SSCs which are unproblematic in proliferation with GDNF alone. However, different mouse strains such as C57BL/6 or 129/SvCP produce SSCs that are dependent on the soluble GDNF family receptor alpha 1 (GFR α 1) and basic FGF (bFGF or FGF2) to proliferate steadily *in vitro* (6). Kanatsu-Shinohara et al. (14) have already detected the beneficial growth patterns of DBA/2-derived SSCs. According to Sariola et al. (37), a multicomponent receptor complex including RET receptor tyrosine kinase and a glycosyl phosphatidylinositol-anchored ligand-binding subunit, termed GFR α 1, trigger the cellular responses to GDNF. In the majority of mouse strains, *in vitro* proliferation of SSCs critically depends on the addition of soluble GFR α 1, since the downstream signaling is supported by RET stimulation with soluble GFR α 1 (38).

In contrast, STO feeders express the insulin-like growth factor binding protein 4 and the growth factor pigment epithelium-derived factor (39). Their various expression of growth factors may explain the greater effect of MEFs on the proliferation and colony formation of SSCs.

Further transcriptomic and proteomic analysis should aim to identify the membrane-bound and secreted molecules by MEFs facilitating the proliferation of mouse SSCs in culture. The identification of these molecules might lead to the development of a more robust culture system for SSC proliferation. A similar approach would be of tremendous advantage for the improvement of short- and long-term culturing of human SSCs.

Conclusion

Our data showed that the markers *VASA*, *DAZL*, *PLZF*, and *OCT4* are specific for the characterization of SSCs, but CD9, GPR125, and INTEGRIN-B1 are also expressed in STO and TSCs somatic cells. Therefore, CD9, GPR125, and INTEGRIN-B1 markers are not unique for SSC identification. While some reports showed that SSCs could be cultivated and expanded on STO and somatic testicular feeder, our data showed that STO and TSC feeder could not be an ideal feeder layer for the short-term cultivation of SSCs. Our findings indicate that in comparison to STO, neonate, and adult TSC feeders, MEF feeder cells are able to better enhance SSC proliferation and expansion in the short-term cultures. In the future, it would be interesting to identify the contact-mediated substrates and soluble

growth factors produced by MEF feeder cells which might be beneficial for self-renewal and expansion of mouse SSCs in short-term cultures.

Acknowledgments

This research project was financially supported by the Iranian National Science Foundation (INSF), the International Scientific Meeting Office, Ministry of Science, Research and Technology of Islamic Republic of Iran and the University of Heidelberg, Institute for Anatomy and Cell Biology III, Department of Neuroanatomy, Germany. There is no conflict of interest in this study.

Authors' Contributions

H.A.; Wrote the manuscript, carried out and design the experiment. H.G.H., T.S.; Provided critical feedback and data analysis. T.S.; Edited the manuscript. The authors read and approved the final manuscript.

References

- Oatley JM, Brinster RL. The germline stem cell niche unit in mammalian testes. *Physiol Rev*. 2012; 92(2): 577-595.
- Rossi P, Dolci S. Paracrine mechanisms involved in the control of early stages of mammalian spermatogenesis. *Front Endocrinol (Lausanne)*. 2013; 4: 181.
- Kubota H, Brinster RL. Culture of rodent spermatogonial stem cells, male germline stem cells of the postnatal animal. *Methods Cell Biol*. 2008; 86: 59-84.
- Naughton CK, Jain S, Strickland AM, Gupta A, Milbrandt J. Glial cell-line derived neurotrophic factor-mediated RET signaling regulates spermatogonial stem cell fate. *Biol Reprod*. 2006; 74(2): 314-321.
- Meng X, Lindahl M, Hyvönen ME, Parvinen M, de Rooij DG, Hess MW, et al. Regulation of cell fate decision of undifferentiated spermatogonia by GDNF. *Science*. 2000; 287(5475): 1489-1493.
- Azizi H, Conrad S, Hinz U, Asgari B, Nanus D, Peterziel H, et al. Derivation of pluripotent cells from mouse SSCs seems to be age dependent. *Stem Cells Int*. 2016; 2016: 8216312.
- Choi NY, Park YS, Ryu JS, Lee HJ, Arauzo-Bravo MJ, Ko K, et al. A novel feeder-free culture system for expansion of mouse spermatogonial stem cells. *Mol Cells*. 2014; 6(37): 437-479.
- Kanatsu-Shinohara M, Miki H, Inoue K, Ogonuki N, Toyokuni S, Ogura A, et al. Long-term culture of mouse male germline stem cells under serum- or feeder-free conditions. *Biol Reprod*. 2005; 72(4): 985-991.
- Kanatsu-Shinohara M, Inoue K, Ogonuki N, Morimoto H, Ogura A, Shinohara T. Serum- and feeder-free culture of mouse germline stem cells. *Biol Reprod*. 2011; 84(1): 97-105.
- Moscattelli D, Presta M, Joseph-Silverstein J, Rifkin DB. Both normal and tumor cells produce basic fibroblast growth factor. *J Cell Physiol*. 1986; 129(2): 273-276.
- Chen S, Choo A, Chin A, Oh SK. TGF- β 2 allows pluripotent human embryonic stem cell proliferation on E6/E7 immortalized mouse embryonic fibroblasts. *J Biotechnol*. 2006; 122(3): 341-361.
- Conrad S, Azizi H, Hatami M, Kubista M, Bonin M, Hennenlotter J, et al. Expression of Genes Related to Germ Cell Lineage and Pluripotency in Single Cells and Colonies of Human Adult Germ Stem Cells. *Stem Cells Int*. 2016; 2016: 8582526.
- Prowse AB, McQuade LR, Bryant KJ, Marcal H, Gray PP. Identification of potential pluripotency determinants for human embryonic stem cells following proteomic analysis of human and mouse fibroblast conditioned media. *J Proteome Res*. 2007; 6(9): 3796-3807.
- Kanatsu-Shinohara M, Ogonuki N, Inoue K, Miki H, Ogura A, Toyokuni S, et al. Long-term proliferation in culture and germline transmission of mouse male germline stem cells. *Biol Reprod*. 2003; 69(2): 612-616.
- Kubota H, Avarbock MR, Brinster RL. Growth factors essential for self-renewal and expansion of mouse spermatogonial stem cells. *Proc Natl Acad Sci USA*. 2004; 101(47): 16489-16494.
- Nagano M, Avarbock MR, Leonida EB, Brinster CJ, Brinster RL. Culture of mouse spermatogonial stem cells. *Tissue Cell*. 1998; 30(4): 389-397.
- Oatley JM, Avarbock MR, Brinster RL. Glial cell line-derived neurotrophic factor regulation of genes essential for self-renewal of mouse spermatogonial stem cells is dependent on Src family kinase signaling. *J Biol Chem*. 2007; 282(35): 25842-25851.
- Mohamadi SM, Movahedin M, Koruji SM, Jafarabadi MA, Makoolati Z. Comparison of colony formation in adult mouse spermatogonial stem cells developed in Sertoli and STO coculture systems. *Andrologia*. 2012; 44 Suppl 1: 431-437.
- Kubota H, Wu X, Goodyear SM, Avarbock MR, Brinster RL. Glial cell line-derived neurotrophic factor and endothelial cells promote self-renewal of rabbit germ cells with spermatogonial stem cell properties. *FASEB J*. 2011; 25(8): 2604-2614.
- Seandel M, James D, Shmelkov SV, Falciatori I, Kim J, Chavala S, et al. Generation of functional multipotent adult stem cells from GPR125+ germline progenitors. *Nature*. 2007; 449(7160): 346-350.
- Schlüter C, Duchrow M, Wohlenberg C, Becker MH, Key G, Flad HD, et al. The cell proliferation-associated antigen of antibody Ki-67: a very large, ubiquitous nuclear protein with numerous repeated elements, representing a new kind of cell cycle-maintaining proteins. *J Cell Biol*. 1993; 123(3): 513-522.
- Nazm Bojnordi M, Movahedin M, Tiraihi T, Javan M, Ghasemi Hamidabadi H. Oligoprogenitor cells derived from spermatogonia stem cells improve remyelination in demyelination model. *Mol Biotechnol*. 2014; 56(5): 387-393.
- Ghasemi Hamidabadi H, Rezvani Z, Nazm Bojnordi M, Shirinzadeh H, Seifalian AM, Joghataei MT, et al. Chitosan-intercalated montmorillonite/poly(vinyl alcohol) nanofibers as a platform to guide neuronlike differentiation of human dental pulp stem cells. *ACS Appl Mater Interfaces*. 2017; 9(13): 11392-11404.
- Bojnordi MN, Azizi H, Skutella T, Movahedin M, Pourabdolhossein F, Shojaei A, et al. Differentiation of Spermatogonia Stem Cells into Functional Mature Neurons Characterized with Differential Gene Expression. *Mol Neurobiol*. 2017; 54(7): 5676-5682.
- Azizi H, Mehrjardi NZ, Shahbazi E, Hemmesi K, Bahmani MK, Baharvand H. Dehydroepiandrosterone stimulates neurogenesis in mouse embryonal carcinoma cell- and human embryonic stem cell-derived neural progenitors and induces dopaminergic neurons. *Stem Cells Dev*. 2010; 19(6): 809-818.
- West FD, Machacek DW, Boyd NL, Pandiyan K, Robbins KR, Stice SL. Enrichment and differentiation of human germ-like cells mediated by feeder cells and basic fibroblast growth factor signaling. *Stem Cells*. 2008; 26(11): 2768-2776.
- Shlush E, Maghen L, Swanson S, Kenigsberg S, Moskovtsev S, Barretto T, et al. In vitro generation of Sertoli-like and haploid spermatid-like cells from human umbilical cord perivascular cells. *Stem Cell Res Ther*. 2017; 8(1): 37.
- Shinohara T, Avarbock MR, Brinster RL. β 1- and α 6-integrin are surface markers on mouse spermatogonial stem cells. *Proc Natl Acad Sci USA*. 1999; 96(10): 5504-5509.
- Bojnordi MN, Azizi H, Skutella T, Movahedin M, Pourabdolhossein F, Shojaei A, et al. Differentiation of spermatogonia stem cells into functional mature neurons characterized with differential gene expression. *Mol Neurobiol*. 2017; 54(7): 5676-5682.
- Rastegar T, Minaee MB, Habibi Roudkenar M, Raghadi Kashani I, Amidi F, Abolhasani F, et al. Improvement of Expression of α 6 and β 1 Integrins by the Co-culture of Adult Mouse Spermatogonial Stem Cells with SIM Mouse Embryonic Fibroblast Cells (STO) and Growth Factors. *Iran J Basic Med Sci*. 2013; 16(2): 134-139.
- Smith JF, Yango P, Altman E, Choudhry S, Poelzl A, Zamah AM, et al. Testicular niche required for human spermatogonial stem cell expansion. *Stem Cells Transl Med*. 2014; 3(9): 1043-1054.

32. Izadyar F, Wong J, Maki C, Pacchiarotti J, Ramos T, Hower-ton K, et al. Identification and characterization of repopulating spermatogonial stem cells from the adult human testis. *Hum Reprod.* 2011; 26(6): 1296-1306.
 33. Shinohara T, Orwig KE, Avarbock MR, Brinster RL. Spermatogo-nial stem cell enrichment by multiparameter selection of mouse testis cells. *Proc Natl Acad Sci USA.* 2000; 97(15): 8346-8351.
 34. Kubota H, Avarbock MR, Brinster RL. Culture conditions and single growth factors affect fate determination of mouse sper-matogonial stem cells. *Biol Reprod.* 2004; 71(3): 722-731.
 35. Nasiri Z, Hosseini SM, Hajian M, Abedi P, Bahadorani M, Baha-rvand H, et al. Effects of different feeder layers on short-term culture of prepubertal bovine testicular germ cells in-vitro. *The-riogenology.* 2012; 77(8): 1519-1528.
 36. Nagano M, Ryu BY, Brinster CJ, Avarbock MR, Brinster RL. Maintenance of mouse male germ line stem cells in vitro. *Biol Reprod.* 2003; 68(6): 2207-2214.
 37. Sariola H, Saarma M. Novel functions and signalling pathways for GDNF. *J Cell Sci.* 2003; 116(Pt 19): 3855-3862.
 38. Paratcha G, Ledda F, Baars L, Couplier M, Besset V, Anders J, et al. Released GFRalpha1 potentiates downstream signaling, neuronal survival, and differentiation via a novel mechanism of recruitment of c-Ret to lipid rafts. *Neuron.* 2001; 29(1): 171-184.
 39. Sarkar P, Randall SM, Muddiman DC, Rao BM. Targeted pro-teomics of the secretory pathway reveals the secretome of mouse embryonic fibroblasts and human embryonic stem cells. *Mol Cell Proteomics.* 2012; 11(12): 1829-1839.
-

Dynamics of The Expression of Pluripotency and Lineage Specific Genes in The Pre and Peri-Implantation Goat Embryo

Pouria HosseinNia, Ph.D.^{1,2,3}, Mehdi Hajian, Ph.D.¹, Farnoosh Jafarpour, Ph.D.¹, Seyed Morteza Hosseini, Ph.D.¹, Mojtaba Tahmoorespur, Ph.D.², Mohammad Hossein Nasr-Esfahani, Ph.D.^{1*}

1. Department of Reproductive Biotechnology, Reproductive Biomedicine Research Center, Royan Institute for Biotechnology, ACECR, Isfahan, Iran
2. Department of Animal Science, Faculty of Agriculture, Ferdowsi University of Mashhad, Mashhad, Iran
3. Department of Research and Development, ROJETechnologies, Yazd, Iran

*Corresponding Address: P.O.Box: 81593-58686, Department of Reproduction and Development, Royan Institute for Biotechnology, ACECR, Isfahan, Iran

Email: mh.nasr-esfahani@royaninstitute.org

Received: 28/January/2018, Accepted: 19/August/2018

Abstract

Objective: Two critical points of early development are the first and second lineage segregations, which are regulated by a wide spectrum of molecular and cellular factors. Gene regulatory networks, are one of the important components which handle inner cell mass (ICM) and trophoctoderm (TE) fates and the pluripotency status across different mammalian species. Considering the importance of goats in agriculture and biotechnology, this study set out to investigate the dynamics of expression of the core pluripotency markers at the mRNA and protein levels.

Materials and Methods: In this experimental study, the expression pattern of three pluripotency markers (*Oct4*, *Nanog* and *Sox2*) and the lineage specific markers (*Rex1*, *Gata4* and *Cdx2*) were quantitatively assessed in *in vitro* matured (MII) oocytes and embryos at three distinctive stages: 8-16 cell stage, day-7 (D7) blastocysts and D14 blastocysts. Moreover, expression of *Nanog*, *Oct4*, *Sox2* proteins, and their localization in the goat blastocyst was observed through immunocytochemistry.

Results: Relative levels of mRNA transcripts for *Nanog* and *Sox2* in D3 (8-16 cell) embryos were significantly higher than D7 blastocysts and mature oocytes, while *Oct4* was only significantly higher than D7 blastocysts. However, the expression pattern of *Rex1*, as an epiblast lineage marker, decreased from the oocyte to the D14 stage. The expression pattern of *Gata4* and *Cdx2*, as extra embryonic lineage markers, also showed a similar trend from oocyte to D3 while their expressions were up-regulated in D14 blastocysts.

Conclusion: Reduction in *Nanog*, *Oct4*, *Sox2* mRNA transcription and a late increase in extra embryonic lineage markers suggests that the developmental program of lineage differentiation is retarded in goat embryos compared to previously reported data on mice and humans. This is likely related to late the implantation in goats.

Keywords: Blastocyst, Embryo, Goat, Oocyte

Cell Journal(yakhteh), Vol 21, No 2, July-September (Summer) 2019, Pages: 194-203

Citation: HosseinNia P, Hajian M, Jafarpour F, Hosseini SM, Tahmoorespur M, Nasr-Esfahani MH. Dynamics of the expression of pluripotency and lineage specific genes in the pre and peri-implantation goat embryo. Cell J. 2019; 21(2): 194-203. doi: 10.22074/cellj.2019.5732.

Introduction

A distinguishing feature of blastocyst formation in mammals is regulation of the trophoctoderm (TE) and specification of the pluripotent inner cell mass (ICM) through a series of highly orchestrated events directed by spatial and temporal patterns of gene expression, cell polarization, and cell-cell interactions (1). The TE will differentiate into the placenta while the ICM differentiates into the epiblast and the hypoblast or primitive endoderm. Subsequently, the embryo proper is derived from the epiblast while extra-embryonic tissues are derived from the primitive endoderm and trophoblast. As the ICM of the newly developed blastocyst is the main source of embryonic stem cell (ESC) derivation in the mouse and human, it is obviously important to provide a clear understanding of the molecular circuitry governing ICM and TE ontogeny and to expand our knowledge of *in vitro* derivation of ESC and for their future applications in the goat species.

Despite initial concepts proposing the equivalence

of gene networks governing the delineation of ICM and TE and pluripotency across different mammalian species, recent comparative studies suggest that different pathways may be involved in controlling ICM-TE ontogeny in different species. For example, during first lineage segregation, TE and ICM are committed and marked by reciprocal expression of *Cdx2* and *Oct4* in mouse blastocysts while derivation of the epiblast and primitive endoderm in second lineage segregation is modulate by *Nanog* and *Gata6*, respectively (2). In humans, although a similar pattern of regulation exists, *OCT4* is not restricted to the ICM and it has been demonstrated that in primates ESCs and isolated ICMs fail to incorporate into host embryos and develop into chimeras (3). More importantly, it has been recently shown that primate ESCs are more equivalent to mouse epiblast stem cells (EpiSCs), which are driven from post implantation embryos and are developmentally more advanced relative to naive ESCs (4).

Ungulates may be a unique case, having some

similar regulatory pathways to mouse and human cells but is coupled with dramatically distinct expression patterns. For example, comparative immunocytochemical studies have shown that *Cdx2* and *Gata6* expression in porcine and bovine blastocysts resembled that of the mouse, however, *Oct4* is expressed in both the ICM and TE (5). Importantly, through exchanging mouse and bovine *Oct4* reporters, Berg et al. (6) elegantly demonstrated that the mouse *Oct4* promoter, which is normally repressed in the mouse TE remained active in the bovine TE; and vice versa, while bovine *Oct4* promoter also remains active in the mouse TE, suggesting that the TE is not committed at an equivalent stage in the bovine embryo as it is in newly developed mouse blastocysts. In this regard, a recent study by Simmet et al. (7) showed that *Oct4* is expressed during early stages of embryonic development (oocyte to morula stage) and regulates *Nanog*, *Gata6* and *Gata4* expression in bovine embryos as it does in the mouse (8), however, unlike in the mouse this is not mediated through fibroblast growth factors (FGF) signaling.

The great difference between ICM and TE cells, commonly occurs within two cell cycles from morula to the blastocyst (9). A growing body of evidence indicating that the core pluripotency triad in humans (*OCT4*, *NANOG*, *SOX2*) and mice (*Oct4*, *Nanog*, *Sox2*) is the main regulator of the establishment and maintenance of pluripotency in the ICM. The expression levels of the core pluripotency triad during ICM emergence in mice and humans have been well established at the mRNA and protein levels. However, the actual status of *Oct4*, *Nanog*, and *Sox2* genes is poorly understood in other mammals. Such studies will provide a roadmap for differentiating definitive species-specific differences and help to understand why authentic ESCs are not established in ungulates (4, 7).

The goat is a valuable livestock with promising importance in agriculture, biomedicine and transgenic production of pharmaceutical drugs. Therefore, this study set out to investigate the dynamics of the expression of the core pluripotency triad in *in vitro* produced goat embryos at the mRNA and protein levels. Moreover, since implantation in ungulates, unlike in human and mouse embryos, occurs with a delay of around 7 days, this period of "delay" in implantation should likely "influence" the pattern of developmentally important genes (10). Therefore, we further planned to evaluate the expression status of peri-implantation goat embryos cultured *in vitro* until D14.

Materials and Methods

Unless otherwise stated, all chemicals and media were obtained from Sigma Chemical Co. (St. Louis, MO, USA) and Gibco (Grand Island, NY, USA), respectively.

Selection of the gene set

In order to select the genes that could predominantly be involved in the regulation of early embryonic development and pluripotency, and due to a lack of sufficient data on the goat species, we followed the strategy used by McGraw et al. (11). In brief, we sought the related information using gene

expression databases that profile gene expression and gene ontologies (GOs) in human and mouse embryos and ESCs. To be a candidate, the potential genes had to be commonly present in ESCs and either in the oocyte or the blastocyst, while playing a critical role in transcription regulation and pluripotency. This survey provided a list of 6 genes including, *Oct4*, *Rex1*, *Sox2*, *Nanog*, *Gata4*, *Cdx2* genes.

In vitro production of goat embryos

The procedure for *in vitro* production of goat embryos was as has been described previously (12). In brief, goat ovaries were used for *in vitro* maturation of cumulus-oocyte complexes (COCs) in tissue culture medium-199 (TCM199) plus 10% fetal calf serum (FCS), 2.5 mM sodium pyruvate, 100 IU/mL penicillin, 100 mg/mL streptomycin, 10 mg/mL follicle stimulating hormone (FSH), 10 mg/mL luteinizing hormone (LH), 1 mg/mL estradiol-17 β , and 0.1 mM cysteamine under mineral oil for 20-22 hours at 39°C, 5% CO₂, and maximum humidity before being used for embryo development in groups of six in 20 μ L droplets of a modified formulation of synthetic oviductal fluid (mSOF) (13) at 39°C, 6% CO₂, 5% O₂, and maximum humidity. MII oocytes were collected 20-22 hours post maturation, D3 developing embryos at the 8-16 cell stage, and D7 blastocysts, were washed thrice in phosphate buffered saline (PBS) without calcium and magnesium, and collected. Pools of 60 oocytes, 35-40 day 3 embryos, 20 day 7 blastocysts were collected in 500 μ L microtubes containing 20 μ L RLT buffer, frozen and stored at -70°C until RNA extraction. All oocyte and embryo pools used for RNA extractions were collected and analyzed in triplicates. This system of embryo development supported quite good rates of *in vitro* embryo development with cleavage and blastocyst rates ranging between 85-92% and 40-45%, respectively (14). In order to extend *in vitro* culture of goat blastocysts, we prepared a feeder layer of caprine fetal fibroblasts (CFFs) as described by Behboodi et al. (10). For this purpose, a CFF line was derived from three 40-day male fetuses. Single cell suspension was prepared by mincing fetal tissue and culturing the cells in Dulbecco's modified eagle medium and ham's F12 (DMEM/F12) supplemented with 10% FBS, 0.25 μ g/ml amphotericin-B, 1% penicillin-streptomycin, 1% gentamycin in 25 cm² culture flasks and incubated at 37°C, 6% CO₂, until the appearance of a confluent monolayer from day 4 onwards. The monolayer was trypsinized and further cultured for proliferation of the CFF source, each passage took around 3-4 days until becoming confluent. CFFs at passages 2-4 were treated with mitomycin (10 mg/mL) for 2 hours. Mitomycin-treated cells were washed twice with DMEM/F12, and treated with 0.25% trypsin-EDTA and dissociated into single cells by gentle pipetting. Cells were then seeded at concentration of 1 \times 10⁵ cells/mL in 100 μ L drops of DMEM/F12 in the vicinity of feeder-free 100 μ L droplets of DMEM/F12 supplemented with 10% FBS, 1% L-glutamine, 1% non-essential amino acid, and 0.1% β -mercaptoethanol under mineral oil. Five to six D7 blastocysts were transferred to each 100 μ L droplet of feeder-free DMEM/F12. Using of the tip of a drawn glass pipette, the DMEM/F12 drops containing blastocysts were gently connected to their adjacent DMEM/F12 drop containing the CFF monolayer. This joined culture system

provides the beneficial effects of a feeder layer for extended *in vitro* embryo culture, while preventing attachment and flattening of the growing blastocysts. The joined droplets were refreshed every other day until D14 of embryo development, when pools of 7-10 well developed spherical D14 embryos were pooled for RNA extraction as described above.

RNA extraction and reverse transcription polymerase chain reaction

The procedure for quantitative real-time polymerase chain reaction (qRT-PCR) was as described previously (15). In brief, total RNA of MII-oocytes, 8-16 cell embryos, blastocysts on days 7 & 14 was extracted using RNeasy Micro kit (Qiagen, ON, Canada) followed by the treatment with DNase I (Ambion, ON, Canada) according to the manufacturer's protocol. The quality and quantity of the extracted RNA was determined using a WPA Biowave spectrophotometer (Cambridge, UK). For reverse transcription, 10 µL of total RNA was used in a reaction with a final volume of 20 µL containing 1 µL of Random Hexamers, 4 µL RT buffer (10 x), 2 µL of dNTP, 1 µL of RNase inhibitor (20 IU), and 1 µL of reverse transcriptase (Fermentas, Glen Burnie, Ontario, Canada). Reverse transcription was carried out at 25°C for 10 minute, 42°C for 1hour and 70°C for 10 minutes.

Quantitative analysis of transcripts by real time-polymerase chain reaction

The transcript level of the aforementioned genes and ACTB, as a housekeeping gene, were measured using real time-PCR (RT-PCR). Briefly, total RNA of oocytes, day3 embryos, day 7 and 14 blastocysts was extracted and then each RNA sample was used for cDNA synthesis. RT-PCR was carried out using 1 µL of cDNA (50 ng), 5 µL of the SYBR Green/0.2

µl ROX qPCR Master Mix (2X) (Fermentas, Germany) and 1 µL of forward and reverse primers (5 pM) adjusted to a total volume of 10 µL using nuclease-free water. The primer sequences, annealing temperatures and size of the amplified products are shown in Table 1.

Embryo immunostaining

Expression of Nanog, Oct4 and Sox2 proteins and their localization in the goat blastocyst was observed through immunocytochemistry (ICC). *In vitro*-derived embryos were washed in PBS containing 1 mg/ml polyvinyl alcohol (PVA), and then fixed in 4.0% paraformaldehyde for 30 minutes. Subsequently the embryos were washed in PBS/PVA with 0.5 µl/ml tween 20 (solution1). Permeabilization was carried out in 0.5% Triton X-100 (Sigma-Aldrich) solution in PBS for 15 minutes at room temperature (RT), and then washed with solution1. In order to block non-specific binding sites, embryos were incubated in blocking solution containing PBS/PVA containing 1% bovine serum albumin (BSA)+10% normal goat serum for 60 minutes at RT. Subsequently, embryos were incubated with the primary antibody, either rabbit polyclonal antibody against Nanog (1:300 dilution, Abcame, ab21603), rabbit monoclonal anti-human Sox2 antibody (1:300 dilution, cell signaling, 3579) and rabbit polyclonal anti-mouse Oct4 (1:300 dilution, lifespan, c48532), for 60 minutes at 37°C. Then, embryos were washed 3-4 times in PBS/PVA for 15 minutes at 37°C and subsequently incubated in goat anti-rabbit IgG fluorescein conjugated (1:50 dilution, Sigma, F1262) for 45 minutes at RT. After washing 3-4 times in PBS/PVA at 37°C, all embryos were counterstained with 1 µg/mL Hoechst for 5-10 minute and then washed 3-4 times in PBS/PVA for 15 minute at 37°C, Embryos were mounted in 10ml light diagnostics mounting fluid (Merck, Germany) on a slide before observation. Fluorescent signals were visualized using a fluorescent microscope (Olympus, Japan).

Table 1: Specific real-time primers were designed for gene sequences

Gene	Primer sequences (5'-3')	Length of PCR product	Tm
<i>OCT4</i>	F: GCCAGAAGGGCAAACGAT R: GAGGAAAGGATACGGGTC	96	56
<i>REX1</i>	F: GCAGCGAGCCCTACACAC R: ACAACAGCGTCATCGTCCG	94	61
<i>SOX2</i>	F: ATGGGCTCGGTGGTGA R: CTCTGGTAGTGCTGGGA	182	54
<i>NANOG</i>	F: GATTCTCCACAAGCCCT R: TCATTGAGCACACACAGC	137	54
<i>GATA4</i>	F: TCCCCTTCGGGCTCAGTGC R: GTTGCCAGGTAGCGAGTTTGC	128	64
<i>CDX2</i>	F: CCCCAAGTGAAAACCAG R: TGAGAGCCCCAGTGTG	144	53
<i>ACTB</i>	F: CCATCGGCAATGAGCGGT R: CGTGTTGGCGTAGAGGTC	146	60

PCR; Polymerase chain reaction and Tm; Melting temperature.

Statistical analysis

Statistical significance was considered to be $P < 0.05$ and determined by two-tailed Fisher's exact test in SPSS software version 20 for developmental data, two-tailed student's t test with equal variance for cell counts and real-time PCR data was used.

Results

Gene expression pattern

In order to understand the relation between the stages of embryonic development and lineage segregation properties, we investigated expression of several pluripotency-related genes (*Oct4*, *Sox2* and *Nanog*), a lineage specific marker for TE development (*Cdx2*), as well as markers for the

development of the primitive endoderm and the ICM (*Gata4* and *Rex1*, respectively) at various embryonic development stages. Oocytes, day 3 embryo (D3), day 7 (D7) and 14 (D14) blastocysts were collected and mRNA transcript levels were determined by RT-PCR CT-values for the aforementioned markers (Fig.1).

In the case of *Nanog*, the relative expression levels of mRNA transcripts in day 3 embryos and D14 blastocysts were significantly higher than oocytes and D7 blastocysts. The expression of *Sox2* was relatively low in the oocytes and significantly increased by day 3 embryos and subsequently decreased to significantly lower values compared to oocytes. The pattern of expression for *Oct4* was not significantly lower in D3 embryos compared to oocyte but it significantly decreased by D7 and D14 compared to D3 embryos.

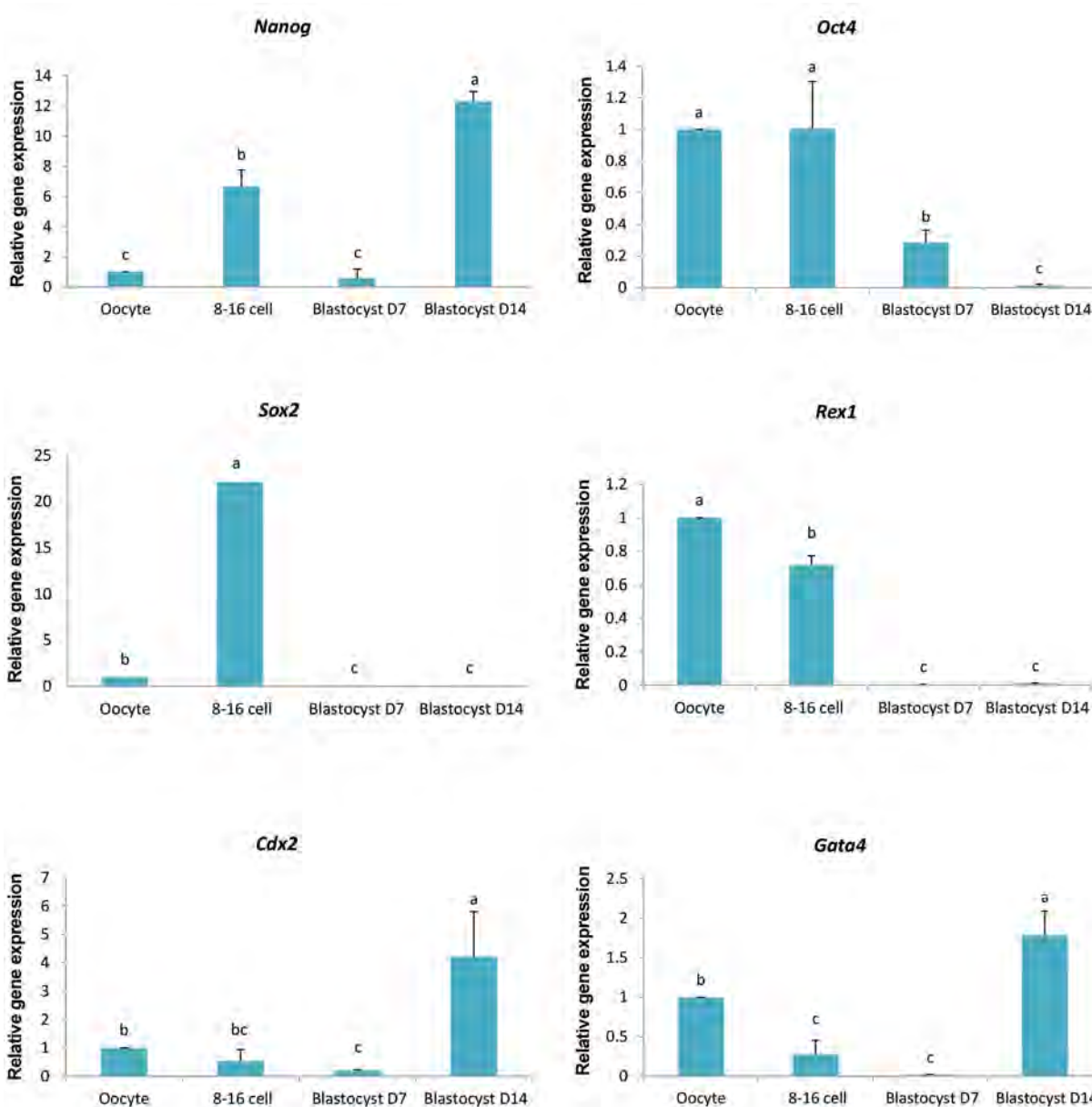


Fig.1: Relative gene expression of specific lineage markers for the ICM, TE, or PE in goat oocytes and preimplantation embryos. a, b, c symbols showed significant differences between the developmental stages. Error bars represent standard deviation. ICM; Inner cell mass, TE; Trophectoderm, and PE; Primitive endoderm.

Rex1 expression was similar to that of *Oct4* and its expression was significantly higher in oocytes compared to D3 embryos and it significantly decreased in D7 and D14 blastocysts compared to oocytes and D3 embryos. *Cdx2* mRNA was detected between oocytes and D14 blastocyst, but its expression was meaningfully up-

regulated in D14 blastocysts, when compared with previous stages. The expression pattern of the lineage marker *Gata4* was highest in D14 blastocysts, when compared to earlier stages. *Gata4* expression gradually decreased from oocytes to D7 blastocysts and became significantly elevated by D14.

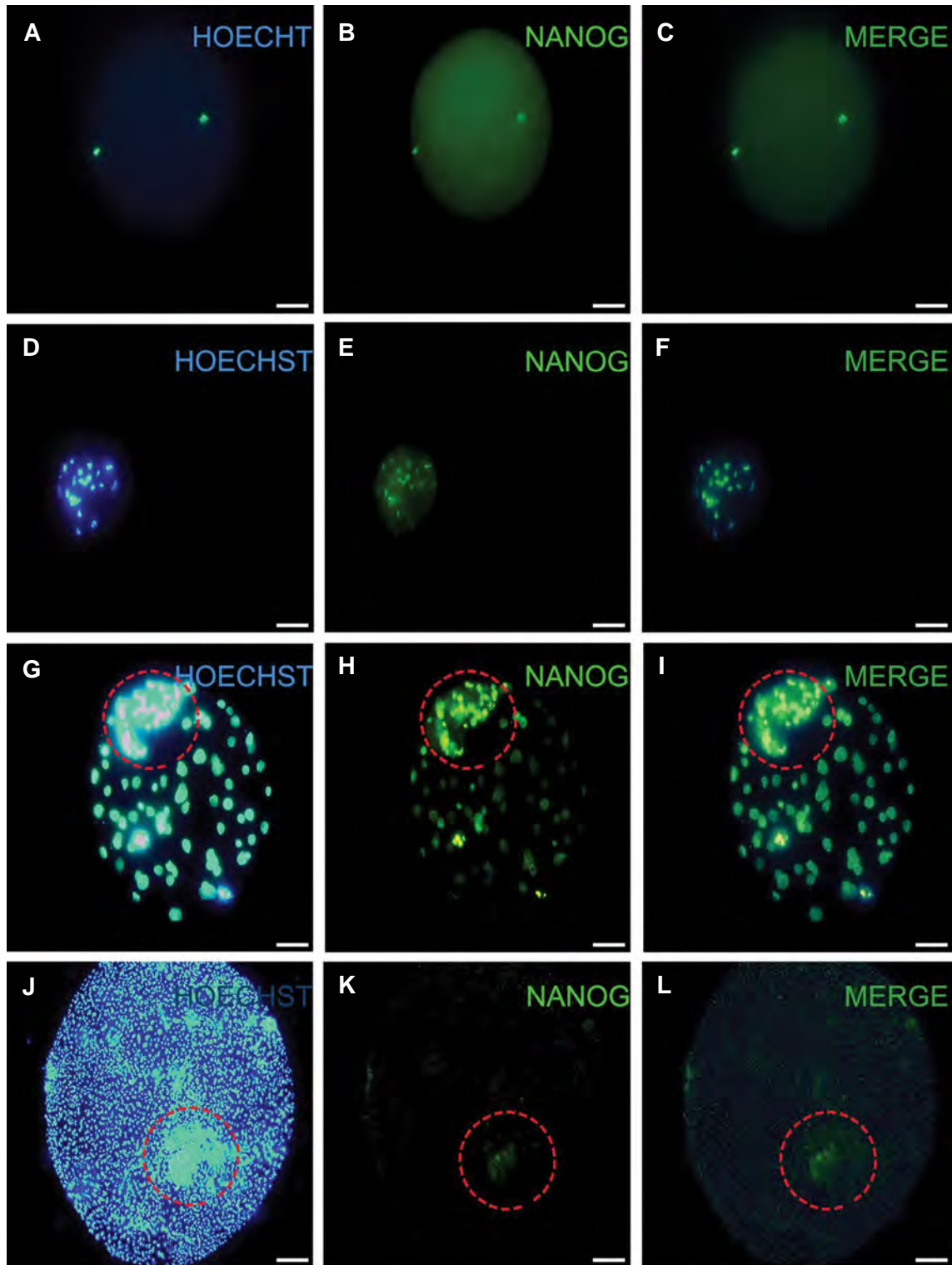


Fig.2: Nanog immunofluorescence results for *in vitro*-produced goat oocyte, 8-16 cell stage, blastocyst day at 7 stage, blastocyst day at 14 developmental stage. **A-C.** Staining of nuclear and embryo cells with HOECHT, Nanog antibody and merge respectively in oocyte stage, **D-F.** Staining of embryo cell in 8-16 cell stage in the above manner, **G-I.** Staining of embryo cells in blastocyst at day 7 stage in the above manner, and **J-L.** Staining of embryo cells in blastocyst at day 14 stage in the above manner. Dashed line denotes inner cell mass (ICM) (scale bar: 200 μ M).

Immunostaining results

Nanog, Oct4 and Sox2 protein expression and localization in goat blastocysts were observed using ICC. Since, the ICM in the goat blastocyst is not very clear or distinguishable, whole immunostaining was used to examine the expression and localization of factors associated with lineage segregation.

Nanog expression was detectable in goat oocytes, D3 embryos, D7 and D14 blastocysts. Expression of Nanog appeared to be localized in the nuclei and nucleoplasm of ICM cells and it appeared to be restricted to the nuclei of TE cells. In D7 blastocysts, the fluorescent intensity of Nanog in the ICM appeared to be higher than in the TE, but in D14 blastocysts, Nanog was expressed exclusively in the ICM (Fig.2).

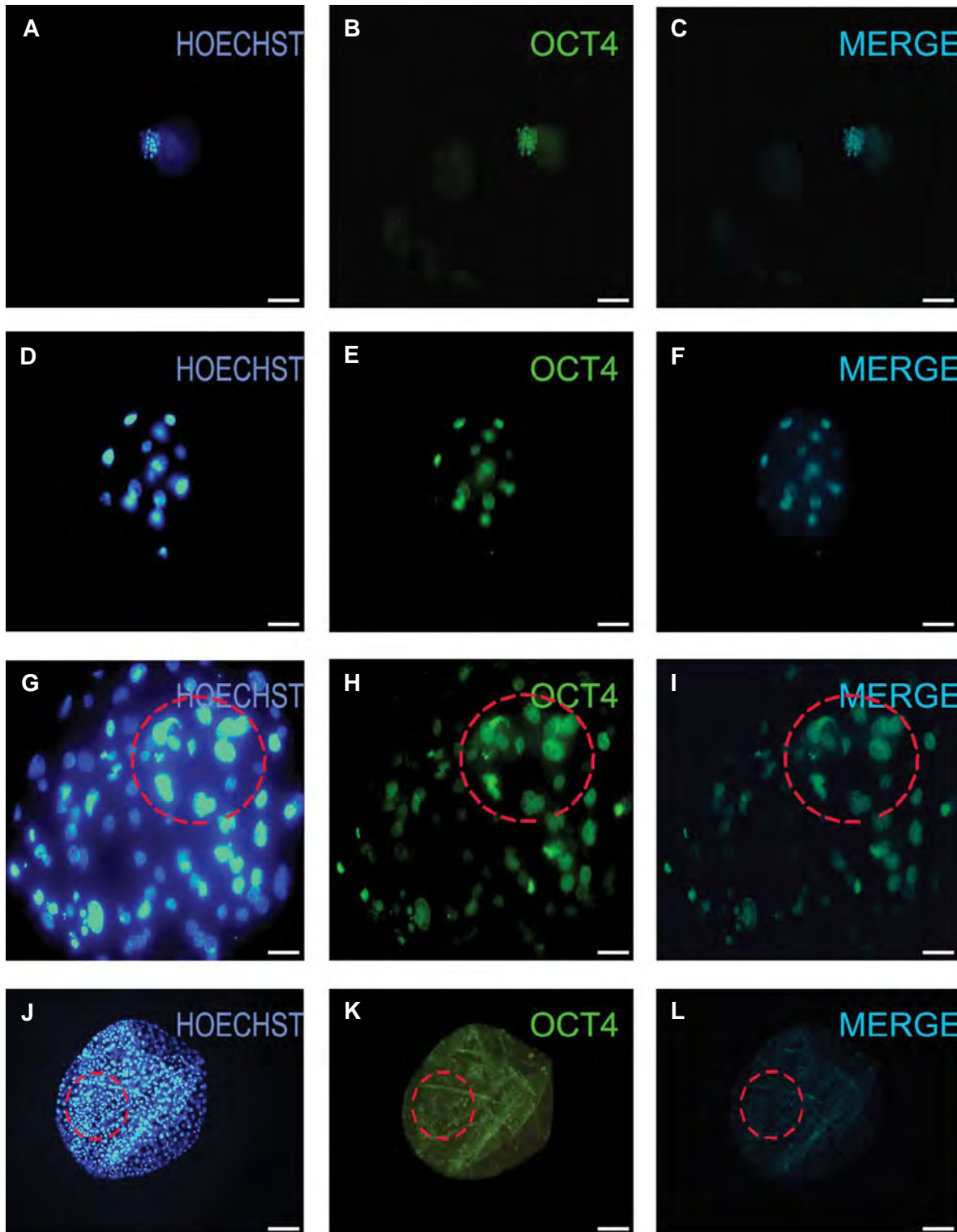


Fig.3: Oct4 immunofluorescence results for *in vitro*-produced goat oocyte, 8-16 cell stage, blastocyst day at 7 stage, blastocyst day at 14 developmental stage. **A-C.** Staining of nuclear and embryo cells by HOECHT, Oct4 antibody and merge respectively in oocyte stage, **D-F.** Staining of embryo cell in 8-16 cell stage in the above manner, **G-I.** Staining of embryo cell in blastocyst at day 7 stage in the above manner, and **J-L.** Staining of embryo cells in blastocyst at day 14 stage in the above manner. Dashed line denotes inner cell mass (ICM) (scale bar: 200 μm).

Oct4 expression was detected from the oocyte to the D14 blastocyst stage. Its expression appeared to be restricted to the nuclear area but it was difficult to discern its distribution between ICM and TE (Fig.3).

Sox2 protein expression was also limited to ICM cells especially in blastocysts on D14, however in D7 goat blastocyst also appeared to be expressing it in the TE (Fig.4, 5).

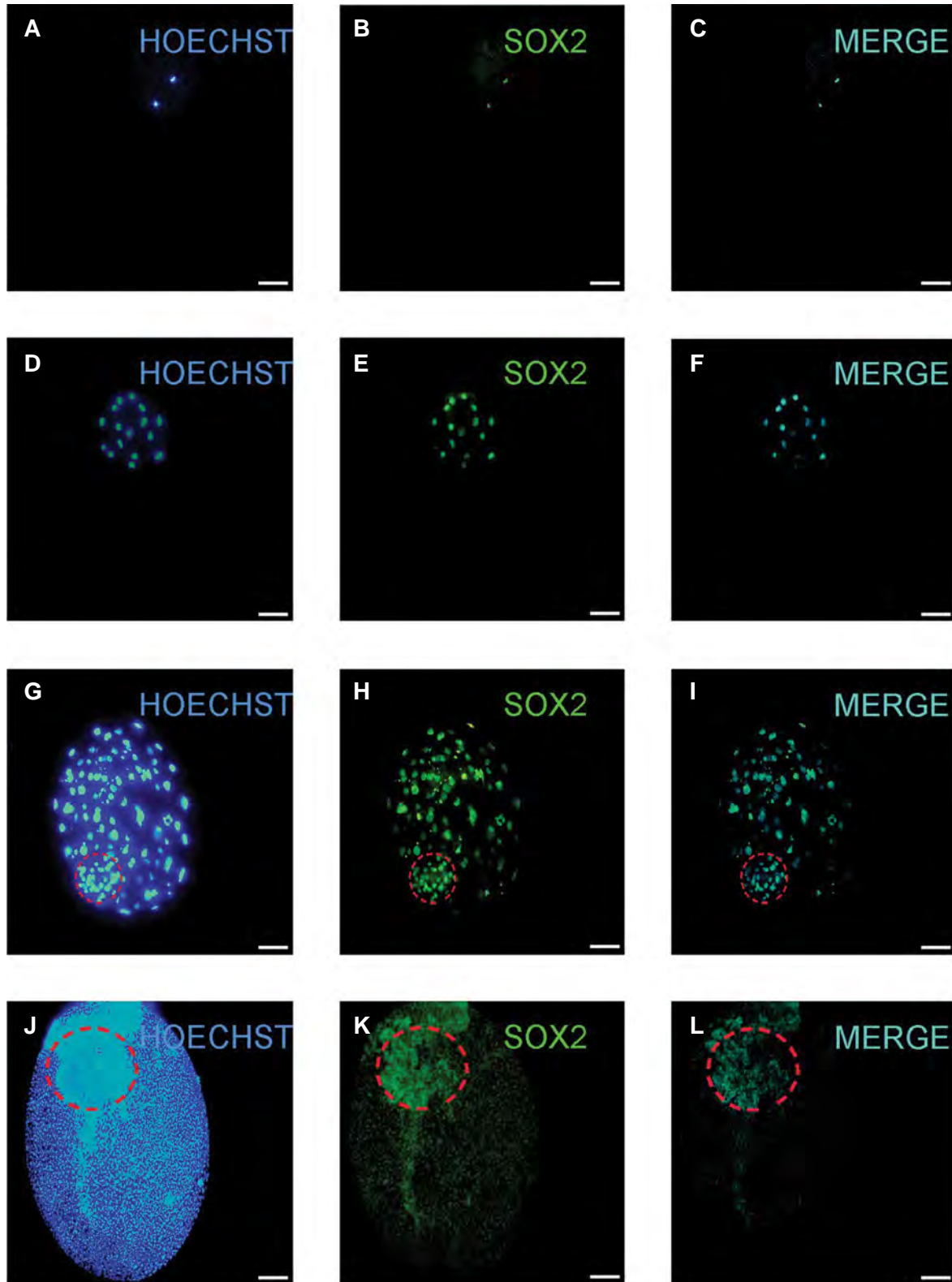


Fig.4: Sox2 immunofluorescence results for *in vitro*-produced goat oocyte, 8-16 cell stage, blastocyst day at 7 stage, blastocyst day at 14 developmental stage. **A-C.** Staining of nuclear and embryo cells by HOECHT, Sox2 antibody and merge respectively in oocyte stage, **D-F.** Staining of embryo cell in 8-16 cell stage in the above manner, **G-I.** Staining of embryo cell in blastocyst at day 7 stage in the above manner, and **J-L.** Stain of embryo cell in blastocyst at day 14 stage in the above manner. Dashed line denotes inner cell mass (ICM) (scale bar: 200 μ M).

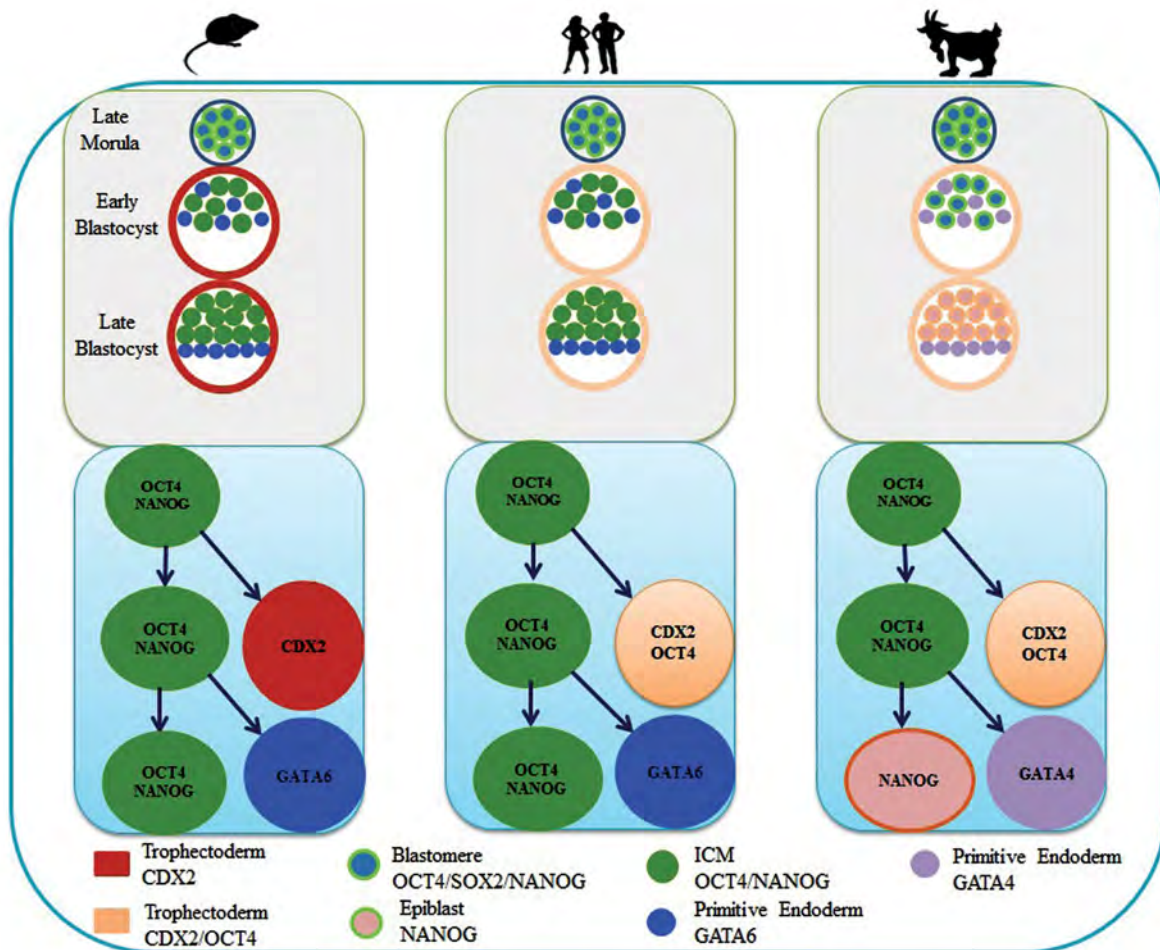


Fig.5: Early lineage segregation in mouse, human, and goat. Oct4, Nanog and Sox2 have been expressed in a different manner in goat embryos compared to mouse or human embryos, where these factors play a role in the formation of the pluripotent primitive ectoderm.

Discussion

Most of the information that we have about the development and genetics of the embryo is derived from studies carried out on mouse and human embryos. These studies mark two fundamental stages of lineage segregation. The first one is the distinction of TE from ICM, which occurs after a reciprocal constraining of *Oct4* and *Cdx2* (2, 16) and the second lineage segregation, which occurs as a result of the mosaic expression of *Nanog* and *Gata6* which occurs in the ICM and causes the separation of the primitive ectoderm and primitive endoderm (17). To assess the same concept in goats, we also assessed the expression of the core pluripotency triad (*Oct4*, *Nanog* and *Sox2*) at both RNA and protein levels and the expression of lineage markers (*Rex1*, *Gata4* and *Cdx2*) during goat pre-implantation embryo development.

Nanog mRNA was presented in goat oocytes and has two waves of expression, peaking at around the 8 cell stage (D3), and D14, while being low in D7 blastocysts. Localization assessment of *Nanog* revealed its expression is similar between different blastomeres and appears to be present mainly in the nucleus but by D7, a salt and pepper appearance is observed in the ICM as in other species

(18). This is likely due to lineage-specific markers *Gata6* and *Nanog*. Unlike in the mouse it is expressed in the nucleus of trophoblast cells and finally becomes restricted to the ICM by D14. The "salt and pepper" appearance of *Nanog* in the ICM, as in other species, may reflect its differentiation to epiblast and hypoblast or primitive endoderm. FGF4 appears to be the main mediator of this segregation in mouse embryos and lack of FGF4 results in *Nanog* enrichment but in bovine embryos as an ungulate this effect is not mediated through FGF and in the goat it remains to be defined. Expression of *Nanog* protein in the nucleus of trophoblast cells may be related to proliferation of the trophoblast known as embryo elongation which occurs before embryo implantation during D7-14 post fertilization in goats (10).

The first peak in the expression of *Nanog* may be related to embryonic genome activation, which is required for the maintenance of pluripotent cells for early gastrulation, as *Nanog* is also considered as a pluripotent lineage specific marker in bovine cells (19). The second peak may be related to the increased number of epiblast cells required by embryos to undergo the process of gastrulation. It is interesting to note that, unlike in the mouse and human, in most ungulates, *Nanog* decreases during

transition from D3 to D7 (20) but as stated, presence of the protein in the nucleus of trophoblast cells may be related to embryo elongation. Indeed, in this regard, it has been shown that *Nanog*^{-/-} cells expand more slowly than wild-type cells (21) and that *Nanog* plays a role in proliferation of cancer cells (22) and can also increase proliferation in somatic cells (23).

The reduction in expression of *Nanog* from day 3 to 7 is very likely related to the time of implantation and gastrulation between these species. Indeed, Sun et al. (24) have stated that the second peak of *Nanog* mRNA expression (D14) is associated with the increased number of epiblast cells, as it has been shown in mice, that *Nanog* through Nodal/Smad2 signaling leads to consolidation of epiblast pluripotency. *Nanog* is also a prerequisite for the formation of the primitive endoderm through an independent mechanism (25).

Unlike *Nanog*, the expression of *Oct4* in goats gradually decreases from oocyte through to day 14. In this species *Oct4* is expressed in all the nuclei of the morula-stage embryos. By blastocyst stage a differential expression of *Oct4* is observed but it is not completely extinguished as cells where very rarely found to be *Oct4* positive in day 14 blastocysts. Indeed, high *Oct4* levels in the oocyte is likely to be related to the acquisition of meiotic competence (26) as it has been stated " that a primary role of *Oct4* at the initiation of genome activation may be more related to maintenance rather than transcriptional regulation required for the initial establishment of the inner-cell mass. In mice expression of *Oct4* in the oocyte does not appear be essential until later in development, i.e. formation of the PE and when the expression of multiple EPI and PE genes such as *Gata6* and *FGF4* are required, but exploration of this issue in other species reveals a different story. In both human and bovine development, *Oct4* appears to be essential for first lineage differentiation and thereby blastocyst formation (7). The presence of *Oct4* in all the nuclei in the morula stage is consistent with the pattern of *Oct4* expression in other species. Its differential expression in day 7 blastocysts is consistent with observations in human and bovine embryos but is in contrast to the mouse where expression of *Oct4* becomes non-existent in TE cells which has been attributed to the speedy differentiation of the TE required for implantation of the embryo. In ungulates, *Cdx2* and *Oct4* are co-expressed in the TE until the time of implantation (14) and reciprocal expression of *Cdx2* and *Oct4* in goats by D14 may suggest that a similar trend is taking place except for the fact that this trend is delayed by 7 day required for the elongation of the embryo which is mainly mediated through the expansion of TE cells.

Assessment of the relative expression of *Sox2* revealed that its low expression in the oocyte and increased expression around day3 coincides with the time of maternal embryonic transition. Differential expression of *Sox2* by different cells of the embryo is apparent on day3 and gradually becomes restricted to the ICM by day14.

Indeed, in mice, it has been reported that a limited level of *Sox2* expression is required to allow development past the morula (27). Moreover, *Sox2* has been considered as the main "driver of the earliest heterogeneity within the ICM, a heterogeneity that leads to the EPI/PE cell fate decision" based on *Sox2* concentration (28). *Sox2*, despite being an *Oct4* binding partner, its expression in bovine embryos appears to be independent of *Oct4*, as the absence of *Oct4* does not prevent the expression of *Sox2* (7), despite embryos arresting at the morula stage (29). In addition, *Sox2* appears to be essential for formation of TE cells in mice (28). Detection of *Sox2* through immunostaining and gradual reduction in expression of *Sox2* mRNA by D14 may suggest that the remaining mRNA might be stable and may account for its protein expression observed in the ICM in day 14. A second possibility for the decrease in relative expression of *Sox2* mRNA by day 7 and 14, and detection of its protein by means of immunostaining may also be related to the skewed ratio of expression of *Sox2* in the ICM relative to TE cells, but this possibility needs further exploration.

Based on cell tracing studies, *Cdx2* is considered as the main regulator of the TE lineage in mice and many other species including bovine and porcine embryos (30-32). In bovine embryos, the expression of *Cdx2* is also high in TE relative to ICM (18), unlike in the mouse, which is considerably low in the ICM. In the goat, the increased expression of *Cdx2* and decreased expression of *Oct4* on day14 may suggest that, similar to the mouse, the regulation of *Cdx2* is also controlled by decreased expression of *Oct4*. But this is an associative effect, which needs further verification in this species. Increase in expression of *Gata4* on day 14, as the marker of the primitive endoderm, also supports the possibility of an inverse relation between *Oct4* with *Cdx2* and *Gata4*, but as stated, it needs further verification. It is of interest to note that, as in the mouse, decreased expression of *Oct4* in the goat is also concomitant with the formation of embryonic layers on day 14. *Rex1* plays an important role in maintaining pluripotency (33) in goats and the decreased expression of *Rex1* is likely to be due to the outstanding increase in the rate of TE proliferation compared to ICM cells, which is very likely to be related to embryo elongation in this species.

This study has a few shortcomings which need to be considered in future studies. These included: i. The antibodies used are not specific to goat, ii. The ICM and TE need to be separated to discern the differential expression of these markers, and iii. The role of each gene in development needs to be assessed in knockout and knockdown studies.

Conclusion

In this study for the first time we assessed the triad of pluripotency genes and lineage specific markers at the mRNA level and we used immunostaining to assess pluripotency markers. Overall, the pattern of expression for the triad markers and their restriction between ICM

and TE in the goat is similar to previous reports in the mouse and human. However, the pattern of expression of lineage specific markers appears to be delayed in D7 blastocysts. This difference appears to be due to delayed implantation in ungulates.

Acknowledgments

This research was financially supported by Royan Institute. Also the authors would like to express their gratitude to Royan Institute for its full support. There are no conflicts of interest in this study.

Authors' Contributions

P.H.; Conception and design, collection and/or assembly of data, data analysis and interpretation, manuscript writing. M.H.; Conception and design, data analysis and interpretation, writing of manuscript. F.J.; Data analysis and interpretation. S.M.H., M.T.; Conception and design, data analysis and interpretation. M.H.N-E; Conception and design, data analysis and interpretation, manuscript writing. All authors read and approved the final manuscript.

References

- Adjaye J, Huntriss J, Herwig R, BenKahla A, Brink TC, Wierling C, et al. Primary differentiation in the human blastocyst: comparative molecular portraits of inner cell mass and trophectoderm cells. *Stem Cells*. 2005; 23(10): 1514-1525.
- Strumpf D, Mao CA, Yamanaka Y, Ralston A, Chawengsaksophak K, Beck F, et al. Cdx2 is required for correct cell fate specification and differentiation of trophectoderm in the mouse blastocyst. *Development*. 2005; 132(9): 2093-2102.
- Tachibana M, Amato P, Sparman M, Gutierrez NM, Tippner-Hedgess R, Ma H, et al. Human embryonic stem cells derived by somatic cell nuclear transfer. *Cell*. 2013; 153(6): 1228-1238.
- Hanna J, Cheng AW, Saha K, Kim J, Lengner CJ, Soldner F, et al. Human embryonic stem cells with biological and epigenetic characteristics similar to those of mouse ESCs. *Proc Natl Acad Sci USA*. 2010; 107(20): 9222-9227.
- Kuijk EW, van Tol LT, Van de Velde H, Wubbolts R, Welling M, Geijsen N, et al. The roles of FGF and MAP kinase signaling in the segregation of the epiblast and hypoblast cell lineages in bovine and human embryos. *Development*. 2012; 139(5): 871-882.
- Berg DK, Smith CS, Pearton DJ, Wells DN, Broadhurst R, Donnison M, et al. Trophectoderm lineage determination in cattle. *Dev Cell*. 2011; 20(2): 244-255.
- Simmet K, Zakhartchenko V, Philippou-Massier J, Blum H, Klymiuk N, Wolf E. OCT4/POU5F1 is required for NANOG expression in bovine blastocysts. *Proc Natl Acad Sci USA*. 2018; 115(11): 2770-2775.
- Fogarty NME, McCarthy A, Snijders KE, Powell BE, Kubikova N, Blakeley P, et al. Genome editing reveals a role for OCT4 in human embryogenesis. *Nature*. 2017; 550(7674): 67-73.
- Rossant J, Tam PP. Blastocyst lineage formation, early embryonic asymmetries and axis patterning in the mouse. *Development*. 2009; 136(5): 701-713.
- Behboodi E, Bondareva A, Begin I, Rao K, Neveu N, Pierson JT, et al. Establishment of goat embryonic stem cells from in vivo produced blastocyst-stage embryos. *Mol Reprod Dev*. 2011; 78(3): 202-211.
- McGraw S, Vigneault C, Sirard MA. Temporal expression of factors involved in chromatin remodeling and in gene regulation during early bovine in vitro embryo development. *Reproduction*. 2007; 133(3): 597-608.
- Hajian M, Hosseini SM, Ostadhosseini S, Nasr-Esfahani MH. Targeting the transforming growth factor- β signaling during pre-implantation development in embryos of cattle, sheep and goats. *Growth Factors*. 2016; 34(3-4): 141-148.
- Hosseini SM, Hajian M, Ostadhosseini S, Forouzanfar M, Abedi P, Jafarpour F, et al. Contrasting effects of G1.2/G2.2 and SOF1/SOF2 embryo culture media on pre-and post-implantation development of non-transgenic and transgenic cloned goat embryos. *Reprod Biomed Online*. 2015; 31(3): 372-383.
- Hosseini SM, Dufort I, Caballero J, Moulavi F, Ghanaei HR, Sirard MA. Transcriptome profiling of bovine inner cell mass and trophectoderm derived from in vivo generated blastocysts. *BMC Dev Biol*. 2015; 15: 49.
- HosseinNia P, Tahmoorespur M, Hosseini SM, Hajian M, Ostadhosseini S, Nasiri MR, et al. Stage-specific profiling of transforming growth factor- β , fibroblast growth factor and wingless-int signaling pathways during early embryo development in the goat. *Cell J*. 2016; 17(4): 648-658.
- Niwa H, Toyooka Y, Shimosato D, Strumpf D, Takahashi K, Yagi R, et al. Interaction between Oct3/4 and Cdx2 determines trophectoderm differentiation. *Cell*. 2005; 123(5): 917-929.
- Chazaud C, Yamanaka Y, Pawson T, Rossant J. Early lineage segregation between epiblast and primitive endoderm in mouse blastocysts through the Grb2-MAPK pathway. *Dev Cell*. 2006; 10(5): 615-624.
- Oron E, Ivanova N. Cell fate regulation in early mammalian development. *Phys Biol*. 2012; 9(4): 045002.
- Harris D, Huang B, Oback B. Inhibition of MAP2K and GSK3 signaling promotes bovine blastocyst development and epiblast-associated expression of pluripotency factors. *Biol Reprod*. 2013; 88(3): 74.
- Khan DR, Dubé D, Gall L, Peynot N, Ruffini S, Laffont L, et al. Expression of pluripotency master regulators during two key developmental transitions: EGA and early lineage specification in the bovine embryo. *PLoS One*. 2012; 7(3): e34110.
- Chambers I, Colby D, Robertson M, Nichols J, Lee S, Tweedie S, et al. Functional expression cloning of Nanog, a pluripotency sustaining factor in embryonic stem cells. *Cell*. 2003; 113(5): 643-55.
- Arif K, Hussain I, Rea C, El-Sheemy M. The role of Nanog expression in tamoxifen-resistant breast cancer cells. *Onco Targets Ther*. 2015; 8: 1327-1334.
- Münst B, Thier MC, Winnemöller D, Helfen M, Thummer RP, Edenhofer F. Nanog induces suppression of senescence through downregulation of p27KIP1 expression. *J Cell Sci*. 2016; 129(5): 912-920.
- Sun LT, Yamaguchi S, Hirano K, Ichisaka T, Kuroda T, Tada T. Nanog co-regulated by Nodal/Smad2 and Oct4 is required for pluripotency in developing mouse epiblast. *Dev Biol*. 2014; 392(2): 182-189.
- Messerschmidt DM, Kemler R. Nanog is required for primitive endoderm formation through a non-cell autonomous mechanism. *Dev Biol*. 2010; 344(1): 129-137.
- Pesce M, Wang X, Wolgemuth DJ, Schöler HR. Differential expression of the Oct-4 transcription factor during mouse germ cell differentiation. *Mech Dev*. 1998; 71(1-2): 89-98.
- Keramari M, Razavi J, Ingman KA, Patsch C, Edenhofer F, Ward CM, et al. Sox2 is essential for formation of trophectoderm in the preimplantation embryo. *PLoS One*. 2010; 5(11): e13952.
- Mistri TK, Arindrarto W, Ng WP, Wang C, Lim LH, Sun L, et al. Dynamic changes in Sox2 spatio-temporal expression promote the second cell fate decision through Fgf4/Fgfr2 signalling in preimplantation mouse embryos. *Biochem J*. 2018; 475(6): 1075-1089.
- Goissis MD, Cibelli JB. Functional characterization of SOX2 in bovine preimplantation embryos. *Biol Reprod*. 2014; 90(2): 30.
- Dietrich J-E, Hiiragi T. Stochastic patterning in the mouse pre-implantation embryo. *Development*. 2007; 134(23): 4219-4231.
- Ralston A, Rossant J. Cdx2 acts downstream of cell polarization to cell-autonomously promote trophectoderm fate in the early mouse embryo. *Dev Biol*. 2008; 313(2): 614-629.
- Jedrusik A, Parfitt D-E, Guo G, Skamagki M, Grabarek JB, Johnson MH, et al. Role of Cdx2 and cell polarity in cell allocation and specification of trophectoderm and inner cell mass in the mouse embryo. *Genes Dev*. 2008; 22(19): 2692-2706.
- Son MY, Choi H, Han YM, Cho YS. Unveiling the critical role of REX1 in the regulation of human stem cell pluripotency. *Stem Cells*. 2013; 31(11): 2374-2387.

Synergetic Effect of Silver Nanoparticles and UVC Irradiation on H2AX Gene Expression in TK6 Cells

Tahereh Zare, M.Sc.¹, Reza Fardid, Ph.D.^{1,2*}, Samaneh Naderi, M.Sc.³

1. Department of Radiology, School of Paramedical Sciences, Shiraz University of Medical Sciences, Shiraz, Iran

2. Ionizing and Non-Ionizing Radiation Protection Research Center (INIRPRC), Shiraz University of Medical Sciences, Shiraz, Iran

3. Diagnostic Laboratory Sciences and Technology Research Center, School of Paramedical Sciences, Shiraz University of Medical Sciences, Shiraz, Iran

*Corresponding Address: P.O.Box: 7193636578, Department of Radiology, School of Paramedical Sciences, Shiraz University of Medical Sciences, Shiraz, Iran
Email: rfardid@sums.ac.ir

Received: 12/Mar/2018, Accepted: 24/Jun/2018

Abstract

Objective: The use of nanoscale particles, for instance silver nanoparticles (Ag NPs) has considerably increased recently. Since Ag NPs can be transmuted into silver ions; the toxicity and genotoxicity of these NPs along with other external factors such as ultraviolet type C (UVC) irradiation must be evaluated. In the present study, the aim was to investigate the genotoxic effects Ag NPs and UVC co-exposure on human lymphoblastoid TK6 cells.

Materials and Methods: In this experimental study, Ag NPs (~20 nm) were purchased from US Research Nanomaterials Inc. and H2AX gene expression was evaluated using quantitative real time polymerase chain reaction (qRT-PCR), 1 and 24 hours post Ag NPs and UVC treatment.

Results: Results showed that treatment of TK6 cells with different Ag NP concentrations without exposure to UVC can reduce H2AX gene expression, but treatment of these cells with Ag NPs in combination UVC irradiation can reduce viability that leads to a synergistic increase in the amount of H2AX gene expression.

Conclusion: According to our findings, Ag NPs can act to sensitize cells to UVC radiation when used for cancer treatment. So, combination of Ag NPs and UVC irradiation could be used in radiotherapy.

Keywords: Genotoxicity, H2AX, Nanoparticles, Silver, Ultraviolet

Cell Journal (Yakhteh), Vol 21, No 2, July-September (Summer) 2019, Pages: 204-209

Citation: Zare T, Fardid R, Naderi S. Synergetic effect of silver nanoparticles and UVC irradiation on H2AX gene expression in TK6 cells. Cell J. 2019; 21(2): 204-209. doi: 10.22074/cellj.2019.5898.

Introduction

In recent years nanotechnology has attracted a great deal of attention in numerous fields such as biochemistry, physics, biology, material science etc. (1). Over past decades, silver (Ag) has been the subject of extensive research for antibacterial and anti-fungal purposes (2). Ag is of particular interest in health care, the food industry, water purification, and household products (3, 4). One of the applications of Ag NPs in medicine is for cancer treatment (5, 6). Nowadays the use of Ag at the nano scale has increased due to recent development in nanotechnology. Previously, silver was considered as a non-toxic metal; however, recent studies have shown that Ag is the second most harmful metal after mercury to freshwater fish and invertebrates (7-9). Nanoparticles (NPs) are commonly considered to be more toxic than micro-sized particles due to their individual physicochemical characteristics, and the small size of the particles (10). Therefore, the toxicity of Ag nanoparticles (Ag NPs) must be determined for safe and effective usage, especially in mammalian cells because Ag NPs dissolve into Ag ions (11), and can directly bind to RNA polymerase, leading to the inhabitation of RNA polymerase activity, and over all RNA transcription. This is process is separate from the cytotoxic effects of Ag ions (12).

Sunlight ultraviolet (UV) radiation can have harmful effects on all living organisms including animals and humans (13). Generally, UV radiation is divided in to

three segments based on the wavelength: ultraviolet type A (UVA) (320-400 nm), ultraviolet type B (UVB) (280-320 nm) and ultraviolet type C (UVC) (200-280 nm). UVA and UVB penetrate the ozone layer and have significance physiological effects (14), but UVC is absorbed by the ozone layer and cannot reach the surface of the earth. One of the main applications of UVC is in disinfection technologies for water and liquid food products due to its advantages over alternatives (15). UVC has an antimicrobial effect on different types of microorganisms due to photochemical changes induced in the pyrimidines of DNA and RNA (16). DNA breaks produced by UV radiation, prevent DNA replication and transcription leading to impaired cellular function, and eventually cell death (17). It can therefore also be used in treating cancer. The lethal effects of UV radiation depend on the radiation dosage, and the capability of the cell to repair the damage (16).

Many studies have been conducted to investigate the genotoxic effects of Ag NPs by evaluating γ -H2AX as a marker for detecting DNA double strand breaks (DSB) in mammalian cells (10, 18, 19). However, the genotoxic effects of Ag NPs in combination with UV radiation in humans have not been determined yet.

As mentioned above UVC irradiation and Ag NPs can

be used in cancer therapy. In this study we evaluate the effect of Ag NPs as a sensitizer to UVC irradiation in order to kill cancer cells. The present study aimed to investigate the genotoxic effects of Ag NPs in combination with UVC irradiation via evaluating *H2AX* gene expression. To do this, human lymphoblastoid TK6 cells were pretreated with Ag NPs (~20 nm) followed by exposure to UVC irradiation. Next, we measured the *H2AX* gene expression in TK6 cells via quantitative real time polymerase chain reaction (qRT-PCR) to determine the synergistic effects of treatment with Ag NPs plus UVC radiation at 1 and 24 hours post UVC irradiation.

Materials and Methods

Cell culture

In this experimental study, the human lymphoblastoid TK6 cell line was purchased from American Type Culture Collection (ATCC® CRL-8015™) and were maintained in RPMI-1640 medium (Gibco, USA) supplemented with 10% heat incubated fetal bovine serum (FBS, Gibco, USA) and 100 U/ml of penicillin-streptomycin (Gibco, USA), and incubated at 37°C in a humidified atmosphere containing 5% CO₂. Cells in the exponential growth phase were used in this study. To maintain a culture density of less than 1.2×10⁶ cell/ml, TK6 cells were sub cultured every 2-3 days.

Ag NPs preparation

Ag NPs (~20 nm: according to Transmission Electron Microscopy (TEM) and XRD pattern by US Research Nanomaterials) were purchased from the US Research Nanomaterials Inc. (Stock#: US1038). To do this study, Ag NPs were suspended in deionized water, and various concentrations were prepared (0, 5, 10 and 15 µg/ml in each well). Ag NPs were immediately sonicating (Hielscher ultrasound technology, UP100H, Germany) before being applied to cells.

Treatment with Ag NPs and UVC irradiation

Cells were treated with different concentrations of Ag NPs for 1hr, and then exposed 20 minutes to a germicidal UVC lamp (λ~254 nm) at 1 mW/cm², which was determined with a radiometer (UV-254, Lutron, Taiwan). The cells were returned to an incubator for 1 and 24 hours at 37°C in an atmosphere of 5% CO₂ in a humidified environment. Non-irradiated cells were handled similar to the UVC irradiated samples, only without being exposed to UVC lamp.

Cell viability and MTT assay

The cells were removed from the incubator twice (1 and 24 hours) post UVC irradiation. Next, the cells were mixed with try-pan blue solution [0.3 % (v/v); 1:1], and cell viability (%) was calculated for all conditions using the following equation:

$$\text{Cell viability (\%)} = (\text{viable cells}) / (\text{total cells}) \times 100$$

The cytotoxicity of Ag NPs in different concentration, and UVC irradiation were investigated by a MTT cell proliferation assay. MTT is reduced to purple formazan crystals in functional mitochondria. The total formazan produced is proportional to the number of viable cells. To perform the MTT assay, TK6 cells at a density of 2.5×10⁴ cells per well were cultured in 96-well culture plates. Then the plate was incubated at 37°C in 5% CO₂ for 24 hours. The TK6 cells were then treated with different Ag NPs concentration (0, 5, 10 and 15 µg/ml in each well), and irradiated with a germicidal UVC lamp (λ254~ nm). The plate was then returned to the incubator for 1 hour (37°C, 5% CO₂) after which the MTT solution (5 mg/ml, Sigma Aldrich, M2128, USA) was added (20 µg in each well) and cells were incubated for 4hrs at 37°C in 5% CO₂. Following this, the plate was centrifuged (2500 rpm for 40 minutes) and the cell culture medium was discarded. Then dimethyl sulfoxide (DMSO) was added to dissolve the formazan crystals, and the plate was put on a shaker for 30 minutes in a dark room. The absorbance of each well was measured at 545 nm using an ELISA reader (Fax Reader, England). Each experiment was repeated at least three times independently and 0 µg/ml of Ag NPs and UVC was considered as the control group.

RNA isolation and quantitative real time polymerase chain reaction

At the 1 hour and 24 hours after UVC irradiation time points, total RNA from each sample was extracted using a RNX-Plus solution (CinaClon Co., Iran) according to the instruction provided by the manufacturer. A Nano drop spectrometer (Helma, USA) was used to determine the quality and concentration of the RNA samples. Approximately 1 µg of total RNA was used for complementary DNA (cDNA) synthesis using RevertAid First Strand cDNA synthesis kit (Thermo Scientific, Lithuania), with a gradient thermal cycler (ASTEC, Japan). cDNA samples were stored at -20°C. The generated cDNA samples were mixed with a master mix (SYBR Green Method with low ROX, Amplicon,) to prepare the qRT-PCR reaction. The qRT-PCR Mixture consisted of 10 µl SYBR green PCR master mix, 0.5 µl forward primer, 0.5 µl reverse primer (10 µM), and 8 µl nuclease free water. Then 1 µl of the cDNA samples were added to qRT-PCR master mix. The specific primers and reaction conditions used in this study are shown in Table 1. The 48-well plates containing all reagents were briefly centrifuged and analyzed on an ABI Step One Real-Time PCR System (Applied Biosystems, ABI, USA). *β-actin* was considered as the housekeeping gene for analyses of this study.

Statistical analysis

All experiments were repeated in triplicates. Data are expressed as the mean ± SD. Statistical comparison was done using one-way ANOVA and P<0.05 was considered to be statistically significant. In the cases where the means were compared from the two independent groups, independent t test was used and in the groups that were dependent, paired t test was used.

Table 1: Quantitative real-time polymerase chain reaction primers, and reaction conditions for quantitative real time polymerase chain reaction (qRT-PCR)

Gene	Primer sequence (5'-3')
<i>H2AFX</i>	F: CAACAAGAAGACGCGAATCA
	R: CGGGCCCTCTTAGTACTCT
β -actin	F: ATC GTG CGT GAC ATT AAG GAG
	R: GAA GGA AGG CTG GAA GAG TG

Three-step qRT-PCR program		
Cycles	Cycles duration	Temperature (°C)
1	2 minutes	95
40	30 seconds	95
	40 seconds	60
	30 seconds	72
1	5 minutes	72

Results

Cytotoxicity in combined treatment of TK6 cells with Ag NPs and UVC irradiation

In this study the cytotoxic effect of simultaneous exposure of TK6 cells to Ag and UVC irradiation was examined using try-pan blue dye. In two separate time points following UV irradiation (1 hour and 24 hours) cell viability was reduced at all Ag NP concentrations, which revealed a significant increase in cytotoxicity of Ag NPs with UVC irradiation (Fig.1).

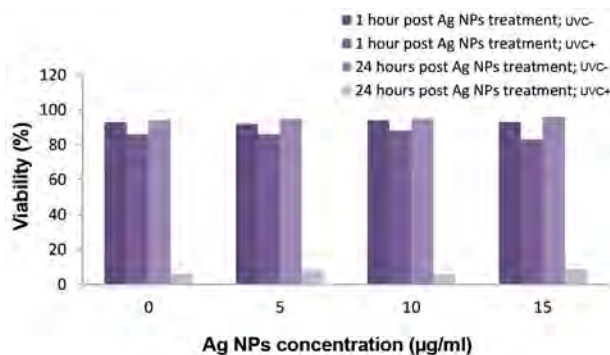


Fig.1: TK6 cell viability after combined treatment with Ag NPs and ultraviolet type C (UVC) irradiation using the try-pan blue assay; cells were harvested 1 hour and 24 hours post UVC exposure (1 mW/cm²).

A MTT colorimetric assay for TK6 cells in the presence of Ag NPs and UVC irradiation was performed. MTT results showed a dose dependent cytotoxicity of Ag NPs with UVC irradiation. On the other hand, various Ag NPs concentrations also showed a significant decrease in cell viability. Also results show, cell viability was reduced by increasing the concentration of the NPs alongside UVC irradiation (Fig.2). These differences were significant in comparison with when each factor was applied separately. Therefore, the MTT test shows increased cytotoxic effects

of simultaneous exposure to Ag NPs and UVC irradiation.

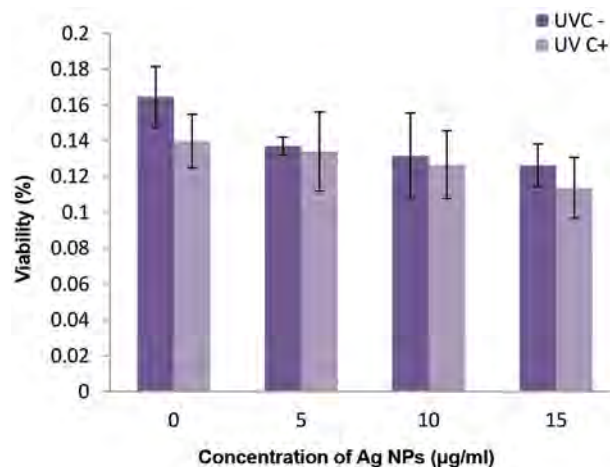
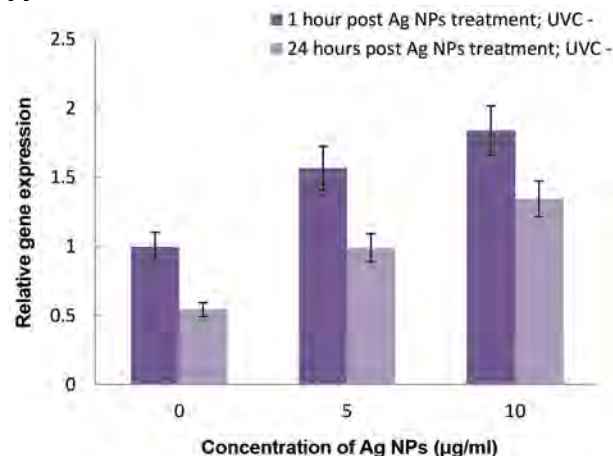


Fig.2: Cytotoxicity of co-exposure to different concentration of Ag NPs and ultraviolet type C (UVC) irradiation (1 mW/cm²) by means of MTT assay. 0 µg/ml of Ag NPs and UVC were considered as the control groups. Data are presented as the mean ± SD.

Genotoxic effects of Ag NPs and UVC irradiation co-treatment on TK6 cells

In this study, we investigated the genotoxic effects of Ag NPs on TK6 cells post UVC irradiation with qRT-PCR. In the present study, showed that treatment of TK6 cells with Ag NPs can significantly increase *H2AX* gene expression in the absence of UVC irradiation after 1 hour and 24 hours post UVC irradiation (Fig.3A). This trend was observed in all Ag NPs concentrations. Also the results show that UVC irradiation alone can increase *H2AX* gene expression in TK6 cells (Fig.3B). We observed that *H2AX* expression was increased 1 hour and 24 hours after UVC irradiation (P<0.01). The gene expression in TK6 cells after co-treatment with Ag NPs and UVC irradiation was compared with their control groups. *H2AX* gene expression after being treated with 10 and 5 µg/ml of Ag NPs post UV exposure was significantly increased, both 1 hour and 24 hours after UVC treatment (Fig.4A, B, P<0.05).

A



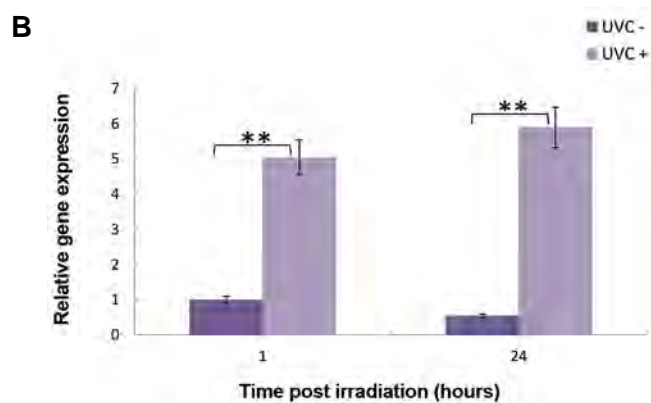


Fig.3: The effect of Ag NPs and ultraviolet type C (UVC) irradiation on *H2AX* gene expression on TK6 cells. *H2AX* gene expression 1 hour and 24 hours after treatment with **A.** Ag NPs in different concentration (5, 10 and 15 $\mu\text{g}/\text{ml}$) and **B.** *H2AX* gene expression post UVC irradiation (1 mW/cm^2) (**; $P < 0.001$). Data are presented as the mean \pm SD. $P < 0.05$ were considered as significant.

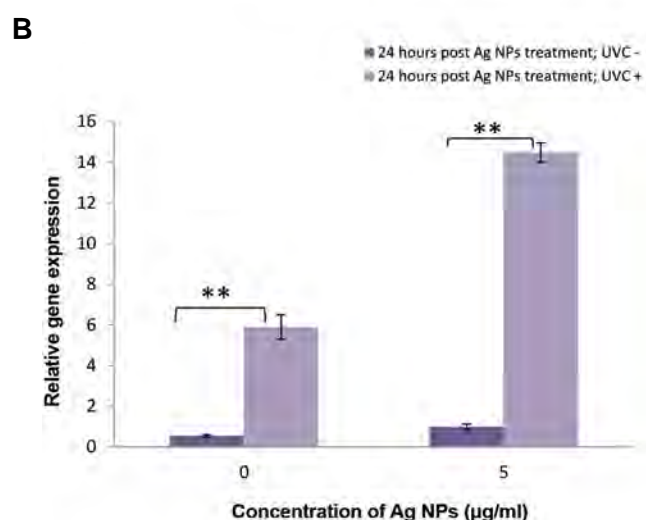
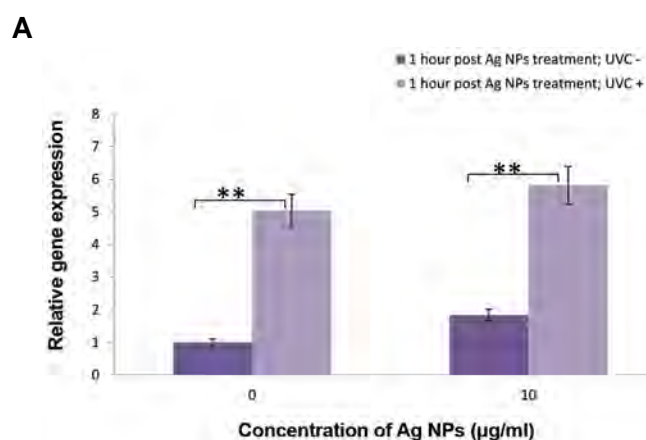


Fig.4: *H2AX* gene expression of Ag NPs and ultraviolet type C (UVC) co-treated cells. TK6 cells were harvested **A.** 1 hour with 10 $\mu\text{g}/\text{ml}$ Ag NPs, and **B.** 24 hours with 5 $\mu\text{g}/\text{ml}$ Ag NPs post exposure to UVC (1 mW/cm^2) (**; $P < 0.001$). Data are presented as the mean \pm SD. $P < 0.05$ were considered as significant.

Discussion

In recent years, increasing usage of Ag NPs has

led to the need for evaluating their cytotoxicity and genotoxicity. Recently, the cytotoxic effects of Ag NPs in various types of cells such as Hella cells (20), human glioblastoma cells (U251) (21), BRL 3A rat liver cells (22) have been evaluated. The sun's UV radiation can have many biological effects, including changes in the structure of DNA, proteins and other biological molecules (23, 24). For instance, Glover et al. (25) showed that after irradiation TK6 cells with UVC, the sensitivity to DNA damage was increased. It also increased the amount of apoptosis, delayed DNA repair and caused changes in the expression of P53-target genes.

Xu et al. (20) showed that the viability of Hella cells treated with Ag NPs (0-30 $\mu\text{g}/\text{ml}$ Ag NPs) were decreased after 24 and 48 hours. Similarly, an increase in cytotoxicity was observed in cells treated with Ag NPs by Hussain et al. in BRL 3A rat liver cells (22). In the present study, cytotoxicity of Ag NPs combined treatment with UVC irradiation in TK6 cells revealed that combined treatment can reduce TK6 viability at two separate time points (1 hour and 24 hours) post UVC irradiation. Furthermore, MTT colorimetric assay showed a time dependent reduction of cell viability of TK6 cells. A decrease in survival rate was observed at all NP concentrations, which was in line with previous studies (10, 20, 22, 26).

There are several studies that have evaluated the effects of UVA and UVB. For example, the genotoxicity of Ag ions and UVB combined treatment was investigated by Zhao et al. (2). They showed that UVB and Ag ions simultaneous exposure in a human keratinocyte cell line, HaCaT, can induce DNA breaks by measuring an increase in *H2AX*. Induction of marked toxic effects against bacteria through combined treatment using Ag NPs and UVA was also investigated by Zhao et al. (27). γ -*H2AX* expression was measured 1 hour and 24 hours post ionizing radiation by Li et al. (28) and they observed that expression of *H2AX* significantly increased 1 hour post irradiation. Also Zhang et al. (29) showed that after whole body irradiation of mice, *H2AX* mRNA expression increased significantly in comparison with control groups. Recently γ -*H2AX* foci, gene expression, miRNA and protein profile were used as biomarkers for radiation (30-34). *H2AX* gene expression is proportional to the early cellular response to DSBs (18), which can be induced by UV irradiation (35). Therefore, due to the release of silver ions from Ag NPs that leads to *H2AX* gene expression; the present study aimed to investigate the potential genotoxicity of Ag NPs along with UV exposure by measuring *H2AX* gene expression using qRT-PCR.

Without applying UVC radiation *H2AX* gene expression increased with the increase in nanoparticle concentration. Results show that UVC alone can induce a significant enhancement in *H2AX* gene expression. When the cells were co-exposed to Ag NPs and UVC, a significant increase in relative gene expression in comparison with its control group was observed 1 hour after irradiation with 10 $\mu\text{g}/\text{ml}$ Ag NPs. As post treatment time increased from 1 hour to 24 hours, we found that there was a significant

increase in *H2AX* gene expression (in 5 µg/ml Ag NPs) in comparison to its control group. In a study by Glover et al. (25) the effects of DNA damage response in TK6 cells treated with 12-O-Tetradecanoylphorbol-13-acetate (TPA)+UVC was evaluated using γ -*H2AX* formation in various times, after UVC irradiation (0-24 hours). Results showed that cell treatment with TPA and UVC caused a significant increase in γ -*H2AX*, 2 hours after UVC exposure. In our study, we observed *H2AX* synergistic gene expression in 24 hours post UVC treatment in cells treated with 5 µg/ml Ag NPs.

Uddin et al. (36) evaluated the effect of low concentrations of arsenite and showed that it can increase the risk of skin cancer after UV irradiation. Hence, to investigate the effects of Ag NPs in low concentrations we chose 5 and 10 µg/ml of NPs, and it was observed that in these two concentrations, at 1 hour and 24 hours after UVC irradiation *H2AX* gene expression was increased. Based on these results, co-treatment of TK6 cells with Ag NPs and UVC irradiation can have a synergic effect and significantly increase *H2AX* gene expression. Therefore, the use of Ag NPs and UVC irradiation can be effective in death of cancer cells. This means that Ag NPs can be used as a sensitizing agent for UVC irradiation to combat cancer cells.

Conclusion

Try-pan blue and MTT tests revealed that simultaneous use of silver nanoparticles and UVC irradiation can lead to increased cytotoxicity. We have found that exposing human lymphoblastoid TK6 cells to UVC after treatment with increasing concentrations of Ag NPs can induce dose dependent cellular toxicity. In addition, evaluating the *in vitro* genotoxicity of Ag NPs at different concentrations alongside UVC exposure revealed that UVC irradiation can enhance the genotoxic effects Ag NPs as revealed by increased *H2AX* gene expression. The results of this study show a significant synergistic increase in *H2AX* gene expression could occur in TK6 cells co-exposed to Ag NPs and UVC irradiation. Consequently, combination of Ag NPs and UVC irradiation could be used in cancer therapy.

Acknowledgements

This work was extracted from the proposal financially supported by the Research Council of Shiraz University of Medical Sciences (12598). The authors wish to thank Mr. H. Argasi at the Research Consolation Center (RCC) at Shiraz University of Medical Sciences for his invaluable assistance in editing this manuscript. The authors declare no conflicts of interest.

Authors' Contributions

T.Z., S.N.; Contributed to all experimental work and molecular experiments. T.Z., R.F.; Contributed to conception, design data, statistical analysis, and interpretation of data. Drafted the manuscript, which was

revised by R.F., T.Z. R.F.; Was responsible for overall supervision. All authors performed editing, read and approved the final manuscript.

References

1. Hoet PH, Nemmar A, Nemery B. Health impact of nanomaterials? *Nat Biotechnol.* 2004; 22(1): 19.
2. Zhao X, Toyooka T, Ibuki Y. Silver ions enhance UVB-induced phosphorylation of histone H2AX. *Environ Mol Mutagen.* 2014; 55(7): 556-565.
3. Nowack B, Krug HF, Height M. 120 years of nanosilver history: implications for policy makers. *Environ Sci Technol.* 2011; 45(4): 1177-1183.
4. Chernousova S, Epple M. Silver as antibacterial agent: ion, nanoparticle, and metal. *Angew Chem Int Ed Engl.* 2013; 52(6): 1636-1653.
5. Sibbald RG, Contreras-Ruiz J, Coutts P, Fierheller M, Rothman A, Woo K. Bacteriology, inflammation, and healing: a study of nanocrystalline silver dressings in chronic venous leg ulcers. *Adv Skin Wound Care.* 2007; 20(10): 549-558.
6. Loo C, Lowery A, Halas N, West J, Drezek R. Immunotargeted nanoshells for integrated cancer imaging and therapy. *Nano Lett.* 2005; 5(4): 709-711.
7. De Boeck G, Grosell M, Wood C. Sensitivity of the spiny dogfish (*Squalus acanthias*) to waterborne silver exposure. *Aquat Toxicol.* 2001; 54(3-4): 261-275.
8. Bianchini A, Bowles KC, Brauner CJ, Gorsuch JW, Kramer JR, Wood CM. Evaluation of the effect of reactive sulfide on the acute toxicity of silver (I) to *Daphnia magna*. part 2: toxicity results. *Environ Toxicol Chem.* 2002; 21(6): 1294-1300.
9. Webb NA, Shaw JR, Morgan J, Hogstrand C, Wood CM. Acute and chronic physiological effects of silver exposure in three marine teleosts. *Aquat Toxicol.* 2001; 54(3): 161-178.
10. Zhao X, Takabayashi F, Ibuki Y. Coexposure to silver nanoparticles and ultraviolet A synergistically enhances the phosphorylation of histone H2AX. *J Photochem Photobiol B.* 2016; 162: 213-222.
11. Loza K, Diendorf J, Sengstock C, Ruiz-Gonzalez L, Gonzalez-Calbet JM, Vallet-Regi M, et al. The dissolution and biological effects of silver nanoparticles in biological media. *J Mater Chem B.* 2014; 2(12): 1634-1643.
12. Wang Z, Liu S, Ma J, Qu G, Wang X, Yu S, et al. Silver nanoparticles induced RNA polymerase-silver binding and RNA transcription inhibition in erythroid progenitor cells. *ACS Nano.* 2013; 7(5): 4171-4186.
13. Sinha RP, Häder DP. UV-induced DNA damage and repair: a review. *Photochem Photobiol Sci.* 2002; 1(4): 225-236.
14. Svobodova A, Walterova D, Vostalova J. Ultraviolet light induced alteration to the skin. *Biomed Pap Med Fac Univ Palacky Olomouc Czech Repub.* 2006; 150(1): 25-38.
15. Hijnen WA, Beerendonk EF, Medema GJ. Inactivation credit of UV radiation for viruses, bacteria and protozoan (oo) cysts in water: a review. *Water Res.* 2006; 40(1): 3-22.
16. Gayán E, Mañas P, Álvarez I, Condón S. Mechanism of the synergistic inactivation of *Escherichia coli* by UV-C light at mild temperatures. *App Environ Microbiol.* 2013; 79(14): 4465-4473.
17. Ramasamy K, Shanmugam M, Balupillai A, Govindhasamy K, Gunaseelan S, Muthusamy G, et al. Ultraviolet radiation-induced carcinogenesis: Mechanisms and experimental models. *J Radiat Cancer Res.* 2017; 8(1): 4-19.
18. Rogakou EP, Pilch DR, Orr AH, Ivanova VS, Bonner WM. DNA double-stranded breaks induce histone H2AX phosphorylation on serine 139. *J Biol Chem.* 1998; 273(10): 5858-5868.
19. Zare T, Fardid R, Naderi S. Synergistic genotoxic effects of co-exposure to Ag NPs and UVC on TK6 cells Using H2AX gene expression evaluation. Poster session presented at: second Nanomedicine and Nanosafety Conference (NMNS); 2017 Nov 29-30; Tehran University of Medical Sciences (TUMS); Tehran, Islamic Republic of Iran.
20. Xu L, Takemura T, Xu M, Hanagata N. Toxicity of silver nanoparticles as assessed by global gene expression analysis. *Mater Express.* 2011; 1(1): 74-79.
21. AshaRani P, Low Kah Mun G, Hande MP, Valiyaveetil S. Cytotoxicity and genotoxicity of silver nanoparticles in human cells. *ACS nano.* 2008; 3(2): 279-290.
22. Hussain SM, Hess KL, Gearhart JM, Geiss KT, Schlager JJ. In vitro toxicity of nanoparticles in BRL 3A rat liver cells. *Toxicol In Vitro.*

- 2005; 19(7): 975-983.
23. Sinha R, Rastogi RP, Ambasht NK, Häder D. Life of wetland cyanobacteria under enhancing solar UV-B radiation. *Proc Natl Acad Sci India B*. 2008; 78: 53-65.
 24. Zeeshan M, Prasad SM. Differential response of growth, photosynthesis, antioxidant enzymes and lipid peroxidation to UV-B radiation in three cyanobacteria. *S Afr J Bot*. 2009; 75(3): 466-474.
 25. Glover KP, Markell LK, Donner EM, Han X. Protein kinase C-activating tumor promoters modulate the DNA damage response in UVC-irradiated TK6 cells. *Toxicol Lett*. 2014; 229(1): 210-219.
 26. Eftekhari Z, Fardid R, Zare T. the bystander effects (BSE) of ultraviolet radiation (UVR) and silver nanoparticles (Ag NPs) on TK6 cells. Poster session presented at: second Nanomedicine and Nanosafety Conference (NMNS); 2017 Nov 29-30; Tehran University of Medical Sciences (TUMS); Tehran, Islamic Republic of Iran.
 27. Zhao X, Toyooka T, Ibuki Y. Synergistic bactericidal effect by combined exposure to Ag nanoparticles and UVA. *Sci Total Environ*. 2013; 458-460: 54-62.
 28. Li Y, Liu F, Wang Y, Li D, Guo F, Xu L, et al. Rapamycin-induced autophagy sensitizes A549 cells to radiation associated with DNA damage repair inhibition. *Thorac Cancer*. 2016; 7(4): 379-386.
 29. Zhang J, He Y, Shen X, Jiang D, Wang Q, Liu Q, et al. γ -H2AX responds to DNA damage induced by long-term exposure to combined low-dose-rate neutron and γ -ray radiation. *Mutat Res Genet Toxicol Environ Mutagen*. 2016; 795: 36-40.
 30. Jain V, Kumar PR, Koya PK, Jaikrishan G, Das B. Lack of increased DNA double-strand breaks in peripheral blood mononuclear cells of individuals from high level natural radiation areas of Kerala coast in India. *Mutat Res*. 2016; 788: 50-57.
 31. Chaudhry MA, Omaruddin RA, Kreger B, de Toledo SM, Azzam EI. Micro RNA responses to chronic or acute exposures to low dose ionizing radiation. *Mol Biol Rep*. 2012; 39(7): 7549-7558.
 32. Nylund R, Kuster N, Leszczynski D. Analysis of proteome response to the mobile phone radiation in two types of human primary endothelial cells. *Proteome Sci*. 2010; 8: 52.
 33. Sokolov M, Neumann R. Global gene expression alterations as a crucial constituent of human cell response to low doses of ionizing radiation exposure. *Int J Mol Sci*. 2015; 17(1): pii: E55.
 34. Rothkamm K, Löbrich M. Evidence for a lack of DNA double-strand break repair in human cells exposed to very low x-ray doses. *Proc Natl Acad Sci USA*. 2003; 100(9): 5057-5062.
 35. Bonner WM, Redon CE, Dickey JS, Nakamura AJ, Sedelnikova OA, Solier S, et al. GammaH2AX and cancer. *Nat Rev Cancer*. 2008; 8(12): 957-967.
 36. Uddin AN, Burns FJ, Rossman TG, Chen H, Kluz T, Costa M. Dietary chromium and nickel enhance UV-carcinogenesis in skin of hairless mice. *Toxicol Appl Pharmacol*. 2007; 221(3): 329-338.
-

Panax ginseng Extract Improves Follicular Development after Mouse Preantral Follicle 3D Culture

Abbas Majdi Seghinsara, Ph.D.¹, Hamed Shoorei, Ph.D.^{1,2*}, Mohammad Mehdi Hassanzadeh Taheri, Ph.D.², Arash Khaki, D.V.M, Ph.D.³, Majid Shokoohi, M.Sc.¹, Moloud Tahmasebi, M.Sc.⁴, Amir Afshin Khaki, Ph.D.¹, Hossein Eyni, M.Sc.⁴, Sadegh Ghorbani, M.Sc.⁴, Khadijeh Riahi Rad, Ph.D.⁵, Hossein Kalarestaghi, Ph.D.⁶, Leila Roshangar, Ph.D.⁷

1. Department of Anatomical Sciences, Faculty of Medicine, Tabriz University of Medical Sciences, Tabriz, Iran
2. Department of Anatomical Sciences, Faculty of Medicine, Birjand University of Medical Sciences, Birjand, Iran
3. Department of Pathology, Islamic Azad University, Tabriz Branch, Tabriz, Iran

4. Department of Anatomical Sciences, Faculty of Medicine, Tarbiat Modares University, Tehran, Iran
5. Department of Horticulture Science, Tarbiat Modares University, Tehran, Iran

6. Research laboratory for Embryology and Stem Cells, Department of Anatomical Sciences and Pathology, School of Medicine, Ardabil University of Medical Sciences, Ardabil, Iran
7. Stem Cell Research Center, Tabriz University of Medical Sciences, Tabriz, Iran

*Corresponding Address: P.O.Box: 5166614766, Department of Anatomical Sciences, Faculty of Medicine, Tabriz University of Medical Sciences, Tabriz, Iran
Email: h.shoorei@gmail.com

Received: 28/January/2018, Accepted: 26/June/2018

Abstract

Objective: *Panax ginseng* is a popular traditional herb that has been used in complementary and alternative medicine in eastern Asia, and it possesses pharmacologically active compounds like ginsenosides (GSs). This study aimed to investigate the impact of *Panax ginseng* extract (PGE) at different concentrations on *in vitro* follicular function and development in a three-dimensional (3D) culture system fabricated using sodium alginate after 12 days of culture.

Materials and Methods: In this experimental study, preantral follicles (n=661) were mechanically isolated from the ovaries of 14-day-old female NMRI mice using 29-gauge insulin syringes. Follicles were individually capsulated within sodium alginate, and divided into four groups including control and experimental groups 1, 2, and 3. Then, they were cultured for 12 days in the medium supplemented with different concentrations of PGE (0, 50, 100, and 500 µg/mL, for control groups and groups 1, 2 and 3, respectively). At the end of the culture period, the mean diameter and maturation of follicles, follicular steroid production, mRNA expression level of proliferating cell nuclear antigen (PCNA) and follicle stimulating hormone receptor (FSH-R), and reactive oxygen species (ROS) levels in collected metaphase-II (MII) oocytes were determined.

Results: The mean diameter of follicles in group 2 was significantly increased as compared to other groups (P<0.001). The percentages of the survival and maturation rate and levels of secreted hormones were higher in group 2 than the other groups (P<0.05). Follicles cultured in the presence of PGE 100 µg/mL had higher levels of proliferation cell nuclear antigen (PCNA) and follicle stimulating hormone receptor (FSH-R) mRNA expression in comparison to other groups (P<0.05). Moreover, oocytes collected from groups 2 and 3 had lower levels of ROS as compared to other groups (P<0.05).

Conclusion: Our results suggest that PGE at the concentration of 100 µg/mL induces higher follicular function and development in the 3D culture system.

Keywords: Gene Expression, Ovarian Follicle, *Panax ginseng*, Steroid Hormone

Cell Journal (Yakhteh), Vol 21, No 2, July-September (Summer) 2019, Pages: 210-219

Citation: Majdi Seghinsara A, Shoorei H, Hassanzadeh Taheri MM, Khaki A, Shokoohi M, Tahmasebi M, Khaki AA, Eyni H, Ghorbani S, Riahi Rad Kh, Kalarestaghi H, Roshangar L. *Panax ginseng* extract improves follicular development after mouse preantral follicle 3D culture. Cell J. 2019; 21(2): 210-219. doi: 10.22074/cellj.2019.5733.

Introduction

Folliculogenesis is a complex and dynamic process which has a key role in maintaining the continuity of mankind's life (1-3). Folliculogenesis is regulated by several autocrine and paracrine factors (4).

In vitro culture and maturation (IVC-IVM) of primordial and preantral follicles as well as IVM of cumulus-oocyte complexes (COCs) have been developed for investigating follicular growth and oocyte maturation mechanisms, and used as a source for *in vitro* fertilization (IVF) of the matured oocytes in assisted reproductive technology (ART) (5). Therefore, to investigate mechanisms

underlying the folliculogenesis and explore the effects of factors such as antioxidant, hormones, and growth factors on the growth and maturation of follicles and oocytes, a myriad types of cell culture systems including two- and three-dimensional (3D) methods have been suggested and developed (4).

In two-dimensional (2D) IVC system, isolated follicles (i.e. preantral) or granulosa cell (GC)-oocyte complexes grow in multi-well plates or dishes, then, GCs attach to the surface of culture vessel and migrate away from the oocyte (4). This system is not sufficient to sustain the normal architecture of follicles similar to that seen

in vivo; therefore, follicles are unable to complete the maturation process because of partial loss of the oocyte-follicle cells interactions (4, 6). On the other hand, in 3D IVC models, each isolated follicle is encapsulated in extracellular matrices (ECM), such as agar/agarose, hyaluronic acid (HA), alginate, collagen, and chitosan. Thus, encapsulated follicles not only do not attach to the bottom of the culture vessel, but also keep their spherical growth and native morphology. Moreover, in 3D systems, good interactions between the somatic cell and oocyte occur when optimized for the follicular growth and oocyte development (7). It has been suggested that, compared to other types of culture, gene expression profile of cells grown in a 3D culture system, is closer to that of cells grown *in vivo* (8).

In each mentioned type of cell culture systems, since ovarian follicles are maintained in an incubator under higher concentrations of O₂, the reactive oxygen species (ROS) are continuously produced (9). Overproduction of ROS can affect the IVC of preantral follicles because they can act as second messengers and lead to the opening of a nonspecific pore in the inner mitochondrial membrane, release of cytochrome c, and activation of caspase cascades ultimately resulting in apoptosis. Although overproduction of oxidative agents can cause cell damage and loss of follicular function, antioxidants can attenuate deleterious effects of oxidative stress (9, 10).

Antioxidants are natural or man-made substances that bind free radicals and subsequently neutralize their destructive properties such as peroxidation of lipids and DNA breakage; hence, they can act as protective agents via scavenging free radicals (11, 12). Ginseng (*Panax ginseng*) is one of the most popular members of the family *Araliaceae* (13).

For thousands of years, ginseng has been used in traditional herbal medicine due to its pharmacological properties. It has been reported that ginseng root has various cellular activities, including anti-aging, anti-inflammatory, anti-tumor, and antioxidant effects. Several lines of evidence have reported GSs, polysaccharides, peptides, phenolic acids, phytosterols, tocopherols, policosanols, and fatty acids as the main components of ginseng, but recent pieces of evidence showed that GSs (ginseng saponins) are the major components of ginseng.

Ginsenosides are derived from dammarane-type triterpenoid with a steroid-like structure that consists of 30 carbon atoms and four trans-rings with a modified side chain at C-20. It has been reported that the molecular target of GSs is located not only in the cellular membrane but also inside the cell. Moreover, GSs can regulate cellular functions through non-genomic or the genomic pathways. In the non-genomic pathway, GSs are able to bind the membrane-associated receptors that can initiate the activation of the phosphorylation cascade and therefore, lead to the generation of so-called second messengers within the cell (13). Additionally, GSs by binding the intracellular nuclear hormone receptors, such

as the proliferator-activated receptor, androgen receptor (AR), estrogen receptor (ER), and progesterone receptor (PR), can activate the genomic pathway.

P. ginseng has also been considered a phytoestrogenic herb that has potent estrogenic activity (14, 15). Phytoestrogens can exert estrogenic properties, directly through binding ERs (i.e. ER α or β), which are mainly expressed in reproductive tissues or indirectly by activating ERs (13, 16). It has been reported that ERs mediate cellular effects of estrogens, as female steroid hormones mainly produced by the ovaries (13). One study found that *P. ginseng* could upregulate both ER α and ER β in the uterus and vagina. It could also enhance the serum level of estradiol in ovariectomized mice (15). Another study reported that addition of GSs to the culture media promoted the proliferation of cultured chicken ovarian germ cells (17).

However, the impact of *P. ginseng* extract (PGE) on the growth and maturation of preantral follicles *in vitro*, remains unknown. Therefore, the main purpose of the present study was to investigate the effects of different doses of PGE on the development and function of follicles cultured for 12 days by assessment of follicular growth, the rates of antrum formation and oocyte maturation, hormonal production, and ROS level in collected MII oocytes, as well as evaluation of the mRNA expression levels of follicle stimulating hormone receptor (*FSH-R*) and proliferation cell nuclear antigen (*PCNA*).

Materials and Methods

Animals and collection of ovarian follicles

In this experimental study, 14 day-old female NMRI mice (n=100) were used. Animals were maintained in the laboratory animals of the Tabriz University of Medical Sciences under standard conditions (temperature 22 \pm 2°C, humidity 55 \pm 2%, and 12 hours/12 hours light/dark cycle). To remove mice ovaries, animals were sacrificed by dislocating the cervical vertebrae, then their bilateral ovaries were immediately dissected from oviducts, connective tissues (mesentery), and fat by 29-gauge insulin needles and transferred to dissection medium containing alpha-minimum essential medium (α -MEM, WelGENE, Korea) supplemented with antibiotics and 5% fetal bovine serum (FBS, Gibco, UK). The Ethical Committee of Tabriz University of Medical Sciences, Iran approved the present study (IR.TBZMED.REC.1396.555).

Study design

Under a stereomicroscope (Olympus, Japan), intact preantral follicles (n=661) of 150-160 micrometer (μ m) in diameter, were mechanically isolated from immature mice ovaries using 29-gauge insulin syringes, and immediately collected by a micropipette. Then, only those with more centrally-located spherical oocytes which were surrounded by two or three layers of GCs and no apparent sign of necrosis were randomly divided into one control group and three experimental groups. The control group

(G1) containing 5% FBS without *P. ginseng* extract and experimental groups 1 (Exp. 1), 2 (Exp. 2), and 3 (Exp. 3) were respectively treated with 50, 100, and 500 µg/mL of *P. ginseng* extract (G115 or PGE) (commercially obtained from Pharmaton Company, Switzerland). One study quantified GSs content of the PGE powder (Pharmaton Company, Switzerland) and found Rg1 (4.61 ± 0.43 mg/g), Rb1 (1.39 ± 0.12 mg/g), Rb2 (11.59 ± 1.30 mg/g), Rf (2.36 ± 0.25 mg/g), Rd (9.06 ± 1.05 mg/g), Rc (3.99 ± 0.20 mg/g), and Re (9.59 ± 0.85 mg/g) in PGE (18). In this study, the base of culture medium of follicles for all groups was composed of α -MEM supplemented with 0.33 mM sodium pyruvate, 1% insulin, transferrin, and sodium selenite (ITS, Gibco, UK), 100 mIU/mL rFSH (Gonal-f, Switzerland), antibiotics (100 IU/mL penicillin and 50 mg/mL streptomycin), and 5% FBS. Moreover, in the present study, PGE (10 g/mL) was prepared in dimethylsulfoxide (DMSO, Sigma-Aldrich, Germany), then diluted with media to provide different concentrations of PGE (i.e. 50, 100, and 500 µg/mL) for *in vitro* ovarian follicle culture. Furthermore, in this study, all experiments performed at least in three replicates.

***In vitro* three-dimensional culture system**

Three-dimensional culture system could increase follicular growth, GC differentiation, somatic cell proliferation, oocyte growth, and hormone production by maintaining cell-cell communication and paracrine signalling between the follicular cells and oocytes that eventually promote the growth of both cell types (4). In this stage, isolated follicles were encapsulated in sodium alginate (Sigma-Aldrich, Germany). In brief, sodium alginate was dissolved in deionized water to reach the concentration of 1% (w/v). Then, it was mixed with activated charcoal (0.5 g charcoal was added to 1 g sodium alginate) to improve alginate purity and also remove organic impurities. After charcoal treatment, sodium alginate solution was centrifuged at 5000 rpm for 5 minutes; then, it was passed through 0.22 µm filters (Millipore Filtration, Sigma-Aldrich, Germany). At the end of the process, aliquots of sodium alginate and charcoal-stripped were diluted with 1 X sterilized phosphate buffered saline (PBS) to reach the concentration of 0.5% (w/v). Then, each isolated follicle was transferred to 10 mL of alginate droplet. Droplets were slowly falling into the chemical cross-linking solution (140 mM NaCl and 50 mM CaCl₂) and left for 2-3 minutes (4). Each alginate droplet was removed and washed in α -MEM media, then transferred into 35-mm Petri dishes (SPL Life Science, Korea), which had been filled with 25-35 droplets of culture medium (the volume of each droplet was 50 µL) overlaid together with mineral oil (Sigma-Aldrich, Germany). All capsulated follicles were cultured for 12 days under standard conditions (at 37°C with 5% CO₂).

Morphological and diametrical assessment of follicles

During the culture period, the morphology of follicles was checked using an inverted microscope (Olympus,

Japan) and of follicles photographs were taken at $\times 100$ magnification. Follicles with extrusion of denuded oocytes or darkened oocytes, a disorganized arrangement of GCs, and darkening were considered “degenerated follicles”. To measure the diameter of follicles, the photographs were imported into ImageJ Software (<http://rsbweb.nih.gov/ij>) (n=30/each group). After calibration of ImageJ Software, the mean diameter of each follicle was calculated as the mean length of two perpendicular axes.

Induction of *in vitro* ovulation

For induction of *in vitro* ovulation and oocyte maturation, 1.5 IU/mL human chorionic gonadotropin (hCG, Organon, Netherlands) on day 12 of culture, was added to the culture media. About 24 hours after adding HCG to culture media, the oocytes were scored as a germinal vesicle (GV), GV breakdown (GVBD), and metaphase II (MII) stages based on the appearance of the GV or polar body in the perivitelline space.

Assessment of steroid hormones

The levels of hormones including 17- β estradiol (E2), progesterone (P4), as well as dehydroepiandrosterone (DHEA) were measured by a Microplate Enzyme Immunoassay kit (sensitivity=6.5 pg/mL, Monobind Inc., USA), an enzyme-linked immunosorbent (ELISA) assay kit (sensitivity=0.1 ng/mL, DiaPlus Inc., USA), and a Microplate Enzyme Immunoassay kit (sensitivity=0.04 mg/mL, Monobind Inc., USA), respectively. On the last day of culture, half of the culture media was collected.

RNA extraction, cDNA synthesis for molecular assessment and real-time quantitative reverse transcription polymerase chain reaction

To evaluate gene expression, on culture day 12, follicles in all of the studied groups were collected (15 follicles/each replicate). Briefly, total RNA was extracted from each group using a TRIzol reagent extraction method (Invitrogen, Paisley, UK) according to the manufacturer's instructions. To eliminate any genomic DNA contamination, DNase I treatment was performed after RNA extraction using the RNeasy Micro kit (Invitrogen Life Technologies, Carlsbad, CA, USA). Then, RNA concentration was determined by spectrophotometry and adjusted to a concentration of 600 ng/mL. Subsequently, the cDNA was synthesized by a commercial kit (Thermo Scientific, EU) using oligo dT and reverse transcriptase according to the manufacturer's instructions. Then, cDNA synthesis reaction which was performed for 60 minutes at 42°C, was terminated by heating for 5 minutes at 70°C. The obtained cDNA was stored at -70°C until use. Sequences of specific primers for *PCNA*, *FSH-R*, and glyceraldehyde-3-phosphate dehydrogenase (*GAPDH*) genes are shown in Table 1 (4). *GAPDH* gene was used as an internal control. The RT-qPCR was performed on Applied Biosystems (UK) according to the manufacturer's instructions in a 48-well plate using 20 µL reaction volume consisting of 7 µL RNase/DNase free water, 1 µL

forward primer, 1 mL reverse primer, and 10 mL SYBR Green Master Mix (Sigma-Aldrich, Germany). The real-time thermal condition included a holding step (the initial denaturation) of 1 cycle at 95°C for 10 minutes, a cycling step of 40 cycles of 95°C for 15 seconds, 58°C for 30 seconds and 72°C for 30 seconds, and the final extension step (the melt curve step) at 95°C for 15 seconds, 60°C for 1 minute, and 95°C for 15 seconds. Then, relative quantitative analysis of target genes was done by Pfaffl method (i.e. $2^{-\Delta\Delta CT}$, $\Delta\Delta CT = \Delta Ct_{\text{Sample}} - \Delta Ct_{\text{Control}}$).

Reactive oxygen species assay

The levels of ROS in the obtained MII oocytes after HCG treatment (n=10 for each group) were measured based on the method reported in our previous study (4). Briefly, in the first stage that was done in a dark room, 10 pooled MII oocytes were incubated in assay buffer (40 mmol/L Tris-HCl, pH=7 at 37°C) containing 5 mmol/L 2', 7'-dichlorodihydrofluorescein diacetate (Sigma-Aldrich, Germany) for 25 minutes. In the second stage, incubated oocytes were washed with PBS and sonicated at 50W for 3 minutes, then immediately centrifuged at 3000 rpm for 12 minutes at 4°C. Finally, the supernatants were collected and monitored by a spectrofluorimetric method at excitation and emission wavelengths of 480 and 520 nm, respectively (4). Data related to the ROS levels are presented as mM H₂O₂.

Statistical analysis

Data were analyzed by SPSS version 22 software (SPSS Inc., USA). The results of different groups were compared using one-way ANOVA followed by Tukey post-hoc test and expressed as mean \pm SD. Differences were considered statistically significant when the P<0.05.

Results

Effect of *P. Ginseng* extract on the diameter of cultured isolated preantral follicles

One of the objectives of this study was to investigate the impact of different concentrations of *P. ginseng* extract on the growth of isolated preantral follicles cultured in 0.5% alginate hydrogels for 12 days. In this regard, Figure 1 shows an invert micrograph of isolated cultured follicles. At the beginning of culture, the mean diameter of follicles was $151.48 \pm 7 \mu\text{m}$ for all studied groups; however, during 12-day IVC period, in all of the studied groups, follicles increased in size and GC layers expanded (Fig.2). On the other hand, on days 6 and 12 of the culture, the mean diameter of cultured follicles which were treated with PGE 100 $\mu\text{g}/\text{mL}$ was significantly increased compared to other groups (P<0.001). Moreover, on day 12 of culture, the mean diameter of follicles was significantly increased in experimental group 1 compared to control group (P<0.001).

Table 1: The characteristic of primer sequences used in real-time quantitative reverse transcription polymerase chain reaction assays

Genes	Primer sequence (5'-3')	GenBank accession numbers	Product size (bp)
<i>PCNA</i>	F: AGGAGGCGGTAACCATAG R: ACTCTACAACAAGGGGCACATC	NM-011045	76
<i>FSH-R</i>	F: CCAGGCTGAGTCGTAGCATC R: GGCGGCAAACCTCTGAACT	NM-013523.3	79
<i>GAPDH</i>	F: GGAAAAGAGCCTAGGGCAT R: CTGCCTGACGGCCAGG	NM-007393	64

Table 2: Developmental rates of isolated preantral follicles after 12-day *in vitro* culture

Groups	Number of follicles	Number of survived	Number of antrum formation	Number of MII
Control	149	105 (70.48 \pm 0.7)	44 (41.9 \pm 2.49)	26 (24.64 \pm 2.38)
Exp.1	167	121 (72.55 \pm 1.58) ^a	52 (42.8 \pm 2.37)	32 (25.51 \pm 1.98)
Exp.2	174	140 (80.45 \pm 0.76) ^{abc}	71 (50.78 \pm 3.22) ^{abc}	44 (31.48 \pm 2.00) ^{abc}
Exp.3	171	122 (71.49 \pm 1.14)	52 (42.70 \pm 1.33)	31 (25.39 \pm 1.06)

The control group containing 10% fetal bovine serum (FBS) without *Panax ginseng* extract (PGE), Exp.1, (group 1) that was treated with 50 $\mu\text{g}/\text{ml}$ PGE, Exp.2, (group 2) that was treated with 100 $\mu\text{g}/\text{ml}$ PGE, and Exp.3, (group 3) that was treated with 500 $\mu\text{g}/\text{ml}$ PGE. ^a, ^b, and ^c show significant differences compared to the control group (P<0.05), group 1 (P<0.001), and group 3 (P<0.001), respectively. Values are given as mean \pm SD.

Effect of *P. Ginseng* extract on follicular developmental rate

The developmental rate of follicles, including survival rate, antrum formation, as well as MII rate, are summarized in Table 2. Although the survival rate of follicles was significantly increased in experimental

group 1 (treated with PGE 50 µg/mL) in comparison to control group ($P < 0.05$), the highest percentage of survival rate was observed in group 2 (treated with PGE 100 µg/mL) compared to other groups ($P \leq 0.001$). Moreover, the highest percentages of antrum formation and MII rate were observed in group 2 compared to other groups ($P \leq 0.001$).

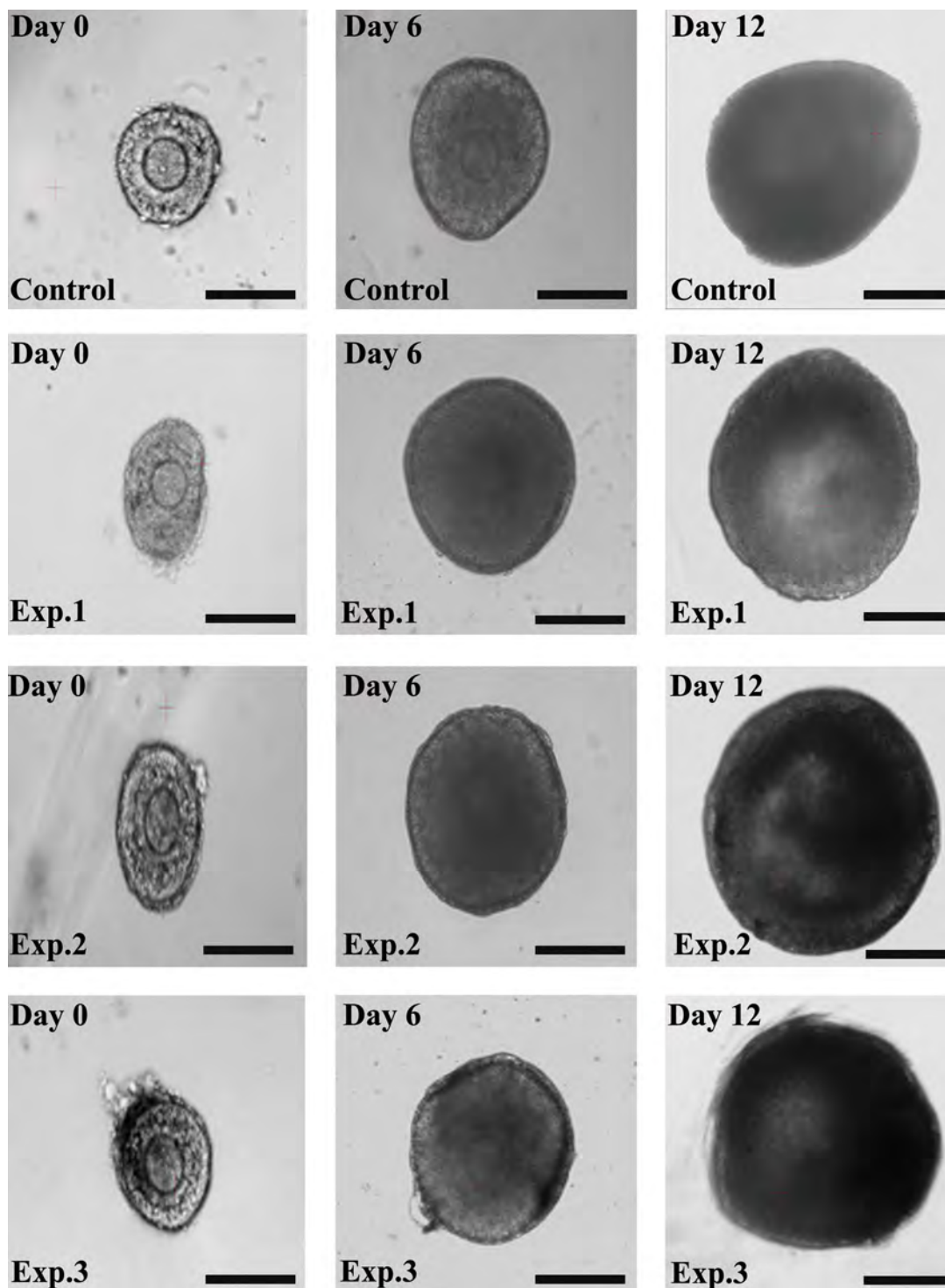


Fig.1: Images of the inverted microscope during *in vitro* three-dimensional follicular development in the alginate droplet on day 0 (first column), day 6 (second column), and day 12 (third column) in different groups. The control group containing 10% fetal bovine serum (FBS) without *Panax ginseng* extract (PGE), Exp.1, (group 1) that was treated with 50 µg/ml PGE, Exp.2, (group 2) that was treated with 100 µg/ml PGE, and Exp.3, (group 3) that was treated with 500 µg/ml PGE (scale bar: 100 µm).

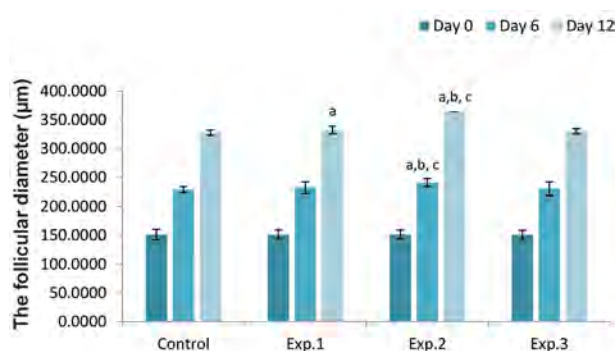


Fig.2: The average diameter of isolated preantral follicles (μm) during *in vitro* three-dimensional culture. a, b, and c show significant differences compared to control group ($P<0.05$), group 1 ($P<0.001$), and group 3 ($P<0.001$), respectively. Values are given as mean \pm SD. Exp; Experimental group.

Effect of *P. ginseng* extract on hormonal productions of follicles

To investigate the effects of PGE on hormonal productions of cultured follicles, on the last day of the culture i.e. day 12), the levels of steroid hormones namely, E2, P4, and DHEA in media collected from

cultured follicles, were measured (Table 3). The levels of these hormones were significantly higher in the media of follicles cultured in the presence of PGE 100 $\mu\text{g}/\text{mL}$ compared to other groups ($P<0.05$). Also, the hormonal productions were significantly higher in group 1 compared to the control group ($P<0.05$). Additionally, the level of E2 was significantly increased in group 3 in comparison to control group ($P<0.05$). On the other hand, no significant difference was observed in P4 and DHEA hormones levels between group 3 and control group.

Real-time quantitative reverse transcription polymerase chain reaction analysis

On the last day of culture, the effects of *P. ginseng* extract on the expression levels of *PCNA* and *FSH-R* mRNA were investigated by RT-qPCR (Fig.3A, B). The results showed increased expression of *PCNA* and *FSH-R* mRNA in group 1 when compared with control ($P<0.05$). Also, they were significantly higher in group 2 than the other groups ($P<0.05$). On the other hand, the relative expression of mentioned genes in group 3 was not significantly different from that of the control group.

Table 3: The levels of steroid hormones (E2, P4, and dehydroepiandrosterone) in media collected on the last day of culture

Groups	17- β estradiol (E2) (ng/ml)	Progesterone (P4) (ng/ml)	DHEA ($\mu\text{g}/\text{ml}$)
Control	1.99 \pm 6.80	27.74 \pm 2.09	22.47 \pm 1.74
Exp.1	2.26 \pm 6.30 ^a	33.56 \pm 2.25 ^a	25.86 \pm 2.11 ^a
Exp.2	2.56 \pm 4.54 ^{abc}	81.69 \pm 1.65 ^{abc}	29.58 \pm 1.12 ^{abc}
Exp.3	2.23 \pm 6.30 ^a	31.24 \pm 1.41	23.19 \pm 1.10

The control group containing 10% fetal bovine serum (FBS) without *Panax ginseng* extract (PGE), Exp.1, (group 1) that was treated with 50 $\mu\text{g}/\text{ml}$ PGE, Exp.2, (group 2) that was treated with 100 $\mu\text{g}/\text{ml}$ PGE, and Exp.3, (group 3) that was treated with 500 $\mu\text{g}/\text{ml}$ PGE. ^a, ^b, and ^c show significant differences compared to control group ($P<0.05$), group 1 ($P<0.05$), and group 3 ($P<0.05$), respectively. Values are given as mean \pm SD. DHEA; Dehydroepiandrosterone.

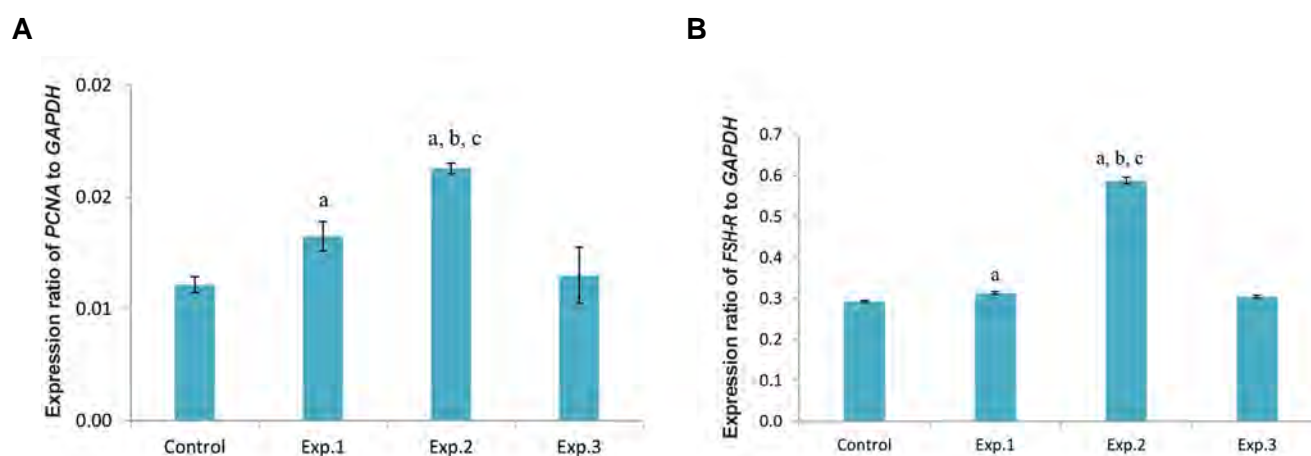


Fig.3: Effects of *Panax ginseng* extract on expression levels of *PCNA* and *FSH-R* mRNA on day 12 of culture as analyzed by real-time quantitative reverse transcription polymerase chain reaction (qRT-PCR). **A.** The mRNA expression of *PCNA*. a, b, and c show significant differences compared to control group ($P<0.05$), group 1 ($P<0.05$), and group 3 ($P<0.001$), respectively and **B.** The mRNA expression of *FSH-R*. a, b, and c show significant differences compared to control group ($P<0.05$), group 1 ($P<0.001$), and group 3 ($P<0.001$), respectively. Exp; Experimental group.

Effect of *P. Ginseng* extract on intracellular reactive oxygen species levels in collected metaphase-II oocytes

The antioxidant benefits of *P. ginseng* extract on MII oocytes, which were released after hCG treatment, were evaluated by measuring the abundance of intracellular ROS in oocytes using the spectrofluorimetric method (at excitation and emission wavelengths of 480 nm and 520 nm, respectively). The levels of ROS in collected MII oocytes in different groups are shown in Figure 4. Measuring the levels of ROS in collected MII oocytes revealed a significant difference between groups that received PGE and the control group ($P < 0.05$). Also, there was a significant decrease in the levels of ROS of MII oocytes collected from groups 2 and 3 when compared to group 1 ($P \leq 0.002$). Additionally, no significant difference was observed between groups 2 and 3 in this regard.

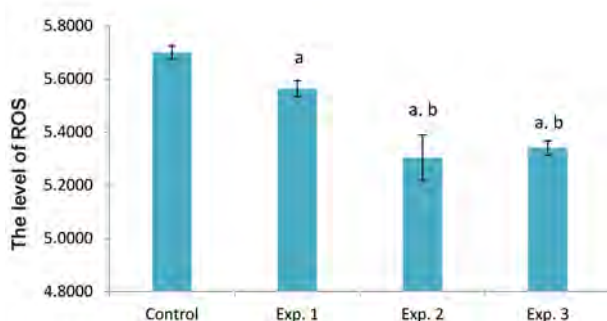


Fig.4: Reactive oxygen species (ROS) levels in different groups on the last day of culture (i.e. day 12). The control group containing 10% fetal bovine serum (FBS) without *Panax ginseng* extract (PGE), Exp.1, (group 1) that was treated with 50 µg/ml PGE, Exp.2, (group 2) that was treated with 100 µg/ml PGE, and Exp.3, (group 3) that was treated with 500 µg/ml PGE. a and b show significant differences compared to control group ($P < 0.05$), and group 1 ($P \leq 0.002$), respectively. Values are given as mean \pm SD. Exp: Experimental group.

Discussion

This study investigated the impacts of different concentrations of *P. ginseng* extract on the growth and maturation of isolated preantral follicles after 12-day culture in a 3D culture system fabricated using the sodium-alginate scaffold.

However, during IVM of isolated preantral follicles, the average diameter of follicles was increased in all groups. But, follicles cultured in the media supplemented with PGE 100 µg/mL showed larger diameters compared to other groups.

Moreover, our results showed that the follicles cultured in PGE 100 µg/mL -supplemented media had the highest follicular survival rate compared to other groups. Of note, in group 1, the survival rate was higher than that of the control group. Developmental rates namely the antrum formation and MII oocytes were significantly increased in group 2 (treated with PGE 100 µg/mL) compared to other groups.

Also, in the medium containing PGE 100 µg/mL (group 2), production of steroid hormones by follicles (E2, P4, and DHEA) was higher than other groups. Moreover, the levels of steroid hormones in the media of group 1 (treated with PGE 50 µg/mL) were significantly increased in comparison to the control group. Consistently, the level of E2 in group 3 was significantly higher than that of the control group.

Furthermore, expression levels of *PCNA* and *FSH-R* mRNA were significantly increased in group 2 (treated with PGE 100 µg/mL).

Among the treated groups, follicles in the group (treated with PGE 100 µg/mL) had better growth and maturation compared to other groups. It seems the highest concentration of *ginseng* (500 µg/mL) may not be beneficial for *in vitro* ovarian follicle culture; hence, the growth and maturation of follicles were not improved as much as that observed in group 2 (treated with 100 µg/mL PGE). One study that investigated the antiviral effects of *Korean red ginseng* (KRG) at different concentrations (0, 5, 6.7, 10, 20 µg/mL), showed that the highest concentration (20 µg/mL) of KRG extract had cytotoxic effects on cell lines (19). Accordingly, it has been demonstrated that GSs are capable of binding directly to ERs or stimulating estrogenic responses independently of binding to ER. This phenomenon can enhance the estrogenic response even at low concentrations (20). However, the results of the present study showed that different concentrations of *P. ginseng* extract have different impacts on the growth and maturation of follicles. Hence, it appears that the effect of *ginseng* on *in vitro* growth and maturation of follicles and oocytes is dose-dependent and this extract acts as an anti-oxidant and anti-proliferative agent at doses of 50 and 100 µg/mL. Since there was no sufficient information about the improvement of follicular growth and maturation by supplementing the culture media with PGE, we performed this research to examine the effect of this herbal extract.

For several centuries, ginseng has been used as one of the most important herbal medicines in the East because of its diverse pharmacological effects on many systems, such as the immune system, central nervous system (CNS) and endocrine system (13, 17). Moreover, it has been reported that the major active components of ginseng are GSs or ginseng saponins. Moreover, more than 100 different GSs with various pharmacological activities have been isolated from the root of *P. ginseng* (13, 21). Furthermore, the most abundant GSs are Rb1, Rb2, Rg1, and Re (13). It has been proven that ginseng due to its antioxidant activity, enhances the function of reproductive organs (13). One study found that treatment with *Korean ginseng* saponins (GSs) modulated the process of steroidogenesis and improved the oocyte quality in the ovary of immature rats which were pre-treated with a super-ovulatory dose of pregnant

mare serum gonadotropin (PMSG) (22). On the other hand, a clinical trial done on women experiencing menopausal disorders showed that intake of *Korean ginseng* powder improves the ovarian function via its estrogenic activity and increasing blood supply into the ovary (23). Another study reported that *American ginseng* could protect the ovary against premature ovarian failure (POF) by preventing the ovarian aging and regulating ovulation (24). Liu and Zhang (17) reported that adding GS at concentrations of 0.1, 1, and 10 µg/mL, could increase the number of chicken ovarian germ cells and elevate PCNA expression.

PCNA is a 36 kDa protein expressed in fetal and adult ovaries of several mammals and it is considered a marker for GCs proliferation (4). The crucial symbol of follicles development is the proliferation of GCs. It has been shown that GCs or oocytes of primordial follicles of rat, do not express PCNA; however, the expression of PCNA would be enhanced with the initiation of follicle growth (25). The higher PCNA expression has been considered a characteristic of actively growing follicles. Furthermore, it has been indicated that PCNA acts as a key factor in DNA replication and repair, the development of ovarian follicles as well as cell survival (4). Alternatively, although the mechanism underlying GS's effects on follicular development and oocyte maturation is not fully elucidated, the meiotic maturation-induced effect of GSs on the oocytes of the mouse has been reported (26). Moreover, the pro-proliferation effects of GSs on diverse cells, such as ovarian germ cells, neurons and endothelial cells have been proven (17, 27). Several studies showed that GSs have a direct pro-proliferative effect on GCs of chicken pre-hierarchical follicles, chicken primordial germ cells and mouse spermatogonia through activating protein kinase C (PKC) (27-29). The PKC family has been implicated in the control of cell proliferation, apoptosis, differentiation and neuronal activity in many cell types; also, PKC signalling pathways promote the steroidogenesis in differentiated GCs of pre-ovulatory follicles (30). One study found that GSs enhance the proliferation of chicken GCs and development of chicken pre-hierarchical follicles in a dose-dependent manner through activating PKC signalling pathways involved in up-regulation of *cyclin E-CDK2* and *cyclin D1-CDK6* genes (27). Therefore, in our study, enhancement of *PCNA* expression at mRNA levels in follicles cultured in the presence of PGE 50 and 100 µg/mL may be due to the direct proliferative effect of *P. ginseng* extract on GCs in a dose-dependent manner.

Furthermore, our results showed that treatment with PGE 50 and 100 µg/mL increases the expression of *FSH-R* mRNA. In females, FSH and its cognate receptor (i.e. *FSH-R*), which are exclusively located on GCs, are essential for the ovarian function and fertility (4). FSH stimulates preantral follicles to grow and promote estradiol production in GCs and regulates

the expression of *FSH-R* in GCs (4). *FSH-R* is a glycoprotein that belongs to the family of G protein-coupled receptors and is expressed in growing follicles (31). When the FSH binds its cognate receptor, it induces the follicular transition from preantral to antral follicles and promotes cytochrome P450. It can also increase the transcription of *CYP19A1* in GCs involved in converting theca cell-derived androgens namely, dehydroepiandrosterone and androstenedione into estrogens, estradiol, and estrone (32). It has been indicated that estrogens stimulate the proliferation of GCs and are absolutely necessary for the normal follicle growth (33). In a study that investigated the effects of ginsenoside Rg1 (one of the main compounds of PGE and a kind of natural estrogen) on POF induced by D-galactose (D-gal), it was shown that treatment with Rg1 could up-regulate the protein expression of *FSH-R* in GCs (34). Moreover, Lee et al. (35) reported that KRG could attenuate sub-chronic psychological stress-induced testicular damage and male sterility by modulating the proteins and mRNA expression levels of sex hormone receptors such as *FSH-R*, *LH-R* and *AR*. Therefore, it is suggested that PGE by up-regulating the expression level of *FSH-R* mRNA, could prevent the follicular regression and subsequently enhance the follicular development.

It has been reported that GSs act through steroid hormone receptors (36). In this regard, it has been indicated that KRG could upregulate the steroidogenic enzyme P450 (*CYP11A1*) in senescent rat testes (37). In females, in the estradiol biosynthesis pathways, cholesterol in the inner membrane of the mitochondria is converted into pregnenolone by *CYP11A1* and then into estradiol by different pathways (38). Therefore, high concentrations of estradiol hormone in the media of cultured follicles supplemented with PGE 100 µg/mL may stem from this phenomena. He et al. (34) reported that treatment with ginsenoside Rg1 could increase serum level of E2 in mice model of D-gal-induced POF. Furthermore, high production of steroid hormones, P4 and DHEA, is associated with the activity of theca cells in the secretion of androgens through increasing the proliferation and differentiation of follicle cells, as well as increasing the aromatase activity in GCs numbers during IVC (39).

In the present study, the level of ROS in oocytes was significantly decreased in groups 2 and 3 compared to other groups. It has been reported that *Korean red ginseng* oil prevents cell/tissue damages directly by scavenging ROS and inhibiting lipid peroxidation. The ability of PGE in reducing the level of ROS in oocytes is due to its antioxidant properties (40).

Conclusion

According to our results, *P. ginseng* extract exerts its effects on follicular development in a dose-dependent manner. Moreover, results of the present study demonstrated that *P. ginseng* extract 100 µg/mL not only

increased the growth of isolated preantral follicles from the ovaries of pre-pubertal mice, but also enhanced their maturation rate after 12-day *in vitro* 3D culture. Further studies are warranted to illuminate the mechanism underlying the findings of the present experiment.

Acknowledgements

The authors thank members of the Stem Cell Research Center for technical support. This work received a grant (grant number: 510867-2) from the Stem Cell Research Center, Tabriz University of Medical Sciences, Tabriz, Iran. There is no conflict of interest.

Authors' Contributions

A.A.Kh., H.Sh., M.M.H.T., A.M.S.; Participated in study design, data collection and evaluation, drafted and statistical analysis. M.T., H.Sh., M.Sh.; Performed follicle collection and follicle culture. A.Kh., L.R., S.Gh., Kh.R.R.; Contributed extensively in interpretation of the data and the conclusion. H.E., H.K.; Conducted molecular, hormonal and, and oxidative experiments and RT-qPCR analysis. All authors performed editing and approving the final version of this manuscript for submission, also participated in the finalization of the manuscript and approved the final draft.

References

- Hsueh AJ, Kawamura K, Cheng Y, Fauser BC. Intraovarian control of early folliculogenesis. *Endocr Rev.* 2015; 36(1): 1-24.
- Roushangar L, Soleymanirad J, Nikpou P, Sayahmeli M. Effect of oxytocin injection on folliculogenesis, ovulation and endometrial growth in mice. *Iranian Journal of Reproductive Biomedicine.* 2009; 7(2): 91-95.
- Roshangar L, Rad JS, Afsordeh K. Maternal tamoxifen treatment alters oocyte differentiation in the neonatal mice: Inhibition of oocyte development and decreased folliculogenesis. *J Obstet Gynaecol Res.* 2010; 36(2): 224-231.
- Shoorei H, Khaki A, Ainehchi N, Hassanzadeh Taheri MM, Tahmasebi M, Seyedghiasi G, et al. Effects of matricaria chamomilla extract on growth and maturation of isolated mouse ovarian follicles in a three-dimensional culture system. *Chin Med J (Engl).* 2018; 131(2): 218-225.
- Liebenthron J, Köster M, Drengner C, Reinsberg J, van der Ven H, Montag M. The impact of culture conditions on early follicle recruitment and growth from human ovarian cortex biopsies *in vitro*. *Fertil Steril.* 2013; 100(2): 483-491. e5.
- Gook DA, Edgar DH, Lewis K, Sheedy JR, Gardner DK. Impact of oxygen concentration on adult murine pre-antral follicle development *in vitro* and the corresponding metabolic profile. *Mol Hum Reprod.* 2014; 20(1): 31-41.
- Zhang C, Wang X, Wang Z, Niu W, Zhu B, Xia G. Effect of different culture systems and 3, 5, 3'-triiodothyronine/follicle-stimulating hormone on preantral follicle development in mice. *PLoS One.* 2013; 8(4): e61947.
- Antoni D, Burckel H, Josset E, Noel G. Three-dimensional cell culture: a breakthrough *in vivo*. *Int J Mol Sci.* 2015; 16(3): 5517-5527.
- Agarwal A, Gupta S, Sikka S. The role of free radicals and antioxidants in reproduction. *Curr Opin Obstet Gynecol.* 2006; 18(3): 325-332.
- Shokoohi M, Shoorei H, Soltani M, Abtahi-Eivari SH, Salimnejad R, Moghimian M. Protective effects of the hydroalcoholic extract of *Fumaria parviflora* on testicular injury induced by torsion/detorsion in adult rats. *Andrologia.* 2018; e13047.
- Devine PJ, Perreault SD, Luderer U. Roles of reactive oxygen species and antioxidants in ovarian toxicity. *Biol Reprod.* 2012; 86(2): 27.
- Soltani M, Moghimian M, Abtahi-Eivari SH, Shoorei H, Khaki A, Shokoohi M. Protective effects of matricaria chamomilla extract on torsion/detorsion-induced tissue damage and oxidative stress in adult rat testis. *Int J Fertil Steril.* 2018; 12(3): 242-248.
- Park J, Song H, Kim SK, Lee MS, Rhee DK, Lee Y. Effects of ginseng on two main sex steroid hormone receptors: estrogen and androgen receptors. *J Ginseng Res.* 2017; 41(2): 215-221.
- Ding J, Xu Y, Ma X, An J, Yang X, Liu Z, et al. Estrogenic effect of the extract of Renshen (*Radix Ginseng*) on reproductive tissues in immature mice. *J Tradit Chin Med.* 2015; 35(4): 460-467.
- Xu Y, Ding J, Ma XP, Ma YH, Liu ZQ, Lin N. Treatment with Panax ginseng antagonizes the estrogen decline in ovariectomized mice. *Int J Mol Sci.* 2014; 15(5): 7827-7840.
- Paterni I, Granchi C, Katzenellenbogen JA, Minutolo F. Estrogen receptors alpha (ER α) and beta (ER β): subtype-selective ligands and clinical potential. *Steroids.* 2014; 90: 13-29.
- Liu H, Zhang C. Ginsenosides promote proliferation of cultured ovarian germ cells involving protein kinase C-mediated system in embryonic chickens. *Asian-Australas J Anim Sci.* 2006; 19(7): 958-963.
- Cabral de Oliveira AC, Perez AC, Merino G, Prieto JG, Alvarez AI. Protective effects of Panax ginseng on muscle injury and inflammation after eccentric exercise. *Comp Biochem Physiol C Toxicol Pharmacol.* 2001; 130(3): 369-377.
- Lee MH, Lee BH, Jung JY, Cheon DS, Kim KT, Choi C. Antiviral effect of Korean red ginseng extract and ginsenosides on murine norovirus and feline calicivirus as surrogates for human norovirus. *J Ginseng Res.* 2011; 35(4): 429-435.
- King ML, Adler SR, Murphy LL. Extraction-dependent effects of American ginseng (*Panax quinquefolium*) on human breast cancer cell proliferation and estrogen receptor activation. *Integr Cancer Ther.* 2006; 5(3): 236-243.
- Lee CH, Kim JH. A review on the medicinal potentials of ginseng and ginsenosides on cardiovascular diseases. *J Ginseng Res.* 2014; 38(3): 161-166.
- Yu WJ, Lee BJ, Nam SY, Yang DC, Yun YW. Modulating effects of Korean ginseng saponins on ovarian function in immature rats. *Biol Pharm Bull.* 2003; 26(11): 1574-1580.
- Vogler BK, Pittler MH, Ernst E. The efficacy of ginseng. A systematic review of randomised clinical trials. *Eur J Clin Pharmacol.* 1999; 55(8): 567-575.
- Zhu L, Li J, Xing N, Han D, Kuang H, Ge P. American ginseng regulates gene expression to protect against premature ovarian failure in rats. *Biomed Res Int.* 2015; 2015: 767124.
- Oktay K, Schenken RS, Nelson JF. Proliferating cell nuclear antigen marks the initiation of follicular growth in the rat. *Biol Reprod.* 1995; 53(2): 295-301.
- Zhang D, Zhang C, Liu J, Hu S. Ginsenosides promote meiotic maturation of mouse oocytes in cumulus-oocyte complexes involving increased expression of nitric oxide synthase. *Nutr Res.* 2006; 26(11): 585-590.
- Tan TQ, Ge C, Mi Y, Jin Y, Zhang C. Ginsenosides promote proliferation of granulosa cells from chicken prehierarchal follicles through PKC activation and up-regulated cyclin gene expression. *Cell Biol Int.* 2010; 34(7): 769-775.
- Ge C, Zhang C, Ye J, Tang X, Wu Y. Ginsenosides promote proliferation of chicken primordial germ cells via PKC-involved activation of NF-kappaB. *Cell Biol Int.* 2007; 31(10): 1251-1256.
- Zhang DL, Wang KM, Zhang CQ. Ginsenosides stimulated the proliferation of mouse spermatogonia involving activation of protein kinase C. *J Zhejiang Univ Sci B.* 2009; 10(2): 87-92.
- Woods DC, Johnson AL. Protein kinase C activity mediates LH-induced ErbB/Erk signaling in differentiated hen granulosa cells. *Reproduction.* 2007; 133(4): 733-741.
- Oktay K, Briggs D, Gosden RG. Ontogeny of follicle-stimulating hormone receptor gene expression in isolated human ovarian follicles. *J Clin Endocrinol Metab.* 1997; 82(11): 3748-3751.
- Hernández-Ochoa I, Gao L, Peretz J, Basavarajappa MS, Bunting SL, Karman BN, et al. Follicle-stimulating hormone responsiveness in antral follicles from aryl hydrocarbon receptor knockout mice. *Reprod Biol Endocrinol.* 2013; 11: 26.
- Chaffin CL, VandeVoort CA. Follicle growth, ovulation, and luteal

- formation in primates and rodents: a comparative perspective. *Exp Biol Med (Maywood)*. 2013; 238(5): 539-548.
34. He L, Ling L, Wei T, Wang Y, Xiong Z. Ginsenoside Rg1 improves fertility and reduces ovarian pathological damages in premature ovarian failure model of mice. *Exp Biol Med (Maywood)*. 2017; 242(7): 683-691.
 35. Lee SH, Choi KH, Cha KM, Hwang SY, Park UK, Jeong MS, et al. Protective effects of Korean Red Ginseng against sub-acute immobilization stress-induced testicular damage in experimental rats. *J Ginseng Res*. 2017; 1-10.
 36. Nah SY. Ginseng ginsenoside pharmacology in the nervous system: involvement in the regulation of ion channels and receptors. *Front Physiol*. 2014; 5: 98.
 37. Kim I-H, Kim S-K, Kim E-H, Kim S-W, Sohn S-H, Lee SC, et al. Korean red ginseng up-regulates C21-steroid hormone metabolism via Cyp11a1 gene in senescent rat testes. *J Ginseng Res*. 2011; 35(3): 272-282.
 38. Payne AH, Hales DB. Overview of steroidogenic enzymes in the pathway from cholesterol to active steroid hormones. Payne AH, Hales DB. Overview of steroidogenic enzymes in the pathway from cholesterol to active steroid hormones. *Endocr Rev*. 2004; 25(6): 947-970.
 39. Peng X, Yang M, Wang L, Tong C, Guo Z. In vitro culture of sheep lamb ovarian cortical tissue in a sequential culture medium. *J Assist Reprod Genet*. 2010; 27(5): 247-257.
 40. Bak MJ, Jun M, Jeong WS. Antioxidant and hepatoprotective effects of the red ginseng essential oil in H₂O₂-treated HepG2 cells and CCl₄-treated mice. *Int J Mol Sci*. 2012; 13(2): 2314-2330.
-

Neuroprotective Effects of Combined Treatment with Minocycline and Olfactory Ensheathing Cells Transplantation against Inflammation and Oxidative Stress after Spinal Cord Injury

Soheila Pourkhodadad, Ph.D.^{1*}, Shahrbanoo Oryan, Ph.D.^{1*}, Gholamreza Kaka, Ph.D.²,
Seyed Homayoon Sadraie, Ph.D.³

1. Department of Animal Physiology, Faculty of Biology, Kharazmi University, Tehran, Iran
2. Neuroscience Research Center, Baqiyatallah University of Medical Sciences, Tehran, Iran
3. Department of Anatomy, School of Medicine, Baqiyatallah University of Medical Sciences, Tehran, Iran

*Corresponding Address: P.O.Box: 15815-3587, Department of Animal Physiology, Faculty of Biology, Kharazmi University, Tehran, Iran

Emails: s.porkhodadad@yahoo.com, Sh_oryan@yahoo.com

Received: 27/June/2018, Accepted: 2/September/2018

Abstract

Objective: Traumatic spinal cord injury (SCI) is considered one of the most devastating injuries leading to neuronal disruption. Olfactory ensheathing cells (OECs) and minocycline have been shown to promote locomotor function after spinal cord injury. In this study, we have tested the efficacy of combined treatment with minocycline and OECs after contusive spinal cord injury.

Materials and Methods: In this experimental study, adult female Wistar rats were randomly divided into five groups. Rats received an intraperitoneal injection of minocycline immediately after SCI, and then 24 hours after the injury. Transplantations were performed 7 days after the injury. Functional recovery was evaluated using the Basso, Beattie and Bresnahan scale (BBB). After that, the animals were sacrificed, and T11 segment of the spinal cord was removed after 5 weeks, and then used for histopathological, immunohistochemical, and biochemical assessments. Western blot analysis was applied to determine the protein expression of tumor necrosis factor alpha (TNF- α), interleukin 1 beta (IL1 β) and caspase3.

Results: The results of this study showed that the combination of OECs graft and minocycline reduced the functional deficits and diminished cavitation and astrogliosis in spinal tissue. The analysis of protein expression by western blotting revealed that minocycline treatment along with OECs transplantation further decreased the level of IL-1 β , TNF- α , caspase-3, and the oxidative stress as compared with when minocycline or OECs transplantation was used alone.

Conclusion: The combinatory treatment with OECs graft and minocycline induced a more effective response to the repair of spinal cord injury, and it is considered a therapeutic potential for the treatment of SCI.

Keywords: Inflammation, Minocycline, Olfactory Ensheathing Cells, Oxidative Stress, Spinal Cord Injury

Cell Journal (Yakhteh), Vol 21, No 2, July-September (Summer) 2019, Pages: 220-228

Citation: Pourkhodadad S, Oryan Sh, Kaka Gh, Sadraie SH. Neuroprotective effects of combined treatment with minocycline and olfactory ensheathing cells transplantation against inflammation and oxidative stress after spinal cord injury. Cell J. 2019; 21(2): 220-228. doi: 10.22074/cellj.2019.6126.

Introduction

Spinal cord injury (SCI) is considered one of the most devastating conditions leading to neurological dysfunction and disability in young people (1). Traumatic SCI which is resulted in functional deficits causes degeneration and disruption of axonal tracks leading to secondary injury and cell death that occur hours and days after the primary trauma (2, 3). It is thought that inflammation, the oxidative stress, and apoptosis are significant factors precipitating in post-traumatic degeneration due to secondary injury in SCI. Although the molecular pathway of secondary damage is still controversial, therapeutic strategies that inhibit and delay oxidative stress and apoptosis may contribute to motor functional recovery (4, 5).

Minocycline, a semi-synthetic second-generation tetracycline, has several mechanisms of action including anti-inflammatory (6) and anti-apoptotic effects (7). It also reduces the microglial activation made it an attractive

neuroprotective agent (8). Many studies indicated that minocycline exerts neuroprotective effects in several rodent models of the central nervous system disorders including ischemia, Huntington's disease, amyotrophic lateral sclerosis, and spinal cord injury (6, 9, 10). In another experiment, it has been revealed that minocycline provides neuroprotection against 6-hydroxydopamine or glutamate-induced toxicity by inhibiting microglial activation (11, 12). These experimental studies demonstrate that minocycline provides neuroprotection via an anti-inflammatory mechanism that may help the survival of transplanted cells.

Numerous investigators sought strategies to promote axonal regeneration following SCI, and cellular transplantation has been emerged as a promising tool to achieve this goal. Among cellular manipulation strategies, olfactory ensheathing cells (OECs) have attracted much attention as potential therapeutic agents for the treatment of SCI due to their ability to secrete

neurotrophic factors and remyelinate the regenerated axons (13, 14). Despite the transplantation of OECs after SCI has been successful so far, the functional recovery after the injury is achieved only to a partial degree (15). To date, the underlying mechanism of SCI is complex, and many factors are involved in the development of the disease. Although the application of OECs has opened up a new horizon for the treatment of neurodegenerative diseases, it is not useful for spinal cord repair in animal models when employed alone. Thus combined therapies are recommended to boost the efficacy of this therapeutic approach. The previous studies reported the transplantation of OECs in addition to the administration of FK506 and methylprednisolone. However, the restoration of functions was not achieved completely post-injury (16, 17). According to former studies, minocycline and OECs transplantation have been indicated to possess suitable effects on SCI. Thus, the aim of this study was to determine whether the restorative properties of OECs graft is improved when combined with minocycline administration after spinal cord contusion injury.

Materials and Methods

In this experimental study, adult female Wistar rats (220-250 g) were used in this study. The animals were maintained on a 12 hours dark/light cycle at 20°C. Food and water were available ad libitum. All procedures that pertained to animals were approved by the animal care and ethics in Baqiyatallah University of Medical Sciences, Tehran, Iran. For inducing SCI, we used 50 rats in the following five groups (10 rats in each group): sham group in which only laminectomy was performed; control group in which the animals underwent laminectomy, SCI, and the phosphate-buffered saline (PBS) treatment (i.p) following the transplantation of Dulbecco's Modified Eagle's medium (DMEM) into spinal cord 7 days post-injury; OECs group in which the animals underwent laminectomy, SCI, and the PBS treatment followed by the transplantation of OECs (450000 cells/6 µl) at 7 days post-injury; minocycline group in which the animals underwent laminectomy, SCI, and the minocycline treatment (90 mg, i.p, given the first and 24 hours after SCI) followed by the transplantation of DMEM (6 µl) into the spinal cord at 7 days post-injury, and finally, OECs+minocycline group in which the animals underwent laminectomy, SCI, and minocycline treatment (90 mg/kg, i.p) followed by the transplantation of OECs (450000 cells/6 µl) at 7 days post-injury. We also used 10 rats for OECs culture.

Olfactory ensheathing cells culture and immunopurification

OECs were obtained from the nerve fibers and olfactory bulbs of adult rats using Nash methods (18). Briefly, rats were anesthetized with an overdose of chloral hydrate, then, the olfactory nerve rootlets and olfactory bulbs were dissected and placed into calcium and magnesium-free Hank's balanced salt solution (HBSS, Sigma, USA). All meninges and blood vessels were divested of the tissue. The tissues were minced and incubated within a solution of 0.1 % trypsin (Gibco, USA) in DMEM/F12 (Gibco,

USA) in 5% CO₂ at 37°C for 30 minutes. Trypsinization was inactivated by the addition of fetal bovine serum (FBS, Sigma, USA). The suspension was centrifuged at 1000 rpm for 5 minutes and seeded into an uncoated cell culture flask in DMEM/F12 (Gibco, USA) supplemented with 10% fetal bovine serum, 2 Mm L-glutamine (Gibco, USA), 100 IU/ml penicillin and 100 µg/ml streptomycin (Gibco, USA), a process allowing most of the fibroblasts to attach to the plate during the first incubation period for 18 hours. The supernatant from the culture was removed and plated onto uncoated culture flasks. After 36 hours of incubation, the supernatant was seeded in flasks pre-coated with poly L-lysine (Sigma, USA), and the OECs attached within 48 hours. The media were changed every 2 days. After reaching confluence, OECs were identified by immunohistochemistry (IHC) staining with p75 nerve growth factor receptor (NGFRp75) antibody (1:100, Rabbit polyclonal, N3908, Sigma, USA) to determine cell purity.

The animal model of spinal cord injury

Rats were anesthetized with intraperitoneal chloral hydrate (450 mg/kg). A laminectomy was done at vertebral level T11, and the spinal cord was exposed. The injury was produced by dropping a 10 g rod from a height of 25 mm onto the rat spinal cord at T11, following the procedural guidelines established by a multicenter consortium. After the injury, the muscles and skin were closed separately, and the rats were placed in a chamber overnight. Gentamicin was administered for 3 days after contusion to prevent wound and bladder infections; also, acetaminophen was added to drinking water for 7 days, and urinary bladder expression was performed twice daily until reflexive bladder emptying was achieved.

Minocycline administration

Minocycline was dissolved in sterile PBS and administered intraperitoneally (i.p) after injury in the treatment group. Rats receiving 25 mm insult received 90 mg/kg of minocycline immediately after SCI, and then 24 hours after SCI (19). The control group received an injection of sterile PBS. For the sham groups, the animals underwent T11 laminectomy without contusion injury, received non-pharmacological treatment, and were sacrificed at the same time intervals as the treatment groups.

Transplantation

The transplantation was performed 7 days after the initial surgery (14). All rats were anesthetized, and the laminectomy site was re-exposed. Six microliters of cell suspension (450,000 cells/6 µl for OECs) were injected using a Hamilton syringe, which remain in place after each injection for 5 minutes. The cell suspension was injected at a depth of 0.8 mm of the lesion epicenter and 1 mm rostral and caudal to the epicenter (2 µl per injection). Control animals were injected with an equal volume of DMEM at the same sites. After injection, the muscle and skin were sutured.

Behavioral assessment

Behavioral tests were performed according to the Basso, Beattie and Bresnahan scale (BBB scale) to evaluate the functional recovery (20). The scale used for measuring hind limb function ranged from 0 (paralysis) to 21 (normal score), with an increasing score indicating the use of individual joints, coordinated joint movement, coordinated limb movement, weight-bearing, and the other functions. All scores were obtained on days 1, 7, 14, 21, 28, and 35 by two examiners who were blinded by treatment. The average scores were calculated according to the progression of locomotion recovery after SCI.

Histological and immunohistochemical analyses

The spinal cord segment at the level of T11 was dissected (1cm on each side of the lesion) 35 days after SCI, and then, were paraffin embedded and cut into 5 μm -thick transverse sections by a microtome. Sections were then deparaffinized with xylene, rehydrated with decreasing alcohol concentrations, then stained with hematoxylin and eosin (H&E). Cavity volume in all sections was studied using an image analyzing software (Motic 2.1, Italy, Cagli). The transverse sections were stained with a primary antibody against the glial fibrillary acidic protein (Rabbit anti-GFAP, 1:100; PAB12325; Abnova, Taiwan) to visualize the astroglial reactivity and the formation of glial scar around the lesion. Segments of the spinal cord centered on the impact site were cut into serial 5- μm -thick sagittal sections for histopathology, (n=3 rats/group). The sections were permeabilized and blocked with 0.3 % Triton X-100 and 10% normal goat serum in 0.01 M PBS for 2 hours. Then sections were incubated at 4°C with polyclonal rabbit anti-glial fibrillary acidic protein (GFAP, 1:100) for astrocytes in a wet chamber overnight. After washing with PBS 4 times, the sections were incubated with HRP-conjugated secondary antibodies (1:200; Abnova, Taiwan) for 2 hours at room temperature. After incubation with 0.02% 3,3'-Diaminobenzidine (DAB) for 5 minutes, the sections were counterstained with hematoxylin. The positive area counting was performed in a defined square perimeter of 1,000 μm^2 in three different segments of the ventral horn.

Western blot assay

Western blot was used to detect the protein expression of tumor necrosis factor alpha (TNF- α), interleukin 1 beta (IL1 β), and caspase-3. After being treated with the transplantation of OECs and minocycline for 35 days, 5 mm lengths of the spinal cord centered on T11 were rapidly removed, weighted, and the tissues were homogenized in 0.2 mL of homogenization buffer; then, centrifuged for 10 minutes (12,000 rpm/minutes, at 4°C). The supernatants were applied for protein determination. 20 μg protein samples were separated by 10% sodium dodecyl sulfate-polyacrylamide gel electrophoresis (SDS-PAGE) and transferred from the gel onto polyvinylidene fluoride (PVDF) membranes (150 mA, 1.5 hour) (Millipore Corporation, USA). After blocking with 5% nonfat dry milk for 2 hours, the membranes were incubated overnight at 4°C with

different primary antibodies including anti-TNF α (Abcam, Cambridge, UK), anti-IL1 β (Abcam, Cambridge, UK), anti-caspase3 (Abcam, Cambridge, UK), and anti-GAPDH (Abcam, UK). After washing membranes with TBST, the membranes were incubated with goat anti-rabbit IgG-HRP conjugated secondary antibody (Sigma, USA) at a 1:1000 dilution for 2 hours at room temperature. Then, the membranes were rinsed three times for 10 minutes and incubated with enhanced chemiluminescence (ECL) kit. GAPDH served as the internal control, and the analysis of the images was performed using the ImageJ software.

Tissue preparation and protein quantification

At 35 days after SCI, the spinal cord tissues were removed and homogenized in cooled radioimmunoprecipitation assay (RIPA) buffer supplemented with phenyl methanesulfonyl fluoride, then centrifuged at 15,000 \times g for 15 minutes at 4°C. Next, the supernatant was aliquoted and stored at 20°C until used for the measurement of the oxidative stress parameters analysis. The concentration of protein was measured using the Lowry method (21).

Measurement of tissue malondialdehyde

The concentration of malondialdehyde (MDA) was determined based on its reaction with thiobarbituric acid (TBA) at 95°C (15). Briefly, 150 μl supernatant was mixed with 300 μl trichloroacetic acid (10%, Sigma, USA) and TBA (0.67%, Sigma, USA) and heated at 95°C for 15 minutes. After cooling at room temperature, the samples were centrifuged at 3500 \times g for 10 minutes. The absorbance of the samples was read at 532 nm. Tetramethoxypropane (Sigma, USA) was used to prepare the standard curve. The malondialdehyde (MDA) concentrations were reported as nmol/mg protein.

Measurement of catalase activity

Catalase activity was calculated according to the method of Aebi (22). The reaction was started by the addition of tissue homogenate (50 μg) in 2 ml of 30 mM hydrogen peroxide (H₂O₂) in 50 mM phosphate buffer (pH=7.0). The activity was measured by the reduced absorbance of H₂O₂ at 240 nm. The results are expressed as units per mg of protein (U/mg of protein).

Levels of the glutathione

Glutathione (GSH) levels were determined based on the reaction between dithionitrobenzoic acid (DTNB) and the reduced GSH. The yellow mixture was measured spectrophotometrically at 412 nm. GSH content was expressed as mg GSH/g protein.

Nitrite oxide assay (nitrite content)

To measure tissue levels of nitrite oxide (NO) in spinal cord samples, 50 μL of supernatant was mixed with an equal volume of Griess reagent (1% sulphanilamide and 0.1% N-1-naphthylethylene diamine dihydrochloride in 0.5% H₃PO₄).

After incubation for 10 minutes at room temperature, the absorbance was measured at 540 nm in a microplate reader (23). The average concentration of nitrite was calculated through a comparison with a standard calibration curve with sodium nitrite (NaNO_2 : 0-110 $\mu\text{mol/l}$).

Statistical analysis

All data are expressed as the mean \pm SEM and were analyzed using the GraphPad Prism software, version 5.0 (GraphPad Software, Inc., La Jolla, CA, USA). The statistical differences were determined using one-way analysis of variance (ANOVA) with post-hoc Bonferroni's multiple comparison tests. Differences were considered significant if $P < 0.05$.

Results

A week after the cells were plated, various forms of classic cells of OECs were observed under microscopy as bipolar and multipolar cells (Fig.1A). To identify OECs, immunocytochemical staining was utilized for the detection of NGFRp75 (Fig.1B).

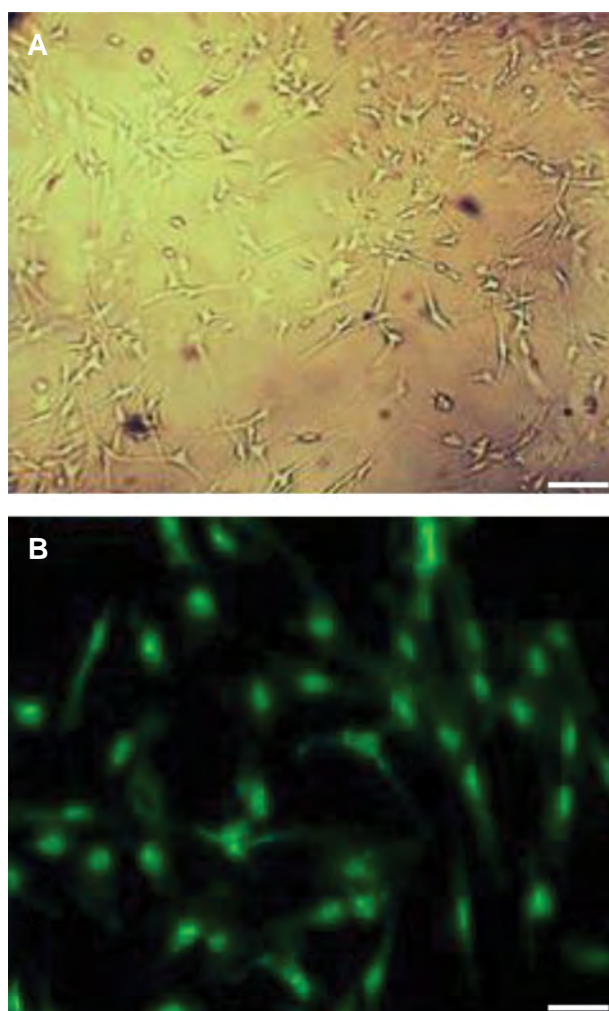


Fig.1: Characterization of primary cultured olfactory ensheathing cells (OECs). **A.** The morphology of OECs in culture and **B.** Immunofluorescence analysis of NGFRp75 (shown in green) in the cells. The purity of OECs is 85% (scale bar: 100 μm).

Locomotor recovery

The locomotor behavior for both hind limbs was impaired in all groups immediately after contusion injury. The motor function of the four groups exhibited gradual improvements in the hind limb during 35 days of the experiment. Although motor functions were gradually improved, the scores of motor function were significantly lower ($P < 0.001$) than those of the sham group. Similarly, an improved motor function was also found in the minocycline treatment on day 14, 21, 28 ($P < 0.05$), and 35 ($P < 0.01$) and in the OECs transplantation group on day 35 ($P < 0.05$) as compared with the SCI group. The combined treatment group showed a markedly better functional recovery, with a significantly increased BBB locomotor score on day 14, 21 ($P < 0.05$), 28 ($P < 0.01$), and 35 ($P < 0.001$) compared to the SCI group (Fig.2).

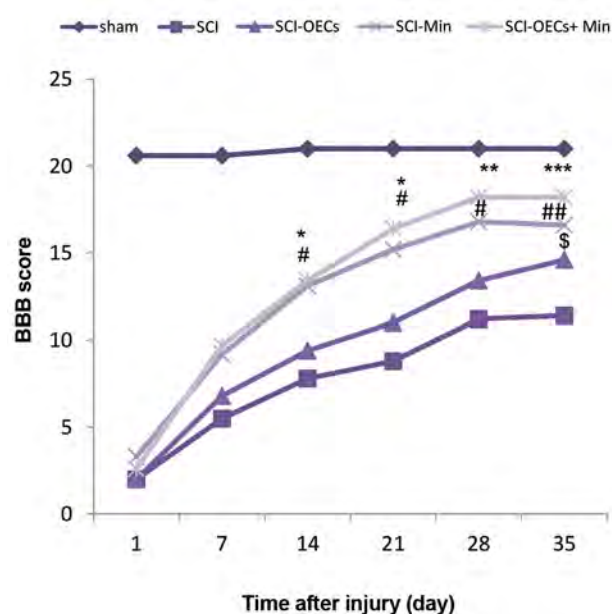


Fig.2: Effect of combination therapy on hind limb behavioral motor function after SCI. Data are expressed as the means \pm SEM. SCI; Spinal cord injury, OECs; Olfactory ensheathing cells, BBB; Basso, Beattie and Bresnahan scale, ***; $P < 0.001$, **; $P < 0.01$, *; $P < 0.05$ in SCI-OECs-Min group versus SCI group, #; $P < 0.05$, ##; $P < 0.01$ in SCI-Min group vs. SCI group, and \$; $P < 0.05$ in SCI-OECs group versus SCI group.

Cavitation analysis

The mean cavity size was calculated after H&E staining. At 35 days after injury, the SCI control group showed a maximum injury and minimum recovery from SCI, and severe tissue damage was observed in the gray and white matter. In the sham group, the white and gray matter of the spinal cord segments were intact (Fig.3A).

The results indicated that the mean cavity size was significantly lower in the minocycline- and OECs-treated groups in comparison with the SCI group

($P < 0.01$, $P < 0.05$). Although the percentage of the cavitation in the OECs transplantation group showed a slight decrease compared to the minocycline group, the difference was not statistically significant ($P > 0.05$). Moreover, the mean cavity area in the minocycline+OECs group was significantly reduced in comparison with the SCI ($P < 0.001$, Fig.3B).

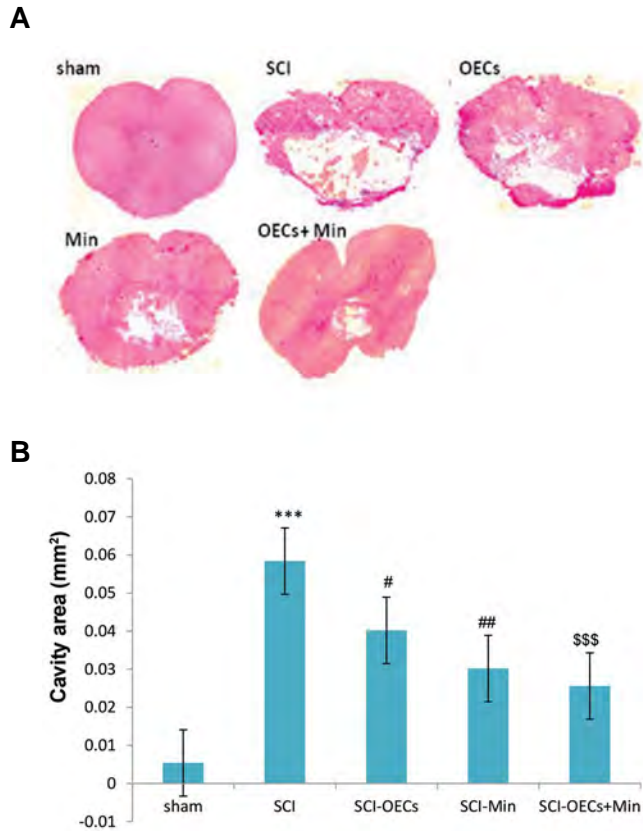


Fig.3: Histopathological assessment of combined treatment with OECs and minocycline on the cavity area at the epicenter of injured spinal cord. **A.** The H&E stained paraffin sections of cavity area ($\times 10$) and **B.** Percentage of the cavity area at the epicenter of injury between injury groups at 35 days after SCI. Data are presented as mean \pm SEM.

SCI; Spinal cord injury, OECs; Olfactory ensheathing cells, ***; $P < 0.001$ versus sham group, #; $P < 0.05$, ##; $P < 0.01$, and \$\$\$; $P < 0.001$ versus SCI group.

Effects of combined treatment with minocycline and olfactory ensheathing cells transplantation on GFAP after spinal cord injury

To identify whether the different treatment groups inhibited posttraumatic astrogliosis, the GFAP expression was compared between experimental groups. There was strong, robust immunoreactivity in the grey matter throughout all sections of the SCI group. The statistical analysis revealed that the number of GFAP⁺ astrocytes was significantly increased in the SCI group. Nevertheless, this activation was significantly attenuated in the minocycline and minocycline+OECs groups, whereas the OECs group had intermediate values. Regarding the obtained results, the density of astrogliosis in the grey matter

of the spinal cord was significantly increased in the SCI group in comparison with the sham group ($P < 0.001$). Moreover, the statistical analysis showed that the density of gliosis was significantly reduced in the minocycline+OECs ($P < 0.001$), and minocycline ($P < 0.01$) groups when compared with the SCI group (Fig.4A, B). There were no significant differences between the OECs and SCI groups.

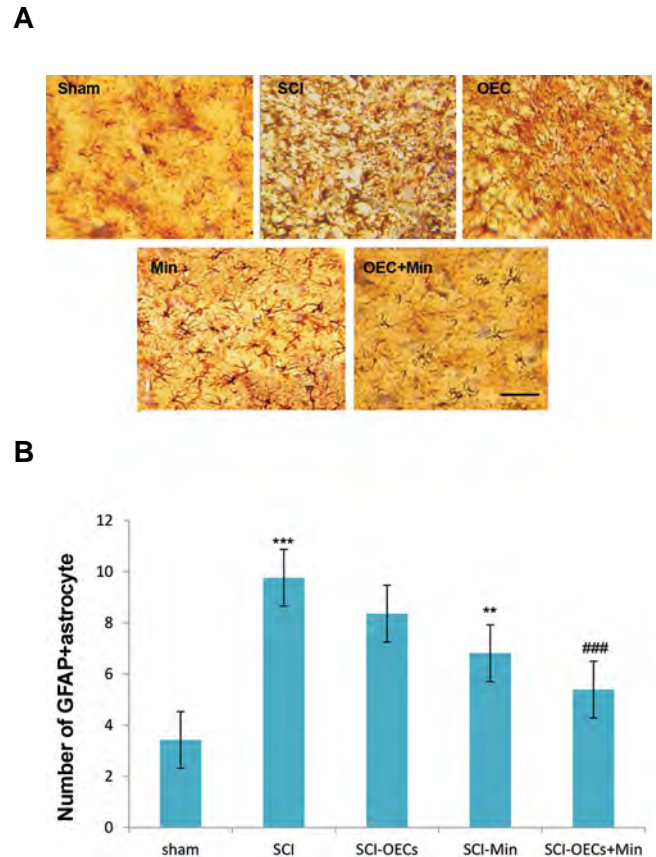


Fig.4: Immunohistochemistry assessment of combined treatment on the GFAP in the ventral horn of spinal cord at 35 days after SCI. **A.** The immunohistochemistry staining ($\times 40$) (scale bars: 50 μ m) and **B.** Number of the GFAP-positive glial. Data are presented as the mean \pm SEM.

GFAP; glial fibrillary acidic protein, SCI; Spinal cord injury, OECs; Olfactory ensheathing cells, ***; $P < 0.001$ vs. sham group, **; $P < 0.01$, and ###; $P < 0.001$ vs. SCI group.

Effect of combined treatment with minocycline and olfactory ensheathing cells transplantation on expression levels of pro-inflammatory factors after spinal cord injury

The expression of proinflammatory factors was also determined to elucidate the functions and mechanisms of inflammatory cells. The analysis of protein levels by western blotting revealed that minocycline treatment and OECs transplantation significantly decreased the level of IL-1 β , TNF α , as compared with that of the SCI group ($P < 0.01$, $P < 0.05$, Fig.5A, B). Also, the results showed that the transplantation of OECs with minocycline reduced the levels of IL-1 β and TNF- α ($P < 0.001$, Fig.5A, B). These results suggested that the

transplantation of OECs with minocycline can reduce further the expression of pro-inflammatory factors (TNF- α and IL-1 β) in SCI.

Effects of combined treatment with minocycline and olfactory ensheathing cells on caspase-3 activation after spinal cord injury

Western blot analysis was used to detect the expression of caspase-3 in the spinal cord tissue at 35 days after SCI. In comparison to the sham group, the expression level of caspase-3 was significantly elevated after SCI ($P < 0.001$). Nevertheless, minocycline and combined treatment with minocycline and OECs significantly decreased SCI-induced increase in caspase-3 activity ($P < 0.01$). However, the transplantation of OECs had no significant effect on the expression of caspase-3 (Fig.5).

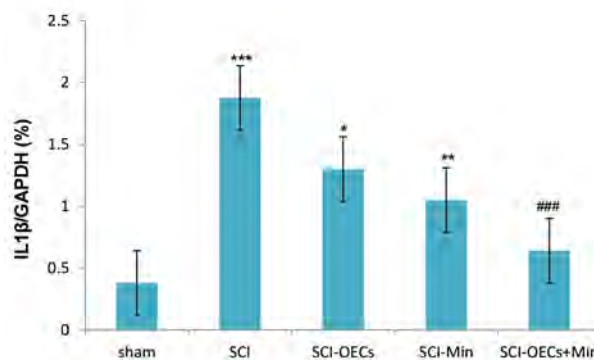
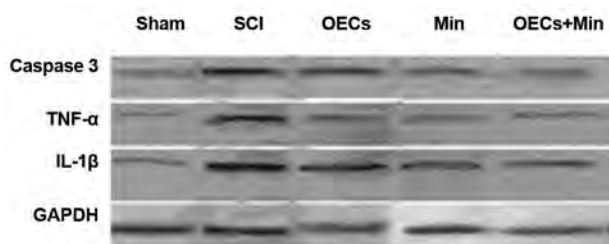
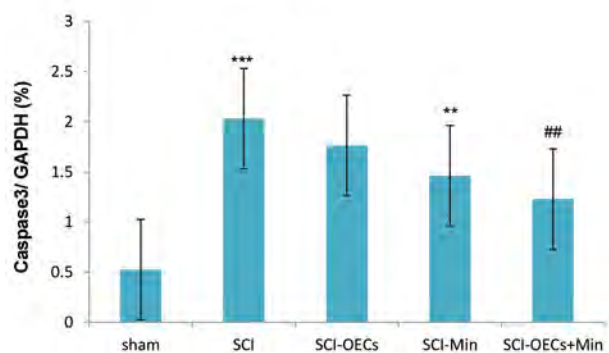
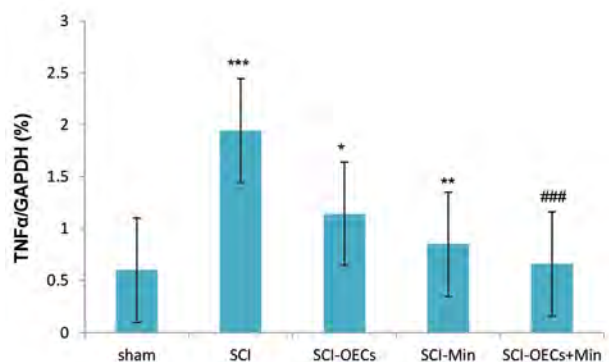


Fig.5: The effect of combined treatment on the levels of TNF- α , IL-1 β and caspase-3. **A.** Western blotting for TNF- α , IL-1 β and caspase-3 in different groups and **B.** The quantification of protein expression of TNF- α , IL-1 β , and caspase-3 at 35 days after SCI. Data are presented as mean \pm SEM (n=4, each). TNF- α ; Tumor necrosis factor alpha, IL-1 β ; Interleukin 1 beta, ***; $P < 0.001$ vs. sham group, *; $P < 0.05$, **; $P < 0.01$, and ###; $P < 0.001$ vs. SCI group.

A



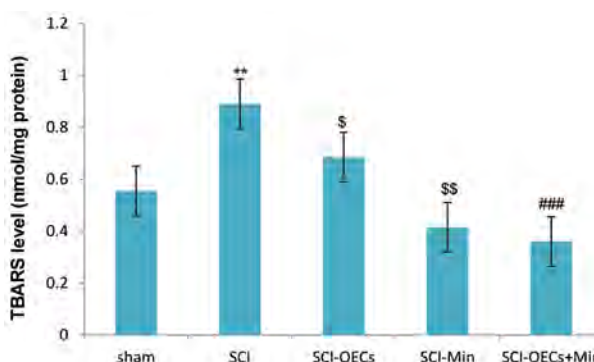
B



Biochemical findings

The levels of GSH and CAT were significantly lowered in the SCI control animals compared to the sham group ($P < 0.001$, $P < 0.01$). The OECs transplantation had no significant effects on GSH activity when compared to the SCI group, but it increased the levels of CAT ($P < 0.05$). However, SCI animals treated with minocycline and combined treatment with the minocycline+OECs exhibited a significant ameliorating effect on the level of GSH compared to the SCI group ($P < 0.05$, Fig.6). Both treatment with minocycline and minocycline+OECs significantly increased the tissue CAT activity compared to the SCI group ($P < 0.05$, $P < 0.01$, Fig.6).

The results of TBARS indicated that SCI significantly stimulated the level of TBARS activity compared to the sham group ($P < 0.01$). However, SCI animals treated with either OECs or minocycline alone, or in combination with each other were significantly mitigated compared to the SCI group ($P < 0.05$, $P < 0.01$, $P < 0.001$). Tissue NO levels were found to be significantly increased in the SCI group when compared with the sham group ($P < 0.01$). In the minocycline and combined treatment groups, tissue NO levels were significantly decreased compared to the SCI group ($P < 0.05$, $P < 0.01$). In the OECs but didn't show significant difference in the NO levels compared to the SCI group (Fig.6).



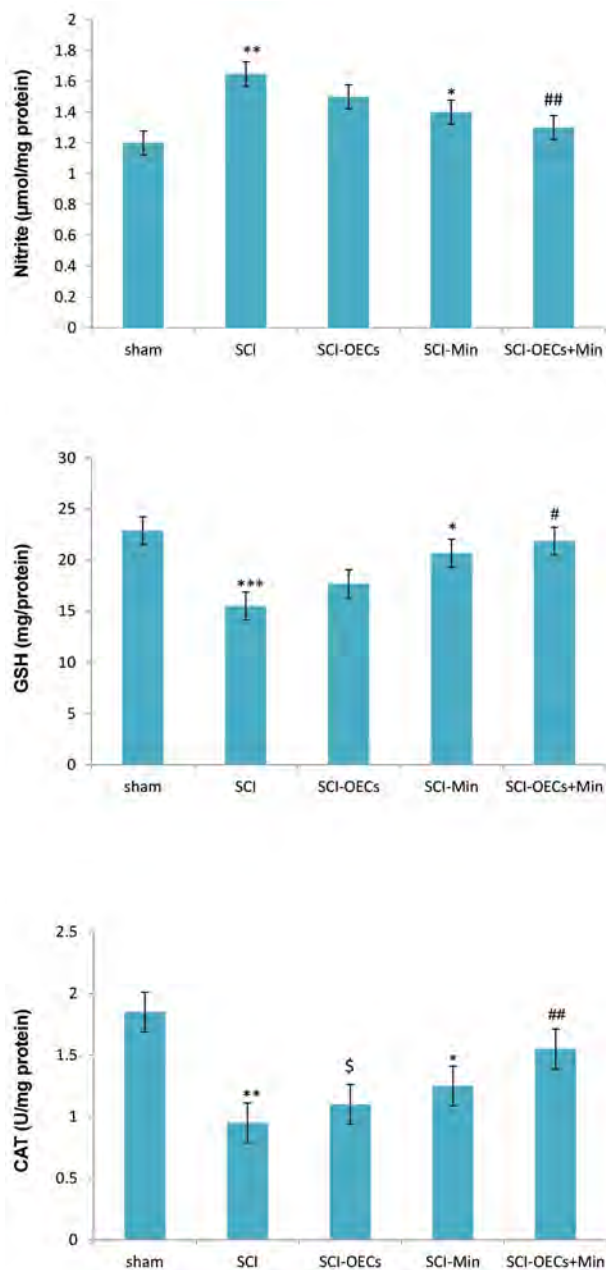


Fig.6: The effect of combined treatment on the levels of MDA, NO, CAT, and GSH at 35 days after SCI. The error bars indicate mean \pm SEM. MDA; Malondialdehyde, NO; Nitric oxide, CAT; Catalase, GSH; Glutathione, SCI; Spinal cord injury, OECs; Olfactory ensheathing cell, **; $P < 0.01$, ***; $P < 0.001$ vs. sham, \$\$; $P < 0.01$, *; $P < 0.05$, \$; $P < 0.05$, ###; $P < 0.001$, ##; $P < 0.01$, #; $P < 0.05$ vs. SCI group (n=6/group).

Discussion

The secondary injury after SCI leads to significant loss of neurons and the formation of an inhibitory glial scar. A variety of single therapies have targeted single obstacles that limit the recovery of post-injury, which provide small improvements in functional recovery (24). Earlier studies have indicated that axonal regeneration in SCI is possible if the inhibitory milieu or glial scar is prevented at a low level to allow CNS axons to grow (25, 26). Herein, we combined promising therapies namely, transplantation of OECs and minocycline to overcome

the multitude of obstacles limiting the recovery with the aim of enhancing recovery over single therapies. Also, in this study, for the first time, we investigated the effect of OECs alone and in combination with minocycline on the oxidative stress in contusive SCI model. The results of this study indicated that the effect of combined treatment with OECs and minocycline on biochemical factors and apoptosis is more effective than single treatment with OECs or minocycline.

The results showed that the combination of minocycline with OECs grafting results in a significant improvement in BBB score than the SCI group, also an increase in tissue sparing observed in the combination of minocycline and OECs transplantation compared to minocycline and OECs transplantation alone. OECs transplantation after moderate contusive thoracic SCI of adult rats promoted the partial recovery of motor function that is in agreement with the study of Plant et al. (14). The most recovery rate was apparent in the minocycline and minocycline+OECs groups, which exhibited the improvement in the functional recovery with an increased rate of recovery between 2-5 weeks after SCI. This may be explained by this fact that the injection of minocycline prior to OECs transplantation provides a favorable environment for grafted cells by reducing proinflammatory molecules and glial scar formation. On the other hand, GFAP expression is increased during the first week of spinal cord injury; therefore, OECs grafting, one week after injury, may be too delayed to prevent the formation of the glial scar and secretion of inhibitory molecules. In one study performed by López-Vales et al. (15) showed that the delayed OECs transplants had intermediate effects on the GFAP expression after SCI. Therefore, the protective effects after contusion SCI and the enhanced locomotor function were observed when the combination of minocycline and OECs transplantation was applied that may mediate the inhibition of the posttraumatic astrogliosis. These findings are in agreement with the results of similar studies. Festof et al. in 2006 reported that modulating apoptosis, caspases, and microglia by minocycline provide promising therapeutic targets for limiting the degree of functional loss after CNS trauma (9). Besides, neuroprotection effect of minocycline has been also reported to promote axonal regeneration through the suppression of RGMA in rat MCAO/reperfusion model (27). Consistent with these studies, we indicated that minocycline enhanced the functional recovery after moderate contusive spinal cord injury. On the other hand, the results observed the restorative effects of OECs transplant after SCI that are in agreement with previous studies (28-30).

Also, the histological results indicated that the cavitation volume in animals receiving minocycline was significantly reduced as compared with those received OECs graft. It was shown that the minocycline group had the increased volume of tissue sparing 35 days post-injury, but the combination of OECs transplantation with minocycline further reduced the cavity size compared with the single strategies. Furthermore, the combination

therapy was more effective in increasing the tissue sparing than minocycline and OECs transplantation alone. These results would be expected due to the difference in the timing of the injection of minocycline immediately after the injury, during the peak of secondary injury, versus transplantation of OECs one week after injury when considerable secondary tissue loss had already occurred. Moreover, the secondary injury was increased because of the delayed treatment, and the injury cascade that stems from the neurodestructive events is likely to be more extensive. Besides, the immunomodulatory effect of minocycline was exerted through the protection of the spinal cord tissue and reduced neuronal and glial death during the acute phase of the injury, such as inhibition of caspase-3 activity (9) and the release of cytochrome c from mitochondria (10). Lee et al. (31) indicated that minocycline reduces neuronal death and the cyst cavity, and it improves the locomotor function after traumatic SCI in rats. On the other hand, tissue protection mediated by OECs is due to the ability of OECs in secretion of several factors that may promote not only axonal regeneration but also provide neurotrophic support that permit the survival of the damaged neural cells, including nerve growth factor, brain-derived neurotrophic factor, glial derived neurotrophic factor, and neurotrophin 4/5 factor, as well as the prevention of the progression of cavity (32). Because each treatment modulates some common factors involved in the pathophysiology of SCI through the different mechanisms; therefore, the combination of tissue protective agents and the later transplantation of cell may exert additive tissue sparing over the use of each treatment alone.

It was previously reported that the reactive astrocytes secrete cytotoxic proinflammatory factors and chondroitin sulfate proteoglycans that initiate the effective cascades, which not only increase the inflammatory responses but also destroy the internal environment of the CNS resulting in cell death and inhibition of the axonal regeneration (33, 34). Thus, reducing the levels of pro-inflammatory factors can prevent the subsequent cytotoxic and apoptotic effects. Herein, in accordance with the others studies, we demonstrated that both minocycline injection and OECs transplantation reduced proinflammatory cytokines such as TNF- α and IL-1 β . However, OECs treatment did not decrease the expression of caspase-3 after SCI. Nevertheless, the combination of both treatments further reduced proinflammatory cytokines and caspase-3 in the contusion SCI model.

In the present study, lipid peroxidation measured as thiobarbituric acid-reactive substances in tissue (MDA), NO, and ROS levels as an indicator of oxidative damage were analyzed for the mechanisms underlying the neuroprotective action of OEC grafts for the first time in SCI. The previous studies have reported that the transplanting of OECs into the sub-retinal space of rats with light-induced retinal damage reduced the oxidative stress and the loss of photoreceptors (35). Also, in another study, it was shown that OEC-conditioned medium may also promote the antioxidant defense, leading to suppression of 6OHDA-induced oxidative damage by

enhancing Akt survival signaling (36). A study carried out by Liu et al. (37) indicated that OEC-conditioned medium may protect astrocytes from the oxidative damage by promoting the cell survival while reducing apoptosis of the damaged cells.

In the present study the levels of MDA, and NO were significantly increased following SCI. In addition, due to elevated levels of the oxidative stress in the spinal cord, tissue antioxidants namely GSH and CAT were decreased (38). Minocycline and OECs alone and in combination with each other significantly decreased the levels of MDA, and NO when compared with the SCI group. These results have shown that OECs transplantation one week after injury could affect the oxidative stress and proinflammatory factors. However, the underlying mechanisms of the protective effect of OECs have not been fully understood and need further studies. These results suggest noticeable protection against the oxidative stress and significant antioxidant effect of combined treatment in rats with contusive spinal cord injury. Similarly, Ahmad et al. (39) also reported that minocycline treatment decreased tissue MDA and MPO levels and prevented the inhibition of GSH and CAT in SCI tissues. Furthermore, other studies have determined that minocycline potentially targets a broad range of secondary injury mechanisms, and protect neural tissue from multiple neurotoxic insults via its anti-inflammatory, anti-oxidant, and anti-apoptotic properties as well as inhibitory impacts on lipid peroxidation and oligodendrocyte apoptosis. It was demonstrated that the treatment with minocycline improved the functional recovery after SCI (40).

Conclusion

The results of the present study showed that minocycline and OECs grafts can modulate some common mechanisms involved in the pathophysiology of spinal cord injury, and therefore, the combination of both treatments may exert better effects. The injection of minocycline prior to OECs transplantation can reduce the cavity volume, astrogliosis, and the release of proinflammatory cytokines, providing unfavorable microenvironment and increasing the ability of OECs to enhance the axonal regeneration. According to the complexity of SCI pathophysiology, these results indicate that the combination therapy is more effective to improve SCI damage, and this study may be another promising step to the development of a combined treatment for refining the functional recovery after spinal cord injury.

Acknowledgments

This work was financially supported by Iran National Science Foundation (INSF, grant number 94803041). The authors declare that they have no conflict of interest.

Authors' Contributions

S.P.; Carried out the study design and experiments. S.O.; Contributed to the discussion, and reviewed the manuscript and was responsible for overall supervision.

S.H.S.; Contributed to the discussion, and analyzed data. G.K.; Performed a part of the experiment and analyzed data. All authors read and approved the manuscript.

References

- Lim PA, Tow AM. Recovery and regeneration after spinal cord injury: a review and summary of recent literature. *Ann Acad Med Singapore*. 2007; 36(1): 49-57.
- Oyinbo CA. Secondary injury mechanisms in traumatic spinal cord injury: a nugget of this multiply cascade. *Acta Neurobiol Exp (Wars)*. 2011; 71(2): 281-299.
- Dumont RJ, Okonkwo DO, Verma S, Hurlbert RJ, Boulos PT, Ellegala DB, et al. Acute spinal cord injury, part I: pathophysiologic mechanisms. *Clin Neuropharmacol*. 2001; 24(5): 254-264.
- van den Berg ME, Castellote JM, Mahillo-Fernandez I, de Pedro-Cuesta J. Incidence of spinal cord injury worldwide: a systematic review. *Neuroepidemiology*. 2010; 34(3): 184-192.
- Young W. Secondary injury mechanisms in acute spinal cord injury. *J Emerg Med*. 1993; 11 Suppl 1: 13-22.
- Golub LM, Ramamurthy NS, McNamara TF, Greenwald RA, Rifkin BR. Tetracyclines inhibit connective tissue breakdown: new therapeutic implications for an old family of drugs. *Crit Rev Oral Biol Med*. 1991; 2(3): 297-321.
- Chen M, Ona VO, Li M, Ferrante RJ, Fink KB, Zhu S, et al. Minocycline inhibits caspase-1 and caspase-3 expression and delays mortality in a transgenic mouse model of Huntington disease. *Nat Med*. 2000; 6(7): 797-801.
- Yrjänheikki J, Tikka T, Keinänen R, Goldsteins G, Chan PH, Koistinaho J. A tetracycline derivative, minocycline, reduces inflammation and protects against focal cerebral ischemia with a wide therapeutic window. *Proc Natl Acad Sci USA*. 1999; 96(23): 13496-13500.
- Festoff BW, Ameenuddin S, Arnold PM, Wong A, Santacruz KS, Citron BA. Minocycline neuroprotects, reduces microgliosis, and inhibits caspase protease expression early after spinal cord injury. *J Neurochem*. 2006; 97(5): 1314-1326.
- Teng YD, Choi H, Onario RC, Zhu S, Desilets FC, Lan S, et al. Minocycline inhibits contusion-triggered mitochondrial cytochrome c release and mitigates functional deficits after spinal cord injury. *Proc Natl Acad Sci USA*. 2004; 101(9): 3071-3076.
- Tikka TM, Koistinaho JE. Minocycline provides neuroprotection against N-methyl-D-aspartate neurotoxicity by inhibiting microglia. *J Immunol*. 2001; 166(12): 7527-7533.
- He Y, Appel S, Le W. Minocycline inhibits microglial activation and protects nigral cells after 6-hydroxydopamine injection into mouse striatum. *Brain Res*. 2001; 909(1-2): 187-193.
- Li Y, Field PM, Raisman G. Regeneration of adult rat corticospinal axons induced by transplanted olfactory ensheathing cells. *J Neurosci*. 1998; 18(24): 10514-10524.
- Plant GW, Christensen CL, Oudega M, Bunge MB. Delayed transplantation of olfactory ensheathing glia promotes sparing/regeneration of supraspinal axons in the contused adult rat spinal cord. *J Neurotrauma*. 2003; 20(1): 1-16.
- López-Vales R, Forés J, Verdú E, Navarro X. Acute and delayed transplantation of olfactory ensheathing cells promote partial recovery after complete transection of the spinal cord. *Neurobiol Dis*. 2006; 21(1): 57-68.
- López-Vales R, Forés J, Navarro X, Verdú E. Olfactory ensheathing glia graft in combination with FK506 administration promote repair after spinal cord injury. *Neurobiol Dis*. 2006; 24(3): 443-454.
- Pearse DD, Marcillo AE, Oudega M, Lynch MP, Wood PM, Bunge MB. Transplantation of Schwann cells and olfactory ensheathing glia after spinal cord injury: does pretreatment with methylprednisolone and interleukin-10 enhance recovery? *J Neurotrauma*. 2004; 21(9): 1223-1239.
- Nash HH, Borke RC, Anders JJ. New method of purification for establishing primary cultures of ensheathing cells from the adult olfactory bulb. *Glia*. 2001; 34(2): 81-87.
- Aras M, Altas M, Motor S, Dokuyucu R, Yilmaz A, Ozgiray E, et al. Protective effects of minocycline on experimental spinal cord injury in rats. *Injury*. 2015; 46(8): 1471-1474.
- Basso DM, Beattie MS, Bresnahan JC. A sensitive and reliable locomotor rating scale for open field testing in rats. *J Neurotrauma*. 1995; 12(1): 1-21.
- Lowry OH, Rosebrough NJ, Farr AL, Randall RJ. Protein measurement with the Folin phenol reagent. *J Biol Chem*. 1951; 193(1): 265-275.
- Aebi H. Catalase. *Methods of enzymatic analysis*. 2nd edition. Elsevier; 1974; 673-684.
- Petrola MJ, de Castro AJ, Pitombeira MH, Barbosa MC, Quixadá AT, Duarte FB, et al. Serum concentrations of nitrite and malondialdehyde as markers of oxidative stress in chronic myeloid leukemia patients treated with tyrosine kinase inhibitors. *Rev Bras Hematol Hemoter*. 2012; 34(5): 352-355.
- Wilems TS, Pardieck J, Iyer N, Sakiyama-Elbert SE. Combination therapy of stem cell derived neural progenitors and drug delivery of anti-inhibitory molecules for spinal cord injury. *Acta Biomater*. 2015; 28: 23-32.
- Bradbury EJ, McMahon SB. Spinal cord repair strategies: why do they work? *Nat Rev Neurosci*. 2006; 7(8): 644-653.
- Yiu G, He Z. Glial inhibition of CNS axon regeneration. *Nat Rev Neurosci*. 2006; 7(8): 617-627.
- Tao T, Xu G, Si Chen C, Feng J, Kong Y, Qin X. Minocycline promotes axonal regeneration through suppression of RGMA in rat MCAO/reperfusion model. *Synapse*. 2013; 67(4): 189-198.
- Lu J, Féron F, Mackay-Sim A, Waite PM. Olfactory ensheathing cells promote locomotor recovery after delayed transplantation into transected spinal cord. *Brain*. 2002; 125(Pt 1): 14-21.
- Ramón-Cueto A, Cordero MI, Santos-Benito FF, Avila J. Functional recovery of paraplegic rats and motor axon regeneration in their spinal cords by olfactory ensheathing glia. *Neuron*. 2000; 25(2): 425-435.
- Ramer LM, Au E, Richter MW, Liu J, Tetzlaff W, Roskams AJ. Peripheral olfactory ensheathing cells reduce scar and cavity formation and promote regeneration after spinal cord injury. *J Comp Neurol*. 2004; 473(1): 1-15.
- Lee SM, Yune TY, Kim SJ, Park DW, Lee YK, Kim YC, et al. Minocycline reduces cell death and improves functional recovery after traumatic spinal cord injury in the rat. *J Neurotrauma*. 2003; 20(10): 1017-1027.
- Lipson AC, Widenfalk J, Lindqvist E, Ebendal T, Olson L. Neurotrophic properties of olfactory ensheathing glia. *Exp Neurol*. 2003; 180(2): 167-171.
- Schwab ME, Bartholdi D. Degeneration and regeneration of axons in the lesioned spinal cord. *Physiol Rev*. 1996; 76(2): 319-370.
- Bovolenta P, Fernaud-Espinosa I. Nervous system proteoglycans as modulators of neurite outgrowth. *Prog Neurobiol*. 2000; 61(2): 113-132.
- Xue L, Zeng Y, Li Q, Li Y, Li Z, Xu H, et al. Transplanted olfactory ensheathing cells restore retinal function in a rat model of light-induced retinal damage by inhibiting oxidative stress. *Oncotarget*. 2017; 8(54): 93087-93102.
- Shukla A, Mohapatra TM, Parmar D, Seth K. Neuroprotective potentials of neurotrophin rich olfactory ensheathing cell's conditioned media against 6OHDA-induced oxidative damage. *Free Radic Res*. 2014; 48(5): 560-571.
- Liu J, Qiu J, Xiong Y, Liu Z, Gao J. The mitochondrial protective mechanism of olfactory ensheathing cells conditioned medium protects against H₂O₂-induced injury in astrocytes. *Neurosci Lett*. 2013; 555: 91-96.
- Azbill RD, Mu X, Bruce-Keller AJ, Mattson MP, Springer JE. Impaired mitochondrial function, oxidative stress and altered antioxidant enzyme activities following traumatic spinal cord injury. *Brain Res*. 1997; 765(2): 283-290.
- Ahmad M, Zakaria A, Almutairi KM. Effectiveness of minocycline and FK506 alone and in combination on enhanced behavioral and biochemical recovery from spinal cord injury in rats. *Pharmacol Biochem Behav*. 2016; 145: 45-54.
- Sonmez E, Kabatas S, Ozen O, Karabay G, Turkoglu S, Ogun E, et al. Minocycline treatment inhibits lipid peroxidation, preserves spinal cord ultrastructure, and improves functional outcome after traumatic spinal cord injury in the rat. *Spine (Phila Pa 1976)*. 2013; 38(15): 1253-1259.